Universidad Autónoma de Madrid

Departamento de Bioquímica

Functional implication of the calmodulin-binding domain of the adaptor protein Grb7

Irene García Palmero

Madrid, 2012

Departamento de Bioquímica

Facultad de Medicina

Universidad Autónoma de Madrid

Functional implication of the calmodulin-binding domain of the adaptor protein Grb7

Memoria de Tesis Doctoral presentada por:

Irene García Palmero

Licenciada en Bioquímica, para optar al grado de Doctor

por la Universidad Autónoma de Madrid

Director de tesis:

Dr. Antonio Villalobo

Profesor de Investigación del CSIC

INSTITUTO DE INVESTIGACIONES BIOMÉDICAS “ALBERTO SOLS”

CONSEJO SUPERIOR DE INVESTIGACIONES CIENTÍFICAS

UNIVERSIDAD AUTÓNOMA DE MADRID

Antonio Villalobo, Profesor de Investigación del Consejo Superior de Investigaciones Científicas y Profesor Honorario de la Universidad Autónoma de Madrid, certifica que:

Irene García Palmero, Licenciada en Bioquímica por la Universidad Autónoma de Madrid, ha realizado bajo mi dirección el trabajo de investigación titulado: **"Functional implication of the calmodulin-binding domain of the adaptor protein Grb7"** en el Instituto de Investigaciones Biomédicas "Alberto Sols".

Considero que el mencionado trabajo es apto para poder optar al grado de Doctor por la Universidad Autónoma de Madrid.

Y para que así conste a todos los efectos, firmo el presente certificado en Madrid, a 12 de Junio de 2012.

Fdo.: Antonio Villalobo

Director de la Tesis
Profesor de Investigación, CSIC

Vº Bº Tutor: Mario Vallejo

Profesor de Investigación, CSIC
Profesor Honorario del Departamento de Bioquímica de la Universidad Autónoma de Madrid

Este trabajo ha sido realizado en el Departamento de Biología del Cáncer del Instituto de Investigaciones Biomédicas “Alberto Sols” (CSIC-UAM), gracias a una Ayuda a la Formación del Profesorado Universitario (FPU) del Ministerio de Educación.

A mis padres

A mi hermana

A David

"*Logic will get you from A to B.*

Imagination will take you everywhere"

A. Einstein

AGRADECIMIENTOS

Parece que fue ayer cuando llegué por primera vez al IIB y la verdad es que han pasado ya casi 6 años. Realizar una Tesis doctoral ha sido un proyecto duro, pero una experiencia muy gratificante tanto a nivel profesional como personal, que he compartido con muchas personas a las que me gustaría dar las gracias de manera muy especial.

En primer lugar quiero dar las gracias al Prof. Antonio Villalobo, mi director de Tesis, por haberme dado la oportunidad de incorporarme a su laboratorio y haber puesto a mi disposición todos sus conocimientos, por la importante labor de dirección, y sobre todo por el apoyo recibido durante estos años. También quiero dar las gracias a mi tutor, el Prof. Mario Vallejo por su labor en la supervisión de esta Tesis.

Quiero agradecer también la ayuda que he recibido para el desarrollo de mis experimentos de MRI. En primer lugar al Prof. Sebastián Cerdán y a todo el equipo del SIERMAC y muy especialmente a la Dra. Pilar López Larrubia y a Patricia Sánchez, por su gran ayuda y apoyo en mis experimentos y en el buen desarrollo de esta tesis, y sobre todo por esos inolvidables momentos que hemos pasado jornaleando. También quiero dar las gracias al Dr. Eduardo Villalobo por la preparación del mutante de delección del dominio de unión a calmodulina Grb14Δ, y a la Dra. Mª Carmen Grijota por su ayuda con la parte histológica de la Tesis.

I would like to thank Prof. Jacques Haiech and his laboratory for performing the fluorescent polarization analysis and calorimetric titration assays to test the binding of calmodulin with the calmodulin-binding domain peptides for us.

También quiero dar las gracias a los servicios del IIB, cultivos, imagen, informática, biblioteca, secretaria, almacén, lavado, mantenimiento, prevención de riesgos laborales, microscopia, y a los laboratorios de confocal y citometría del SIDI y a toda la gente que hay detrás de ellos por sus buenas palabras y por su inestimable ayuda.

Por la que ha sido mi segunda casa durante estos años, el labo 1.8, han pasado muchas personas con las que he compartido más o menos tiempo, pero que me han aportado y me han ayudado mucho a crecer como persona. Espero no olvidarme de nadie. En primer lugar, y por orden de llegada, me gustaría acordarme de Óscar, y de cómo él me enseñó todo lo que sabía durante mis inicios y de cómo yo le enseñé a reciclar. De Carmen y Elisa, y de el cerdo que pensábamos que iba a hacer estallar el iib. De Amandeep y de Jihene, de esa persona con tan buen corazón, Karim, y de Célia, la dulzura francesa en persona. Gracias a Patri, por “estar completa”, a Christian por nuestras charlas sobre el Atleti, a Lucía, por enseñarme que las pipetas Pasteur de plástico también existen, a Lara por su gran apoyo en el labo y por su ayuda

con el dicroísmo circular, y por supuesto a Miguel, con quien tanto me reí. A Celia muchas gracias por los panetones y por esos zuecos rojos de Papá Noel. También me quiero acordar de aquel verano polaco que pasé con Kate y con Michael, gracias por ser cómo eres y por considerarme "your Lady Grb7". Como no, a mi Martita, terremoto y locura hecha persona, "muchas grassiass mi amol". Gracias a mi Paulita, a la que yo intenté enseñar y resultó que ella me enseñó mucho más. Y no me quiero olvidar de otras personas que también han pasado por el labo como Juan, María, Ana, Gonzalo, Silviya, Clara, Laura y Cristina, mi guardiola preferida. Especialmente me gustaría recordar a mi compañero de tesis, de laboratorio, de día a día, Pablo, y dar las gracias a esa belga que llegó revolucionando el laboratorio, por ser una persona tan especial a la que echo mucho de menos y a la que me quiero parecer de mayor. Pero sobre todo me gustaría dar las gracias a esa personita que es el alma del laboratorio, que tiene una luz tan especial y con olor a azahar, mi Amparito. Gracias por estar siempre ahí, por tu ayuda, por tus consejos, por nuestros cafés, risas, y sobre todo por haberme tratado siempre, desde que llegué al labo, con una vocecita que no oías, como a una hija.

Y saliendo del 1.8, me quiero acordar especialmente de mi segundo cobijo, el 1.4. Muchas gracias en especial a Alberto, mi amigo, apoyo y compañero de siempre, a Isa, por toda esa locura y cariño que desbordas porque saben los chinos que voy a echar mucho de menos tus chistes y nuestros cotilleos desayunando, a Yenny, por su tranquilidad y buenas palabras. Quiero dar las gracias también a la Dra. Carmela Calés, por preocuparse siempre por mí durante estos años. No me quiero olvidar de gente que ya no están por ahí, como David, Rafa e Irma, me lo pasé genial con vosotros, y también de María, Dani, Camino, Bárbara y Leti.

Quería dar las gracias a todas esas personas con las que he compartido pasillos, sonrisas y buenos momentos durante estos años. Los vecinos del 1.9, a Jose, Marina, Sandra, Diana y Elena, por sus risas, canciones de cumpleaños delante de toda la sala de personal y por alegrarme cada tarde que estaba en mi mesa cansada y me daba la vuelta para veros hacer carreras de sillas por el pasillo. También quiero agradecer todo el apoyo y el cariño recibido de los niños del 1.3.1, Jose y María V. Gracias Jose por hacerme reír cuando más lo he necesitado y a ti, María muchas gracias por tu apoyo durante esos momentos difíciles que he pasado en la biblio. Gracias a Jorge, mi arbitro de tenis preferido. Gracias también a Carlos y a Diego por alegrarme todos los días la entrada y salida del centro. No me puedo olvidar de gente con la que he compartido horas y horas en el cuarto de cultivos, como Jaime, Pilar, Rosa, Sole, María P, Bea, Cris y Álvaro. Ni tampoco de otras personas con las que he convivido estos últimos meses en la biblio, Dani, Ana y María G con quien he compartido agobios, estreses y sobre todo risas. También me quiero acordar de mis compañeras de cafés, en primer lugar Lali y

Anabel, muchas gracias por vuestros sabios consejos, y de Laura, ha sido un placer compartir cafecitos y confidencias durante estos meses.

I want to say a big thank you to everybody who helped me during my aussie adventure. First of all I would like to thank Prof. Roger Daly for housing me in his lab and making me feel part of it since the first day. I also want to thank all the members of the lab, Naveid, for helping me with all the MS experiments, Brigid, Ling, Brian, Luxi, Carole and Emily for all your support during my stay. And special thanks to Ruth for all your help and good advice. I also would like to say thank you to the rest of the members of the lab 1 and to the cancer department, especially to Dessi and Christa, I miss you so much girls. Y todavia “down under”, no sé como agradecer a David y Fátima toda su ayuda y su apoyo durante esos meses. Muchas gracias por todo chicos.

Y la verdad es que este largo camino de la tesis empezó hace mucho tiempo, allá por 2002, cuando decidí empezar biología en la Autónoma de Madrid, y conocí a mucha gente que me han ayudado a llegar donde estoy ahora. Cris, mi amiga, mi compañera de viajes y no sólo de tren, Laura, mi amiga, que siempre está ahí cuando la necesito, Marta, mi compañera de tesis, de biblio y de aventura, gracias por todo, Tefi, no cambies nunca, gracias por tu alegría, Tere los lunares hechos sonrisa, Dani y su empanamiento, mi Albertito (ver arriba) y mis niños Nacho y Sali. Os quiero a todos.

Muchas gracias a todos mis niños y niñas arancetanos, exiliados o adoptados, gracias por ser cómo sois, y por pasar tan buenos momentos juntos.

Quiero dar las gracias también a mi familia, por estar siempre apoyándome en todo momento, no sólo durante estos años de la tesis, si no durante toda mi vida. Muchas gracias a mis tíos, y a mis abuelos, a los que tanto quiero. También quiero agradecer todo el apoyo recibido por parte de Inma y Jose durante estos años. En especial quiero dar las gracias a mi tati, por ser como es, por tener siempre esa sonrisa en la cara, por su ayuda con los colores de esta tesis, por todos los buenos momentos que hemos pasado juntas, y por los que aún nos quedan (muchos frotis de caritas). También quiero dar las gracias a las dos personas más importantes de mi vida que han dado siempre todo por mí, muchas gracias mamá por toda tu ayuda y muchas gracias papá por tener ese corazón atlético tan fuerte.

Y por último, quiero dar las gracias a David, que tanto me ha ayudado y me ha apoyado, (y aguantado) durante estos años. Gracias por creer en mí, por estar siempre a mi lado, por hacerme siempre reír y por hacerme simplemente feliz. Te quiero.

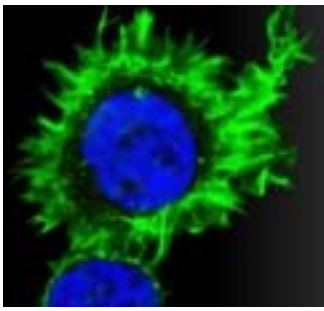

INDEX

INDEX OF FIGURES AND TABLES

- **FIGURES**

- **TABLES**

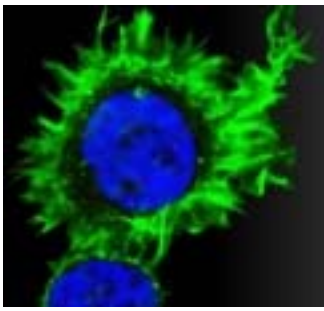

1 ABSTRACT/ RESUMEN

The growth factor receptor bound protein 7 (Grb7) gives name to a mammalian adaptor protein family that also includes Grb10 and Grb14. As an adaptor protein, Grb7 mediates signal transduction events iniciated by tyrosine kinase receptors present in the plasma membrane or other cytosolic kinases through its Src homology 2 (SH2) domain. Our laboratory previously described the presence of a calmodulin (CaM)-binding domain (CaM-BD) located in the proximal region of the pleckstrin homology (PH) domain of Grb7 and described that Grb7 was able to bind CaM in a Ca^{2+}-dependent manner both *in vitro* and in living cells. In this Thesis, we first described that the other Grb7 family members, Grb10 and Grb14, are also CaM-binding proteins (CaM-BP). To investigate the role that CaM plays in Grb7 functionality, we generated a deletion mutant lacking the CaM-BD named Grb7Δ. We report the differential behavior *in vitro* and *in vivo* of cells expressing Grb7Δ, as compared to those expressing either its wild type counterpart or cells lacking expression of this adaptor protein. Our results showed that deletion of the CaM-BD resulted in a lower cell migration rate, impaired cell adhesion ability to the extracellular matrix, and a lower proliferation rate. Additionally, we demonstrated that Grb7Δ was unable to localize in the nuclear fraction and that inhibition of CaM favored the nuclear localization of wild type Grb7. Therefore, we proposed that the CaM-BD of Grb7 overlapped its nuclear localization sequence (NLS). Besides, we performed *in vivo* experiments to study the role of the CaM-BD of Grb7 in tumor growth and tumor-associated angiogenesis by implanting glioma C6 cells stably expressing EYFP, EYFP-Grb7 or EYFP-Grb7Δ in the brain of rats and monitoring the tumor growth and its associated angiogenesis using Magnetic Resonance Imaging (MRI). We found that tumors generated by EYFP-Grb7Δ-expressing cells were smaller and less vascularized than those grown from cells expressing its wild type EYFP-Grb7 counterpart or EYFP-expressing control cells, suggesting an anti-angiogenic effect of the mutant protein. Finally, using co-immunoprecipitation and Mass Spectrometry-based proteomics, we described novel Grb7 and/or Grb7Δ binding partners. We validated by Western blot Hsc70 (heat shock cognate 70 protein) and caprin-1 (cytoplasmic activation/proliferation-associated protein-1) as Grb7 and Grb7Δ associated partners, and Nedd4 (neural precursor cell expressed developmentally down-regulated protein 4) as a Grb7 binding partner.

La proteína Grb7 *(growth factor receptor bound protein 7)* da nombre a una familia de proteínas adaptadoras que también incluye Grb10 y Grb14. Como proteína adaptadora, Grb7 media la transducción de señales desde receptores tirosina quinasa presentes en la membrana plasmática u otras quinasas citosólicas a través de su dominio SH2 *(Src homology 2)*. Nuestro laboratorio describió la existencia en Grb7 de un CaM-BD (*por calmodulin-binding domain)*, presente en la región proximal del dominio PH *(pleckstrin homology)* y confirmó la capacidad de Grb7 de unir CaM de una forma dependiente de Ca^{2+} tanto *in vitro* como en células. En primer lugar, en esta Tesis, demostramos que Grb10 y Grb14, los otros miembros de la familia de Grb7, son también proteínas de unión a CaM. Con el fin de caracterizar el papel del CaM-BD en la funcionalidad de Grb7, generamos un mutante de delección de dicho dominio, denominado Grb7Δ. En esta Tesis describimos las diferencias encontradas, tanto *in vitro* como *in vivo* entre células que expresaban la forma silvestre de Grb7 con respecto a las que expresaban el mutante de delección del CaM-BD, Grb7Δ. Nuestros resultados muestran que la delección del CaM-BD conllevó una menor capacidad migratoria de las células, una menor adhesión al sustrato, así como una menor capacidad proliferativa. Adicionalmente, demostramos la incapacidad de Grb7Δ de translocarse al núcleo y que la inhibición de la CaM indujo una mayor translocación de la forma silvestre de Grb7 al núcleo, sugiriendo que su CaM-BD solapa con su secuencia de localización nuclear (NLS). Además, realizamos estudios *in vivo* con el fin de investigar el papel que el CaM-BD desempeña en la funcionalidad de Grb7 controlando el crecimiento tumoral y la angiogénesis asociada a los tumores mediante la implantación de células C6 de glioma que expresaban establemente EYFP, EYFP-Grb7 o EYFP-Grb7Δ en el cerebro de ratas y la posterior monitorización de los tumores mediante técnicas de Imagen por Resonancia Magnética. Los tumores generados por células que expresaban el mutante EYFP-Grb7Δ, eran de menor tamaño y presentaban menor vascularización que los generados por células que expresaban la proteína silvestre EYFP-Grb7 y por las células control que expresaban EYFP, sugiriendo que Grb7Δ induce un efecto anti-angiogénico. Finalmente, describimos mediante técnicas de co-inmunoprecipitación y proteómica basada en Espectrometría de Masas y posterior validación por Western blot que tanto Hsc70 *(heat shock cognate 70 protein)* como caprin-1 *(cytoplasmic activation/proliferation-associated protein-1)* son proteínas capaces de asociarse con Grb7 y con su mutante de delección Grb7Δ, mientras que Nedd4 *(neural precursor cell expressed developmentally down-regulated protein 4)* solo se halló asociado con la forma silvestre de la proteína, sugiriendo la importancia del CaM-BD para la correcta unión de ésta.

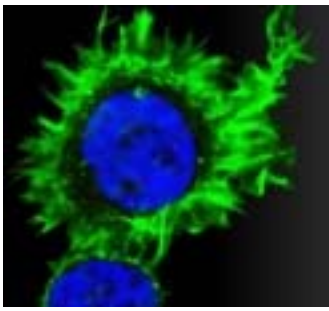

2 ABBREVIATIONS & ACRONYMS

5'-UTR: 5'-untranslated region

ADC: apparent diffusion coefficient

Apo-CaM: apocalmodulin

Akt: v-Akt murine thymoma viral oncogene homolog

Av: average

BCA: bicinchoninic acid

BPS: between PH and SH2

BSA: bovine serum albumin

CaM: calmodulin

CaM-BD: CaM-binding domain

CaM-BP: CaM-binding protein

CaMK: CaM-dependent kinase

Caprin-1: cytoplasmic activation/proliferation-associated protein-1

CBF: cerebral blood flow

CBV: cerebral blood volume

CDK: cyclin dependent kinase

CID: collision-induced dissociation

CLL: chronic lymphocytic leukemia

c-Myc: cellular myelocytomatosis oncogene

CORT: cloning of receptor targets

CRM1: chromosomal region maintenance 1

DAPI: 4',6-diamidino-2-phenylindole

DCC: deleted in colorectal cancer

DMEM: Dulbecco's modified Eagle's medium

DTPA: diethylenetriaminepentaacetic acid

DTT: dithiothreitol

ECL: enhanced chemiluminescence

EDTA: 2-[2-(bis(carboxymethyl)amino)ethyl-(carboxymethyl)amino]acetic acid

EGF: epidermal growth factor

EGFR: EGF receptor

EGTA: ethylene glycol-bis(2-aminoethylether)-*N,N,N',N'*-tetraacetic acid

EphB1: erythropoietin-producing hepatocellular carcinoma cells receptor

EPI: echo-planar imaging

ErbB: erythroblastic leukemia viral oncogene homolog

ERK: extracellular signal-regulated kinase

ESI: electrospray ionization

EV: empty vector

EYFP: enhanced yellow fluorescent protein

FACS: fluorescence-activated cell sorting

FAK: focal adhesion kinase

FAT: focal adhesion targeting

FBS: fetal bovine serum

FDR: false-positive discovery rate

FERM: four 1 protein, erzin, radixin moesin

FGF: fibroblast growth factor

FGFR: FGF receptor

FITC: fluorescein isothiocyanate

FOV: field of view

FRET: fluorescence resonance energy transfer

G3BP-1: GTPase-activating protein (SH3 domain) binding protein 1

GAPDH: glyceraldehyde-3-phosphate dehydrogenase

GFP: green fluorescent protein

GM: Grb and Mig10

Grb7: growth factor receptor-bound protein 7

Grb10: growth factor receptor-bound protein 10

Grb14: growth factor receptor-bound protein 14

GHR: growth hormone receptor

HCC: human hepatocellular carcinoma

HECT: homologous to E6-AP carboxyl terminus

HEK: human embryonic kidney

HEPES: 4-(2-hydroxyethyl)-1-piperazineethanesulfonic acid

HER: human EGFR receptor

hnRNP: heterogeneous nuclear ribonucleoprotein

HPLC: high-pressure liquid chromatography

HR: homologous region

HRGβ1: heregulin β1

Hsc70: heat shock cognate protein 70

HuR: Hu antigen R

IGFR: insulin growth factor receptor

IGF-1R: insulin-like growth factor 1 receptor

IgG: immunoglobulin G

JNK: c-Jun N-terminal kinase

KOR: kappa opioid receptor

K-Ras: Kirsten rat sarcoma viral oncogene homolog

M: mitosis

MAPK: mitogen-activated protein kinase

MRI: magnetic resonance imaging

mRNP: messenger ribonucleoprotein particle

MS: mass spectrometry

MTT: mean transit time

Nedd4: neural precursor cell expressed developmentally down-regulated protein 4

NF: nuclear fraction

NLS: nuclear localization sequence/signal

NMR: nuclear magnetic resonance

NNF: non-nuclear fraction

NP-40: Nonidet P-40

NSE: non-seminomas

NT: non-transfected

ORF: open reading frame

PABP: poly(A)-binding protein

PARP: poly(ADP-ribose) polymerase

PBS: phosphate buffered saline

PDGF: platelet derived growth factor

PDGFR: PDGF receptor

PDZ: post synaptic density protein (PSD95), *Drosophila* disc large tumor suppressor 1 (Dlg1), and zonula occludens-1 protein (zo-1)

PH: pleckstrin homology

Phall: phalloidin

PI3K: phosphatidylinositol 3-kinase

PLCγ1: phospholipase Cγ1

PMSF: phenylmethylsulfonyl fluoride

PR: proline-rich

pRb: retinoblastoma tumor suppressor protein

PVDF: polyvinylidene fluoride

RA: Ras-associating

ROI: region of interest

RPMI: Roswell Park Memorial Institute medium

SAM: sterile alpha motif

SDS: sodium dodecyl sulphate

SDS-PAGE: polyacrylamide gel electrophoresis in the presence of SDS

SE: seminoma

SH2: Src homology 2

SHP-2: SH2 protein tyrosine-phosphatase

MLCK: myosin light chain kinase

SOX: Sry-related high-mobility-box

SRY: sex determining region on the Y chromosome

STRING: search tool for the retrieval of interacting genes

T1: Relaxation time 1 (longitudinal)

T1W: T1-weighted

T2: Relaxation time 2 (transverse)

T2W: T2-weighted

TCA: trichloroacetic acid

TE: time of echo

TGCT: testicular germ cell tumor

TIA-1: T cell intercellular antigen-1

TR: time of repetition

TSAd: T cell–specific adapter

UCH-L3: ubiquitin carboxyl-terminal hydrolase isozyme

UGC: upper gastrointestinal adenocarcinoma

VEGF: vascular endothelial growth factor

VEGFR: VEGF receptor

W-7: *N*-(6-aminohexyl)-5-chloro-1-naphthalenesulfonamide

W-13: *N*-(4-aminobutyl)-5-chloro-1-naphthalenesulfonamide

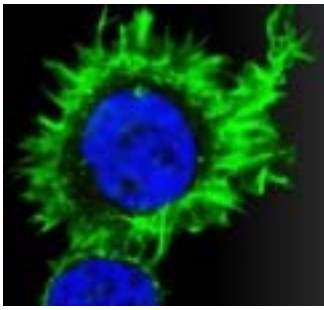

3 INTRODUCTION

The specific and appropriate response of cells to external stimuli requires the integration of multiple signaling pathways. The control of the cross-talk between different signaling cascades and its specificity is mediated in great extent by adaptor proteins among other factors. Adaptor proteins usually lack any intrinsic enzymatic activity, but they contain several domains within their structure which allow specific protein-protein interactions within a given signaling cascade resulting in the transmission of the signal along defined pathways (77).

3.1 The growth factor receptor bound protein 7

The growth factor receptor bound protein 7 (Grb7) is a mammalian adaptor protein that plays important roles in mediating the transmission of signals from tyrosine kinase receptors present in the cell surface, and from other cytoplasmic tyrosine kinases, by coupling protein complexes. This protein is part of the Grb7 family which also includes Grb10 and Grb14 (55, 99, 167, 179, 254, 291). They are phylogenetically related to the *Caenorhabditis elegans* Mig10 protein (177), which is involved in the regulation of embryonic neural cell migration. They all share significant sequence homology and a well conserved molecular structure divided in several domains able not only to modulate the binding to different motifs contained in proteins by identifying short peptide sequences, but also the interaction with membranes (176-177).

3.1.1 Structure

Human (h) Grb7 is a 532 amino acid protein harboring an amino-terminal proline-rich (PR) region, a central GM region (for Grb and Mig10) (179) that includes a Ras-associating (RA) domain, a pleckstrin homology (PH) domain and a BPS domain (for between PH and SH2); and a carboxyl-terminal Src homology 2 (SH2) domain (Fig. 1) (55, 99, 179, 291).

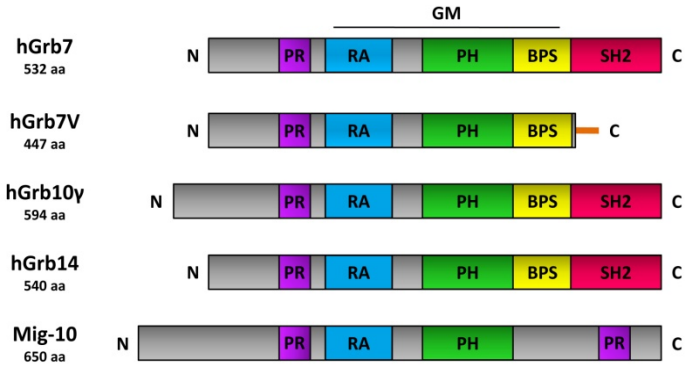

Figure 1: Structure of the human (h) Grb7 protein family. They all share a highly conserved structure differentiated in several domains. A proline-rich (PR) region, a central region denoted GM (for Grb and Mig10) that includes a Ras-associating (RA) domain, a pleckstrin homology (PH) domain and a BPS (for between PH and SH2) domain, and finally a Src homology 2 (SH2) domain located at the carboxy-terminal. The SH2 domain is absent in Grb7V, a naturally occurring truncated variant found in several tumors. The Grb7 family of proteins is phylogenetically related to the *Caenorhabditis elegans* Mig10 protein and they share a similar structure although it does not contain an SH2 domain.

Proline-rich regions are frequently found as multiple tandem repeats of variable length for binding to src-homology 3 (SH3) domain-containing proteins (302). Grb7 has five consensus PxxP motifs that define its PR region where x denotes any amino acid (99). Although previous reports did not assign a known biological function to the PR region of Grb7, novel studies revealed this region as a specific RNA-binding domain (258, 284).

The 300 amino acids-long central GM region shows high sequence homology between the different Grb7 family members and Mig10. This region comprises the RA, the PH and the BPS domains.

The Ras superfamily of GTPases are small monomeric G-proteins known to play critical roles in signal transduction and in the control of many biological functions (301), thus a wide variety of proteins present RA domains allowing their binding to the different members of the Ras superfamily. The RA-like domains were identified in the Grb7 protein family by sequence analysis. Grb7 has been shown to interact with the Ras family members N-Ras, K-Ras and R-Ras3 (238). Additionally, it has been demonstrated that in human breast adenocarcinoma SK-BR-3 cells, that overexpress Grb7, there is a constitutive activation of Ras and its related pathways (46).

The PH domains are protein modules formed by approximately 120 amino acids that can be found in a great variety of signaling molecules involved in intracellular signaling and in proteins that form part of the cytoskeleton. Although the PH domains can interact with other proteins, they fundamentally interact with membrane phosphoinositides. The PH domains can present different specificity for phosphoinositides phosphorylated at distinct sites within the inositol ring (171). Thus, Grb7 is able to bind to different phosphoinositides through its PH domain with distinct affinities. It binds with high affinity to phosphatidylinositol-3-phosphate and phosphatidylinositol-5-phosphate, and also binds to phosphatidylinositol-4-phosphate and phosphatidylinositol-3,5-bisphosphate with lesser affinity. A weaker binding is also found to phosphatidylinositol-3,4-bisphosphate and phosphatidylinositol-3,4,5-triphosphate. This shows that Grb7 preferentially binds to inositides phosphorylated at D3 and D5 positions. However, puntual mutations of Grb7 at some critical residues, such as Arg-239, prevent phosphoinositide binding. It is well known that interaction of the PH domain of Grb7 with phosphatidylinositol phosphates, present in the plasma membrane, is crucial in cell migration processes (99, 255).

The BPS domain is located, as its name indicates, between the PH and the SH2 domains. This protein region of approximately 45 amino acids long and is unique to the Grb7 protein

family. In fact this domain is absent in the homology-related Mig10 protein. The BPS domain seems to enhance the specificity of the binding promoted by the SH2 domain to phospho-tyrosine residues in tyrosine-kinase receptors (62). Crystallographic studies show that this domain appears to be unstructured, lacking stable secondary and tertiary conformations (189). This domain, along with the SH2 domain, plays a crucial role in mediating the interaction of the Grb7 family members with the insulin receptor, with Grb10 and Grb14 negatively regulating its activity (22, 270). However, the relative importance of these domains in the association with its target varies in the different members of the Grb7 protein family. In the case of Grb7, although both the BPS and the SH2 domains are considered to be important, the SH2 domain plays a predominant role in mediating the binding (137), whereas an equally role for both domains has been described in Grb10 (242). However, in the case of Grb14, the interaction is manly driven by the BPS domain (62, 137). These differences might explain the distinct role of the Grb7 protein family members inhibiting the insulin receptor, with Grb14 showing the higher inhibitory activity followed by Grb10 and in lesser extent Grb7 (22).

The SH2 domain is a structurally conserved protein region contained within the Src oncoprotein and in many other intracellular signal transduction proteins. They are characterized for their ability to bind to phospho-tyrosine residues present in phosphoproteins. The SH2 domain of Grb7, located at its carboxy-terminal, has an important role in the interaction of the protein with tyrosine-kinase receptors including all members of the ErbB family such as EGFR/ErbB1/HER1 (180), ErbB2/HER2 (128), ErbB3/HER3 (76) and ErbB4/HER4 (76); and PDGFR (307), FGFR (33), the proto-oncogene c-Kit (280), the insulin receptor (137), the Ret receptor (218), EphB1 (101) and the Tek/Tie2 receptor (131). Furthermore, the SH2 domain of Grb7 also interacts with cytosolic tyrosine kinases, such as FAK (98), and other phospho-proteins including tyrosine-phosphorylated caveolin, a protein involved in endocytosis (156). Grb7 has also been found interacting with the phosphatase SHP-2 through its SH2 domain (143). Besides, Grb7 interacts with the small GTPase Rnd1, a member of the Rho family of GTPases, through its SH2 domain; however, no tyrosine phosphorylation of the GTPase is required for this interaction (286). There is a natural occurring splicing variant of Grb7, denoted Grb7V, which lacks the 88-bp exon in the COOH terminus comprising the SH2 domain and resulting in its substitution by a short hydrophobic amino acid sequence (275) that has been found expressed in some tumors (275, 297). In spite of the 70 % sequence homology found between the SH2 domains of the different members of the Grb7 family; they seem to have different preferences for binding partners (99). The specific recognition of phospho-tyrosine residues by the SH2 domain involves the presence of a

phospho-tyrosine binding pocket, and a binding site that confers specificity for the residues that are next to the phospho-tyrosine (292). The crystallized SH2 domains of Grb7, Grb10 and Grb14 have shown differences in their phospho-tyrosine binding pockets (247, 269) resulting in Grb7 showing more affinity for phospho-peptides with the sequence pYVNQ (where pY represents phospho-tyrosine), than Grb10 or Grb14 (224). Phospho-peptides segments harboring this sequence have been found in ErbB2 (125, 128), a receptor that has been described co-amplified and overexpressed with Grb7 in many tumors, a fact that is related with poor prognosis *(see section 3.1.5)* (54, 178, 267, 274, 293).

Our laboratory described the presence of a calmodulin (CaM)-binding domain (CaM-BD) located at the proximal region of the PH domain of hGrb7 comprising the sequence ^{243}RKLWKRFFCFLRRS^{256} **(Fig. 2A).** This sequence forms a predicted basic amphiphilic α-helix, exposing basic residues on one side of the helical cylinder and most hydrophobic residues on the opposite side **(Fig. 2B)**.

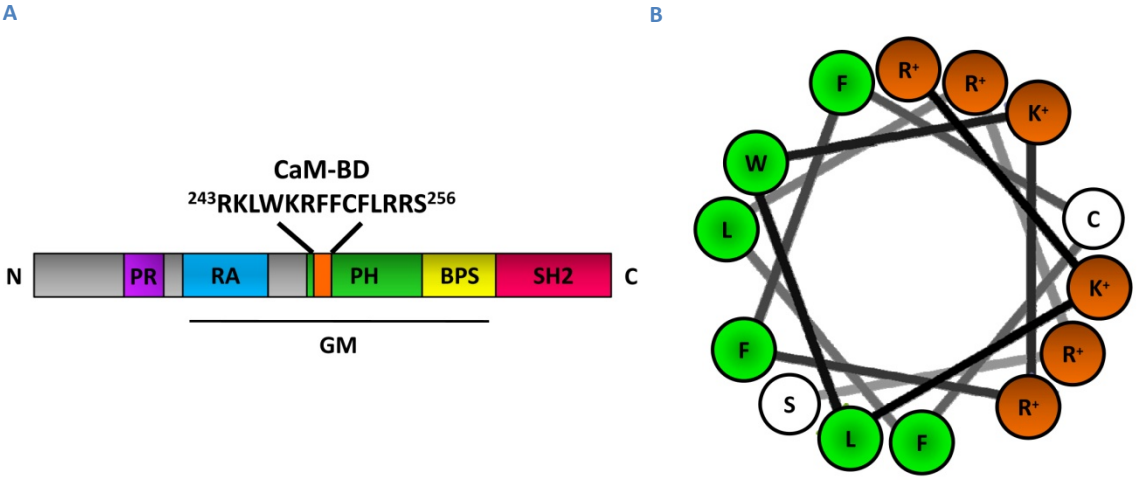

Figure 2: The calmodulin-binding domain (CaM-BD) of Grb7. **(A)** We previously described the presence of a CaM-BD comprising the detailed sequence located at the proximal region of the PH domain. **(B)** The CaM-BD forms a predicted amphiphilic α-helix, where basic (orange) and most hydrophobic (green) residues are exposed in the opposite side of the helix.

Sequence homology analysis shows that the CaM-BD of the truncated splicing variant, Grb7V is identical to the CaM-BD of Grb7. The CaM-BD is also highly conserved in other Grb7 protein family members, with Grb10 sharing 58 % and Grb14 67 % sequence identity. Additionally, the CaM-BD of Grb7 shares 53 % sequence identity with a region found in the Mig10 protein. The CaM-BD is identical in human, rat and mouse Grb7 **(Table 1)** (159).

Protein	Residues	CaM-BD homolog	Identity (%)		References
			CaM-BD	Whole sequence	
Human Grb7	243–256	RKLWKRFFCFLRRS	—	—	(178)
Human Grb7V	243–256	RKLWKRFFCFLRRS	100	97	(275)
Rat Grb7	246–259	RKLWKRFFCFLRRS	100	92	(138)
Mouse Grb7	246–259	RKLWKRFFCFLRRS	100	90	(178)
Human Grb14	248–261	kKSWKkiyFFLRRS	67	52	(56)
Rat Grb14	246–259	kKSWKkAyFFLRRS	67	50	(138)
Mouse Grb14	246–259	kKSWKkAyFFLRRS	67	51	(56)
Human Grb10γ	304–317	kKSWKklyVCLRRS	58	55	(164)
Human Grb10β	246–259	kKSWKklyVCLRRS	58	55	(79)
Human Grb10α	241-256	--	--	49	(164)
Mouse Grb10α	332–345	RKSWKklyVCLRRS	60	56	(213)
Mouse Grb10δ	307-320	RKSWKklyVCLRRS	60	49	(154)
C. elegans Mig10	358–371	RKSWKkHyFVLRPS	53	60	(177)

Table 1: Sequence homology of the calmodulin-binding domain of Grb7 shared between different species and other Grb7 family members. Red letters indicates identities while conservative substitutions are shown by lower-case black letters. The percentages of identity of the CaM-BDs and of the whole protein are also indicated. The human Grb10α isoform lacks the region of the pleckstrin homology (PH) domain where the CaM-BD is located due to alternative splicing.

3.1.2 The *GRB7* gene

Using the cloning of receptor targets (CORT) technique against a mouse library, The *GRB7* gene was first isolated as an EGFR-binding protein (180). The h*GRB7* gene, with a 9,377 pb length, is found in the large arm of chromosome 17, most precisely at the 17q12-q21.1 locus (167, 267). The *GRB7* gene comprises 15 exons; however, only 14 have coding capacity. An alternative splicing process is responsible for the truncated variant Grb7V, lacking the 88-pb exon that codes for the COOH terminus of the protein, resulting in the substitution of the SH2 domain by a short hydrophobic amino acid sequence. The h*GRB7* gene is transcribed into three different transcripts of 2,107, 2,197 and 2,228 pb that differ only in their 5'-UTR encoding all the same 532 amino acids (59.7 kDa) Grb7 protein (119, 167, 275). In normal tissues, Grb7 is highly expressed in liver and kidney and in a lesser extent in placenta, prostate, testis, ovary, lung and small intestine (55, 167).

3.1.3 The other members of the Grb7 family

The other members of the Grb7 protein family, Grb10 and Grb14, also mediate in multiple signal transduction pathways and have been involved in the regulation of many crucial cell functions that are briefly described here.

3.1.3.1 Grb10

The human *GRB10* gene, located at the 7p11.2-p12 locus (167), was also cloned using the CORT technique as a protein interacting with the phosphorylated carboxy-terminal region of the EGFR (179, 213). Several isoforms of the hGrb10 generated by alternative splicing have been described, including hGrb10α, hGrb10β and hGrb10γ (55) **(Fig. 3)**, being the hGrb10γ isoform the longest (67, 89, 165). The hGrb10α isoform is shorter and lacks a 46 amino acids long section corresponding to the PH domain (165, 210). The hGrb10β isoform differs from the hGrb10α isoform in the 5'-UTR and in the 5' coding region, and although presents an intact PH domain as the hGrb10γ isoform, it has a shorter N-terminal region (79). These isoforms differ in their expression pattern, which seems to be cell compartment and tissue-specific (26, 202). The hGrb10α isoform is found in skeletal muscle and pancreas and in lesser extent in heart, brain, placenta, lung, liver and kidney (210). The hGrb10β isoform is expressed in almost all tissues; however, its expression is higher in pancreas and skeletal muscle (79). Finally, hGrb10γ is found in skeletal muscle and in some tumor cells (67). Additionally, other isoforms, not so well characterized, have been described: hGrb10ε, hGrb10σ and hGrb10ζ (196). The h*GRB10* gene can be either paternally or maternally imprinted (one allele silenced), or expressed from both alleles depending on the tissue and the isoform (26). For instance, the transcribed allele for hGrb10γ in skeletal muscle has a maternal origin (26), whereas the paternal allele is the one transcribed for most of the Grb10 isoforms in human fetal brain (26), in contrast to the biallelic expression detected in other fetal tissues (114).

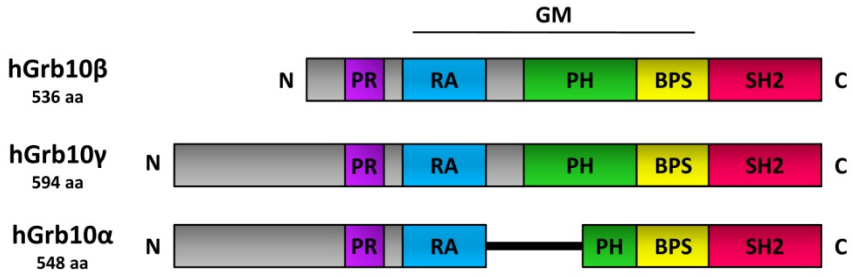

Figure 3: Structure of different human (h) Grb10 isoforms generated by alternative splicing. The hGrb10α and hGrb10γ isoforms present longer N-terminal region than isoform hGrb10β. The isoform hGrb10α lacks a 46 amino acids long section corresponding to the pleckstrin homology (PH) domain and therefore lacking the calmodulin-binding domain (CaM-BD).

Although Grb10 has been found to bind to the GHR (197), as well as to different tyrosine-kinase receptors, such as the EGFR (179), EphB1 (268), Tek/Tie2 (175), PDGFR (79), VEGF (89) and other cytosolic kinases including Raf (203), MEK1 (203) or Bcr-Abl (11), its most important described role is to bind with high affinity to the insulin receptor (103, 165) and the IGF-1R (64, 107, 154, 195, 210) causing the inhibition of the receptors upon ligand stimulation (227). Besides, Grb10 has been found to interact with the ubiquitin ligase Nedd4 (194) triggering the internalization and degradation of the IGF-1R (287).

Maternal disomy of human chromosome 7, where *GRB10* maps, is responsible for the Silver-Russel syndrome whose symptoms include pre- and post-natal growth retardation and other dysmorphologies (148). In fact, genetic screening of patients with this syndrome showed three copies of the *GRB10* gene (73).

3.1.3.2 Grb14

GRB14, mapping at the 2q22-q24 locus, was first cloned using the phosphorylated C-terminus of the EGFR by the CORT technique as the other members of the Grb7 protein family (56). *GRB14* is highly expressed in liver, kidney, pancreas, ovary, testis, heart and skeletal muscles (13).

Grb14 has also been found to inhibit the insulin receptor and IGF-1R (138). In fact, after insulin stimulation, Grb14 is able to interact with the insulin receptor and mediates in the coordinated downregulation of the receptor. The interaction is mediated by the BPS domain of Grb14 (50) that directly binds to the receptor inhibiting its catalytic activity, an inhibition that is enhanced by the SH2 domain (62). The *GRB14* gene is overexpressed in breast and prostate tumors (56, 133), and it has been described several mutations occurring with high recurrence in human colorectal cancers (70).

3.1.4 Grb7 in signaling pathways

3.1.4.1 Cell migration

The fact that Grb7 is phylogenetically related to the *Caenorhabditis elegans* Mig10 protein, which is involved in neuronal cell migration during embryonic development, suggests that Grb7 may play an important role in cellular migration. Indeed, it has been described that Grb7 controls cell migration processes participating in two well known migration pathways: the integrin-mediated signal transduction pathway, by its interaction with FAK; and the EphB1-EphB signaling pathway by interacting with the EphB1 receptor **(Fig. 4)**.

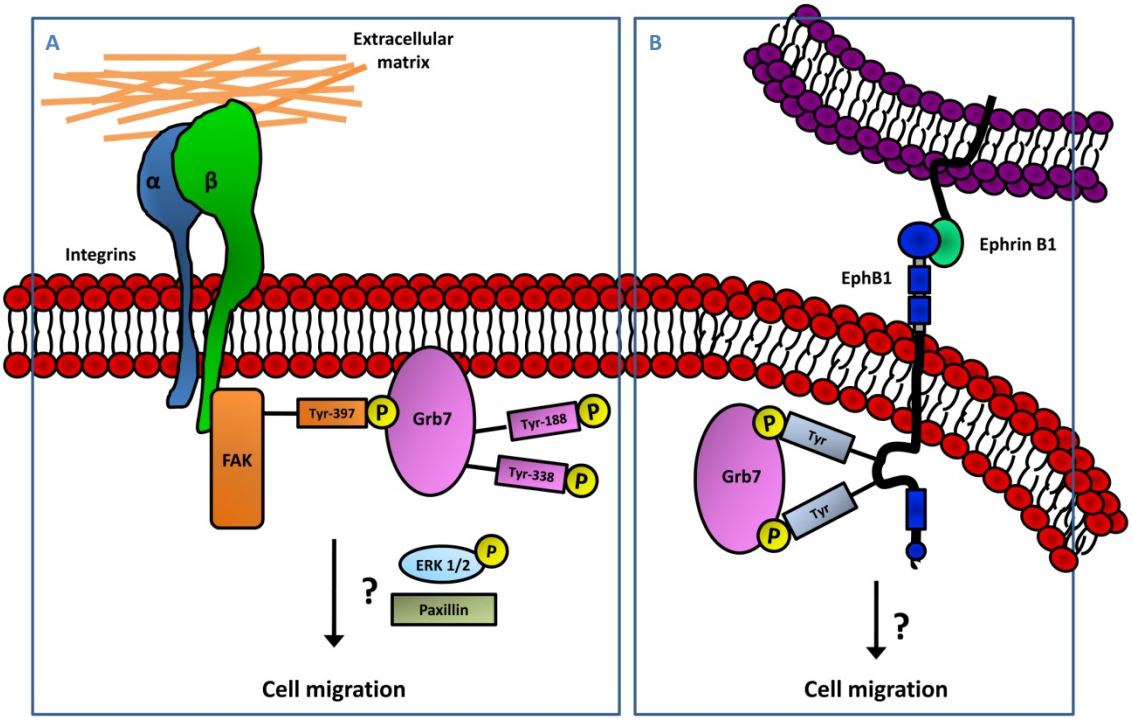

Figure 4: Role of Grb7 promoting cell migration. **(A)** Grb7 has been implicated as a downstream mediator of integrin-FAK signaling pathways in the regulation of cell migration. Integrin activation upon interacting with extracellular matrix components induces auto-phosphorylated FAK at Tyr-397 which is able to recruit Grb7 through its SH2 domain phosphorylating this adaptor protein and triggering a series of unknown mechanisms in which ERK1/2 and paxillin seem to be involved resulting in cell migration. **(B)** Additionally, Grb7 has been found to interact with the EphB1 receptor upon activation by its ligand ephrin B1 located in a neighbor cell promoting cell migration.

3.1.4.1.1 Grb7 and integrin-mediated cell migration

Integrins form a superfamily of cell adhesion receptors that bind extracellular matrix ligand proteins, cell-surface ligands as well as soluble ligands. They are transmembrane heterodimer receptors formed by an α and a β subunit. At least 16 different α subunits and 8 β subunits have been identified in human cells, forming when combined more than 20 heterodimers with distinct ligand-binding specificity (49, 120, 273). According to their ligand specificity, integrins can be divided into four groups: 1) RGD receptors, recognizing the sequence arginine-glycine-aspartic acid, found for instance in fibronectin; 2) Collagen receptors; 3) Laminin receptors; and 4) Leukocyte-specific receptors.

Besides their roles in adhesion to extracellular matrix proteins, integrins can also act as transmembrane mechanical linkers connecting extracellular matrix components to the intracellular cytoskeletal machinery, triggering a large variety of signal transduction events, including proliferation, cytoskeleton reorganization, control of survival/apoptosis, gene expression and cell motility (49).

Clusters of integrins are usually found forming attachment points to the extracellular matrix denoted as focal contacts. Focal contacts not only comprise integrins, but also others molecular complexes that link extracellular matrix components to the cell cytoskeleton and signaling proteins during cell adhesion and migration, including other transmembrane receptors, cytoskeleton proteins such as talin, α-actinin, filamin and vinculin, and intracellular signaling proteins including Src, PI3K and FAK (40, 84).

FAK is a ubiquitously expressed protein tyrosine kinase of 125 KDa that contains an amino-terminal domain denoted as FERM that allows its binding to the integrin β subunit tail promoting FAK activation. FAK has been described to bind β1, β2 and β3 subunits heterodimerizing with any α subunit. Additionally, other membrane-associated proteins such as actin and ezrin, can bind to its FERM domain and increase FAK activation. It has also been described that FAK can be activated upon binding to tyrosine kinase receptors such as the EGFR and the PDGFR through the FERM domain. FAK contains in addition to its central kinase domain, a PR region and a carboxyl-terminal FAT domain that is necessary to localize FAK in the focal contacts (188, 246).

Integrin-mediated stimulation leads to activation and tyrosine auto-phosphorylation of FAK, being Tyr-397 the phosphorylation site. Phospho-Tyr-397 is the binding site for Src family protein kinases, PI3K and Grb7. It is well documented that after Src recruitment to phospho-Tyr-397, Src phosphorylates FAK at Tyr-861 and Tyr-925 creating a SH2-binding site for adaptor proteins such as Grb2, talin and paxillin. The binding of Grb2 to FAK leads to activation of Ras and to the phosphorylation of ERK1/2, among others, resulting in the subsequent activation of MLCK that leads to cytoskeleton reorganization (146, 188, 249). Besides, ERK1/2 phosphorylates paxillin increasing the affinity of the complex formed by FAK and paxillin and promoting the turn-over of other proteins present in the focal contacts (122).

It has been described that upon FAK auto-phosphorylation at Tyr-397, Grb7 can directly interact with the kinase through its SH2 domain resulting in the phosphorylation of Grb7 in at least two tyrosine residues, Tyr-188 and Tyr-338 **(Fig. 4A)**. The binding of the PH domain of Grb7 to phosphoinositides at the plasma membrane, seems to be necessary for proper FAK-mediated Grb7 phosphorylation (100); however, the subsequent downstream signaling events after FAK phosphorylates Grb7 are largely unknown at present, although some reports claim paxillin and ERK1/2 as possible Grb7 downstream targets (45), and that PI3K might be involved since it has been shown that this kinase is also required for FAK-promoted cell migration (231).

3.1.4.1.2 Grb7 and the EphB1-ephrin B signaling pathway

Eph receptors are the largest known subfamily of receptor tyrosine kinases. They can be divided into two subclasses, EphA and EphB, according to sequence similarities and on their binding affinities. EphA receptors typically bind to glycosyl-phosphatidylinositol-linked ephrin A, while EphB receptors bind to transmembrane-bound ephrin B (81). Eph receptors are formed by an extracellular segment composed of a globular ephrin-binding domain, a cystein-rich region and two fibronectin type III domains. Following the single transmembrane domain, the cytoplasmic segment is formed by a juxtamembrane region harboring two conserved tyrosine residues, a tyrosine kinase domain, a SAM region, and a PDZ binding motif (151). When the Eph receptor is activated upon binding to its ligand, ephrin, tyrosine and serine residues present in the juxtamembrane region are phosphorylated, resulting in a conformational change of the cytoplasmic domain that converts the receptor into its active form, subsequently activating or repressing downstream signaling pathways (113, 151).

Eph receptors are able to transmit signals to both the receptor-bearing cell (forward signaling) and to the ephrin-bearing cell (reverse signaling) in a process known as “bi-directional signaling” (59, 72). This process has been implicated in several biological processes including neural synapsis formation and maturation (72), nervous system development (81), cell migration (223), and angiogenic processes such as vascular remodeling during embryogenesis and tumor neovascularization (29, 150).

Grb7 has been reported to associate with the EphB1 receptor through its SH2 domain triggering cell migration **(Fig. 4B)**. This interaction seems to require EphB1 activation and phosphorylation at its Tyr-928; however, the specific mechanisms by which this interaction induces cell migration are still poorly understood (101).

3.1.4.2 Grb7 and translational regulation

Grb7 has been recently identified as an mRNA-binding protein (284). Specifically, Grb7 is able to bind the kappa opioid receptor (KOR) mRNA, interacting through its proline-rich region with the 5’-UTR and mediating the regulation of its translation via netrin-1 signaling. Netrin-1 is a diffusible laminin-related protein, whose major role is to mediate chemo-attraction and chemo-repulsion of axons of neurons during development by its binding to the DCC receptor that interacts with FAK (161, 166, 232). Netrin-1 has been found to regulate the translation of silent KOR mRNAs (283) through a FAK- and Grb7-dependent pathway. It has been demonstrated that hypophosphorylated Grb7 acts as a translational repressor on KOR mRNA

by interacting with its 5'-UTR and blocking the recognition of the capped mRNA by the translational initiator complex (284). After netrin-1 stimulation, FAK binds to the DCC receptor and phosphorylates Grb7 at Tyr-483 and Tyr-495 located in its SH2 domain triggering the release of the KOR mRNA that is now available for recognition and binding to the translational machinery (284).

Additionally, it has been described that Grb7, when bound to KOR mRNA is able to transport the target mRNA from the nucleus to the cytoplasm in an EGF-dependent manner. Upon EGF stimulation, unknown cascade(s) activate the nuclear phosphatase SHP-2, which dephosphorylates Grb7. Grb7 is now able to bind KOR mRNA forming a nuclear export complex with other proteins such as HuR and CRM1, allowing the translocation of the complex to the cytoplasm. As Grb7 is hypophosphorylated and bound to KOR mRNA, the translation process is blocked; however, EGF stimulation also activates cytoplasmic FAK that phosphorylates Grb7 leading to the release of KOR mRNA allowing therefore its translation **(Fig. 5)** (282).

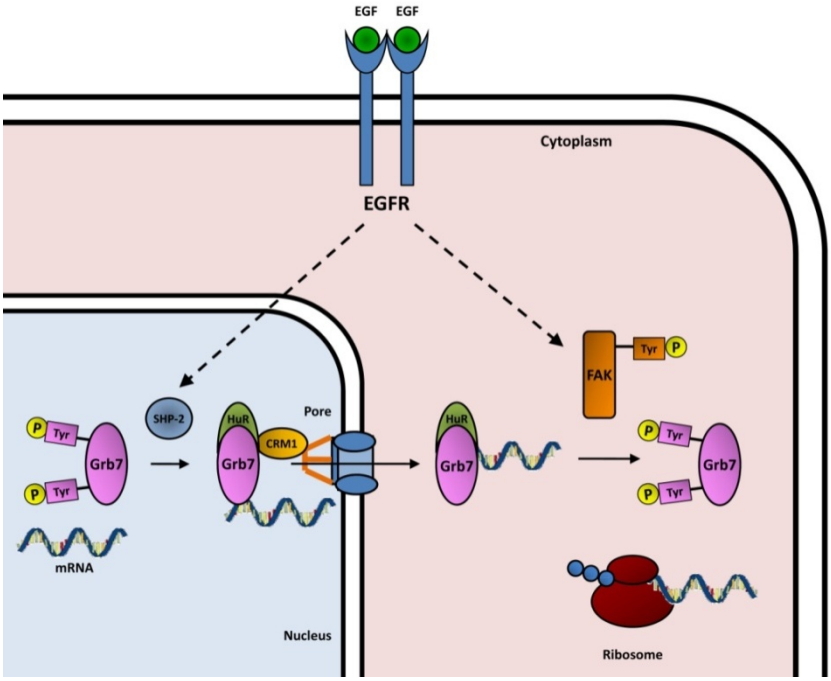

Figure 5: Role of Grb7 regulating translation as a repressor of KOR mRNA. After EGF stimulation, nuclear Grb7 is dephosphorylated by the SHP-2 phosphatase allowing the binding of Grb7 to the target mRNA to form a nuclear export complex with other proteins such as HuR and CRM1. The binding of Grb7 to the target mRNA prevents the binding of the translation initiation complex to the mRNA. When Grb7 is phosphorylated by FAK in the cytosol after EGF stimulation, it releases the target mRNA that is now recognized by the translational machinery.

3.1.4.3 Grb7 and stress granules formation

Under environmental stress conditions the cell stops translation and dense aggregates of proteins and untranslated mRNAs are stored in 100-200 nm size cytoplasm stress granules, not

surrounded by membrane (4). Stress granules assembly is initiated by TIA-1 that binds to a 48S complex promoting polysome disassembly and the location of mRNAs into the stress granules (87). Stress granules are formed in response to numerous signals, including a shift in the cellular redox potential, presence of translation-blocking drugs, the knockdown of specific initiation factors, the overexpression of RNA-binding proteins that repress translation, or the phosphorylation of eIF2α (32, 144). Although the composition of the stress granules might vary, they are mainly composed by poly(A) mRNAs, 40S ribosomal subunits, eIF4E, eIF4G, eIF4A, eIF4B, PABP, eIF3 and eIF2 (32).

Under heat-shock stress, hypophosphorylated Grb7 has been found associated with TIA-1 and HuR promoting the formation of stress granules. During recovery from stress, Grb7 is phosphorylated by FAK leading to disassembly of the stress granules. However, the concrete assembly/disassembly mechanisms are still poorly understood, as well as the identity of the phosphatase(s) that dephosphorylate Grb7 and FAK **(Fig. 6)** (285).

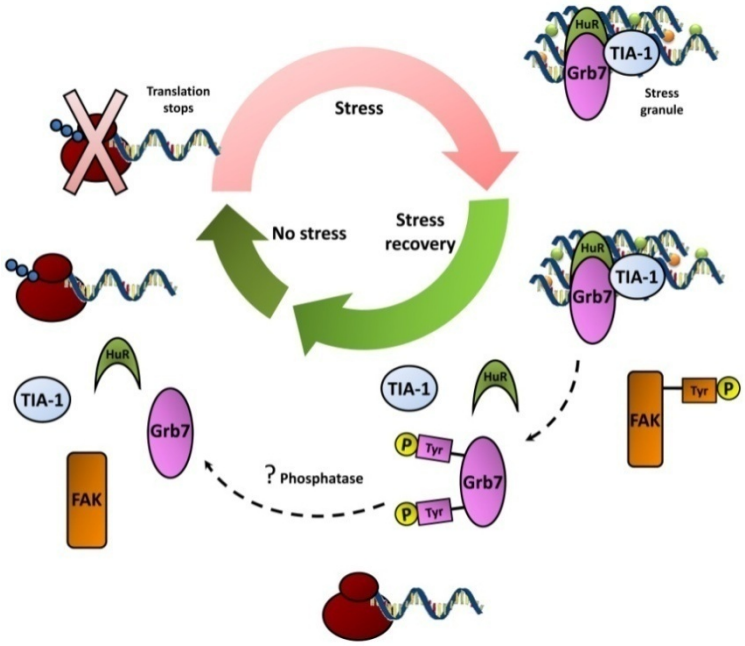

Figure 6: Grb7 regulates stress granules assembly/disassembly. Under stress conditions, Grb7 has been found to co-localize with TIA-1 and HuR promoting stress granules formation. When the stress ceases Grb7 is phosphorylated by FAK triggering the dissociation of the complex formed with HuR and TIA-1 resulting in the disassembly of the stress granules.

3.1.5 Implication of Grb7 in cancer

The adaptor Grb7 has been found overexpressed in highly malignant tumors and it has been related with invasiveness and metastatic processes. In this section we describe the major known roles of Grb7 in cancer development. **Table 2** summarizes the reported implications of Grb7 in different tumors.

Tumor	*GRB7* Amplification	Co-amplification with *ERBB2*	Grb7 over-expression	Co-expression with ErbB2	Metastasis involvement	References
Breast cancer	Yes	Yes	Yes	Yes	Yes	(267, 228)
Upper gastrointestinal adenocarcinoma	Yes	Yes	Yes	Yes	Yes (esophageal tumors)	(274, 293)
Hepatocellular carcinoma	No described	No described	Yes	No described	Yes	(124)
Chronic lymphocytic leukemia	No described	No described	Yes	No described	Increase migration ability reported	(104)
Pancreatic cancer	No described	No described	Yes	No described	Yes	(276)
Testicular germ tumors Seminoma	Yes	Some tumors	Yes	No Co-expressed with KIT	No described	(185)
Testicular germ tumors Non Seminoma	Yes	Some tumors	Yes	Yes Also co-expressed with KRAS2	No described	(185)
Ovarian cancer	No described	No described	Yes	No described	Yes	(297)

Table 2: Implication of Grb7 in tumors. *GRB7* amplification and/or co-amplification with *ERBB2*, as well as their expression pattern are indicated.

3.1.5.1 The ERBB2 amplicon and tumors

Amplicons, amplified genomic regions leading to the deregulated expression of genes, are the major genetic alteration contributing to tumorigenesis (147, 278). The *GRB7* gene is located near the *ERBB2* gene that encodes a transmembrane tyrosine kinase receptor of the ErbB/EGFR family, within the 17q12 amplicon, also called the *ERBB2* amplicon (142). It has been identified a minimal common region of amplification around the *ERBB2* gene comprising a segment of 280 kb that includes the following genes: *NEUROD2, PPP1R1B, STARD3, TCAP, PNMT, PERLD1, ERBB2*, *C17 ORF 37, GRB7* and *ZNFN1A3* (140-142). However, in most tumors, this amplicon spans beyond the minimal common region and therefore genes located outside this region might play as well an important role in tumor progression (141, 261). The co-located genes within the amplicon may influence expression and amplification of *ERBB2*. Additionally, the amplification of one of these genes may result in other tumorigenic effects independent of *ERBB2* (90).

Co-amplification of *GRB7* and *ERBB2* and overexpression of their products have been widely described in many tumors, including breast and gastric cancers, and have been related with poor prognosis (54, 178, 267, 274, 293). Although the SH2 domain of Grb7 has been found to interact with activated ErbB2, the concrete mechanisms by which ErbB2 triggers tumorigenesis in a Grb7-dependent manner are still poorly understood. Recent studies show that Grb7

overexpression leads to ErbB2 activation concomitant with phosphorylation of Akt at Thr-308 and Ser-473 (243).

3.1.5.2 Grb7 and breast cancer

Around 20 % of breast cancers show *ERBB2* gene amplification and overexpression of the ErbB2 receptor. This alteration is associated with a poor clinical outcome. *GRB7* not only has been found amplified and overexpressed with *ERBB2* in breast cancer but also physically associated with the active receptor by its SH2 domain (267). Overexpression of Grb7 and ErbB2, mediates activation of the receptor and activation of the Akt and PLCγ1 downstream pathways (12).

It has been described that in human breast adenocarcinoma SK-BR-3 cells, where both *GRB7* and *ERBB2* genes are overexpressed, EGF induces the phosphorylation of Grb7 resulting in activation of Ras-GTPases and subsequent phosphorylation of ERK1/2, stimulating cell growth (46). However, another study, performed on frozen samples of primary tumors, reported that *GRB7* independent of *ERBB2* overexpression can contribute to solid tumors biology. They described that *GRB7* overexpression is associated with larger tumor size, lymph node involvement, higher tumor grade, negative estrogen and progesterone receptor expression and higher recurrence of the tumors. Therefore, they proposed *GRB7* as an independent prognostic factor in human breast cancer (228).

All these evidences show that *GRB7* is important for the development and/or progression of breast cancer and suggest that *GRB7* is a potential therapy target. In fact, several approaches have been used with this aim. Thus, an inhibitory peptide that binds to the SH2 domain of Grb7 has been developed (225). This peptide called G7-18NATE is able to inhibit the proliferation of SK-BR-3, ZR-75-30, MDA-MB-361 and MDA-MB-231 breast cancer cell lines; however, no significant effect was observed on the breast cancer cell line MCF-7 or 3T3 fibroblasts. Combination treatments with different drugs are nowadays used to increase the therapeutic response of the patients. Co-treatment with G7-18NATE plus doxorubicin, a DNA interacting molecule that blocks replication; or herceptin, a monoclonal antibody against ErbB2 that blocks its tyrosine kinase activity, resulted in an inhibitory synergistic effect on the proliferation of SK-BR-3 cells (220).

3.1.5.3 Grb7 and upper gastrointestinal adenocarcinomas

Upper gastrointestinal adenocarcinomas (UGC)s affect the upper part of the digestive system and include esophageal and gastric (stomach) adenocarcinomas. UGCs are the fourth

most common cancer worldwide and present poor response to therapy (266). Amplification of *ERBB2* and other genes within the *ERBB2* amplicon have also been described in UGCs, with a recurrence rate of ≈ 30 %. This amplification comprises a region of 164 kb and includes eight genes: *PPP1R1B/DARPP-32, STARD3, TACP, PNMT, PERLD1, ERBB2, C17 ORF 37* and *GRB7*. This amplification is more often found in invasive tumors and it is related with poor survival rate (54, 178). *GRB7* and *ERBB2* are found co-amplified and co-expressed in esophageal adenocarcinomas including Barrett's carcinoma (274, 293). Both Grb7 and the truncated splicing variant Grb7V, have been found overexpressed in human esophageal tumors (274). Grb7, and in greater extent Grb7V, expression are highly enhanced in metastatic spread lymph node tissues, suggesting an important role in cell invasion and metastasis. However, Grb7, but not Grb7V that lacks the phospho-tyrosine-binding SH2 domain, is rapidly tyrosyl-phosphorylated in response to EGF stimulation (275). Furthermore, Grb7 has also been found to be phosphorylated in esophageal carcinoma cells after stimulation of the cells with extracellular matrix components such as fibronectin, a process involving the interaction of Grb7 with FAK. The analysis of gastric cancer by integrated array comparative genomic hybridization techniques and expression microarrays, also show gain of the *ERBB2* amplicon, with both *GRB7* and *ERBB2* amplified and overexpressed (178, 200).

3.1.5.4 Role of Grb7 in hepatocellular carcinoma

Human hepatocellular carcinoma (HCC) is the most common type of liver cancer. Most cases of HCC are related with viral hepatitis infection and cirrhosis (296). Grb7 has been found overexpressed in some HCC; in fact, there is a positive correlation between Grb7 overexpression and hepatic venous invasion of tumor cells and metastatic processes. Although the specific mechanisms are still poorly understood, Grb7 expression is also significantly correlated with FAK overexpression. However, it has not been determined if Grb7 phosphorylated by FAK plays a role in HCC cells. Monitoring the overall survival of patients who were resected from HCC shows that the patients with FAK/Grb7 positive expression tumors have a significantly poorer prognosis that those with negative expression tumors (124).

3.1.5.5 Grb7 in chronic lymphocytic leukemia

Chronic lymphocytic leukemia (CLL) is characterized by an uncontrolled growth of B cells, leading to its accumulation in the bone marrow and blood. Grb7 has been found overexpressed in advanced CLL (stage IV) concomitant with an increased migration ability of the neoplasic cells as compared to stage I (104).

3.1.5.6 Role of Grb7 in pancreatic cancer

Pancreatic cancer is one of the most aggressive malignancy in humans, where invasion and metastasis of tumor cells are major risk factors (15). Significantly, *GRB7* has been found overexpressed in 61 % of the pancreatic tumors. These increased levels seem to be associated with regional lymph node and metastatic spread of the tumor cells, an ability that has been previously described in breast and esophageal adenocarcinomas *(See sections 3.1.5.2 and 3.1.5.3)* (276).

3.1.5.7 Grb7 and testicular germ tumors

Testicular germ cell tumors (TGCT)s are the commonest solid tumors in men between the age of 15 and 34. TGCTs can be classified by of the origin of primordial cells in seminomas (SE), formed only by germ cells, and non-seminomas (NSE) composed not only by germ cells but also by embryonal stem cells, that can be differentiated into extra embryonic tissues or somatic elements resulting in tumors composed of a mixture of tissues (27). TGCTs systematically show gain of the chromosomal region 12p11.2-p12.1, a locus that includes the oncogene *KRAS2* encoding for the small G protein K-Ras. Additionally, a gain of the regions 4q12 (where *KIT* is the only amplified gene) and 17q12 (that includes both *ERBB2* and *GRB7*), is found in these tumors (185, 239, 262-263). *GRB7* has been detected overexpressed in TGCTs in primary tumor samples and in derived cell lines (186, 262-263). Also, *GRB7* has been found concurrently overexpressed with *KIT* and *KRAS2* in SE, and only with *KRAS2* and *ERBB2* in NSE, where *KIT* is rarely overexpressed, suggesting a coordinated involvement of these genes in tumor development (186).

3.1.5.8 Grb7 in ovarian cancer

As ovarian cancers are frequently diagnosed in advanced stages, they are considered the most deadly malignancy in women (117). Both Grb7 and Grb7V have been found overexpressed in high-grade ovarian cancers. Furthermore, ovarian cancer cell models, show that overexpression of Grb7 promotes cell migration by a JNK-dependent mechanism, whereas, overexpression of Grb7V leads to an increase in the cell proliferation rate and anchorage-independent growth ability. Both capacities are impaired by ERK1/2 inhibitors, suggesting the involvement of the MAPK pathway (297).

3.2 Calmodulin

The cell receives myriad of external stimuli during its life span that must be translated by intracellular signaling cascades to modulate a proper response to those stimuli. Ca^{2+} is a key signaling ion involved in many cellular processes. Stimulation of many cellular receptors results in the transient increase of the intracellular Ca^{2+} concentration. As a result, Ca^{2+} binds to regulatory proteins amplifying the signal and generating an adequate response. One of the most important Ca^{2+} binding proteins is CaM, able to translate the Ca^{2+} signal into a wide variety of cellular responses (48, 271).

CaM is a 16.5 KDa protein, ubiquitously found in all eukaryotic cells. It has different subcellular locations, including the cytoplasm, within organelles, or associated with the plasma or organelle membranes and also in the nucleus. CaM regulates the activity of multitude of enzymes and other protein targets, affecting many different cellular functions, such as gene transcription, cell migration, cytoskeletal reorganization, osmotic cell volume regulation, endo- and exocitosys, zygote fertilization, cell proliferation, immune response, inflammation, smooth muscle contraction, metabolism, long- and short-term memory and apoptosis, among others (35-36, 145, 271).

3.2.1 Calmodulin structure and Ca^{2+} binding

The crystal structure of CaM was first solved by *Babu et al.* (10) and it has been refined since then by several groups (39, 229). CaM is a dumbbell-shaped protein with two globular domains (at the N- and C- terminal lobes) each connected by a flexible α-helix linker region. Each lobe consists of two EF-hand motifs (helix-loop-helix), with the ability of binding Ca^{2+}, which are joined by a short anti-parallel β-sheet and that are numbered from I to IV (10). The Ca^{2+}-binding affinity is different for the EF-hands in the N- and C-terminal lobes. The Ca^{2+}-binding sites III and IV present higher affinity ($K_d = 10^{-7}$ M) than the sites I and II ($K_d = 10^{-6}$ M) (52, 306).

3.2.2 Calmodulin interaction with target proteins

The reversible binding of up to four Ca^{2+} to CaM induces a conformational change that enables CaM to bind to specific protein targets denoted CaM-binding proteins (CaM-BP)s altering their function and therefore acting as part of Ca^{2+} signal transduction pathways **(Fig. 7A)**. However, Ca^{2+}-free CaM, denoted apocalmodulin (apo-CaM), can also bind to some target proteins resulting in different cellular responses (115, 132, 289). Therefore, CaM can interact

with its target proteins in three different modes: 1) with Ca^{2+} bound to CaM, 2) without Ca^{2+} bound to CaM (apo-CaM interaction) and 3) CaM tightly bound as a constitutive subunit of a given system as it happens, for instance, in the phosphorylase kinase (281), the inducible nitric oxide synthase (43), and the voltage-gated potassium channel KCNQ1 (85). The phosphorylase kinase presents four different subunits denoted as αβγδ, where the γ is the catalytic subunit and α, β and δ are regulatory subunits. The δ subunit has been found to be an intrinsic CaM molecule able to stimulate the activity of the catalytic γ subunit (235).

CaM-BPs share no homology in their CaM binding-sequences, but usually contain a 14-26 amino acid segment with a tendency to form a basic amphiphilic α-helix (209) resulting in the display of large hydrophobic residues in conserved positions (1-10, 1-14 and 1-16) opposed to basic amino acids (115). Other typical CaM-BDs are the "IQ-motif" and the "IQ-like motifs" respectively characterized by the following consensus sequences: [F,I,L,V]Qxxx[R,K]Gxxx[R,K]xx[F,I,L,V,W,Y] and [F,I,L,V]Qxxx[R,K], where x can be any amino acid **(Fig. 7B)** (115, 234, 305).

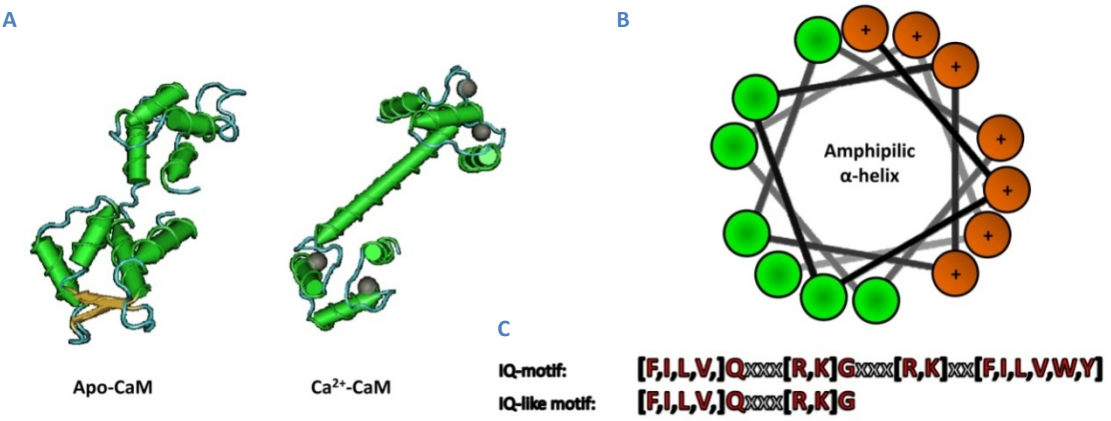

Figure 7: (A) Crystallographic structure of calmodulin (CaM). The non-Ca^{2+} bound form is denoted apocalmodulin (apo-CaM). The binding of Ca^{2+} to CaM triggers sequential conformational changes in the structure of CaM. **(B)** Typical calmodulin-binding domains. The CaM-BD of target proteins can be formed by a basic amphiphilic α-helix with basic (orange) and hydrophobic (green) residues exposed in opposite sides of the helix. **(C)** Alternatively, they can be IQ or IQ-like motifs with the above described consensus sequences. The conserved amino acid residues are represented in red, while x represents any amino acid. Alternative amino acids are shown in parentheses.

Crystallographic and NMR techniques have been very useful to study the conformational changes that CaM binding to its targets can trigger in both CaM and the target proteins. How CaM regulates the activity of its target proteins has been widely studied and three molecular mechanisms has been proposed (115). These are as follows: 1) Rearrangement of the target catalytic site by CaM. An example of this mechanism is given by the activation of the anthrax adenylyl cyclase (69) whose catalytic site suffers a conformational change when bound to CaM that leads to an active site; 2) Release of an autoinhibitory domain that blocks the catalytic site

of an enzyme. In this case when CaM is not bound to the enzyme an autoinhibitory domain is blocking its catalytic domain, and when CaM binds to the enzyme results in a conformational change that triggers the exit of the blocking domain and the subsequent activation of the catalytic domain (129, 295), as for example the plasma-membrane Ca^{2+}-ATPase (168, 205-206); and 3) Formation of dimers, as described in small Ca^{2+}-activated K^+ channels. In this case, CaM is constitutively bound to its α-subunit when Ca^{2+} is absent, resulting in a monomeric closed channel and when Ca^{2+} binds to CaM the complex dimerizes resulting in channel opening and K^+ flux, hence increasing the membrane potential (115).

The structure of CaM is not only affected by the binding of Ca^{2+}, but also by a series of well described post-translational modifications such as acetylation (174), trimethylation at Lys-115 catalyzed by a calmodulin (lysine) N-methyltransferase (199, 299), carboxymethylation (279), phosphorylation (18, 199, 244, 298) and proteolytic cleavage (199), each of which can potentially modulate CaM activity. CaM has been shown to be phosphorylated both *in vitro* and *in vivo* in different cells and tissues by different serine/threonine- and tyrosine-protein kinases including the phosphorylase kinase (222), casein kinase II (201), MLCK (58), the Src family members v-Src (80), c-Src (1) and Fyn (187), the insulin receptor (105) and the EGFR (18-21, 157, 219), among others.

3.3 Grb7 as a calmodulin-binding protein

As previously mentioned, my laboratory described the presence of a CaM-BD in Grb7. This CaM-BD is located in the proximal region of the PH domain **(Fig. 2)**. Grb7 and Grb7V mutants lacking the CaM-BD, respectively called Grb7Δ and Grb7VΔ, were prepared to study the functionality of this site. Our previous studies showed that Grb7Δ lost the ability to bind some phosphoinositides, although a slight binding to phosphatidyl-3-phosphate and phosphatidyl-3,5-bisphosphate remained. Also a competitive effect of CaM on the binding of Grb7 to phosphoinositides was reported (159). Also HRGβ1 stimulation induced Grb7 mobilization from the membrane to the cytosolic fraction in SK-BR-3 cells. This mobilization was inhibited by treatment with the cell-permeable CaM antagonist W-7 and with higher efficiency with CaM inhibitory peptides based on the CaM-BD of MLCK, but not with KN93, an inhibitor of CaMK-II (159). Moreover, conditioned media from Grb7Δ- and Grb7VΔ-expressing HEK293T cells was found to induce anti-angiogenic activity *in vitro*, in contrast to conditioned media from cells expressing their wild type counterparts (159). All these observations suggest that CaM may have an important regulatory role in Grb7 functionality, a role that has been the purpose of the studies for this Thesis.

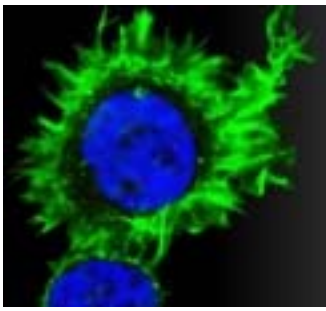

4 OBJECTIVES

The main objectives of this Thesis have been to characterize the functionality of the CaM-BD of Grb7 using its deletion mutant Grb7Δ, and to study *in vitro* and *in vivo* the role of wild type Grb7 and this mutant in different cellular processes including:

1) Cell migration and invasiveness.

2) Cell adhesion and cytoskeletal reorganization.

3) Cell proliferation.

4) Tumor growth and tumor-associated angiogenesis.

Finally, we searched for novel Grb7/Grb7Δ binding partners to better understand some of the functionalities of Grb7 and the alterations induced by the deletion mutant Grb7Δ.

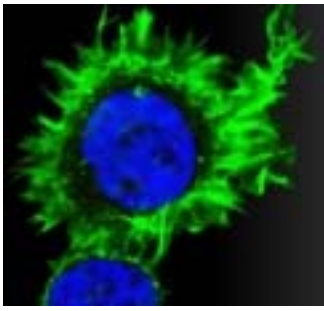

5 MATERIALS & METHODS

5.1 Antibodies

Anti-FLAG®-M2 (clone M2, isotype IgG_1) mouse monoclonal antibody and anti-FLAG®-M2 affinity gel were purchased from Sigma-Aldrich Co. (St. Louis, MO). Anti-caprin-1 rabbit polyclonal antibody was from Proteintech (Chicago, IL). Anti-Nedd4 mouse monoclonal antibody was obtained from BD Transduction Laboratories (Franklin Lakes, NJ). Anti-phospho-tyrosine (clone 4G10, isotype $IgG_{2b\kappa}$) mouse monoclonal antibody, anti-Grb14 mouse monoclonal antibody, anti-HA tag rabbit monoclonal antibody and anti-VEGF rabbit polyclonal antibody were from Upstate-Millipore (Anytown, MA). Anti-Grb7 (N-20) rabbit polyclonal antibody, anti-Grb7 (C-20) rabbit polyclonal antibody, anti-FAK (A-17) rabbit polyclonal antibody, anti-phospho-FAK (Tyr-397) rabbit polyclonal antibody, anti-phospho-ERK1/2 (clone E-4, isotype IgG_{2a}) mouse monoclonal antibody, anti-cyclin E (clone HE12) mouse monoclonal antibody, anti-cyclin A (C-19) rabbit polyclonal antibody, anti-$p19^{Ink4d}$ rabbit polyclonal antibody, anti-lamin B goat (C-20) polyclonal antibody, bovine anti-mouse IgG antibody coupled to FITC and anti-GAPDH mouse monoclonal antibody were purchased from Santa Cruz Biotechnology (Santa Cruz, CA). Anti-Grb10 rabbit polyclonal antibody, Anti-HSPA8 (Hsc70) rabbit monoclonal antibody, anti-phospho-Src family (Tyr-416) rabbit polyclonal antibody, anti-Src (clone 36D10) rabbit monoclonal antibody, anti-ERK1/2 rabbit monoclonal antibody, anti-GAPDH (clone 14C10) rabbit monoclonal antibody, anti-phospho-pRb (Ser-780) rabbit polyclonal antibody, anti-CDK2 (clone 78B2) rabbit monoclonal antibody, anti-phospho-CDK2 (Thr-160) rabbit polyclonal antibody, anti-cyclin D1 (clone DCS6) mouse monoclonal antibody, anti-cyclin B (clone V152) mouse monoclonal antibody, anti-cdc2/CDK1 rabbit polyclonal antibody, anti-phospho-cdc2/CDK1 (Thr-161) rabbit polyclonal antibody, anti-phospho-cdc2/CDK1 (Tyr-15) (clone 10A11) rabbit monoclonal antibody, anti-$p16^{Ink4a}$ mouse monoclonal antibody, anti-$p21^{Cip1/Waf1}$ (clone DCS60) mouse monoclonal antibody, anti-$p27^{Kip1}$ rabbit polyclonal antibody, anti-$p57^{Kip2}$ rabbit polyclonal antibody, anti-PARP (clone 46D11) rabbit monoclonal antibody and anti-ubiquitin (clone P4D1) mouse monoclonal antibody were obtained from Cell Signaling Technology (Danvers, MA). Anti-rabbit IgG Alexa Fluor®-546 antibody was from Invitrogen (Carlsbad, CA). Anti-rabbit IgG goat polyclonal antibody coupled to horseradish peroxidase was from Zymed Laboratories Inc. (San Francisco, CA), Invitrogen or GE Healthcare-Amersham (Buckinghamshire, UK). Anti-GFP (clones 7.1 and 13.1, isotype $IgG_{1\kappa}$) mouse monoclonal antibody, able to recognize also the EYFP protein, was from Roche Applied Science (Penzberg, Germany) and the anti-mouse Fc specific IgG polyclonal (goat) secondary antibody coupled to horseradish peroxidase was from Sigma-Aldrich Co. or GE Healthcare-Amersham.

5.2 Reagents and materials

PVDF membranes were obtained from Pall (Port Washington, NY), DMEM, RPMI-1640, FBS, trypsin/EDTA solution, L-glutamine, geneticin (G418), Hepes, ProLong® Gold Antifade reagent, DAPI, Phall-Alexa Fluor®-488, NuPAGE Bis-Tris Gels (1 mm thickness, 10 wells), Novex® Sharp Unstained Protein Standard, Sypro® Ruby staining solution, protein A-Sepharose 4B and pre-stained molecular mass standards were purchased from Invitrogen. The ECL kit and the CaM-Sepharose 4B columns were obtained from GE Healthcare-Amersham; the X-ray films were from Konika Minolta (Madrid, Spain). Triton X-100, Fast Green FCF, EGTA, crystal violet, toluidine blue, fibronectin (from bovine plasma), paraformaldehyde, D-sucrose, L-glucose, deoxycholic acid, NP-40, trichloroacetic acid (TCA), propidium iodide containing 100 µg/ml RNAse (DNAse-free), iodoacetamide, ammonium bicarbonate (MS grade), acetonitrile, ampicillin, chloroquine, PMSF and glycerol were purchased from Sigma-Aldrich Co. Recombinant UCH-L3 was from Upstate-Millipore (Anytown, MA). Glass-bottom culture dishes (35 mm diameter) coated with collagen or poly-D-lysine for confocal microscopy were obtained from MatTek Corporation (Ashland, MA), and Transwell® 6-well clusters equipped with 24 mm polycarbonate membranes (8 µm pore size) were from Corning Incorporated (Corning, NY). The jetPEI™ transfection kit was obtained from Polyplus Transfection (Illkirch, France). The cloning rings were purchased from Bellco Glass Inc. (Vineland, NJ). The protease inhibitors cocktail (set III), ethylene-glycol, xylol, high grade methanol, high grade ethanol, W-13 and W-7 were from Merk-Calbiochem (Darmstadt, Germany), actrapid insulin (100 UI/ml) was purchased from Novo Nordisk A/S (Bagsvaerd, Denmark); the BCA™ protein assay kit, SuperFrost PLUS microscope slides and heptafluorobutyric acid were purchased from Thermo Scientific (Rockford, IL); lambda phosphatase was obtained from New England Biolabs (Ipswich, UK), and rAPid alkaline phosphatase, Genopure plasmid maxi kit and BSA were from Roche Applied Science. The ExSite mutagenesis kit was from Stratagene (Santa Clara, CA). Tween-20, acrilamide/bisacrilamide solution, precision Plus Protein Standards, Bradford assay kit and ammonium persulfate were purchased from Bio-Rad (Hercules, CA); the fat-free powdered milk was from La Asturiana (Asturias, Spain); ketamine hydrochloride (Imalgen 500) was obtained from Merial Laboratorios (Barcelona, Spain); medetomidine (Domtor) was from Pfizer (New York, NY), sequencing grade trypsin was purchased from Promega (Madison, WI); and GFP-Trap®-A system (also able to bind to EYFP) was from Chromotek (Munich, Germany).

5.3 Vectors preparation

The Grb7 and Grb7V ORFs were amplified by PCR, as previously described (159), using the vectors pCR3/FLAG-Grb7 and pCR3/FLAG-Grb7V as templates and the following oligonucleotides: for Grb7 forward primer 5'-GAT GAC GAT CAT ATG GAG CCG GAT CTG TCT CCA CCT CAT C-3' containing a *NdeI* restriction site (underlined) and reverse primer 5'-GCC AGT CCA CGC TCG AGT CAG AGG GCC ACC CGC GTG CAG C-3', containing a *XhoI* restriction site (underlined). A similar forward primer was used to amplify Grb7V, and the reverse primer was 5'-GCA GGA TGA GAT CTC GAG TCA CTT TCT GCA GGT GGC ACA AAG-3' containing a *XhoI* restriction site. The PCR products were subcloned into the bacterial expression vector pET-14b to obtain pET-Grb7 and pET-Grb7V. Additionally, the CaM-BD (residues 243-256) deletion mutants denoted Grb7Δ and Grb7VΔ were generated by mutagenesis using the ExSite mutagenesis kit using the vectors pCR3/FLAG-Grb7, pCR3/FLAG-Grb7V, pET-Grb7 and pET-Grb7V as template and the following oligonucleotides: forward 5'-TCC TGA ACC CCG CAG CTG CAG AAA GCC CTG-3' and reverse 5' GGC GTC TAT TAC TCC ACC AAG GGC ACC TCT AAG-3'. Alternatively, *EcoRI* and *XhoI* restriction enzymes were used to subclone FLAG-Grb7, FLAG-Grb7Δ, FLAG-Grb7V and FLAG-Grb7VΔ into pcDNA3.1, yielding the pcDNA3/FLAG-Grb7, pcDNA3/FLAG-Grb7Δ, pcDNA3/FLAG-Grb7V and pcDNA3/FLAG-Grb7VΔ vectors. The pEYFP-Grb7 and pEYFP-Grb7Δ vectors were prepared subcloning Grb7 and Grb7Δ from pCR3-FLAG-Grb7 and pCR3-FLAG-Grb7Δ vectors by using the restriction enzymes *XhoI* and *KpnI* and inserting the resultant fragment into pEYFP-C1 after elimination of the FLAG tag as previously described (159). The pCDNA3/Grb10γ-HA vector was kindly provided by Dr. Sophie Gioretti-Peraldi (INSERM, Faculty of Medicine, Nice, France) and was used as template to obtain pcDNA3/Grb10Δ-HA with the ExSite mutagenesis kit and the following oligonucleotides: forward 5' GCA TGT GAA AGA GCT GGG 3' and reverse 5' CTT TGA AGT TCC CTT GGT G 3'. The pRc/CMV/Grb14-FLAG vector was kindly donated by Prof. Roger J. Daly (Garvan Institute of Medical Research, Sydney, Australia) and the pRc/CMV/Grb14Δ-FLAG vector was kindly prepared by Dr. Eduardo Villalobo (Faculty of Biology, Sevilla, Spain). Briefly, the ORF of Grb14 was amplified using pRc/CMV/Grb14-FLAG as a template and the forward primer 5'-ATG ACC ACT TCC CTG CAA GAT G-3'. The resultant PCR product was cloned into pMOSBlue plasmid and used as template for PCR-aided mutagenesis using the forward primer 5'-GGT TTA TAT TTT TCT ACT AAA GGA AC-3' and the reverse primer 5'-TCC CTG TTC TTT CGC ATG TAA GA-3'. The PCR product was purified and re-ligated in the pMOSBlue vector. Finally, the Grb14Δ insert was subcloned into the pRC/CMV/FLAG vector using the *NdeI* and *EcoRI* restriction enzymes. Vectors replication was performed in transformed *Escherichia coli* DH5α grown in Luria broth

with 0.1 mg/ml ampicillin. The isolation of the vectors was performed following the low-copy number procedure of the Genopure plasmid maxi kit.

5.4 Cells culture

Authenticated human embryonic kidney (HEK) 293 cells (ATCC® number CRL-1573 ™), HEK293T cells (ATCC® number CRL-11268™**)**, rat glioma C6 cells (ATCC® number CCL-107 ™) and human breast adenocarcinoma SK-BR-3 cells (ATCC® number HTB-30™) were obtained from the American Type Culture Collection (Manassas, VA). The HEK293, HEK293T and C6 cell lines were grown in DMEM supplemented with 10 % (v/v) FBS, 2 mM L-glutamine, 40 µg/ml gentamicin (plus 1 mg/ml G418 in the case of the stable transfectants) at 37 °C in a humified atmosphere of air containing 5 % CO_2. The SK-BR-3 cells were grown in RPMI-1640 supplemented with 10 % (v/v) FBS, 2 mM L-glutamine, 40 µg/ml gentamicin, 20 mM Hepes-NaOH and 0.25 UI/ml insulin (1 UI of insulin = 0.035 mg human anhydride insulin) in a humified atmosphere of air containing 5 % CO_2.

5.5 Cells transfection

The HEK293 cells were transfected with the following plasmids pcDNA3.1 (empty vector), pcDNA3/FLAG-Grb7, pcDNA3/FLAG-Grb7Δ, pEYFP, pEYFP-Grb7 or pEYFP-Grb7Δ with the calcium phosphate method as previously described (159). Briefly, a cocktail containing 120 mM $CaCl_2$, and HBS medium (25 mM Hepes-NaOH, 150 mM KCl, 50 mM glucose, 250 mM NaCl and 25 mM Na_2HPO_4 pH 7.0) was added to ≈ 80 % confluent cells previously treated with 25 µM chloroquine. When the experiments required follow up for several days, 1 mg/ml G418 was added 24 h post-transfection to ascertain the response of positively transfected cells.

Alternatively, C6 cells were transfected with the following vectors pEYFP, pEYFP-Grb7 or pEYFP-Grb7Δ using the jetPEI™ transfection kit following the manufacturer's instructions. An appropriate amount of DNA for the plate size (1-2 µg of DNA/cm of plate diameter) was suspended in 150 mM NaCl. In parallel, the corresponding volume of jetPEI™ reagent was similarly diluted in 150 mM NaCl. Both solutions were mixed and after 15 min of incubation at room temperature, the resultant mix was added to ≈ 80 % confluent cells. If the experiments required follow up for several days, 1 mg/ml G418 was added 24 h post-transfection to ascertain the response of positively transfected cells. Only during short-term experiments, when the loss of expression was not compromised, transient transfectants were used.

5.6 Generation of stable transfectants

Some of the experiments required long periods of time and hence it was necessary to use stable transfectants to avoid the loss of expression of the proteins occurring in the transient transfectants.

5.6.1 HEK293 transfectants

After transfection of HEK293 cells with pcDNA3/FLAG-Grb7 or pcDNA3/FLAG-Grb7Δ as previously described, stable transfectants were selected by adding 1 mg/ml G418 to eliminate non-transfected cells. Control non-transfected cells were maintained in the same conditions until cell death was apparent to ascertain that resistance to G418 did not developed during the selection procedure. After 15-20 days of selection with G418, the resistant clones were isolated using cloning rings. This process involved rinsing the cells with PBS, positioning the glass cloning rings over selected small clusters of cells and detaching the cells with trypsin/EDTA. The cells were reseeded in 16 mm plates in the presence of DMEM plus 10 % (v/v) FBS containing 1 mg/ml G418 as described above. Regularly, Grb7 and Grb7Δ expression was tested by Western blot using the anti-Grb7 (N-20) antibody as described below. **Fig. 8A** shows the different isolated clones. The chosen clones for the experiments, showing similar levels of expression of Grb7 and Grb7Δ, were HEK293/FLAG-Grb7 (clone 1) and HEK293/FLAG-Grb7Δ (clone 4). The G418 antibiotic was removed from the culture media during the experiments performed with the stable transfectants.

5.6.2 C6 transfectants

C6 cells were stably transfected with the pEYFP, pEYFP-Grb7 or pEYFP-Grb7Δ vectors by the jetPEI™ method as previously described. Twenty-four hours post-transfection the selection was started using 1 mg/ml G418. Non-transfected cells were dead after 15-20 days of antibiotic selection. Positive stable transfected fluorescent cells were submitted to successive enrichment rounds of FACS and finally separated by the same procedure using a FACSVantage SE (Becton Dickinson, San Agustín de Guadalix, Spain) cell-sorting equipment with the 488 nm laser. The cells were individually seeded in 96-wells plates in DMEM plus 10 % (v/v) FBS containing 1 mg/ml G418 to isolate the stable transfectants. Isolated clones were tested by Western blot using both anti-Grb7 (N-20) and anti-GFP (also recognizing EYFP) antibodies to ascertain EYFP, EYFP-Grb7 and EYFP-Grb7Δ expression **(Fig. 8B and C)**. Some negative clones were also obtained. The chosen clones for the experiments, showing similar levels of EYFP-Grb7 and EYFP-Grb7Δ were C6/pEYFP-Grb7 (clone 3), and C6/pEYFP-Grb7Δ (clone 4.2). The

G418 antibiotic was removed from the culture media during the experiments performed with the stable transfectants.

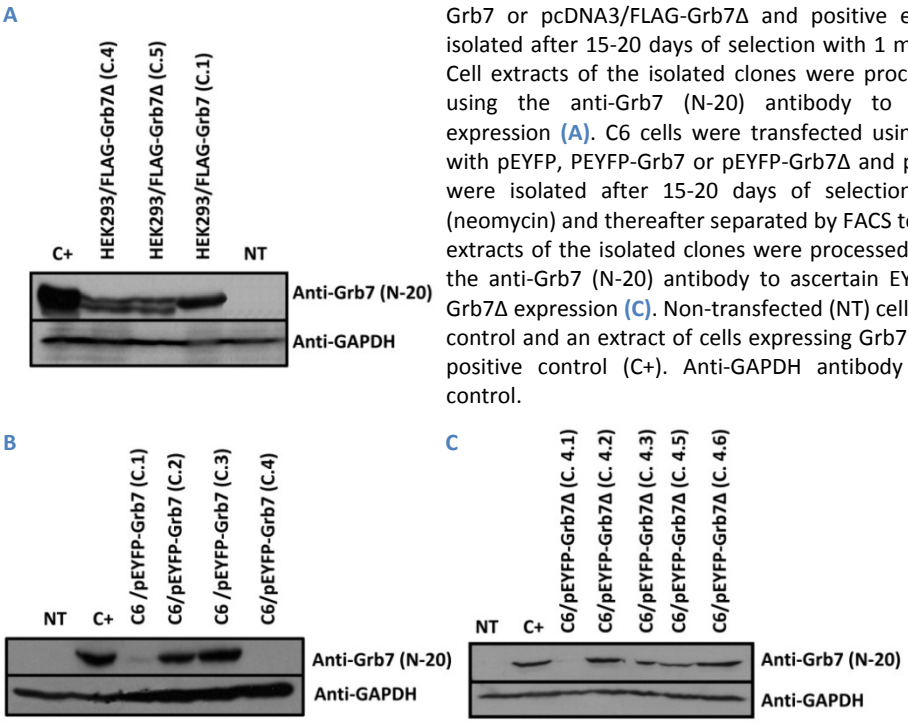

Figure 8: Grb7 and Grb7Δ stable transfectants. HEK293 cells were transfected using the calcium phosphate method with pcDNA3/FLAG-Grb7 or pcDNA3/FLAG-Grb7Δ and positive expressing clones were isolated after 15-20 days of selection with 1 mg/ml G418 (neomycin). Cell extracts of the isolated clones were processed for Western blot using the anti-Grb7 (N-20) antibody to ascertain Grb7/Grb7Δ expression **(A)**. C6 cells were transfected using the JetPEI™ method with pEYFP, PEYFP-Grb7 or pEYFP-Grb7Δ and positive expressing cells were isolated after 15-20 days of selection with 1 mg/ml G418 (neomycin) and thereafter separated by FACS to obtain the clones. Cell extracts of the isolated clones were processed for Western blot using the anti-Grb7 (N-20) antibody to ascertain EYFP-Grb7 **(B)** and EYFP-Grb7Δ expression **(C)**. Non-transfected (NT) cells were used as negative control and an extract of cells expressing Grb7 or Grb7Δ were used as positive control (C+). Anti-GAPDH antibody was used as loading control.

5.7 Preparation of cell extracts

Cells were washed twice with cold PBS and lysed using a RIPA buffer containing 50 mM Tris-HCl (pH 8), 150 mM NaCl, 1 % (w/v) deoxycholic acid, 1 % (v/v) NP-40, phosphatase inhibitors (100 mM NaF and 1 mM Na_3VO_4) and protease inhibitor cocktail (5 µM pepstatin A, 10 µM leupeptin, 0.5 mM 4-(2-aminoethyl)-benzenesulfonyl fluoride, 0.4 µM aprotinin, 7.5 µM N-[N-(L-3-trans-carboxyirane-2-carbonyl)-L-leucyl]-agmatine (E-64) and 25 µM bestatin) supplemented with freshly prepared 1 mM PMSF. Lysates were cleared by centrifugation at 15,000 x g for 30 min at 4 °C.

5.8 Electrophoresis and Western blot

Protein concentration in the cell extracts was determined using the BCA™ method, and thereafter the proper amount of proteins (30-50 µg) was diluted in loading buffer containing 10 % (v/v) glycerol, 50 mM Tris-HCl (pH 6.8), 10 % (v/v) SDS, 0.05 % (w/v) bromophenol blue and 20 % (v/v) β-mercaptoethanol and processed for SDS-PAGE (152). Alternatively, proteins were previously precipitated with 1 % (w/v) TCA and resuspended in loading buffer as described above.

Proteins were electrophoretically separated in 5-20 % (w/v) polyacrylamide gradient slab gels in the presence of 0.1 % (w/v) SDS at pH 8.3 (152) during 16-17 hours at 6 mA. Proteins were electrotransferred from the gels to PVDF membranes for 2 h at 400 mA in a buffer containing 48 mM Tris-base, 36.6 mM L-glycine, 0.04 % (w/v) SDS and 20 % (v/v) methanol (TGSM buffer). Proteins were fixed to the PVDF membrane with 0.2 % (v/v) glutaraldehyde in 10 mM Tris-HCl (pH 8) and 150 mM NaCl (TBS buffer) for 10 min; and transiently stained with a 0.1 % (w/v) Fast Green FCF solution containing 50 % (v/v) methanol and 10 % (v/v) acetic acid to verify the regularity of the transfer procedure. The membranes were blocked with 5 % (w/v) BSA or 5 % (w/v) fat-free powdered milk according to the instructions of the antibodies' manufacturers in TBS containing 0.1 % (v/v) Tween-20 (TBS-T buffer) and incubated overnight at 4 °C using a 1/2000 dilution of the corresponding primary antibody. Membranes were incubated thereafter for 1 h at room temperature using a 1/5000 dilution of the appropriate secondary antibody coupled to horseradish peroxidase. The positive bands were developed using the ECL reagents following instructions from the manufacturer. When required, PVDF membranes were stripped in a buffer containing 62.5 mM Tris-HCl (pH 6.8), 10 mM β-mercaptoethanol and 2 % (w/v) SDS for 30 min at 50 °C, and processed for Western blot with a different antibody.

5.9 Immunoprecipitation and affinity-purification

Cells were washed twice with cold PBS and lysed with an immunoprecipitation lysis buffer containing 50 mM Tris-HCl (pH 7.5), 150 mM NaCl, 0.1 % (v/v) NP-40, 1 % (v/v) Triton X-100, 5 mM EDTA, 20 mM NaF, 1 mM Na_3VO_4, 1 mM PMSF, 70 µg/ml aprotinin and 10 µg/ml leupeptin. Lysates were cleared by centrifugation at 15,000 x g for 30 min at 4 °C and protein concentration was determined by the Bradford's assay (28). Proteins (1 mg) were subjected to immunoprecipitation at 4 °C overnight, by using anti-FLAG®-M2 Affinity Gel for HEK293 cells stably expressing FLAG-Grb7 or FLAG-Grb7Δ, or affinity-purified using the GFP-Trap®-A system, consisting of a peptide coupled to a Sepharose matrix that enabled purification of the protein of interest fused to GFP or EYFP, for C6 cells stably expressing EYFP, EYFP-Grb7 or EYFP-Grb7Δ. The next day, beads were washed four times and the purified complexes were eluted with a loading buffer containing 60 mM Tris-HCl (pH 6.8), 5 % (v/v) glycerol, 1.5 % (w/v) SDS, 100 mM DTT and 0.05 % (w/v) bromophenol blue. Alternatively, Grb7 from SK-BR-3 cells was immunoprecipitated using 40 µg/mg protein of anti-Grb7 (N-20) and protein A-Sepharose 4B.

5.10 Cells immunostaining

HEK293 cells transiently transfected with pCR3/FLAG-Grb7 or pCR3/FLAG-Grb7Δ were grown on glass coverslips placed inside the plates in DMEM plus 10 % (v/v) FBS as described above, washed with PBS and fixed with 4 % (v/v) paraformaldehyde for 5 min. The cells were permeabilized with 0.5 % (v/v) Triton X-100 in a solution containing 10 mM NaCl and 0.3 M sucrose, rinsed with 70 % (v/v) ethanol, and rehydrated with PBS. Samples were blocked with 1 % (w/v) BSA in PBS for 30 min, and probed with an anti-FLAG®-M2 antibody (1/500 dilution) at room temperature for 1 h, and with a FITC-labeled secondary antibody (1/250 dilution) to visualize the expression of the FLAG-tagged Grb7/Grb7Δ. Images were acquired using a Zeiss Axiophot fluorescence microscope equipped with a Plan-Neofluar® 100x/1.30 oil-immersion objective and a Blue/Green BP (470 nm) filter.

5.11 Calmodulin-affinity chromatography

Calcium-dependent CaM-affinity chromatography was performed as previously described (159). Briefly, cells were washed twice with cold PBS and resuspended in a buffer containing 20 mM Hepes-NaOH (pH 7.5), 150 mM NaCl, and the protease inhibitor cocktail mentioned above supplemented with freshly prepared 1 mM PMSF. The cells were sonicated on ice for 5 min with 15 s on/off pulses and centrifuged at 100,000 x g for 30 min at 4 °C. An aliquot of the supernatant (200 µl) was kept and processed for Western blot to have a positive control for input in the column. $CaCl_2$ was added to the rest of the supernatant at a final concentration of 100 µM and the sample was passed through a 2 ml bed volume CaM-Sepharose 4B column previously equilibrated with 25 mM Hepes-NaOH pH 7.5, 135 mM NaCl, 100 µM $CaCl_2$, and the protease inhibitor cocktail supplemented with freshly prepared 1 mM PMSF (Ca^{2+}-buffer). After extensively washing with the same buffer, 0.5 ml fractions were collected before and after elution with a buffer containing 25 mM Hepes-NaOH pH 7.5, 135 mM NaCl, 2 mM EGTA, and the protease inhibitor cocktail supplemented with freshly prepared 1 mM PMSF (EGTA-buffer). The proteins in the fractions were precipitated with 10 % (w/v) TCA and processed for Western blot as previously described.

5.12 Analysis of the interaction of calmodulin with calmodulin-binding domain peptides

These experiments were kindly performed in the laboratory of Prof. J. Haiech (University of Strasbourg, Strasbourg, France) as previously described (53). The three synthetic peptides labeled with TAMRA corresponding to the CaM-BD of hGrb7 (TAMRA-RKLWKRFFCFLRRS), hGrb10γ (TAMRA-KKSWKKLYVCLRRS) and hGrb14 (TAMRA-KKSWKKIYFFLRRS) were synthesized by Schafer-N (Copenhagen, Denmark).

5.13 Ubiquitin carboxyl-terminal hydrolase isozyme L3 treatment

Cells were washed twice with cold PBS and lysed using a buffer containing 20 mM Hepes-NaOH (pH 7.5), 150 mM NaCl, 1 mM EGTA, 1 mM Na_3VO_4, 100 mM NaF and the protease inhibitor cocktail supplemented with freshly prepared 1 mM PMSF, sonicated for 5 min with 15 s on/off pulses and centrifuged at 15,000 x g for 30 min at 4 °C. A reaction mix containing 200 µg of cell extract proteins, 1 mM DTT and 5000 pmol/min/µg UCH-L3 (specific activity 1000 pmol/min/µg determined at 25 °C of with 1 µM ubiquitin-AMC as substrate), previously activated with 1 mM DTT, was incubated for 1 h at room temperature. Non-treated samples as negative control and treated samples were finally processed for Western blot.

5.14 Phosphatases assays

Cells were washed twice with cold PBS and lysed using an appropriate buffer according to the phosphatase treatment as follows.

5.14.1 Alkaline phosphatase

Cells were lysed using a buffer containing 20 mM Tris-HCl (pH 9.8), 150 mM NaCl, 1 mM EGTA, 1% (v/v) Triton X-100, and the protease inhibitor cocktail supplemented with 1 mM PMSF, sonicated for 5 min with 15 s on/off pulses and centrifuged at 15,000 x g for 30 min at 4 °C. Cell extracts with 50 µg of protein were incubated in the same buffer in the absence and in the presence of 119 U/µl of alkaline phosphatase at 37 °C for 30 min (1 U hydrolyzes 1 µmol 4-nitrophenyl phosphate per min at pH 9.8 and 37 °C). The samples were finally processed for Western blot.

5.14.2 Lambda phosphatase

Cells were lysed using a buffer containing 50 mM Hepes-NaOH (pH 7.5), 150 mM NaCl and the protease inhibitor cocktail supplemented with 1 mM PMSF, sonicated for 5 min with 15 s on/off pulses and centrifuged at 15,000 x g for 30 min at 4 °C. Cell extracts with 50 µg of protein were incubated in a buffer containing 50 mM Hepes-NaOH, 100 mM NaCl, 2 mM DTT, 0.01 % (w/v) Brij (pH 7.5) supplemented with 1 mM $MnCl_2$ in the absence and presence of 400 U/µl of lambda phosphatase at 30 °C for 30 min (1 U hydrolyzes 1 nmol 4-nitrophenyl phosphate per min at pH 7.5 and 30 °C). The samples were finally processed for Western blot.

5.15 Artificial wound assays

Artificial wounds were done with a plastic pipette scratching a monolayer of confluent HEK293 cells transiently transfected with pcDNA3.1, pcDNA3/FLAG-Grb7 or pcDNA3/FLAG-Grb7Δ 24 hours post-transfection in the presence of 1 mg/ml G418. Additionally the same procedure was followed on HEK293 cells stably expressing FLAG-Grb7 or FLAG-Grb7Δ, and C6 cells stably expressing EYFP, EYFP-Grb7 or EYFP-Grb7Δ. The wounded monolayers were washed twice with fresh media to remove non-adherent cells before photographs were taken at different times using a Nikon Eclipse TS100 microscope with 4x or 10x objectives to follow the repopulation of the wounds. When testing CaM action, the artificial wound experiments were performed with HEK293 cells expressing FLAG-Grb7 or FLAG-Grb7Δ and non-transfected cells as control adding 15 µM W-7 or 15 µM W-13 to the medium that was changed daily during the course of the experiments.

5.16 Cell motility assays

HEK293 cells transiently transfected with pEYFP-Grb7 or pEYFP-Grb7Δ were seeded 24 hours post-transfection on 35 mm diameter glass-bottom plates coated with collagen or poly-D-lysine. Migrating cells were visualized with a Leica TCS SP5 confocal microscope using 514 nm or 488 nm lasers with a 63x (HCS PL APO lambda blue) oil-immersion objective. Images were acquired every 10 minutes for a 14 hours period to generate a time-lapse video using the Leica Microsystem computer software. Motility rate of each single cell was calculated measuring frame-by-frame the length of the movement of the cell to determine the average migration rate of cells expressing EYFP-Grb7 or EYFP-Grb7Δ.

5.17 Transwell® assays

HEK293 cells (2 x 10^5) transiently transfected with pcDNA3.1, pcDNA3/FLAG-Grb7 or pcDNA3/FLAG-Grb7Δ were seeded 24 hours post-transfection in DMEM supplemented with 10 % (v/v) FBS and 1 mg/ml G418 on the upper chamber of Transwell® plates containing a polycarbonate membrane filter (8 µm diameter pore size). Cells migrating to the lower chamber containing the same medium were photographed using a camera attached to a Nikon Eclipse TS100 microscope with a 4x objective and counted daily up to a maximum of 8 days (Fig. 9).

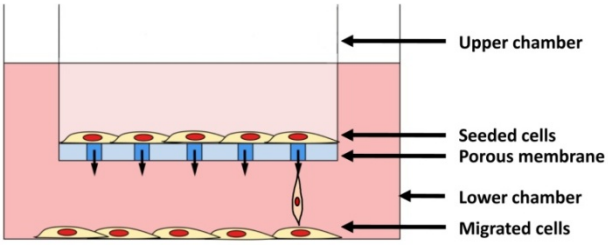

Figure 9: Transwell® assay. A Transwell® plate is formed by two chambers separated by a porous membrane of Matrigel® with 8 µm pore size diameter. The cells are initially seeded in the upper chamber and the cells that migrated across the membrane are found in the lower chamber.

5.18 Cell detachment experiments

HEK293 cells transiently transfected with pcDNA3.1, pcDNA3/FLAG-Grb7 or pcDNA3/FLAG-Grb7Δ were seeded 24 hours post-transfection on 60 mm plates in the presence of DMEM supplemented with 10 % FBS and 1 mg/ml G418. To measure the rate of cell detachment upon trypsin/EDTA treatment, cells were washed twice with PBS to remove trypsin inhibitors contained in the FBS and treated with 1.5 ml of a trypsin/EDTA solution for 1 min at room temperature. After incubation aliquots of the medium were collected every 30 s for a period of 3 min and the cells therein were counted using a Neubauer chamber. The same procedure was followed to measure the detached cells after quelation of extracellular Ca^{2+} with PBS containing 1 mM EGTA. Aliquots of the medium were taken after 2, 6, 12, 22 and 32 min of treatment and the cells were counted as above.

5.19 Cytoskeleton analysis

Serum-deprived non-transfected and stably transfected HEK293 cells expressing FLAG-Grb7 or FLAG-Grb7Δ were seeded on 10 µg/ml fibronectin-coated plates. Not seeded cells were used as negative control. After 15, 30 and 60 min cells were lysed with RIPA buffer and

processed for Western blot as described above. Alternatively, cells were seeded on fibronectin-coated coverslips and fixed after 15, 30 and 60 min with 4 % (w/v) paraformaldehyde in PBS for 20 min. Cells were washed with PBS to remove excess of paraformaldehyde and permeabilized with 0.1 % (v/v) Triton X-100 in PBS for 15 min. Coverslips were transferred to a humidity chamber and blocked with 2 % (w/v) BSA in PBS overnight at 4 °C. Next day, cells were probed with Phall-Alexa Fluor® 488 (1:40 dilution), to detect the actin cytoskeleton, for 1 hour at room temperature. After extensive washing with 0.1 % (v/v) Triton X-100 in PBS to remove unspecific binding, the cells were incubated with a DAPI-containing solution in PBS (1:500 dilution) for 10 min at room temperature to visualize the nuclei. Coverslips were placed faced down on microscope slides using ProLong® Gold Antifade mounting solution. Images were acquired with a Leica TCS SP5 confocal microscope using a 488 nm laser to visualize the actin cytoskeleton labeled with Phall-Alexa Fluor® 488 or the 358 nm (UV) laser to detect the cell nuclei with a 63x (HCS PL APO lambda blue) oil-immersion objective with a 3x zoom focusing the planes at 1 µm intervals to obtain the stacks and processed using the Leica Microsystems computer software.

5.20 Cell proliferation assays

HEK293 cells transiently transfected with pcDNA3.1, pcDNA3/FLAG-Grb7 or pcDNA3/FLAG-Grb7Δ were seeded 24 hours post-transfection on 35 mm plates in DMEM containing 10 % (v/v) FBS in the presence of 1 mg/ml G418. Cell proliferation was determined in triplicate samples every 24 h for a period of 8 days using the Crystal Violet method as previously described (91). Briefly, cells were fixed with 1 % (v/v) glutaraldehyde for 10 min and stained with 0.1 (w/v) crystal violet, a cationic dye that binds to DNA. After several washes with bidestilated water to remove the excess, the dye was extracted with 10 % (v/v) acetic acid and its absorbance was measured in a plate spectrophotometer at 600 nm subtracting background light scattering at 450 nm.

Alternatively, the proliferation of non-transfected and stably transfected HEK293 cells expressing FLAG-Grb7 or FLAG-Grb7Δ was continuously monitored in an xCELLigence RTCA system (Roche Applied Science) during the length of the experiment (174 h). Cells in the presence of DMEM supplemented with 10 % (v/v) FBS were seeded into 8 mm plates provided with sensing gold-microelectrodes at its bottom to detect changes in electrical impedance that was expressed as arbitrary units called the *Cell Index* that is directly proportional to the number of cells in the well. The *Cell Index* at each point was defined as $(R_n-R_b)/15$, where R_n was the cell-electrode impedance of the well when containing cells and R_b was the background

impedance of the well with the media alone. To calculate the doubling time of the cells, we first calculated the growth rate (K') referred to the rate of population increase over time using the following expression:

$$K' = \frac{\ln(N_2/N_1)}{t_2 - t_1}$$

Where N_1 and N_2 correspond to the population of two points of the exponential phase of growth at times t_1 and t_2. Once the K' was obtained, we estimated the doubling time as follows:

$$\text{Divisions per day} = K'/\ln 2$$

$$\text{Doubling time} = 1/Div.day^{-1}$$

5.21 Cell cycle analysis

Serum-deprived non-transfected and stably transfected HEK293 cells expressing FLAG-Grb7 or FLAG-Grb7Δ were stimulated with 10 % (v/v) FBS in DMEM for 2, 4, 6, 8, 24, 26 and 28 h. At those specific time points, cells were detached by trypsin/EDTA treatment, washed with PBS twice, centrifuged at 400 x g for 5 min and resuspended (10^6 cells) in 1 ml of PBS. Cells were fixed with 70 % (v/v) ethanol, kept for at least 18 h at -20 °C and washed thereafter with PBS. Cells were permeabilized with 1.6 % (v/v) NP-40 and stained with 20 µg/ml propidium iodide containing 100 µg/ml RNAse (DNAse-free) for 30 min at room temperature in the dark. FACS analysis was performed in a FACScan instrument (Becton Dickinson) equipped with a 488 nm argon laser using the FL2-A channel after gating intact cells by forward and right-angle light scatter. Integration of the areas in the fluorescence plots corresponding to the G_0/G_1, S and G_2/M phases were determined using the ModFit LT program (Verity Software House, Topsham ME).

5.22 Nuclear fractionation

The nuclear fractions were prepared as previously described (163). Briefly, HEK293 cells transiently transfected with the pcDNA3.1, pcDNA3/FLAG-Grb7, pcDNA3/FLAG-Grb7Δ, pEYFP, pEYFP-Grb7 or pEYFP-Grb7Δ vectors, and stably transfected HEK293 cells expressing FLAG-Grb7 or FLAG-Grb7Δ or C6 cells stably expressing EYFP, EYFP-Grb7 or EYFP-Grb7Δ, were collected in a hypotonic lysis buffer containing 20 mM Hepes-NaOH (pH 7.0), 10 mM KCl, 2 mM $MgCl_2$, 0.5 % (v/v) NP-40, 1 mM Na_3VO_4 and the protease inhibitors cocktail supplemented

with freshly prepared 1 mM PMSF, and homogenized using a Dounce homogenizer. After centrifugation at 1,500 x g for 5 min, the supernatant (non-nuclear fraction) was kept, and the pellet containing the nuclei was washed four times with the same buffer. The nuclei were resuspended in the same buffer supplemented with 0.5 M NaCl to extract the nuclear proteins. The samples were then centrifuged at 15,000 x g for 10 min and the supernatant (nuclear fraction) was collected. The protein concentration in both fractions was determined using the BCA™ protein assay kit.

5.22.1 W-7 treatment and fibronectin seeding

Forty-eight hours post-transfection, serum-starved HEK293 cells were resuspended in DMEM, treated with 15 µM W-7 for 30 min and reseeded on 10 µg/ml fibronectin-coated plastic plates or glass cover slips. Thirty or sixty min thereafter, the cells were respectively collected for nuclear fractionation as previously described, or processed for confocal microscopy as follows: The cells were washed twice with PBS and fixed with 4 % (v/v) paraformaldehyde for 20 min and permeabilized with 0.5 % (v/v) Triton X-100 for 10 min. The cells were washed again with PBS and stained with a DAPI-containing solution in PBS (1:500 dilution) for 10 min. The ProLong® Gold Antifade Reagent was used as mounting solution. Cells were visualized using a Leica TCS SP5 confocal microscope using the 488 nm and the 358 nm (UV) lasers and a 63x (HCS PL APO lambda blue) oil-immersion objective with a 3x zoom focusing the planes at 1 µm intervals to obtain the stacks. Images were acquired and processed using the Leica Microsystems computer software. Long-term treatment was performed by adding 30 µM W-7 daily.

5.23 Magnetic Resonance Imaging

5.23.1 Basic concepts

Magnetic resonance imaging (MRI) is a widely used technique that uses the magnetic properties of hydrogen atoms when they are submitted to an external magnetic field and radio waves to produce highly detailed images of the body. The different content of hydrogen atoms in the tissues, mostly as a result of the different water contents, results in differences in their magnetic properties providing the basis for tissue discrimination and diagnostic by MRI (34, 109).

Hydrogen nuclei consist of a single proton. The proton located in hydrogen atoms are asymmetrically located between them, rotating constantly around an imaginary axis at a

constant velocity described by the intrinsic property denoted as its spin angular momentum. Because a proton has mass, a positive charge, and spins, it produces a small magnetic field. This small magnetic field is referred to as the magnetic momentum of the proton. If we consider an arbitrary volume of tissue containing hydrogen atoms, where each proton has a spin vector of equal magnitude, but orientated randomly in all directions, the sum of their spin vectors is zero, what means no magnetization process is observed in the tissue. If the tissue is submitted to a powerful magnetic field, the average magnetic moment of the protons within becomes aligned with the direction of the field. Because of the spin characteristics of the proton it could assume one of two possible positions. It will align in either a parallel or anti-parallel direction with respect to the magnetic field. Protons aligned in the parallel orientation are said to be in a low energy state, while protons in the antiparallel orientation are said to be in a high-energy state. When a radio frequency transmitter produces an electromagnetic field with the right frequency, known as the resonance frequency, some of the spins in the lower energy state absorb energy from the field and make a transition into the higher energy state. When the electromagnetic field is turned off, the spins of the protons return to their thermodynamic equilibrium and the protons becomes re-aligned with the static magnetic field in a process known as relaxation. During this relaxation, a radio frequency signal is generated, and can be measured with receiver coils. The signal in the coil begins at a given amplitude and fades rapidly away. This initial signal is referred to as the free induction decay. The signal fades as the individual spins contributing to the net magnetization lose their phase coherence, making the vector sum equal to zero again. The free induction decay rate is given by the tissue relaxation parameter known as T2-star (T2*). Some of the spins that had moved into the higher energy state give off their energy to their lattice and return to the lower energy state, causing the net magnetization to recover in the direction of the main magnetic field. This recovering occurs at a rate given by the tissue relaxation parameter known as T1.

Protons in different tissues return to their equilibrium state at different relaxation rates. Different tissue variables, including spin density, T1 and T2 relaxation times and flow and spectral shifts can be used to construct images. This results in a very detailed image of tissues and organs. The distribution of protons in the body can be mathematically recovered from the signal, typically by the use of the inverse Fourier transformation (108-109, 248). We can use T1-weighted scans to depict differences in the spin-lattice T1 parameter and obtain T1-weighted (T1W) images. Similarly, using a T2-weighted scan we can obtain T2-weighted (T2W) images. Thus, proton density, and T1 and T2 times are intrinsic features of biological tissues

and may vary widely from one tissue to the next. Depending of which of these parameters is emphasized in a MRI sequence, the resulting images differ in their tissue-tissue contrast.

Contrast media are pharmaceutical preparations that are administrated in MRI for further enhance the natural contrast and to obtain additional dynamic information. These contrast agents fundamentally alter the intrinsic contrast properties of biological tissues by changing the T1 and/or T2 values (34, 109). A paramagnetic contrast agent, e.g. a gadolinium-containing compound (37), may be injected intravenously resulting in alteration of the signal displayed by the tissues in which it is absorbed. This is very useful to enhance the appearance of new blood vessels, tumors or inflammatory processes (108, 217, 248).

MRI is used to image every part of the body, and it is particularly useful for tissues with high water contents and therefore, many hydrogen nuclei and little density contrast, such as the brain, muscle, connective tissue and most tumors (34, 110).

5.23.2 Diffusion Magnetic Resonance Imaging

Diffusion MRI is widely used to identify histopathologic components of tumors that cannot be clearly distinguished by conventional MRI (31). Water diffusion MRI is physically based on the diffusion of water molecules. In a physiological media, water molecules can move randomly a measurable distance that depends on the temperature, the viscosity of the media and the microstructure of the tissue in which the water molecules are located. This is statistically described by its apparent diffusion coefficient (ADC). Diffusion MRI is based on the principle that water molecules cannot move in the same way through the different tissue structures, thus resulting in different ADCs that can be measured. Therefore, tissues with higher cellularity will present lower ADC values than those with lower cellularity (155, 217).

5.23.3 Perfusion Magnetic Resonance Imaging

This is a special MRI technique for evaluation of microscopic blood flow and it is widely used to study the blood flow in cerebral arterioles, capillaries and venules (14, 214-215, 217). Cerebral perfusion is defined as the volume of blood flowing through a given volume of tissue per unit of time. Many methods using endogenous or exogenous tracers have been developed. In this work, we have employed as exogenous tracer a gadolinium based molecule, Magnevist® (Gd^{3+}-DTPA), to perform bolus-tracking experiments. The basis of a bolus-tracking experiment is that while passing through the microvasculature, a bolus of contrast agent produces changes in the observed MRI signal intensity, where a linear relationship between the concentration of the contrast agent in the blood and the change in transverse relaxation time is assumed.

Tumor vessels are more tortuous than the vascularity of the healthy brain. That increases the distance that blood and the injected contrast agent must travel as they move through the tumor. The intravascular compartmentalization of a contrast agent creates strong microscopic susceptibility gradients that can be detected by MRI and transformed into values for cerebral blood flow (CBF), cerebral blood volume (CBV) and the meant transit time (MTT) of the contrast agent (14, 214-215, 217). When the blood-brain barrier is reasonably intact, the extravasation of the contrast agent from the vascular system to the surrounding tissues during its first-pass through the blood system is zero, however, direct damage of the blood-brain barrier caused by a high-grade tumor results in a disruption of the blood vessels and leakage of the contrast agent to the extravascular space, and this may yield an underestimation of CBV values (8, 216).

5.23.4 Magnetic Resonance Imaging settings

The MRI experiments were performed in the SIERMAC service located in our institute, in collaboration with Prof. Sebastián Cerdán and Dr. Pilar López-Larrubia, using a Bruker Pharmascan system (Bruker Medical GmbH, Ettlingen, Germany) equipped with a 7.0-T horizontal-bore superconducting magnet with a ^{1}H selective birdcage resonator of 38 mm and a Bruker gradient insert with 90 mm of diameter (maximum intensity 360 mT/m). All data were acquired using a Hewlett-Packard console running ParaVision software (Bruker Medical GmbH, Ettlingen, Germany) operating on a Linux platform.

5.23.4.1 Anatomical images

T1W spin-echo images (TR = 400 ms and TE = 10.5 ms) and T2W spin-echo images (TR = 3000 ms and TE = 60 ms) with a rapid acquisition and relaxation enhancement sequence (RARE factor = 8) were acquired in axial, coronal and sagittal orientations for fully coverage of the brain, and employing the following geometric parameters: FOV = 3.8 cm, acquisition matrix = 256 x 256 pixels corresponding to an in-plane resolution of 148 x 148 µm and slice thickness = 1.5 mm.

5.23.4.2 Apparent diffusion coefficient maps

Diffusion weighted imaging studies were acquired employing a diffusion spin-echo sequence with multishot (4 shots) EPI sequence and the following parameters: TR = 2500 ms, TE = 25 ms, Av = 1, diffusion gradient duration = 4 ms, diffusion gradient separation = 16 ms, acquisition matrix = 128 × 128 pixels corresponding to an in-plane resolution of 312 x 312 µm and b factors = 100, 400 and 1000 s/mm^2.

ADC maps were obtained by linear fitting the logarithm of the signal intensity (S) versus the b factor according to the expression:

$$S_b = S_0 \exp(-ADC \times b)$$

Where S_b is the signal intensity at any b value and S_0 is the intensity with the diffusion gradient switched off.

5.23.4.3 Perfusion maps

Perfusion weighted imaging studies were performed using single-shot EPI acquisition, and a 0.3 M Gd^{3+}-DTPA solution (Magnevist®). The contrast agent was injected in the dorsal vein of the tail as a bolus (0.3 mmol/kg body weight) 10 seconds after beginning of acquisition. The parameters employed were as follows: TR = 250 ms, TE = 7.1 ms, Av = 1, flip angle = 30°, acquisition matrix = 64 x 128 pixels corresponding to an in-plane resolution of 297 x 594 µm, number of repetitions = 150, total acquisition time = 38 s, FOV = 3.8 x 3.8 cm, slice thickness 1.5 mm. In order to compute the perfusion maps, pixel time-evolution signals were obtained, and the values corresponding to the first seconds of each temporal series were considered to compute the basal level. Perfusion studies were processed with homemade software using Matlab and the following expression was computed:

$$\Delta R_2^*(t) = -k \cdot \ln\left(\frac{S(t)}{S_\circ(t)}\right)$$

Where *S(t)* are the dynamics of each pixel, $S_0(t)$ denotes the pre-contrast grey levels (basal levels), *k* is a proportionality constant and ΔR_2^* is proportional to the concentration of the contrast agent in the tissue. The parametric images (CBV, MTT, and CBF) were computed based on the following expressions:

$$CBV = \int \Delta R_2^*(t)dt$$

$$MTT = \frac{\int t \cdot \Delta R_2^*(t)dt}{\int \Delta R_2^*(t)dt}$$

$$CBF = \frac{CBV}{MTT}$$

Either in diffusion or perfusion measurements, data were analyzed in the tumoral and non-tumoral control brain areas of interest by measuring the corresponding parameters in the

maps after capturing images with the Image J program (230) that calculates the mean value for all pixels contained in the selected region.

5.24 Tumor cells implantation and animal control

A DMEM solution (10 µl) containing 10^6 C6 cells stably transfected with pEYFP, C6/pEYFP-Grb7 or C6/pEYFPΔ was stereotaxically implanted in the right caudate nucleus of Wistar rats (200-250 g) previously anesthetized using a mixture of ketamine hydrochloride (75 mg/kg) and medetomidine (0.5 mg/kg). To prepare the rats for MRI studies, anesthesia was initiated by inhalation of oxygen (1 l/min) containing 4 % (v/v) isofluorane and maintained during the experiment with 1.5-2 % (v/v) isofluorane in O_2. Animal temperature was maintained at ≈ 37 °C with a heated pad. The physiological constants of the rats ware monitored using a Biotrig physiological monitor (Bruker Medical GmbH, Ettlingen, Germany) that controlled the respiratory rate and the body temperature.

5.25 Animal perfusion

Rats were deeply anesthetized with 0.1 mg/Kg medetomidine and 50 mg/Kg ketamine hydrochloride and transcardially perfused through the left ventricle with 4 % (w/v) paraformaldehyde in 100 mM phosphate buffer (pH 7.4). The brain was removed and post-fixed in the same solution containing 30 % (w/v) sucrose and frozen until used. Coronal sections (25 µm thick) were obtained using a Leica 1900 Cryocut. Sections were stored at -70 °C in a cryoprotectant solution containing 30 % (v/v) ethyleneglycol and 30 % (v/v) glycerol in 100 mM phosphate buffer (pH 7.4) until used.

5.26 Nissl staining

Frozen brain sections were dehydrated overnight with 70 % (v/v) ethanol, washed with bidestilated water and stained with 0.1 % (w/v) toluidine blue (Nissl method) for 15 min. After staining and several washes with bidestilated water, the sections were progressively dehydrated with 70 % (v/v), 96 % (v/v) and 100 % ethanol. Sections were clarified with xylol and progressively rehydrated with 100 %, 96 % (v/v) ethanol and water. The dehydration process was repeated and a second staining step with 0.1 % (w/v) toluidine blue was performed as above. The sections were again clarified with xylol and placed on SuperFrost PLUS microscope slides with DePeX mounting media.

5.27 Immunohistochemistry and measurement of blood vessels

Frozen brain sections were washed with 100 mM phosphate buffer (pH 7.4) and permeabilized with 10 % (v/v) methanol in the same buffer. After several washes with the phosphate buffer, the sections were blocked with 5 % (w/v) BSA and 0.2 % (w/v) Triton X-100 for 1 h and incubated with anti-VEGF antibody (1:100 dilution) in blocking solution overnight. The sections were thereafter incubated with anti-rabbit IgG Alexa Fluor®-546 (1:800 dilution). The sections were mounted on SuperFrost PLUS microscope slides with ProLong® Gold Antifade reagent. The samples were observed using a Leica TCS SP5 confocal microscope using the 546 nm and the 358 nm lasers with 10x/0.4 and 40x/1.25-0.75 oil-immersion objectives focusing the planes at 5 µm intervals to obtain the stacks. The blood vessels were identified by the VEGF staining and their lumen diameter was measured using the Image J program (230).

5.28 Animal care

Adequate measures were taken during housing at the Animal facility of our Institute (license ES280790000188) staffed by specialized personal to care for the animals used in this study and to minimize pain and discomfort during the experiments. The procedures were approved by the Ethical Committee of our Institution (CSIC) and met the national (R.D. 1201/2005) and European Community (86/609/CEE; 1986/ETS123) guidelines on animal experimentation.

5.29 Mass Spectrometry-based proteomics

5.29.1 Basic concepts

In a proteomic study, typically the proteins to be analyzed by mass spectrometry (MS) are isolated from cell lysates by biochemical fractionation or as we did in this Thesis, by immunoprecipitation or affinity selection. A frequently used strategy is to tag the protein of interest with a sequence readily recognizable by an antibody specific for the tag that is then used to purify the tagged protein along with its interacting partners. Isolated proteins are separated by SDS-PAGE to select the bands to be analyzed. Proteins therein are degraded into peptides by using specific endoproteases such as trypsin, and the peptides are separated by one or more steps of HPLC and eluted into an electrospray ionization (ESI) source that ionizes the peptides for MS analysis (75). Following sample ionization, peptide ions are separated based on mass/charge (*m/z*) characteristics in a mass analyzer. Selected precursor ions

typically undergo fragmentation by collision with introduced gas molecules. The most common method of precursor ion fragmentation is termed collision-induced dissociation (CID) (25). Fragmented peptides are submitted to a second round of MS. Mass-to-charge ratios acquired from MS and MS/MS analyses are subsequently searched against protein/genome sequence databases to establish the identity of the analytes (184) **(Fig. 10)**.

Combination of immunoprecipitation/affinity purification and MS has been used to directly isolate from cell lysates multiprotein complexes (2, 66, 88). Co-immunoprecipitation is a commonly used technique to identify relevant protein-protein interactions by using target protein-specific antibodies to capture proteins that are bound to a specific target protein. These protein complexes can be analyzed to identify new binding partners (221).

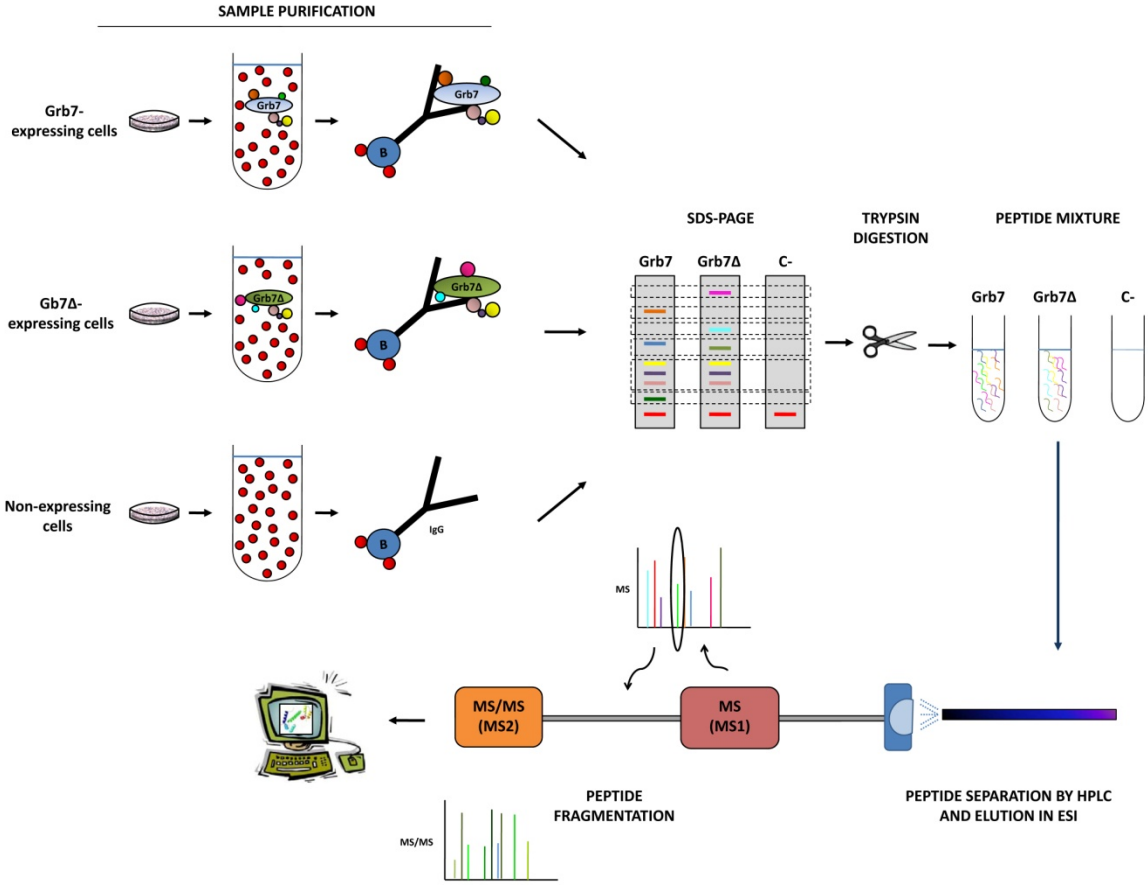

Figure 10: Mass Spectrometry-based proteomics. The proteins of interest (Grb7 and Grb7Δ), bound to other proteins forming protein complexes are purified typically using an antibody coupled to an Agarose matrix bead (B) that is able to recognize the protein of interest. The lysate from non-expressing cells is also incubated with the antibody to detect unspecific binding to the matrix or to the antibody. Immunocomplexes are resolved by SDS-PAGE and different bands are visualized. Those specific bands present only in the lane with the protein of interest and not in the control lane are processed and trypsin digested yielding peptides. The obtained peptides are separated by HPLC chromatography and ionized using electrospray ionization (ESI). Once in the mass analyzer, peptides are separated based on mass/charge (m/z) (see spectra). The peptides undergo fragmentation and a subsequent MS/MS analysis is performed. Finally, the mass/charge spectra are searched against known sequence databases to identify the potential candidates to conform the initial protein complex.

5.29.2 Sypro Ruby staining

After electrophoresis the NuPAGE gels were fixed with a solution containing 50 % (v/v) methanol and 7 % (v/v) acetic acid and stained with Sypro Ruby staining solution for 30 s in a microwave oven, followed by another 30 s of shaking and 30 s more in the microwave oven. After 5 min of staining at room temperature on a shaker, another round of 30 s microwave staining was performed. Finally, the gel was further stained for 23 min at room temperature with constant shaking. After staining, gels were washed with a solution containing 10 % (v/v) methanol and 7 % (v/v) acetic acid for 30 min, rinsed with ultra pure water and visualized using a FLA-5000 laser scanner (Fuji Photo Film Co., Tokyo, Japan) exciting at 450 nm.

5.29.3 In-gel digestion with trypsin

Selected 1D SDS-PAGE separated bands were excised from the gels and destained using 50 % (v/v) acetonitrile in 200 mM ammonium bicarbonate (pH 8.5) multiple times for 15 min each to remove the Sypro Ruby staining. Proteins in the gel sections were reduced with 10 mM DTT in 50 mM ammonium bicarbonate for 30 min. Gel sections were dried by incubation with 100 % acetonitrile for 5 min and then the dehydrated gel sections were alkilated with 55 mM iodoacetamide in 50 mM ammonium bicarbonate protected from light at room temperature for 30 min. Samples were then washed with 50 % (v/v) acetonitrile in 200 mM ammonium bicarbonate (pH 8.5) for 15 min and dehydrated using a vacuum centrifuge prior to enzymatic tryptic digestion with 12.5 ng/µl sequencing grade trypsin at 37 °C overnight. Peptides were extracted by incubation under agitation in 50 µl of 5 % (v/v) formic acid for 15 min at room temperature followed by additional incubations with 50 µl and 100 µl of 100 % acetonitrile for 15 minutes each. Samples were dried using a vacuum centrifuge and stored at -80 ^{o}C until MS analysis.

5.29.4 Mass Spectrometry settings

The dried peptides were resuspended in 1 % (v/v) formic acid, 2 % (v/v) acetonitrile and 0.05 % (v/v) heptafluorobutyric acid. Peptides were separated by nano-LC using an Ultimate 3000 HPLC and autosampler system (Dionex, Amsterdam, Netherlands). Samples (4 µl) were concentrated and desalted onto a micro C18 precolumn (500 µm x 2 mm, Michrom Bioresources, Auburn, CA) with H_2O:CH_3CN (98:2) in 0.05 % (v/v) TFA at 15 µl/min. After a 4 min wash the pre-column was switched (Valco 10 port valve, Dionex) into line with a fritless nano column (75 µm x ≈ 10 cm) containing C18 media (3 µm, 200 Å Magic, Michrom). Peptides were eluted using a linear gradient of H_2O:CH_3CN (98:2) in 0.1 % (v/v) formic acid to

H_2O:CH_3CN (64:36) in 0.1 % (v/v) formic acid at 250 nl/min over 30 min. High voltage 2000 V was applied to low volume tee (Upchurch Scientific) and the column tip positioned at ≈ 0.5 cm from the heated capillary (T = 280 °C) of an Orbitrap Velos (Thermo Electron, Bremen, Germany) mass spectrometer. Alternatively, 1800 V was applied to low volume tee and the column tip positioned at ≈ 0.5 cm from the heated capillary (T = 250 °C) of a LTQ FT Ultra (Thermo Electron, Bremen, Germany) mass spectrometer. Positive ions were generated by electrospray and the Orbitrap Velos or LTQ FT Ultra mass spectrometers operated in data-dependent acquisition (DDA) mode.

A survey scan m/z 350-1750 was acquired in the Orbitrap Velos mass spectrometer (resolution = 30,000 at m/z 400, with an accumulation target value of 1,000,000 ions) with lockmass enabled. Up to the 15 most abundant ions (> 5,000 counts) with charge states > +2 were sequentially isolated and fragmented within the linear ion trap using collisionally induced dissociation with an activation q = 0.25 and activation time of 30 ms at a target value of 30,000 ions. M/z ratios selected for MS/MS were dynamically excluded for 15 seconds.

Alternatively, a survey scan m/z 350-1750 was acquired in the FT ICR mass spectrometer (resolution = 100,000 at m/z 400, with an accumulation target value of 1,000,000 ions). Up to the 6 most abundant ions (> 3,000 counts) with charge states > +2 were sequentially isolated and fragmented within the linear ion trap using collisionally induced dissociation with an activation q = 0.25 and activation time of 30 ms at a target value of 30,000 ions. M/z ratios selected for MS/MS were dynamically excluded for 30 seconds.

5.29.5 MaxQuant-search parameters

Spectral data from the LTQ Orbitrap Velos and FT-ICR mass spectrometers were searched against the UniProt human or rat forward and reversed database (2010) using MaxQuant (ver. 1.1.1.36). The following search parameters were selected and set as follows: peptide, protein and site false discovery rate (FDR) < 0.01; variable modifications, oxidation (M) and phospho (STY), and the fixed modification carbamidomethylation (C) were selected; SILAC multiplicity < 1, MS first search tolerance < 20 ppm, MS/MS tolerance (CID) < 0.5 Da, minimum ratio count < 1, re-quantify, true, reverse and contaminants included.

5.30 Bioinformatics

Putative CaM-BDs were searched using the online calmodulin target database at *http://calcium.uhnres.utoronto.ca/ctdb/ctdb/* (accessed 05/04/2011). Helical projections were

modified from Wheel.pl program, version 1.4 2009-10-20 21:23:36 at *http://rzlab.ucr.edu/scripts/wheel/* (accessed 02/20/2012). Sequence homology was calculated using BLASTP version 2.2.26+ at *http://blast.ncbi.nlm.nih.gov/* (accessed 04/12/2012) (3). Post-translational modifications were predicted using the following web services: site predictor of protein ubiquitination sites (UbPred) at *http://www.ubpred.org/* (accessed 02/14/2012) (226) and Prenylation Prediction Suite (PrePS) database searcher at *http://mendel.imp.ac.at/PrePS/* (accessed 01/20/2012) (183). Prediction of protein interaction networks was obtained from the search tool for the retrieval of interacting genes (STRING) database resource version 9.0 at *http://string-db.org/* using a standard confidence score of 0.4 (accessed 11/30/2011). Additionally, protein gene ontology annotations were obtained from *http://www.geneontology.org/* (accessed 12/30/2011) (9).

5.31 Statistical analysis

The two-way analysis of variance (ANOVA) and the Student's t tests were performed using the GraphPad Prism software program (GraphPad Software Inc., La Jolla, CA). Data were expressed as the mean ± SEM. Differences were considered significant at $p \leq 0.05$ as indicated in the legends of the figures.

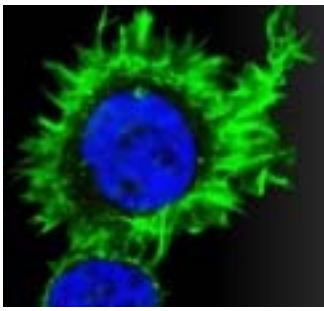

6 RESULTS

6.1 The Grb7 family as calmodulin-binding proteins

CaM-BPs are proteins able to bind CaM, through a CaM-BD, which in some way may regulate their functionality *(see section 3.2.2).* My laboratory previously described the presence of a CaM-BD in hGrb7 comprising the sequence ^{243}RKLWKRFFCFLRRS^{256} and found that this adaptor protein was able to bind CaM both *in vitro* and in living cells (159). To study the functionality of the CaM-BD of Grb7 we prepared a deletion mutant named Grb7Δ lacking the CaM-BD, and diverse techniques were used to ascertain its inability to bind to CaM (159).

Grb10 and Grb14 are the other members of the Grb7 protein family. As previously described they all share a similar protein structure **(Fig. 1)**. Sequence analysis of Grb10 and Grb14 showed that they have significant sequence homology and a well conserved molecular structure with that of Grb7 (177). When we compared the CaM-BD of hGrb7 with the sequences of hGrb10β/hGrb10γ and hGrb14, we observed significant homology with the segments ^{246}KKSWKKLYVCLRRS^{259} in hGrb10γ, ^{304}KKSWKKLYVCLRRS^{317} in hGrb10β, and ^{248}KKSWKKIYFFLRRS^{261} in hGrb14 **(Table 1)**. To study if Grb10 and Grb14 were also CaM-BPs as Grb7, cytosolic fractions of HEK293 cells transiently transfected with pcDNA3/Grb10γ-HA or pcDNA3/FLAG-Grb14 were applied to a CaM-Sepharose 4B column equilibrated with a buffer containing Ca^{2+}. After extensive washing with the Ca^{2+} buffer, the bound proteins were eluted with an EGTA-containing buffer. We also processed a cell extract from HEK293 cells transiently transfected with pcDNA3/FLAG-Grb7 as a positive control. The different fractions were separated by SDS-PAGE, transferred to PVDF and probed with specific antibodies. **Fig. 11** shows that both Grb10 and Grb14 were detected in the EGTA-eluted fractions, as well as Grb7, suggesting their Ca^{2+}-dependent ability to bind to CaM.

Once we identified Grb10 and Grb14 as potential CaM-BPs and described their putative CaM-BDs, we generated deletion mutants lacking these segments, respectively denoted Grb10Δ and Grb14Δ, as described in Materials and Methods. To test if they had lost their ability to bind CaM, we prepared cytosolic fractions of cells transiently transfected with pcDNA3/Grb10Δ-HA or pcDNA3/FLAG-Grb14Δ and subjected them to CaM-affinity chromatography as previously described. We also processed a cell lysate containing Grb7Δ to observe the comparative behavior of the three deletion mutants. Western blot analysis using anti-HA and anti-Grb14 antibodies to respectively detect HA-tagged Grb10Δ and Grb14Δ showed that although they lost in part the ability to bind CaM when compared with their wild type counterparts, they still had significant CaM-binding capacity in contrast to the Grb7 deletion mutant that almost completely lost this ability **(Fig. 11)**.

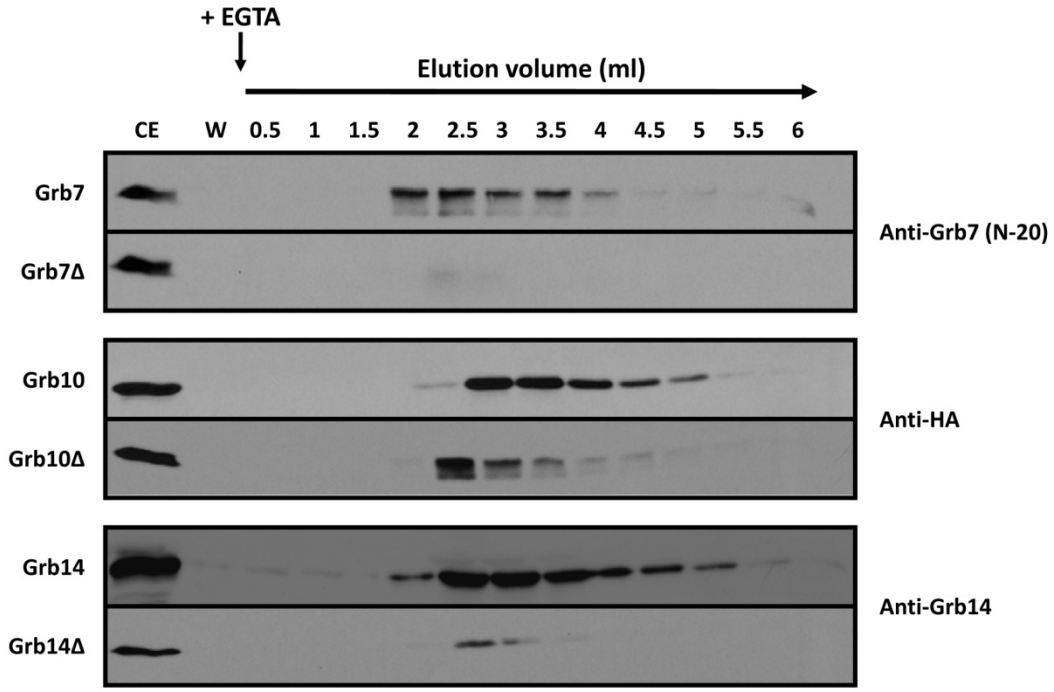

Figure 11: The three Grb7 family members are calmodulin-binding proteins (CaM-BP)s. FLAG-tagged Grb7 and Grb14 and HA-tagged Grb10 and their corresponding calmodulin-binding domain (CaM-BD) deletion mutants Grb7Δ, Grb10Δ and Grb14Δ were respectively transfected in HEK293 cells and their cytosolic fractions were processed by Ca^{2+}-dependent CaM-affinity chromatography. After loading, the column was extensively washed (W) with the Ca^{2+}-buffer to ascertain the absence of proteins unspecifically bound to the matrix. The EGTA-eluted proteins were detected by Western blot using either an anti-Grb7 (N-20) antibody to detect Grb7 and Grb7Δ, an anti-HA antibody to detect the HA-tagged Grb10 and Grb10Δ or an anti-Grb14 antibody to detect Grb14 and Grb14Δ. Total cell extracts (CE) before loading into the column were included to ascertain the positive detection of the proteins.

Interferences with other competing CaM-BPs present in the samples or that the detected proteins were piggy-back bound to other CaM-BPs could not be excluded. Therefore, we decided to estimate the affinity of peptides corresponding to the CaM-BDs of Grb7, Grb10 and Grb14 for CaM. We contacted the laboratory of Prof. Jacques Haiech whose group have developed a brand new technique based on fluorescence polarization to describe the binding affinity of CaM for its target and the minimum number of Ca^{2+} bound to CaM to achieve efficient binding (53), to establish a collaboration and perform these experiments for us.

Peptides corresponding to the above described CaM-BDs of Grb7, Grb10 and Grb14 labeled with the fluorescent probe TAMRA were prepared by Schafer-N **(Figs. 12A and 12B)**. Fluorescent polarization of the CaM/peptide target interaction was measured by using a titration matrix in which both Ca^{2+} and CaM concentrations were changed to determine the minimum number of Ca^{2+} bound to CaM that was required for the interaction to occur with efficiency and the associated kinetics parameters including the association and dissociation constants (K_a and K_d) (53). CaM harbors four EF-hands Ca^{2+}-binding sites in which Ca^{2+} binds sequentially triggering conformational changes that allow the binding of Ca^{2+}/CaM to its target

protein (52, 289) *(see section 3.2)*. We described not only the association/dissociation constants of the peptides for CaM, but also the minimum number of Ca^{2+} required to promote a conformational change in CaM to allow efficient binding to our target peptides. **Fig. 12C** shows the apparent dissociation constants (K'_d) of the fluorescent target peptides corresponding to the CaM-BD of Grb7, Grb10 and Grb14 when they bind to CaM as a function of the Ca^{2+} concentration. The peptide corresponding to the CaM-BD of Grb7 presented a higher affinity for CaM (as given by a lower K'_d) than the Grb14 peptide, while the affinity for CaM of the peptide corresponding to the potential CaM-BD of Grb10 was even lower. CaM is able to bind up to four Ca^{2+} *(see section 3.2.1)*; using isothermal calorimetric titration (53) the association constants of Ca^{2+} to the four binding sites of CaM were calculated to obtain the association constants of the peptides when bound to CaM in the absence of Ca^{2+} and at different Ca^{2+} saturations respectively described as apo-CaM (A), CaM-Ca^{2+} (B), CaM-2Ca^{2+} (C) CaM-3Ca^{2+} (D) and CaM-4Ca^{2+} (E). With this information it was determined the minimum number of Ca^{2+} required to generate a conformational change in CaM to trigger effective binding to the peptides **(Table 3)**. In all cases we found that this change occurred when a single Ca^{2+} was bound to CaM.

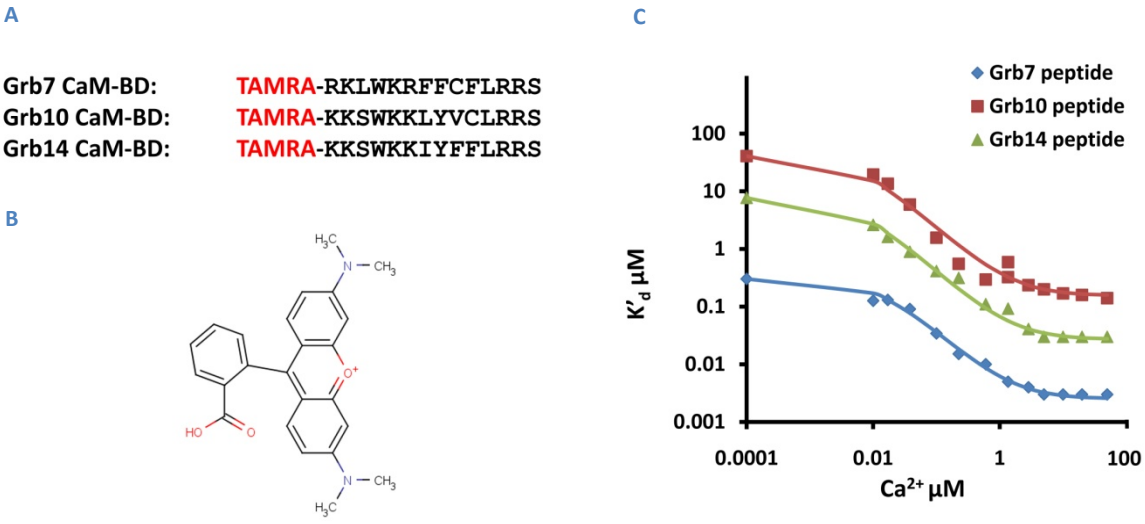

Figure 12: Fluorescence polarization analysis of TAMRA-labeled peptides corresponding to the CaM-BDs of Grb7, Grb10 and Grb14. **(A)** Sequences of the used peptides corresponding to the calmodulin-binding domains (CaM-BD)s of Grb7, Grb10 and Grb14 labeled with the fluorescent probe TAMRA, whose structure is detailed in **(B)**. **(C)** The plot presents the apparent dissociation constants (K'_d) of the peptides corresponding to the CaM-BDs of Grb7, Grb10 and Grb14 to CaM as a function of the Ca^{2+} concentration (Haiech *et al.*, unpublished).

Overall these experiments confirmed that all the Grb7 family members are CaM-BPs. However, their relative affinities for CaM were different between them, resulting in the following sequence: Grb7 >> Grb14 > Grb10.

	A (μM^{-1})	B (μM^{-1})	C (μM^{-1})	D (μM^{-1})	E (μM^{-1})
Grb7 peptide	3.278	293.877	391.877	391.877	391.877
Grb10 peptide	0.024	6.365	6.365	6.365	6.365
Grb14 peptide	0.127	36.473	36.473	36.473	36.473

Table 3: Association constants of calmodulin (CaM) with peptides corresponding to the calmodulin-binding domains (CaM-BD)s of Grb7, Grb10 and Grb14 at different degrees of Ca^{2+} saturation. A, B, C, D and E are the association constants for apo-CaM, CaM-Ca^{2+}, CaM-2Ca^{2+}, CaM-3Ca^{2+} and CaM-4Ca^{2+} respectively. (Haiech *et al.*, unpublished).

6.2 Grb7 expression pattern

To test the expression of Grb7 and its CaM-BD deletion mutant Grb7Δ, HEK293 cells were transiently transfected with pcDNA3/FLAG-Grb7 or pcDNA3/FLAG-Grb7Δ and with pEYFP-Grb7 or pEYFP-Grb7Δ coding for their EYFP chimeric versions. **Fig. 13A** shows that Grb7 was successfully detected by Western blot using the anti-Grb7 (N-20) antibody at ≈ 60 KDa when tagged with FLAG and at ≈ 87 KDa when tagged with EYFP. Grb7Δ was also detected by the anti-Grb7 (N-20) antibody migrating at slightly lower molecular mass as expected. We observed that when transiently transfected Grb7Δ, in its FLAG- or EYFP-tagged versions, tent to aggregate in what appeared to be dimers, as additional bands migrated at approximately the expected double molecular mass **(Fig. 13A)**. Grb7 dimers were also detected when the protein was overloaded or the films were overexposed **(Fig. 13B)**. Solubilization of the cell extract with detergents mostly disaggregated the dimeric forms **(Fig. 13B)**. Additionally, immunocitochemistry using the anti-FLAG®-M2 antibody of HEK293T cells transiently transfected with pcDNA3/FLAG-Grb7 or pcDNA3/FLAG-Grb7Δ **(Fig. 13C)**, and living HEK293 cells transiently transfected with pEYFP-Grb7 or pEYFP-Grb7Δ observed under confocal microscopy showed the presence of Grb7Δ/EYFP-Grb7Δ aggregates **(Fig. 13D)**. In summary, although Grb7 and Grb7Δ were mainly detected in the cytosol, Grb7Δ tent to form some conspicuous intracellular granular/vesicular structures.

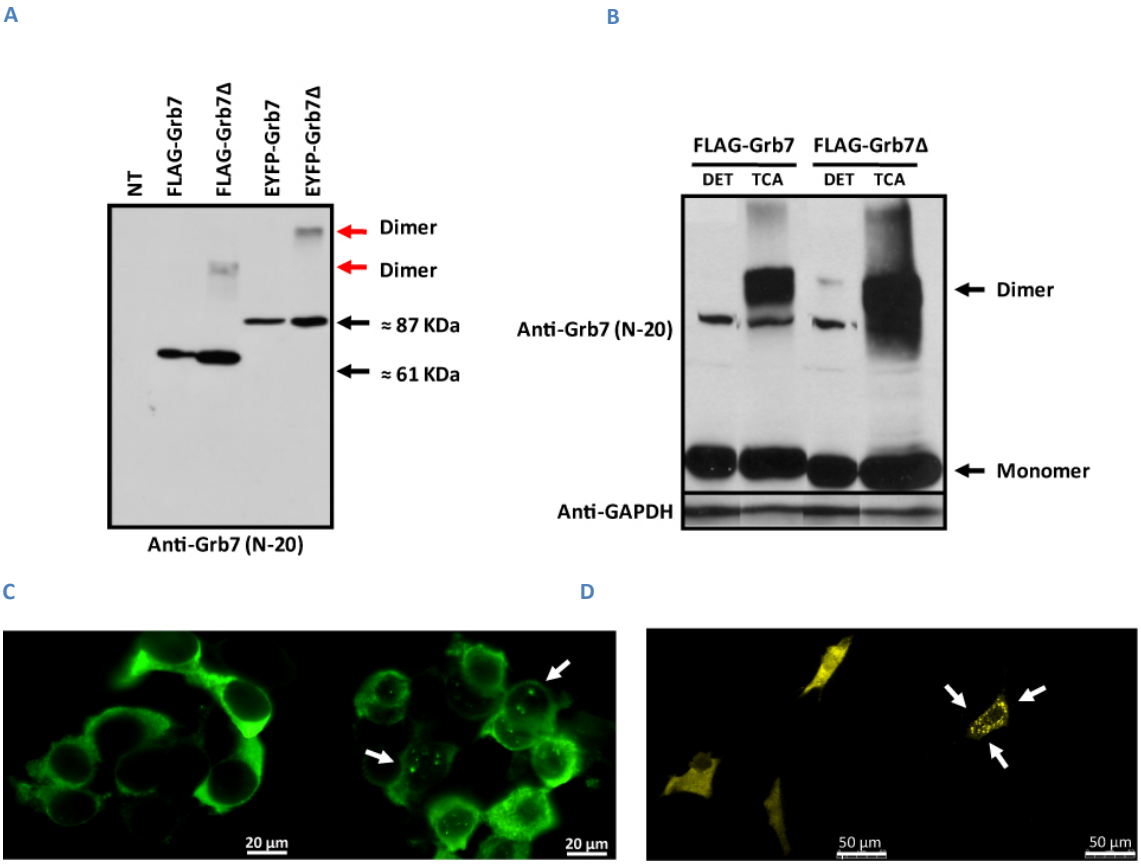

Figure 13: Grb7 and Grb7Δ expression pattern. **(A)** Total cell extracts of non-transfected (NT) and transiently transfected HEK293 cells with pcDNA3/FLAG-Grb7, pcDNA3/FLAG-Grb7Δ, pEYFP-Grb7 or pEYFP-Grb7Δ were processed for Western blot using the anti-Grb7 (N-20) antibody. The deletion mutant Grb7Δ presented a slight higher electrophoretic mobility than its wild type counterpart. **(B)** Both Grb7 and more prominently Grb7Δ presented a tendency to form dimers. Total cell extracts of HEK293 cells transiently transfected with pcDNA3/FLAG-Grb7 or pcDNA3/FLAG-Grb7Δ were either obtained with a detergent (DET)-containing buffer (RIPA buffer) or proteins were precipitated with 10 % (w/v) trichloroacetic acid (TCA) and were processed for Western blot using the anti-Grb7 (N-20) antibody. Anti-GAPDH was used as a loading control. **(C)** Immunocitochemistry using the anti-FLAG®-M2 antibody and the anti-mouse IgG FITC-labeled secondary antibody to detect the FLAG-tagged Grb7/Grb7Δ in HEK293 cells transiently transfected with pcDNA3/FLAG-Grb7 or pcDNA3/FLAG-Grb7Δ. Cells were observed using a Zeiss Axiophot fluorescence microscope equipped with a Plan-Neofluar® 100x/1.30 oil-immersion objective and a Blue/Green BP (470 nm) filter. (D) Living HEK293 cells transiently transfected with pEYFP-Grb7 or pEYFP-Grb7Δ were observed under confocal microscopy using a 63x (HCS PL APO lambda blue) oil-immersion objective and exciting with the 488 nm laser. Arrows point to the appreciable aggregates found mainly in Grb7Δ-expressing cells.

6.3 Post-translational modifications of Grb7/Grb7Δ

We observed that two different isolated clones of HEK293 cells stably expressing Grb7Δ (clones 4 and 5) presented a double band instead of the single band pattern observed in the transient transfectants as detected by Western blot using the anti-Grb7 (N-20) antibody that recognized the N-terminal of the protein. The lower band corresponded with the expected molecular mass of Grb7Δ, while the upper one did not exactly match the molecular mass of wild type Grb7. When the Western blot was performed using the anti-Grb7 (C-20) antibody

recognizing the C-terminal of the protein, only the lower band was detected. This suggested the presence of some conformational impediment in the C-terminal of Grb7Δ that could interfere with the proper recognition of the epitope by the antibody (Fig. 14). Furthermore, we were able to detect the FLAG tag, located at the N-terminal of the protein in both bands (Fig. 14). All this discarded cross-contamination with the Grb7-encoding vector.

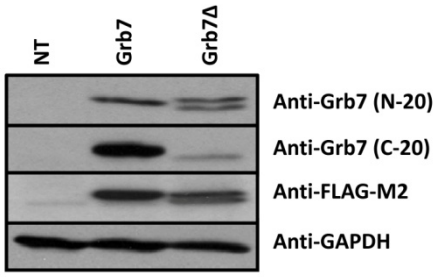

Figure 14: Stably transfected Grb7Δ shows a double band pattern. Total cell extracts of non-transfected (NT) and stably transfected HEK293 cells expressing FLAG-tagged Grb7 or Grb7Δ were processed for Western blot using the anti-Grb7 (N-20) and anti-Grb7 (C-20) antibodies, respectively recognizing the N- and C-terminals of the protein. The anti-FLAG®-M2 antibody recognizing the N-terminal tag of Grb7 and Grb7Δ was also probed. Anti-GAPDH antibody was used as loading control.

To explain the observed double band pattern of Grb7Δ and the differential behavior of the anti-Grb7 N-20 and C-20 antibodies, we hypothesized that Grb7Δ and Grb7 could be differentially affected by some post-translational modifications at the C-terminus. Therefore, we decided to test some post-translational modifications, including: prenylation, ubiquitination and phosphorylation; combining bioinformatic online prediction tests and experimental approaches.

Using the predictor of protein ubiquitination sites (UbPred) on-line data searcher (226), we found that both Grb7 and Grb7Δ were predicted to be ubiquitinated with a high confidence score ($s = 0.92$) at Lys-40 (high confidence $0.84 \leq s \leq 1.00$) and with low confidence score ($s = 0.63$) at Lys-202 (low confidence $0.62 \leq s \leq 0.69$). Although the potential ubiquitination sites were not located near the C-terminal, we tested if ubiquitin bound to Grb7Δ could be responsible for the observed double band. To do so, we treated HEK293, HEK293/Grb7 and HEK293/Grb7Δ cell extracts with the ubiquitin carboxyl-terminal hydrolase UCH-L3, as described in Materials and Methods, to release presumptive ubiquitin molecules bound to Grb7Δ. As Fig. 15A shows, there was no appreciable change in the pattern of the double band after the treatment with the ubiquitin hydrolase. We also checked if Grb7 and/or Grb7Δ were ubiquitinated using an anti-ubiquitin antibody. Fig. 15B shows that despite of the bioinformatic prediction, we could not detect any signal corresponding to Grb7 or Grb7Δ at ≈ 64 KDa. All this discarded the possibility that the double band were due to differential ubiquitination.

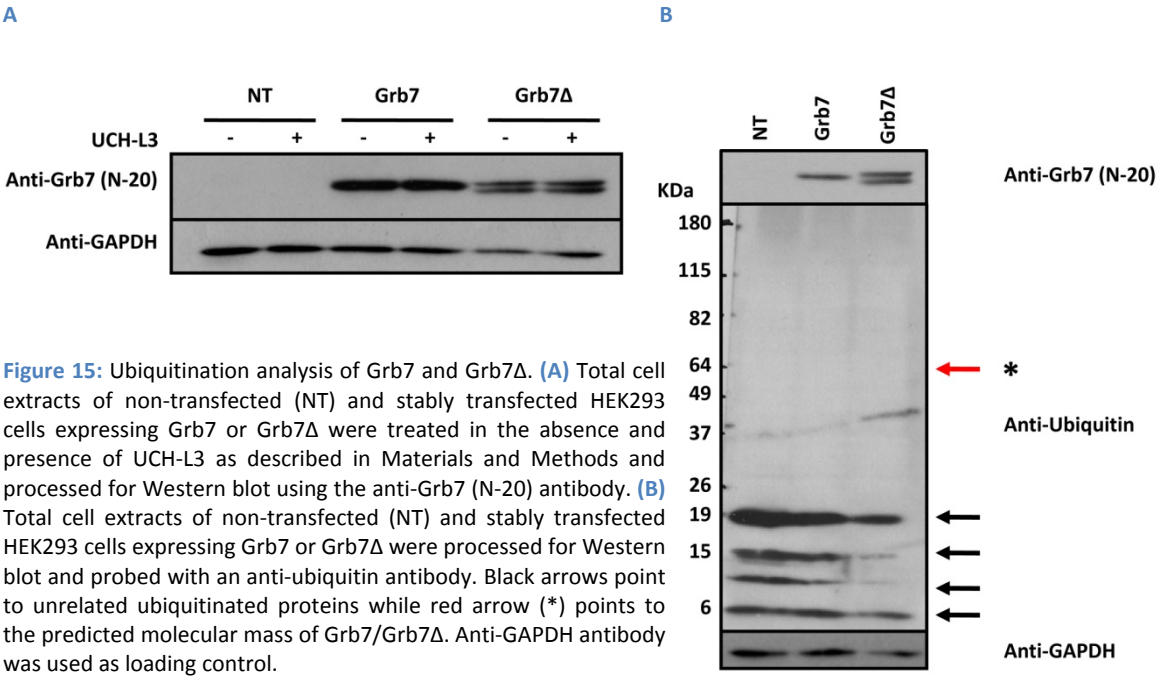

Figure 15: Ubiquitination analysis of Grb7 and Grb7Δ. **(A)** Total cell extracts of non-transfected (NT) and stably transfected HEK293 cells expressing Grb7 or Grb7Δ were treated in the absence and presence of UCH-L3 as described in Materials and Methods and processed for Western blot using the anti-Grb7 (N-20) antibody. **(B)** Total cell extracts of non-transfected (NT) and stably transfected HEK293 cells expressing Grb7 or Grb7Δ were processed for Western blot and probed with an anti-ubiquitin antibody. Black arrows point to unrelated ubiquitinated proteins while red arrow (*) points to the predicted molecular mass of Grb7/Grb7Δ. Anti-GAPDH antibody was used as loading control.

One of the most common post-translational modifications of the C-terminus of proteins is the addition of a lipid anchor to its carboxyl group. This modification allows the protein to be anchored within the membrane (17). We run online prediction tests using the Prenylation Prediction Suite (PrePS) database searcher (183) to analyze if Grb7 and/or Grb7Δ could be prenylated by a farnesyl or geranyl group but all were negative.

We also tested the possibility that the observed double band could be due to phosphorylation. To study this, we treated cell extracts with alkaline or lambda phosphatases as described in Materials and Methods. As **Fig. 16A**, the upper band significantly decreased after the treatment with alkaline phosphatase and in lesser extent with the lambda phosphatase. However, the dephosphorylation was not complete since the double band was still detected after the treatment. **Fig. 16B** shows the densitometric peak of Grb7Δ as given by the upper and lower bands. Despite of the superposition of the signal from both bands, we can appreciate that after the treatment with both phosphatases, but more drastically after alkaline phosphatase treatment, there was a shift in the proportion between the upper and lower bands of Grb7Δ. These evidences suggested that the observed double band pattern of Grb7Δ could be due, at least in part, to phosphorylation.

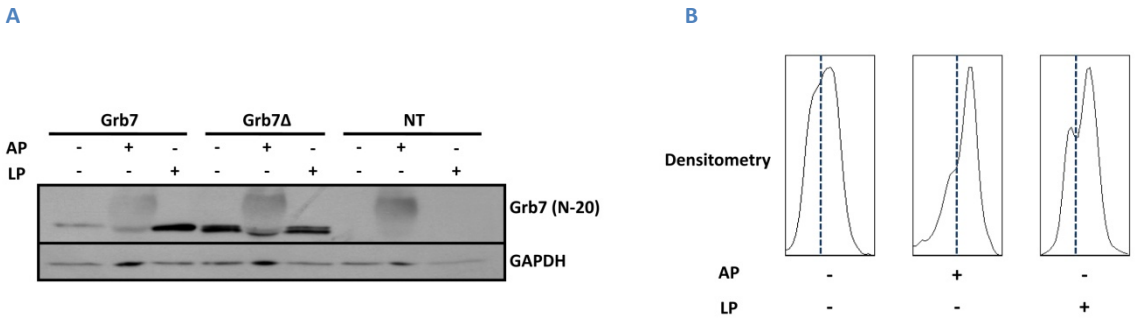

Figure 16: The upper band of Grb7Δ decreases upon phosphatase treatment. (A) Total cell extracts of non-transfected (NT) and stably transfected HEK293 cells expressing Grb7 or Grb7Δ were treated in the absence and presence of alkaline phosphatase (AP) or lambda phosphatase (LP) as described in Materials and Methods and processed for Western blot using the anti-Grb7 (N-20) antibody. Anti-GAPDH antibody was used as loading control. (B) Densitometry pattern of the double band of Grb7Δ before and after treatment with alkaline phosphatase (AP) or lambda phosphatase (LP).

6.4 Grb7Δ impairs cell migration and invasiveness

As Grb7 has been described to promote cell migration we wondered if the CaM-BD had a role controlling this complex process. In order to explore this we followed different approaches.

6.4.1 Artificial wound assays

As a first approach, we transiently transfected HEK293 cells with pcDNA3.1, pcDNA3/FLAG-Grb7 and pcDNA3/FLAG-Grb7Δ as described in Materials and Methods, and performed an artificial wound over a monolayer of confluent cells to follow the closing of the wound along the time. Fig. 17A shows that transiently transfected cells expressing Grb7 fully closed the wound within 24 h, while the empty vector-transfected cells closed the wound at a slightly lower rate. However, those cells transiently transfected with Grb7Δ failed to close the wound even after 53 h. Fig. 17B shows that the average opening of artificial wounds remaining to be closed at different times in a series of experiments performed with transiently transfected cells in similar conditions to those in Fig. 17A.

We performed similar experiments using HEK293 cells stably transfected with Grb7 and Grb7Δ. As shown in Fig. 17C, the expression of Grb7Δ also delayed the closing of the artificial wound as compared to non-transfected or Grb7-expressing cells. Fig. 17D shows the average response in a set of similar experiments to those in Fig 17C carried out with stably transfected cells. Similar results were obtained using rat glioma C6 cells stably transfected with EYFP-Grb7, EYFP-Grb7Δ and EYFP as control (Supplementary Fig. 1S).

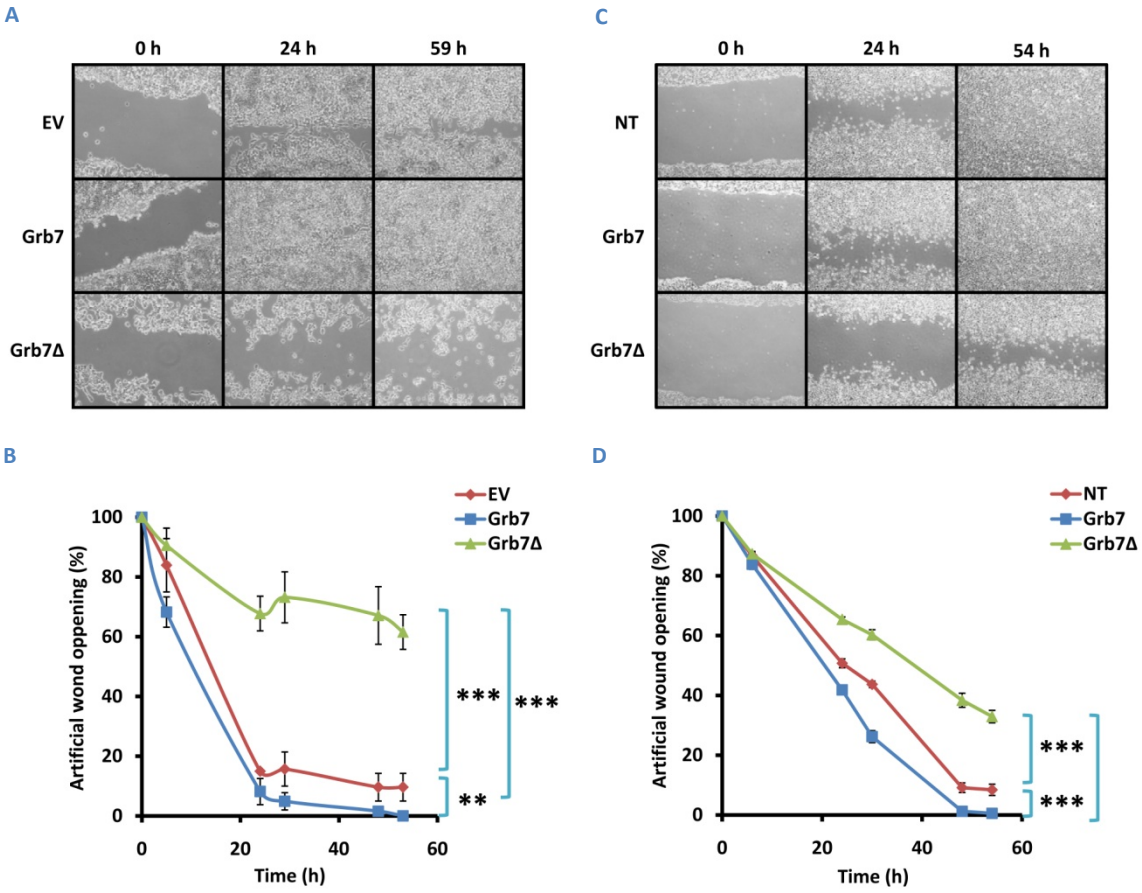

Figure 17: Grb7Δ expressing cells present a low repopulation rate of artificial wounds. Artificial wounds were performed in monolayers of confluent HEK293 cells transiently transfected with the empty vector (EV) pcDNA3.1, pcDNA3/FLAG-Grb7 or pcDNA3/FLAG-Grb7Δ **(A)**. Similar procedure was performed in monolayers of non-transfected (NT) and stably transfected HEK293 cells expressing Grb7 or Grb7Δ **(C)**. Photographs taken at different times, using a Nikon Eclipse TS100 microscope with a 10x objective, to follow the repopulation of the artificial wounds are shown. The plots **(B)** and **(D)** represent the mean ± SEM (n = 4) opening of the wound in a set of experiments respectively similar to those shown in **(A)** and **(C)**. Significant differences were found when comparing the curves using the two-way ANOVA test (*** $p < 0.0001$ and ** $p < 0.001$).

6.4.2 Effect of calmodulin antagonists in artificial wound healing

To study the role of CaM on Grb7 functionality during the cell migration process, we performed artificial wound assays in HEK293 cells stably transfected with Grb7 or Grb7Δ in the absence and presence of cell permeable CaM antagonists. **Figs. 18A and 18B** show that in the presence W-13, and most clearly in the presence of W-7, there was a delay in the closing of the wound by Grb7-expressing cells **(middle panels)**. In contrast, this effect was absent in Grb7Δ-expressing cells **(bottom panels)** and in non-transfected cells **(top panels),** suggesting that CaM was involved in Grb7-mediated cell migration.

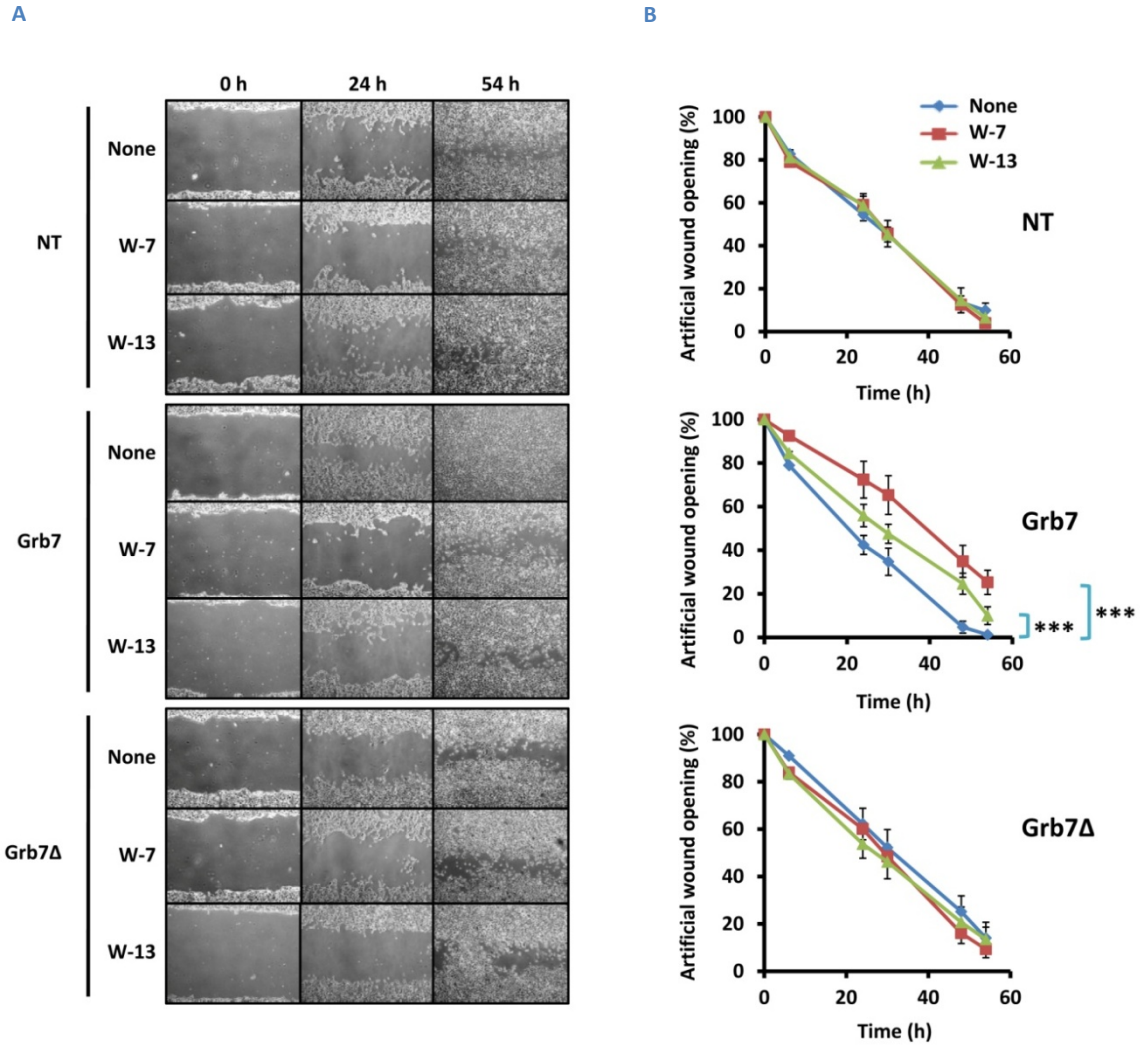

Figure 18: Calmodulin antagonists delay the closing of artificial wounds in cells expressing Grb7, but not in cells expressing Grb7Δ or in non-expressing control cells. Artificial wounds were performed in confluent monolayers of non-transfected (NT) and stably transfected HEK293 cells expressing Grb7 or Grb7Δ treated in the absence (none) or in the presence of the CaM antagonists W-7 (15 µM) and W-13 (15 µM). Photographs were taken at different times to follow the closure of the different wounds using a Nikon Eclipse TS100 microscope with 4x objective. **(A)** Shows a typical set of photographs taken at different times. **(B)** The plots represent the mean ± SEM (n = 4) of the opening of the wound in the three conditions for each cell type. Significant differences were found when comparing the curves using the two-way ANOVA test (*** $p < 0.0001$).

6.4.3 Cell motility analysis in living cells

To ascertain that the differences found in the wound healing assays were due to a different migration rate and not to different proliferation patterns, we directly measured the motility rate in living cells. To do so, we transiently transfected HEK293 cells with pEYFP-Grb7 or pEYFP-Grb7Δ and followed their movement by time-lapse fluorescence confocal microscopy during 14 hours. Typical 3 hours time-lapse images are shown in **Fig. 19A**. We measured the motility rate of each single cell and demonstrated that cells expressing EYFP-Grb7Δ presented on average a lower motility rate than cells expressing its wild type EYFP-Grb7 counterpart **(Fig. 19B)**.

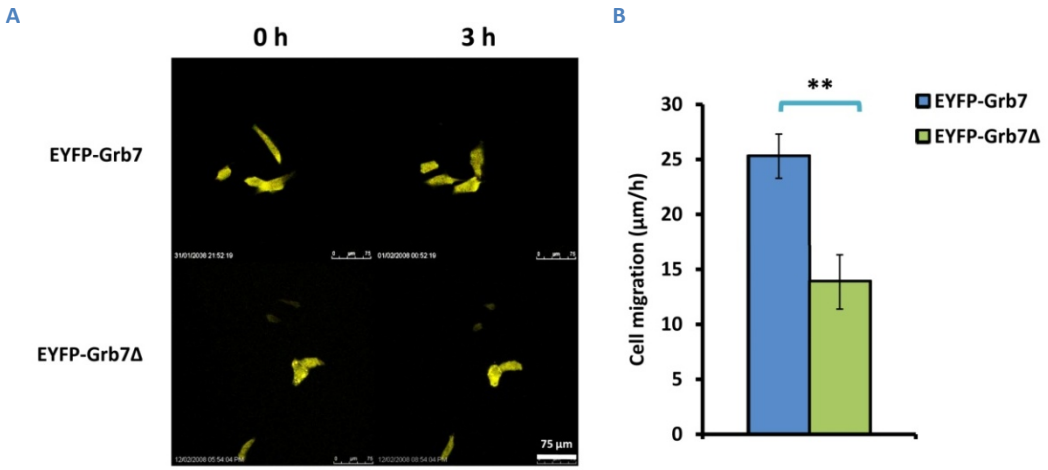

Figure 19: Cells expressing Grb7Δ have low migratory capacity. HEK293 cells transiently transfected with pEYFP-Grb7 or pEYFP-Grb7Δ were seeded on glass-bottom plates pre-coated with either collagen or poly-D-lysine as described in Materials and Methods and their motility was observed for a period of 14 hours by time-lapse fluorescence confocal microscopy using a 63x (HCS PL APO lambda blue) oil-immersion objective and exciting with the 488 nm laser. **(A)** Shows a set of consecutive photographs of cells expressing EYFP-Grb7 or EYFP-Grb7Δ taken three hours apart. **(B)** The plot presents the mean ± SEM rate of migration of individual cells expressing EYFP-Grb7 (n = 22) and EYFP-Grb7Δ (n = 11) from independent experiments measured as described in Materials and Methods. Significant differences were found between EYFP-Grb7 and EYFP-Grb7Δ expressing cells using the Student's t test (** $p < 0.001$).

6.4.4 Transwell® assays

To study whether the deletion of the CaM-BD affected also the ability of the cells to migrate across a porous membrane, we performed Transwell® assays **(Fig. 20)**. This approach is widely used to measure cell invasiveness (233). HEK293 cells were transiently transfected with pcDNA3.1, pcDNA3/FLAG-Grb7 and pcDNA3/FLAG-Grb7Δ and seeded over a porous Matrigel® membrane in the upper chamber of the Transwell®. We counted the number of cells that migrated across the porous membrane for several days colonizing the lower chamber. As **Fig. 20** shows, cells expressing Grb7 colonized the lower chamber significantly more efficiently than cells expressing Grb7Δ or transfected with the empty vector.

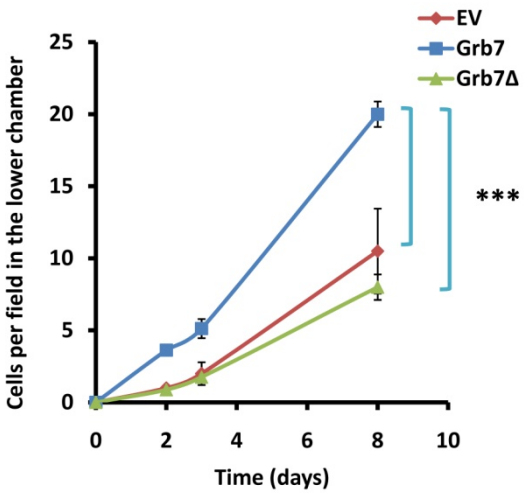

Figure 20: Cells expressing Grb7 present higher invasive ability. HEK293 cells transiently transfected with the empty vector pcDNA3.1 (EV), pcDNA3/FLAG-Grb7 or pcDNA3/FLAG-Grb7Δ were seeded on the porous membrane placed in the upper chamber of a Transwell®. The number of cells colonizing the lower chamber was measured as described in Materials and Methods. The plot presents the mean ± SEM (EV, n = 3; Grb7, n = 7 and Grb7Δ, n = 7) number of cells per field in the lower chamber. Significant differences were found between cells expressing Grb7 and Grb7Δ and between cells expressing Grb7 and non-expressing cells when comparing the curves using the two-way ANOVA test (*** $p < 0.0001$).

6.5 Grb7Δ impairs cell attachment and cytoskeletal reorganization

A successful migratory event not only requires efficient mechanisms to transiently release the cell from the substrate, but also a proper cytoskeletal reorganization to establish new attachment points at the frontal migratory edge (153). To study if the observed differences in cell migration described in the previous sections were correlated with deficiency in the attachment/detachment of the cells, we designed several approaches to study the influence of the CaM-BD of Grb7 in these processes.

6.5.1 Expression of Grb7Δ enhanced cell detachment

We performed a quantitative measurement of the number of detached HEK293 cells transiently transfected with pcDNA3.1, pcDNA3/FLAG-Grb7 and pcDNA3/FLAG-Grb7Δ upon trypsin plus EDTA treatment (Fig. 21A), routinely used to detach cells for reseeding, or just by chelating extracellular Ca^{2+} with EGTA (Fig. 21B). We observed that with both treatments cells expressing Grb7 were more easily detached from its substrate when compared to control cells transfected with the empty vector. However, cells expressing Grb7Δ were even more easily detached than those transfected with its wild type counterpart.

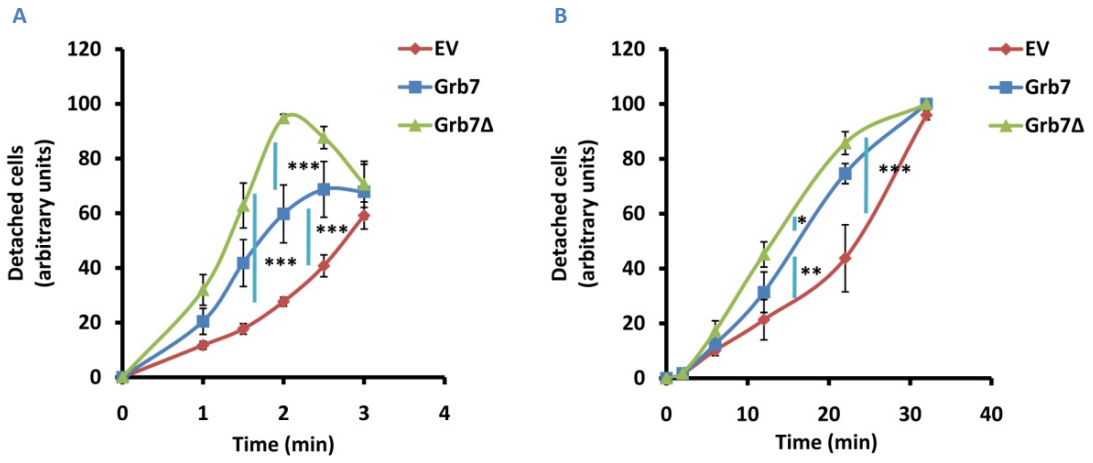

Figure 21: Cells expressing Grb7Δ present high cell detachment ability. A monolayer of HEK293 cells transiently transfected with the empty vector (EV) pcDNA3.1, pcDNA3/Flag-Grb7 or pcDNA3/Flag-Grb7Δ were detached from the plate by using either trypsin/EDTA (A) or 1 mM EGTA to chelate the extracellular Ca^{2+} (B). The plots (A) and (B) represent the mean ± SEM (n = 3) number of detached cells counted at the indicated times. Significant differences were found when comparing the curves by the two-way ANOVA test (*** $p < 0.001$, ** $p < 0.01$ and * $p < 0.05$).

6.5.2 Cytoskeletal reorganization is impaired in cells expressing Grb7Δ

The next step was to analyze the effect of the deletion of the CaM-BD of Grb7 in cell attachment to the substrate and the subsequent cytoskeletal reorganization.

Previous studies have shown that upon integrin-mediated stimulation FAK is recruited to focal adhesions triggering its activation and auto-phosphorylation creating docking sites for a variety of intracellular signaling proteins, such as paxillin, Src and ERK1/2, resulting in the reorganization of cytoskeleton fibers *(see section 3.1.4.1.1)* (49, 51, 120, 146, 188, 246, 249). It has also been described that upon fibronectin stimulation and auto-phosphorylation of FAK at Tyr-397, the kinase recruits Grb7 triggering a series of not well defined signaling cascades that end in the promotion of cell migration (45, 100). Thus we aimed to understand the role of Grb7 and its CaM-BD in this signaling pathway.

To study this, we seeded HEK293 stably expressing Grb7 and Grb7Δ and non-transfected cells over fibronectin-coated plates and analyzed by Western blot the phosphorylation patterns of FAK and ERK1/2 at different time points. **Fig. 22A** shows that not significant differences in the phosphorylation pattern of FAK were observed among the three cell lines. However, its downstream substrate ERK1/2 presented a significant lower and delayed phosphorylation (activation) levels in cells expressing Grb7Δ, as compared to cells expressing wild-type Grb7 or non-expressing cells. This suggested that Grb7Δ could be blocking its downstream signaling pathway controlling cytoskeletal reorganization.

As the phosphorylation of ERK1/2 has been reported to be involved in the reorganization of the cytoskeleton (146, 188, 249), we considered of high relevance to study if this reorganization was impaired in cells expressing Grb7Δ. We observed by confocal fluorescence microscopy the reorganization of the actin cytoskeleton using phalloidin (303), after reseeding HEK293 cells stably expressing Grb7 and Grb7Δ over fibronectin-coated plates. Non-transfected cells were used as control. **Fig. 22B** shows images of cells 15, 30 and 60 min after reseeding on fibronectin plates. It can be observed how the cells expressing Grb7 and in lesser extent the control non-transfected cells, developed fibrilar structures corresponding to the actin cytoskeleton 15 min after reseeding, and how these structures allowed the cells to be completely spread and attached to the fibronectin substrate after 60 min. However, the cells expressing Grb7Δ were unable to develop this kind of fibrilar structures presenting a more circular shape and a pericellular organization of the actin cytoskeleton even 60 min after seeding, although eventually they got attached to the matrix at longer times (not shown).

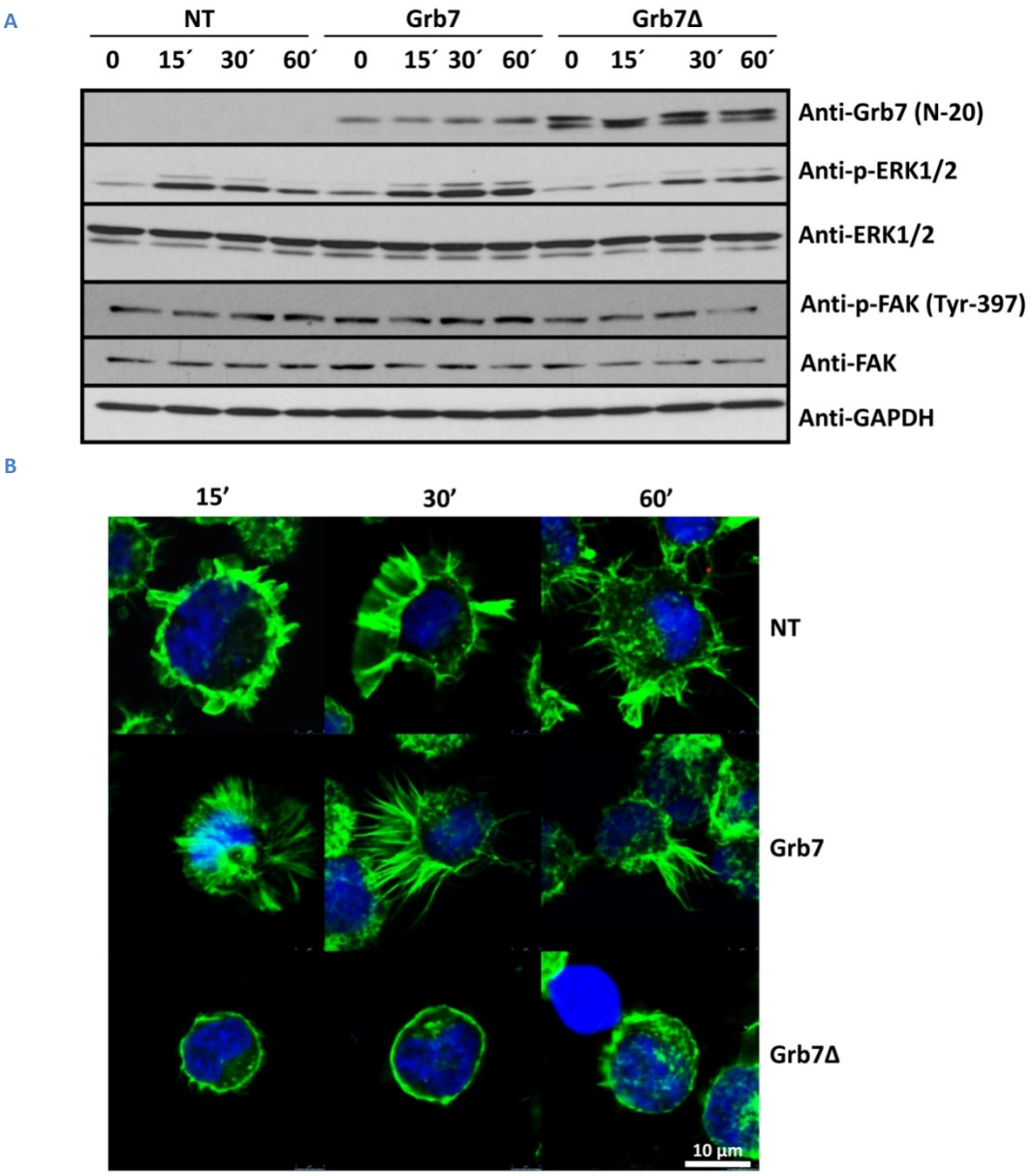

Figure 22: Grb7Δ expressing cells present a delay in cytoskeletal reorganization upon fibronectin-induced cell attachment. Non-transfected (NT) and stably transfected HEK293 cells expressing Grb7 or Grb7Δ were stimulated by seeding on fibronectin-coated plates as described in Materials and Methods. **(A)** Cell extracts were collected at the indicated times after fibronectin-stimulation and the phosphorylation of ERK1/2 and FAK was analyzed by Western blot. Anti-GAPDH, anti-ERK1/2 and anti-FAK antibodies were used as loading control. **(B)** The actin cytoskeletal reorganization after seeding on fibronectin-coated plates was observed at the indicated times using Phall-Alexa Fluor®-488 by confocal microscopy with a 63x (HCS PL APO lambda blue) oil-immersion objective. Cell nuclei were stained with DAPI and visualized using the UV channel.

6.6 Role of Grb7 and Grb7Δ in cell proliferation

Grb7 has been shown to be overexpressed in many tumors, and this phenomenon has been related with poor prognosis *(see section 3.1.5).* One of the main characteristics of tumor cells is their ability to overproliferate. In this context, we studied if Grb7 had any influence in controlling cell proliferation and if its CaM-BD played a role in this process.

Therefore, we tested the effect of Grb7 and Grb7Δ expression on the cell proliferation rate. HEK293 cells were transiently transfected with the empty vector pcDNA3.1, pcDNA3/FLAG-Grb7 or pcDNA3/FLAG-Grb7Δ and the cell proliferation rate was quantitatively measured by using the crystal violet staining method, a cationic dye that binds to DNA. As **Fig. 23** shows, HEK293 cells expressing Grb7 had a lower proliferation rate than non-expressing cells; however, the proliferation rate of cells expressing the deletion mutant Grb7Δ was even lower.

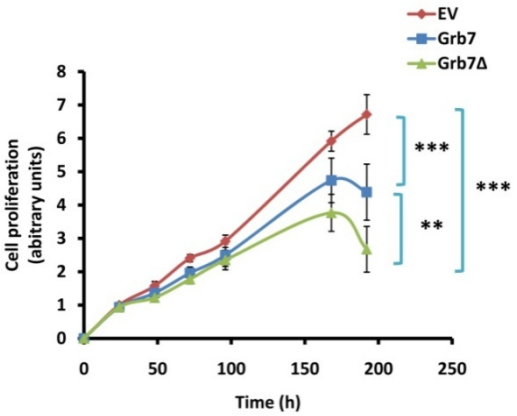

Figure 23: Cells transiently expressing Grb7Δ present lower proliferation rate than Grb7- or non-expressing cells. The proliferation rate of HEK293 cells transiently transfected with the empty vector (EV) pcDNA3.1, pcDNA3/FLAG-Grb7 or pcDNA3/FLAG-Grb7Δ was measured at the indicated times during 196 h by the crystal violet staining method as described in Materials and Methods. The plot represents the mean ± SEM, (n = 11) relative increment of the cell number (arbitrary units). Significant differences were found when comparing the curves using the two-way ANOVA test (*** $p < 0.0001$ and ** $p < 0.001$).

The proliferation rate was also determined in the stably transfected HEK293 cells expressing Grb7 or Grb7Δ. In this case, the proliferation was continuously monitored using the xCELLigence RTCA System that measured the impedance that the cells induced on plates containing gold cover-electrodes. This value, denoted as the *Cell Index*, is proportional to the number of total cells present in the well and can be continuously monitored along the time of the experiment to obtain the proliferation rate. **Fig. 24A** shows the normalized *Cell Index* of non-transfected and of stably transfected HEK293 cells expressing Grb7 or Grb7Δ after initially seeding a different number of cells. As previously observed in the transient transfectants, cells expressing Grb7 presented a lower proliferation rate than non-transfected control cells, and again, the proliferation rate of cells expressing Grb7Δ was even lower. We calculated the average doubling time, as detailed in Materials and Methods, from the curves generated by the xCELLigence System for non-transfected cells and cells expressing Grb7 or Grb7Δ **(Fig. 24B)**. We calculated that the doubling time of HEK293 cells expressing Grb7Δ and Grb7 was respectively 32.3 ± 0.20 and 27.6 ± 0.88 hours, while it was 21.6 ± 1.96 hours in the non-transfected cells.

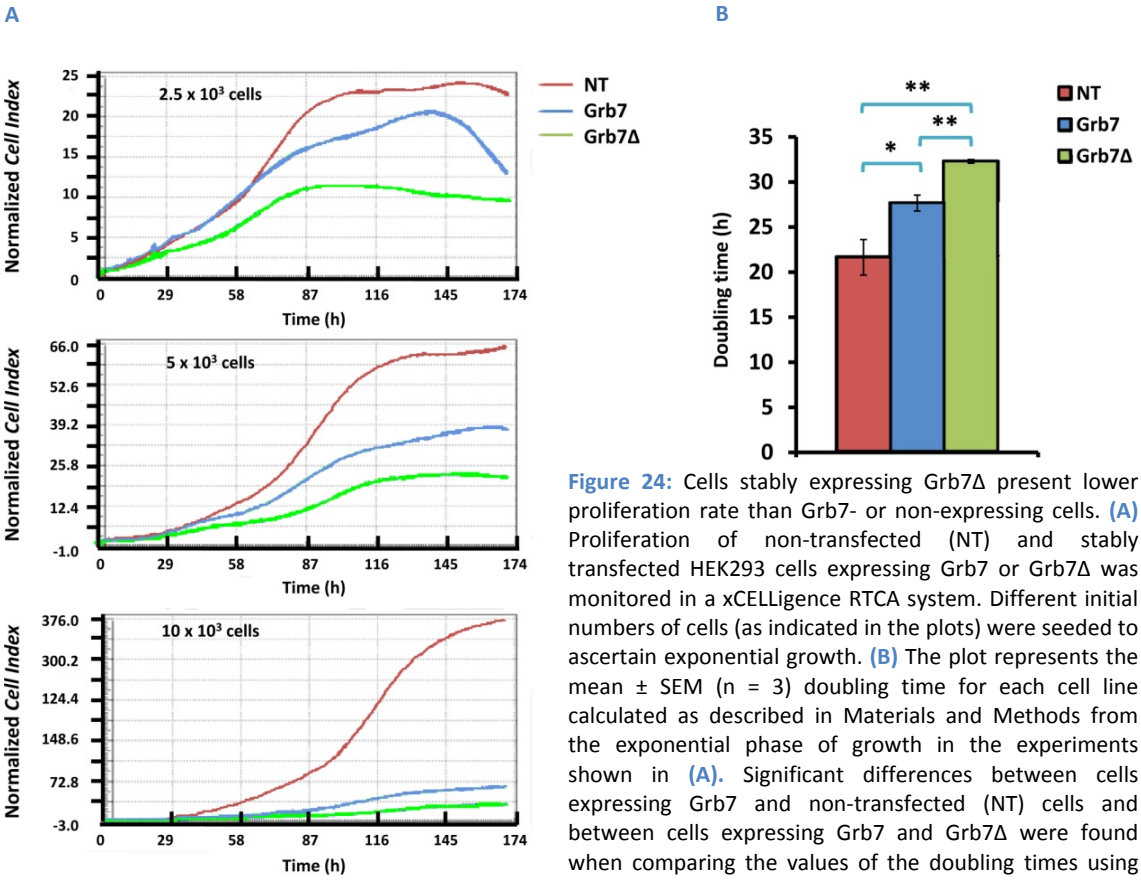

Figure 24: Cells stably expressing Grb7Δ present lower proliferation rate than Grb7- or non-expressing cells. **(A)** Proliferation of non-transfected (NT) and stably transfected HEK293 cells expressing Grb7 or Grb7Δ was monitored in a xCELLigence RTCA system. Different initial numbers of cells (as indicated in the plots) were seeded to ascertain exponential growth. **(B)** The plot represents the mean ± SEM (n = 3) doubling time for each cell line calculated as described in Materials and Methods from the exponential phase of growth in the experiments shown in **(A).** Significant differences between cells expressing Grb7 and non-transfected (NT) cells and between cells expressing Grb7 and Grb7Δ were found when comparing the values of the doubling times using the Student's t test (** $p < 0.001$ and * $p < 0.05$).

The cell cycle includes a series of events that take place in a cell leading to its division. The cell cycle can be divided into different phases: G_0, in which the cell presents a quiescent state of no division; the G_1 phase preparing the cell for DNA replication when exposed to growing stimuli; the S phase, in which DNA is replicated; the G_2 phase, where the cell ensures that everything is ready to enter the division phase; and finally the M phase, or mitosis, in which the cell gets divided into two daughter cells.

To study if the low proliferation rate observed in Grb7Δ-expressing cells was caused by a deficiency in cell cycle progression, we measured the relative number of cells, previously synchronized in G_0 by serum starvation (309), at the different phases of the cell cycle by staining the DNA with propidium iodide and analyzed using flow citometry. We found a slightly lower number of cells expressing Grb7Δ in the S-phase than those found in cells expressing the wild type protein or non-transfected cells **(Fig. 25A)**. Besides, the number of proliferating cells at the G_2/M phases increased more than two-fold after 2 hours of exposure to FBS and slowly decline thereafter but remained high even 28 hours later in non-transfected cells, in contrast to cells expressing Grb7 or Grb7Δ in which this increase was significantly lower **(Fig. 25B)**.

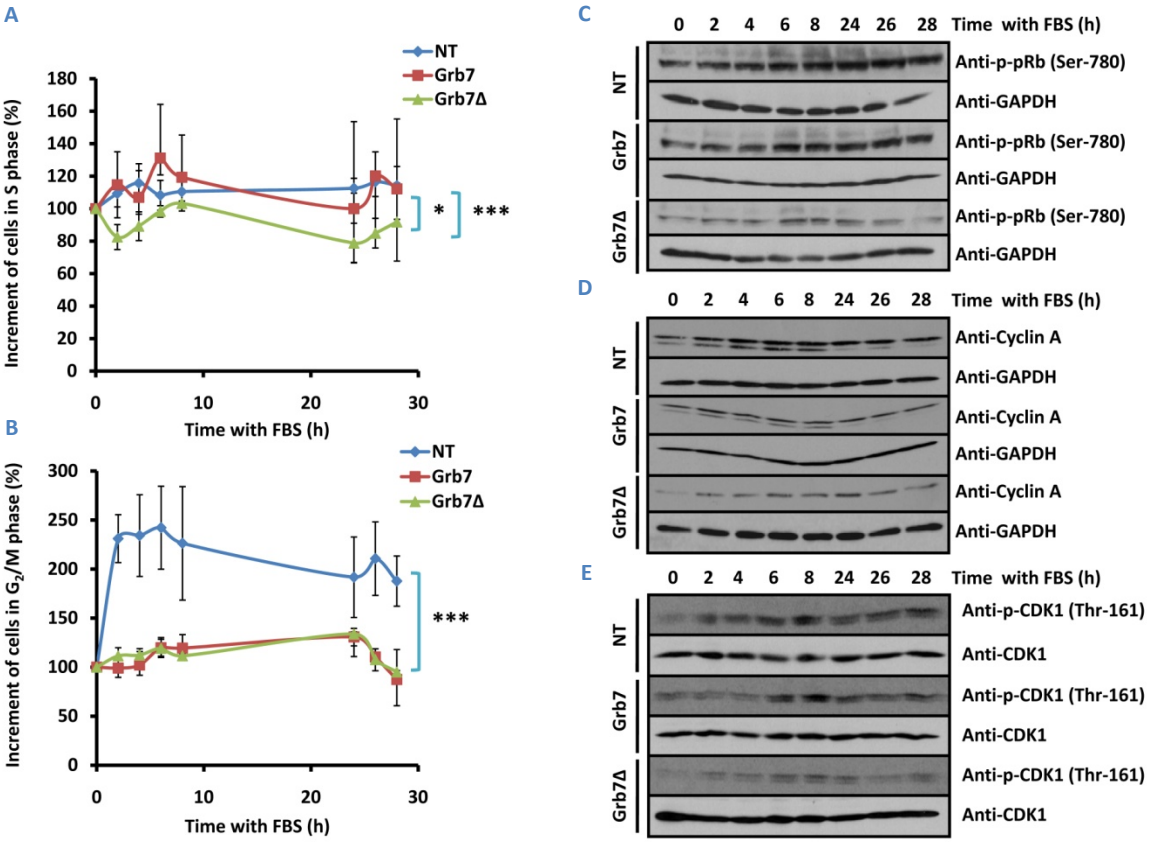

Figure 25: Effect of Grb7 and Grb7Δ expression in cell cycle progression. The cell cycle of non-transfected (NT) and stably transfected HEK293 cells expressing Grb7 or Grb7Δ was synchronized by serum deprivation and proliferation started by the addition of 10 % (v/v) FBS. Cells were collected at the indicated times and the percentage of cells at each cell cycle phase was determined by FACS analysis. The plots represent the mean ± SEM (n = 3) relative increment of cells at the S **(A)** and G_2/M **(B)** phases. Significant differences were found when comparing the curves using the two-way ANOVA test (*** $p < 0.0001$, ** $p < 0.001$ and * $p < 0.05$). **(C-E)** cell extracts were prepared to test by Western blot the expression of cyclin A, and the phosphorylation of pRb and CDK1. Anti-GAPDH or the corresponding antibody against the total protein when comparing phosphorylation patterns, were used as loading controls.

To ascertain a proper replication process, transitions along and between the different cell cycle phases are highly controlled. The major regulators for the transition along the cell cycle are cyclins and cyclin-dependent kinases (CDKs). While CDKs are constitutively expressed in cells, cyclins (the regulatory subunits of the CDKs) are synthesized at specific stages of the cell cycle, in response to various molecular signals (130, 190-191). When a cyclin binds to its corresponding CDK, the kinase gets phosphorylated forming an active complex that determines the progression throughout the cell cycle (130, 190-191).

To further investigate if the activity of these regulators was in some way affected by the expression of Grb7 or Grb7Δ, we analyzed by Western blot their expression and/or phosphorylation along the cell cycle. We first checked the phosphorylation pattern of pRb, that

is repressing cell cycle progression when hypophosphorylated (16, 86). As Fig. 25C shows, we found a significant decrease in the phosphorylation of pRb at Ser-780, substrate of the cyclin D-CDK4/6 (86) and cyclin E-CDK2 (211) complexes, in the cells expressing Grb7Δ and in lesser extent in those expressing wild type Grb7 when compared to non-transfected cells. However, no significant differences were found in the expression pattern of cyclin D between the three cell lines (Supplementary Fig. 2S), neither in the expression of cyclin E nor in the phosphorylation pattern of its associated CDK2 (Supplementary Fig. 2S). We also tested the expression pattern of cyclin A, that in association with CDK2 regulates the progress through the S phase and the G_2 phase (190). We detected that the expression of cyclin A was slightly decreased in cells expressing Grb7 and Grb7Δ (Fig. 25D). Cyclin A, in association with CDK1, also promotes entry in mitosis in late G_2 (190-191). In fact, we also observed a decrease in the FBS-induced phosphorylation of CDK1 (Thr-161) in cells expressing Grb7 and this phosphorylation was even lower in cells expressing Grb7Δ (Fig. 25E). The phosphorylation of CDK1 at Thr-161 is related with activation of the complex cyclins A/B-CDK1 (60). CDK1 also binds to cyclin B in late G_2 and through the mitosis phase (190-191); however no differences were observed in the expression pattern of cyclin B (Supplementary Fig. 2S). We also studied some cell cycle protein inhibitors (24, 170, 288), including $p16^{Ink4a}$, $p19^{Ink4d}$, $p21^{Cip1/Waf1}$ and $p27^{Kip1}$; however not reproducible results were found.

6.7 Calmodulin regulates the translocation of Grb7 into the nucleus

Grb7 has been described as an mRNA binding protein (284). Besides, nuclear Grb7 has been reported to aid in the coordinated exit of mRNAs from the nucleus to the cytoplasm (282). On the other hand, the fact that Grb7 and Grb7Δ appeared to affect the cell cycle progression suggested that they could play an important role in this cellular compartment. Therefore, we tested the nuclear localization of wild type Grb7 and its CaM-BD deletion mutant Grb7Δ.

6.7.1 Grb7Δ failed to localize in the nucleus

We found that Grb7 localized in the nucleus while the CaM-BD deletion mutant Grb7Δ did not. Nuclear fractionation showed that both Grb7 and EYFP-Grb7 were detectable in the nuclear fraction (NF) as well as in the non-nuclear fraction (NNF). However, the CaM-BD deletion mutants Grb7Δ and EYFP-Grb7Δ failed to localize in the NF (Fig. 26A), suggesting that the CaM-BD was essential for Grb7 localization in the nucleus. These observations were supported by immunoprecipitation of the FLAG-tagged Grb7 but not Grb7Δ using anti FLAG®-

M2 affinity gel from the NF obtained from HEK293 cells stably expressing these proteins (Fig. 26B) (82).

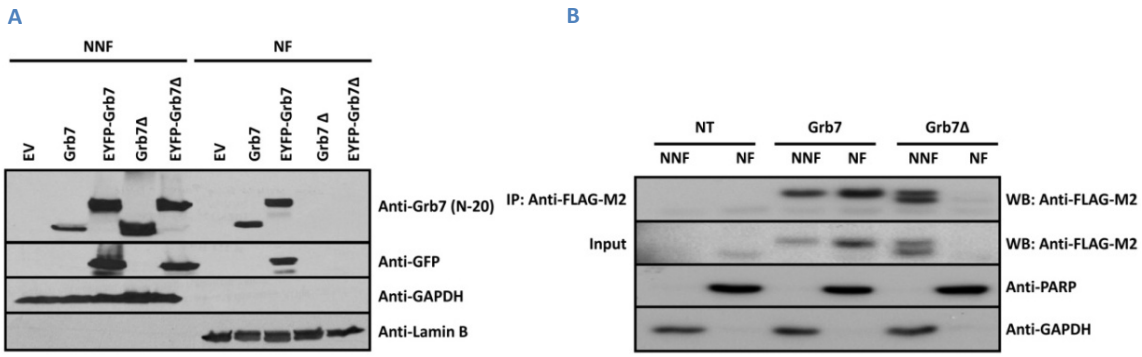

Figure 26: Grb7Δ fails to localize in the nucleus. **(A)** The non-nuclear fraction (NNF) and the nuclear fraction (NF) from HEK293 cells transiently transfected with the empty vector (EV) pcDNA3.1, pcDNA3/FLAG-Grb7, pcDNA3/FLAG-Grb7Δ, pEYFP, pEYFP-Grb7 or pEYFP-Grb7Δ were prepared as described in Materials and Methods. Western blot analysis using the anti-Grb7 (N-20) antibody, or the anti-GFP antibody, also recognizing the EYFP, was used to detect the presence of the proteins in the corresponding cellular fractions. **(B)** FLAG-tagged Grb7 and Grb7Δ were immunoprecipitated (IP) using the anti-FLAG-M2 affinity gel from the NNF and the NF of non-transfected (NT) and stably transfected HEK293 cells. Non-transfected (NT) HEK293 cells were used as negative control. GAPDH (cytosolic localization) and lamin B or PARP (nuclear localization) were detected with their corresponding antibodies to ascertain the absence of cross-contamination between the NNF and NF and as loading controls (82).

Therefore, we hypothesized that the CaM-BD could overlap the NLS of Grb7. As previously described, CaM-BDs are usually formed by basic and hydrophobic residues that are exposed in opposite sides of amphiphilic α-helixes (127). The combination of clusters of basic amino acids separated by approximately 10 unrelated amino acids is also a feature that defines the classical NLS (127). In fact, overlapping of the CaM-BD and the NLS of different proteins frequently occurs as describe in Table 4.

Protein	CaM-BD/NLS	Reference
hGrb7	**RK**LW**KR**FFCFL**RR**S	(82)
BASP1	GG**KL**S**KKKK**	(106)
EGFR	**RRR**HIV**RK**RTL**RR**LLQ	(181, 288)
hSOX1	**KR**PMNAFMVWS**R**GQ**RRK**	(6, 172)
hSOX9	**RR**PMNAFMVWAQAA**RRK**	(6, 172)
hSRY	**KR**PMNAFIVWS**R**DQ**RRK**	(139)
Kir/Gem	**KRK**ESMP**RK**A**RR**	(171)
TAP-Tag	**KRR**WK**K**NFIAVSAAN**R**F**KK**	(239)

Table 4: Overlap of the calmodulin-binding domain and the nuclear localization sequence in different proteins. The sequences corresponding to the CaM-BD and the overlapping NLS of different proteins are shown. Clusters of basic amino acids are highlighted in bold (82).

6.7.2 The SH2 domain of Grb7 contributes to its nuclear localization

To determine whether the SH2 domain of Grb7 was required for its nuclear translocation we compared the presence of Grb7 and Grb7V, a natural occurring truncated variant that lacks the SH2 domain (275), at the nuclear fraction. Figs. 27A and 27B show that Grb7V was detected in the nuclear fraction in far lower extent (≈ 60 %) than wild type Grb7. Again, deletion of the CaM-BD in both wild type Grb7 and its truncated variant Grb7V prevented this localization. This suggested that the SH2 domain, in addition to the NLS/CaM-BD, might play an important role in Grb7 nuclear translocation (82).

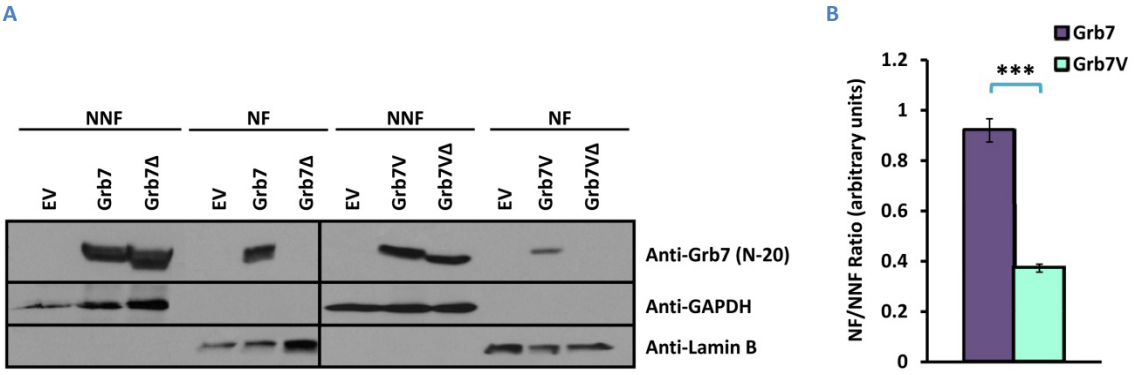

Figure 27: The SH2 domain is important for the nuclear localization of Grb7. **(A)** Non-nuclear fractions (NNF) and nuclear fractions (NF) from HEK293 cells transiently transfected with the empty vector (EV) pcDNA3.1, pcDNA3/FLAG-Grb7 or pcDNA3/FLAG-Grb7Δ were processed by Western blot to analyze the localization of Grb7 and Grb7V and their corresponding calmodulin-binding domain (CaM-BD)-deletion mutants Grb7Δ and Grb7VΔ. GAPDH (cytosolic localization) and lamin B (nuclear localization) were detected to ascertain the absence of cross-contamination between the NNF and NF and as loading controls. **(B)** The plot presents the NF/NNF ratio of the mean ± SEM (n = 3) densitometric signal of Grb7/Grb7V. Significant differences were found when comparing the NF/NNF ratio of Grb7 and Grb7V using the Student's t test (*** $p < 0.0001$) (82).

6.7.3 Inhibition of calmodulin enhances Grb7 translocation into the nucleus

To study the role of CaM in the control of the nuclear translocation of Grb7, we used the cell permeable CaM antagonist W-7, to block a putative CaM effect. Confocal fluorescence microscopy of HEK293 cells transiently transfected with pEYFP-Grb7 and pEYFP-Grb7Δ showed that inhibition of CaM by W-7 led to a massive translocation of EYFP-Grb7 into the nucleus, while W-7 had no effect on EYFP-Grb7Δ localization **(Fig. 28)**. Similar results were obtained in rat glioma C6 cells transiently or stably transfected with EYFP-Grb7 or EYFP-Grb7Δ **(Supplementary Fig. 3S)**

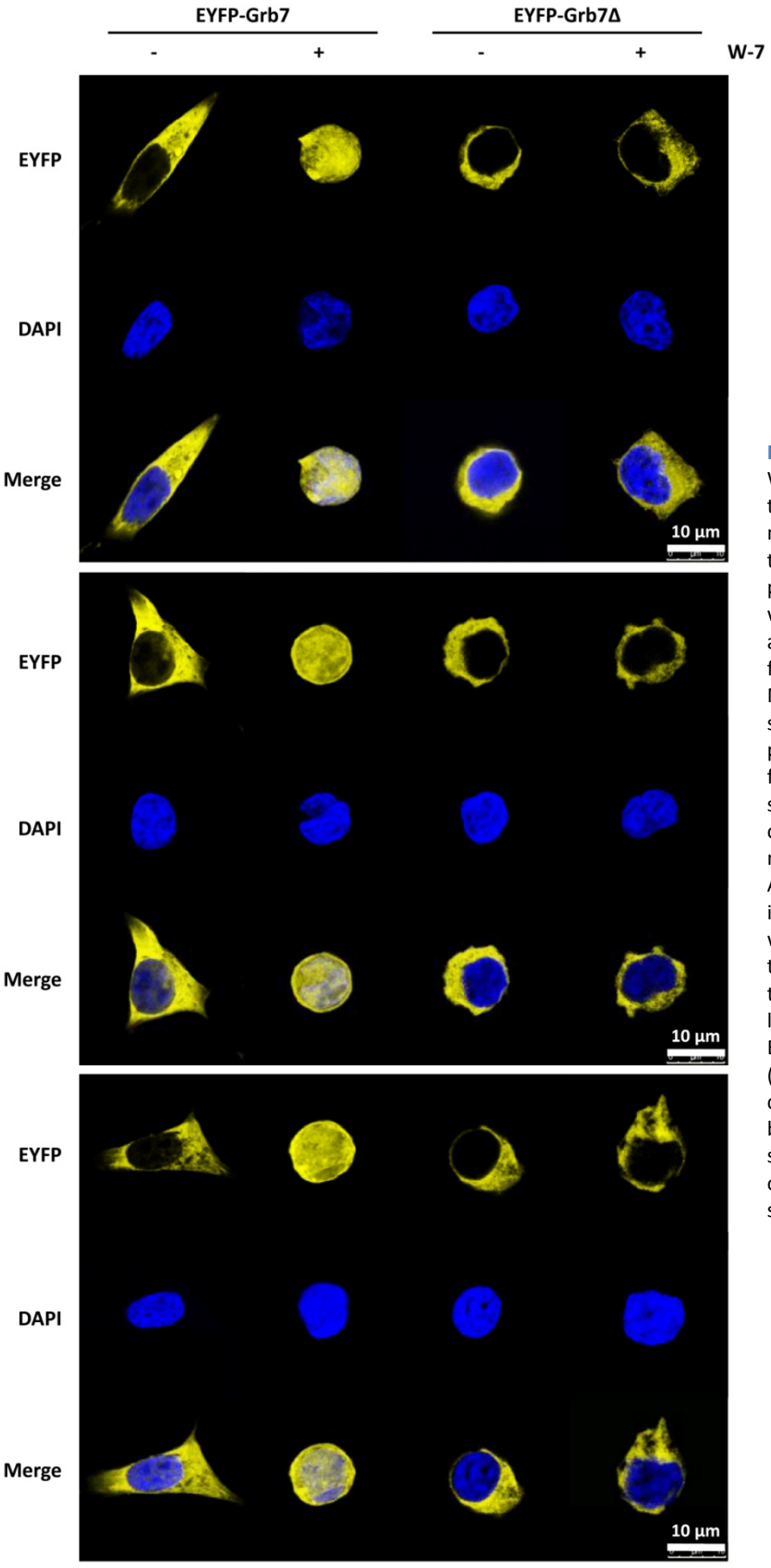

Figure 28: The CaM antagonist W-7 enhances the translocation of Grb7 into the nucleus. HEK293 cells transiently transfected with pEYFP-Grb7 or pEYFP-Grb7Δ were incubated in the absence and presence of W-7 (15 µM) for 30 min as described in Materials and Methods and seeded in fibronectin-coated plates. The cells were then fixed and the nuclei were stained with DAPI to be observed in a confocal microscope using a 63x (HCS PL APO lambda blue) oil-immersion objective exciting with a 488 nm laser to detect the EYFP and the UV channel to observe the nuclei. The localization of the chimeras EYFP-Grb7 and EYFP-Grb7Δ (EYFP) (yellow) and their corresponding nuclei visualized by DAPI staining (blue) are shown. Merge represents the overlay of the EYFP and DAPI signals (82).

The increase of Grb7 in the NF after W-7 treatment was also confirmed by Western blot analysis of the NNF and NF of HEK239 cells transiently transfected with Grb7 **(Figs. 29 A and 29B).** To test for long-term effects, cells were treated with W-7 added daily during 72 hours. **Fig. 29C** presents a typical Western blot showing the presence of Grb7 in the NNF and in the NF. We can appreciate the progressive increase of Grb7 in the NF during the treatment with W-7. **Fig. 29D** shows the average densitometry of a set of experiments similar to the one shown in **Fig. 29C** comparing the NF/NNF ratio of Grb7 in the absence and presence of W-7 after 72 hours of continuous treatment with the CaM inhibitor (82).

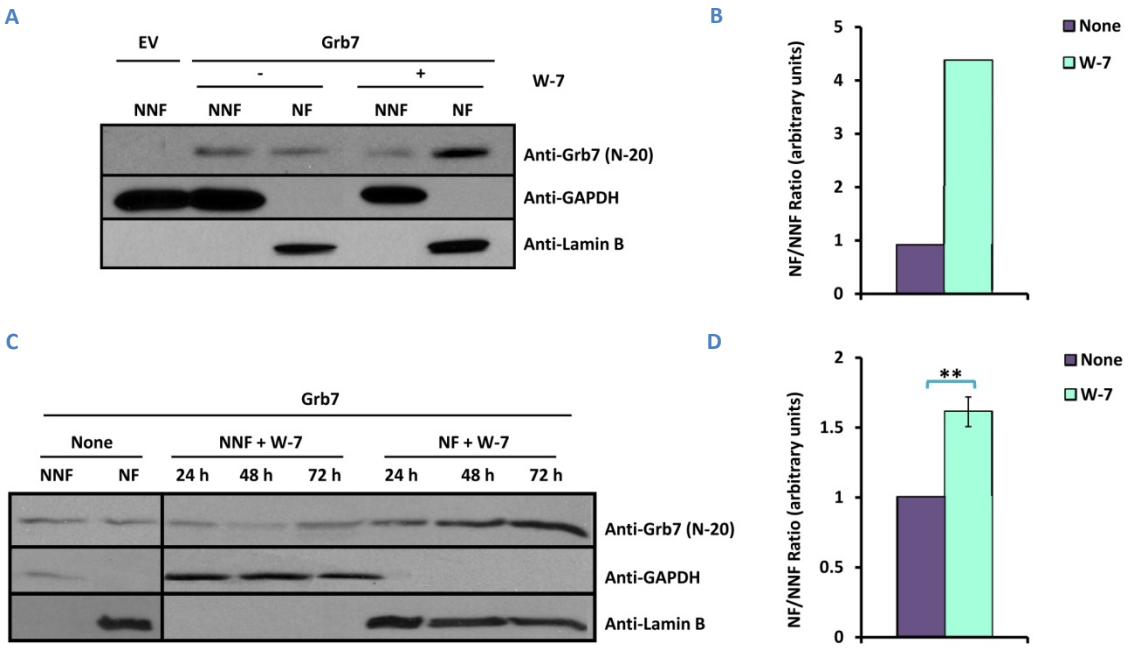

Figure 29: Long-term treatment with W-7 enhances the presence of Grb7 in the nucleus. **(A)** Western blot analysis of the non-nuclear fraction (NNF) and nuclear fraction (NF) of HEK293 cells transiently transfected with the empty vector (EV) pcDNA3.1 or pcDNA3/FLAG-Grb7 treated in the absence and presence of W-7 (30 µM). **(B)** The plot presents the densitometric NF/NNF ratio of Grb7 in the absence and presence of W-7 corresponding to the experiment shown in **(A)**. **(C)** HEK293 cells stably expressing Grb7 were treated with W-7 for 24, 48 and 72 h as described in Materials and Methods and cell lysates were collected and processed for Western blot analysis of the NNF and NF in the absence and presence of W-7. **(D)** The plot presents the NF/NNF ratio of the mean ± SEM (n = 3) densitometric signal of Grb7 at 72 h of continuous treatment with W-7. Significant differences were found when comparing the NF/NNF ratio in the absence and presence of W-7 using the Student's t test (** $p < 0.001$). GAPDH (cytosolic localization) and lamin B (nuclear localization) were detected to ascertain the absence of cross-contamination between the NNF and NF and as loading controls (82).

6.8 Study of tumor growth and tumor-associated angiogenesis *in vivo*

My laboratory previously described that media conditioned by HEK293T cells expressing Grb7Δ presented antiangiogenic activity as determined using an *in vitro* assay system (159). Once, we had characterized in living cells the functional relevance of the CaM-BD of Grb7 using different systems, we aimed to test the effect of the deletion of its CaM-BD in tumor growth and its associated angiogenesis *in vivo*. We looked for a well characterized highly angiogenic

tumor in which Grb7 was not endogenously expressed to study how the gain of the wild type and the deletion mutant proteins was affecting tumor growth and tumor-associated angiogenesis. Therefore, we decided to use the rat glioma C6 cells to generate tumors in rat brain and measure its time-dependent growth and to detect changes in the tumor vascularization by non-invasive MRI techniques using non-extravasable contrast agents (92, 310). Rat glioma C6 cells are widely used as a useful model to study glioblastoma growth and its associated angiogenesis (94). We generated stable transfectants in C6 cells expressing EYFP, EYFP-Grb7 or EYFP-Grb7Δ **(Fig. 30)**. Non-transfected C6 cells were used to show that no endogenous expression of Grb7 was found in this cell line. The cells stably expressing EYFP, EYFP-Grb7 and EYFP-Grb7Δ were stereotaxically implanted in the brain caudate nucleus of the right hemisphere of adult rats as described in Materials and Methods and the development of the tumors was followed by MRI.

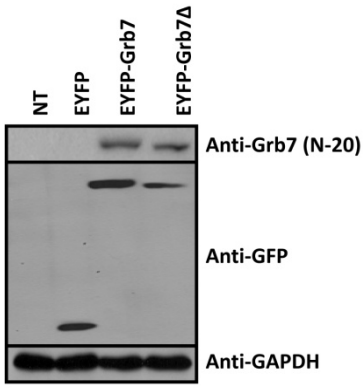

Figure 30: C6 cells stably expressing EYFP-Grb7 and EYFP-Grb7Δ. Total cell extracts of C6 cells stably transfected with pEYFP, pEYFP-Grb7 or pEYFP-Grb7Δ were processed by SDS-PAGE and Western blot using an anti-Grb7 antibody recognizing its N-terminal and an anti-GFP antibody also recognizing the EYFP. Anti-GAPDH antibody was used as loading control.

6.8.1 Grb7Δ inhibits tumor growth *in vivo*

6.8.1.1 Magnetic Resonance Imaging analysis

Fig. 31A shows representative anatomical images of the tumors at different times of development in animals implanted with C6 cells stably expressing EYFP, EYFP-Grb7 or EYFP-Grb7Δ. The panels show anatomical T2W and enhanced T1W images, obtained from the same sections, after a short intra-venous bolus injection of Magnevist® (Gd^{3+}-DTPA), a non-extravasable contrast agent in non-pathological vessels. It should be mentioned that the bright areas, revealing extravasation of the contrast agent through leaky tumor vessels, provide a useful indication of the regional vasculature. **Fig. 31B** shows T2W and enhanced T1W images in axial projection of tumors four weeks post-implantation of the different tumor cell lines in another set of animals.

A

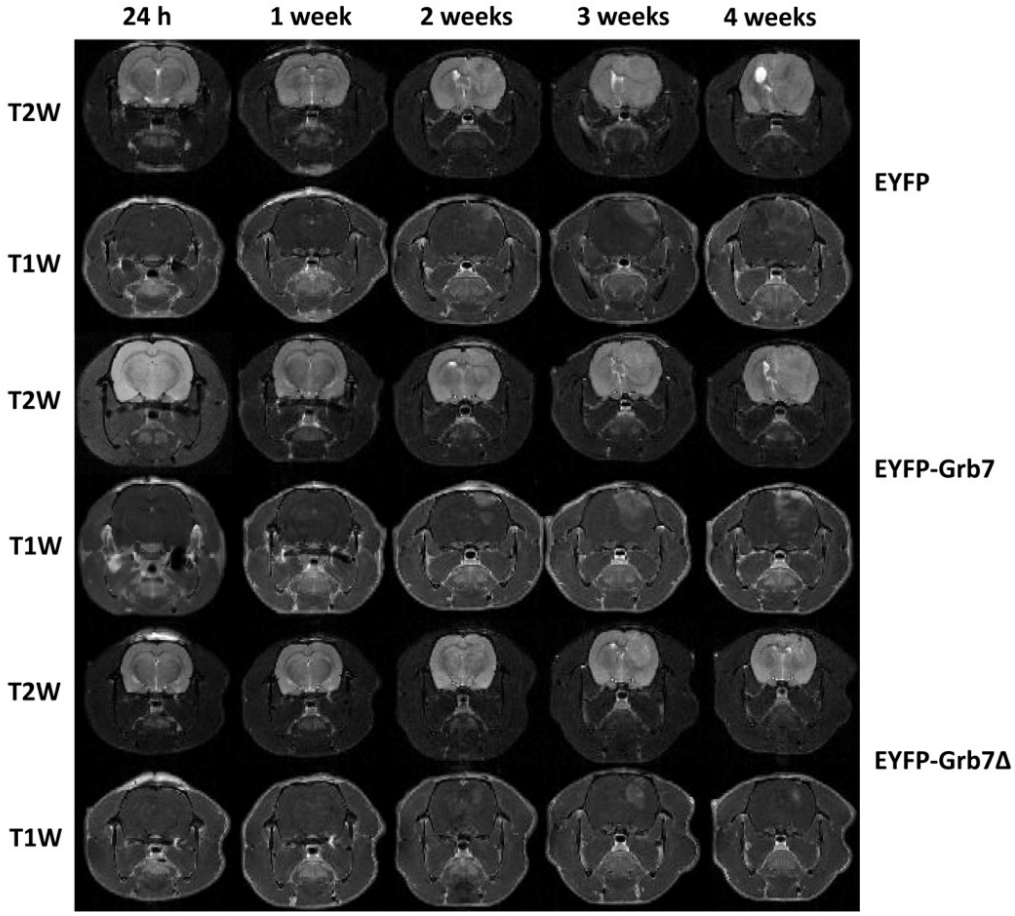

B

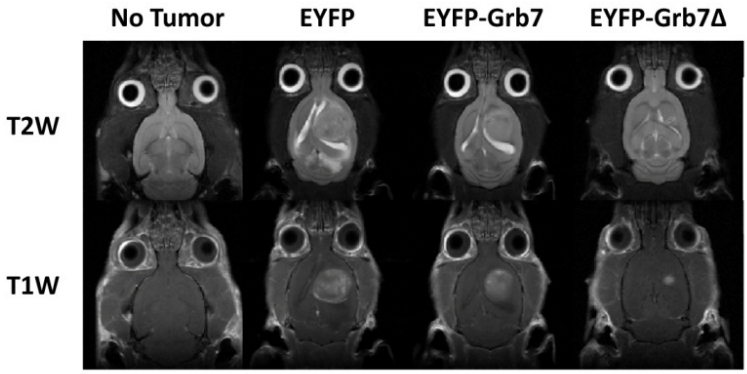

Figure 31: EYFP-Grb7Δ expression, as compared to EYFP or EYFP-Grb7, inhibits tumor growth. Rat glioma C6 cells stably transfected with pEYFP, pEYFP-Grb7 and pEYFP-Grb7Δ were stereotaxically implanted into rat brains as described in Materials and Methods and the tumor growth was followed by non-invasive magnetic resonance imaging (MRI). Coronal **(A)** or axial **(B)** projections of T2W and their corresponding enhanced TW1 images after a short intra-venous bolus injection of Magnevist® (Gd^{3+}-DTPA), a non-extravasable contrast agent, obtained at the indicated times **(A)** or 4 weeks after implantation **(B)** are shown.

As **Fig. 32** shows, when we measured the volume of the tumors generated by the different implanted cell types by integrating the tumor areas of different sections in both T1W **(Fig. 32A)** and T2W **(Fig. 32B)** images, we observed that the tumors derived from implanted EYFP-Grb7-

and EYFP-Grb7Δ-expressing cells were smaller on average than those derived from EYFP-expressing cells. However, the tumors generated from EYFP-Grb7Δ-expressing cells were far smaller than those derived from EYFP-Grb7- and EYFP-expressing cells, and showed a tendency to regression at longer times post-implantation.

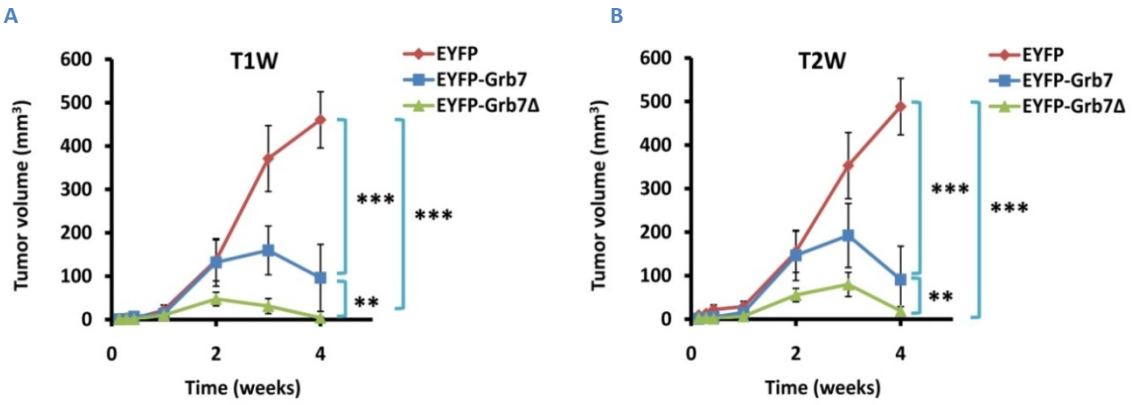

Figure 32: Tumors generated by the EYFP-Grb7Δ-expressing C6 cells are smaller than those generated by EYFP-Grb7 and EYFP-expressing cells. The plots present the mean ± SEM volume of the tumors from a set of animals calculated from similar experiments to those shown in **Fig. 31** generated by implanted C6 cells stably expressing EYFP (n = 6), pEYFP-Grb7 (n = 6) and pEYFP-Grb7Δ (n = 5) calculated from T1W **(A)** or T2W **(B)** images. Significant differences were found when comparing the curves using the two-way ANOVA test (*** $p < 0.0001$, ** $p < 0.001$ and * $p < 0.05$).

6.8.1.2 Diffusion Magnetic Resonance Imaging

We also performed diffusion MRI analysis. The ADC of water is known to provide information, as measured by NMR, on the proliferative behavior of tumors (42, 242), since an increase in the density of the cellular population decreases the observed ADC (265). **Fig. 33A** compares the ADC maps of 3 weeks-old tumors derived from EYFP-, EYFP-Grb7- and EYFP-Grb7Δ-expressing C6 cells. The average ADC was measured within the indicated region of interest (ROI) limited by the black perimeter. The EYFP- and EYFP-Grb7-expressing tumors depicted significant lower ADC values as compared to the EYFP-Grb7Δ-expressing ones. This revealed that the translational movement of water molecules was faster in the latter, consistent with the lower obstruction to diffusion due to reduced cellularity in these tumors. **Fig. 33B** shows the mean ± SEM values of ADC in the three sets of tumors from different animals. These findings are consistent with the lower growth of tumors derived of EYFP-Grb7Δ-expressing C6 cells as shown above.

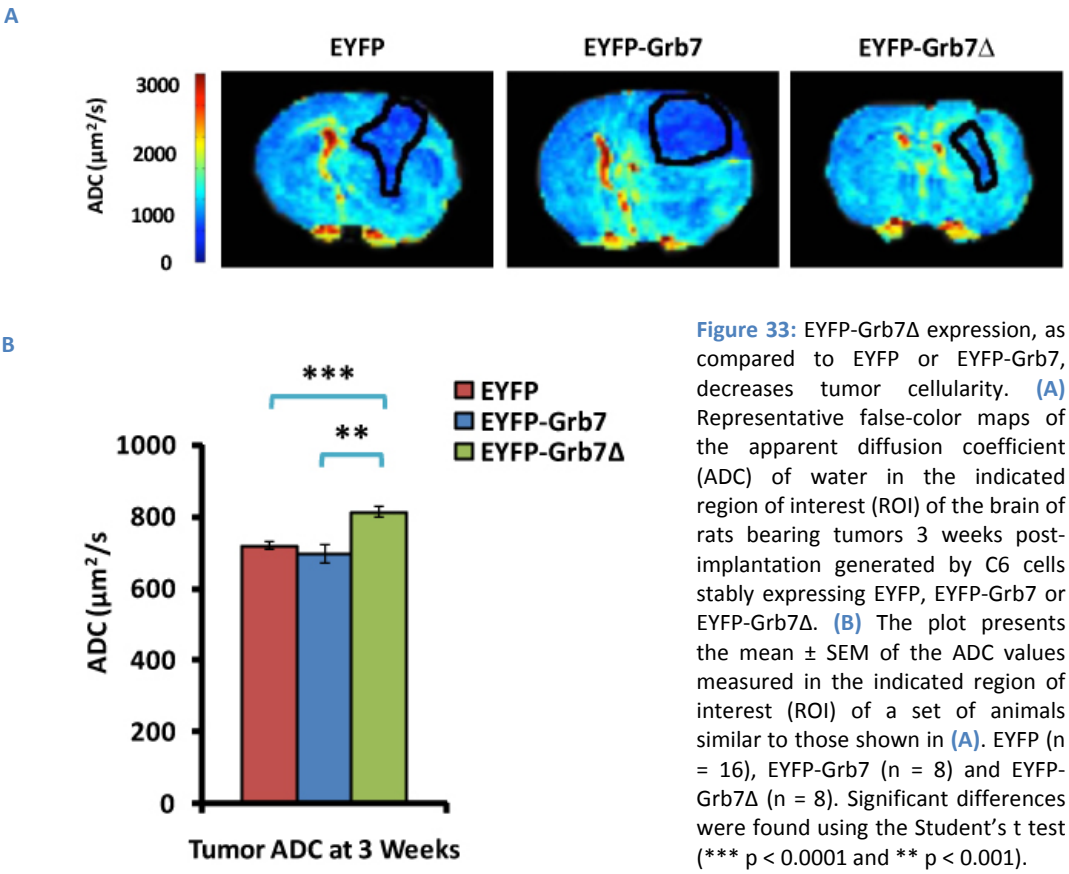

Figure 33: EYFP-Grb7Δ expression, as compared to EYFP or EYFP-Grb7, decreases tumor cellularity. **(A)** Representative false-color maps of the apparent diffusion coefficient (ADC) of water in the indicated region of interest (ROI) of the brain of rats bearing tumors 3 weeks post-implantation generated by C6 cells stably expressing EYFP, EYFP-Grb7 or EYFP-Grb7Δ. **(B)** The plot presents the mean ± SEM of the ADC values measured in the indicated region of interest (ROI) of a set of animals similar to those shown in **(A)**. EYFP (n = 16), EYFP-Grb7 (n = 8) and EYFP-Grb7Δ (n = 8). Significant differences were found using the Student's t test (*** $p < 0.0001$ and ** $p < 0.001$).

6.8.1.3 Histological description of the tumors

To confirm the findings described above using MRI, tumor-bearing rats were sacrificed and brain tissue sections were stained using the Nissl method as described in Materials and Methods, since due to its high number of cytoplasmic ribosomes, C6 cells stain strongly with toluidine blue (23). Rat C6-derived gliomas can be morphologically differentiated in three regions **(Fig. 34)**, a external region of infiltration in which tumor cells are mixed with normal cells, a peripheral proliferative area, and a necrotic center harboring complex vascular aggregates composed of associated microvessels surrounded by variably thickened basement membrane, named glomeruloid formations (241). **Fig. 34** shows representative histological sections of a normal brain without tumor, and brain-bearing tumors four weeks post-implantation of C6 cells expressing EYFP, EYFP-Grb7 or EYFP-Grb7Δ. Active areas of growth, with high cellularity at the periphery of the tumor, and a central necrotized area, were clearly observed in the tumors generated by EYFP- or EYFP-Grb7 expressing cells. In agreement with the MRI results, the peripheral proliferative area of tumors derived from EYFP-Grb7Δ-expresing cells **(Fig. 34D)** was less developed than those from tumors derived from EYFP- and EYFP-Grb7-expressing cells **(Figs. 34B and 34C)**. Notably, the central necrotized region

presented abundant glomeruloid formations in tumors derived from C6 cells expressing EYFP or EYFP-Grb7, while poor or not significant vascular formations were observed in the central scar of tumors derived from EYFP-Grb7Δ-expressing cells.

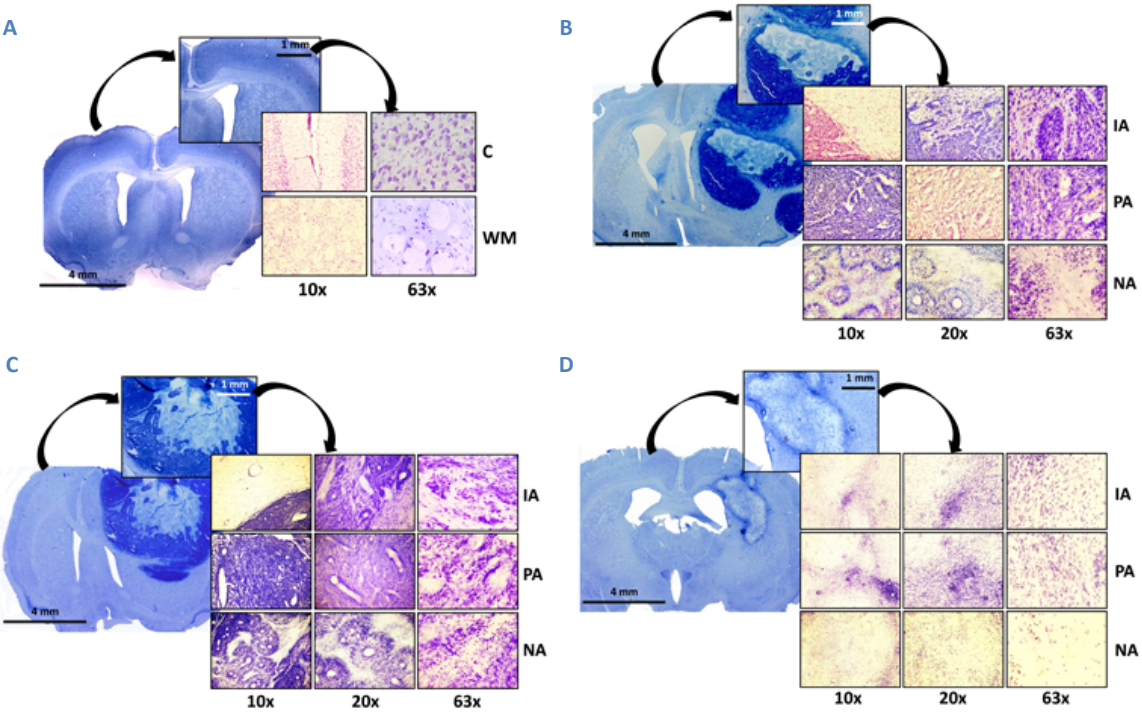

Figure 34: Coronal sections of brains bearing tumors stained with the Nissl method as described in Materials and Methods 4 weeks post-implantation of stably transfected C6 cells expressing EYFP **(B)**, EYFP-Grb7 **(C)** or EYFP-Grb7Δ **(D)** observed at the indicated magnifications. Coronal section of a tumor-free brain is presented in **(A)** showing the whole brain section and magnifications of the brain cortex (C) and the white matter (WM), where the tumors tend to grow. The different areas found in a typical glioblastoma are indicated: infiltration area (IA), proliferative area (PA) and necrotic area (NA).

6.8.2 Grb7Δ inhibits tumor-associated angiogenesis *in vivo*

6.8.2.1 Perfusion Magnetic Resonance Imaging

In order to study the tumor-associated angiogenesis we performed bolus tracking experiments with Magnevist® and generated false-color maps for the CBF, CBV and MTT imaging of coronal planes of the brain (214) that allowed comparing the vascular competence between the ipsilateral tumor-bearing and the contralateral tumor-free hemispheres. As **Fig. 35A** shows, we observed an increase in the values of these parameters in the tumor-bearing hemisphere derived from C6 cells expressing EYFP and EYFP-Grb7 (note the red rim of the tumor in the CBV and MTT maps), as compared to the tumor-free hemisphere. In contrast, no significant increase was observed in tumors grown from EYFP-Grb7Δ-expressing cells. When we normalized the obtained values comparing the area of the tumor with a similar area in the contralateral tumor-free hemisphere **(Fig. 35B)**, we obtained lower mean ± SEM values for

CBF, CBV and MTT in tumors generated by EYFP-Grb7Δ-expressing C6 cells than in those generated by cells expressing either EYFP or EYFP-Grb7, confirming decreased vascular competence in the former.

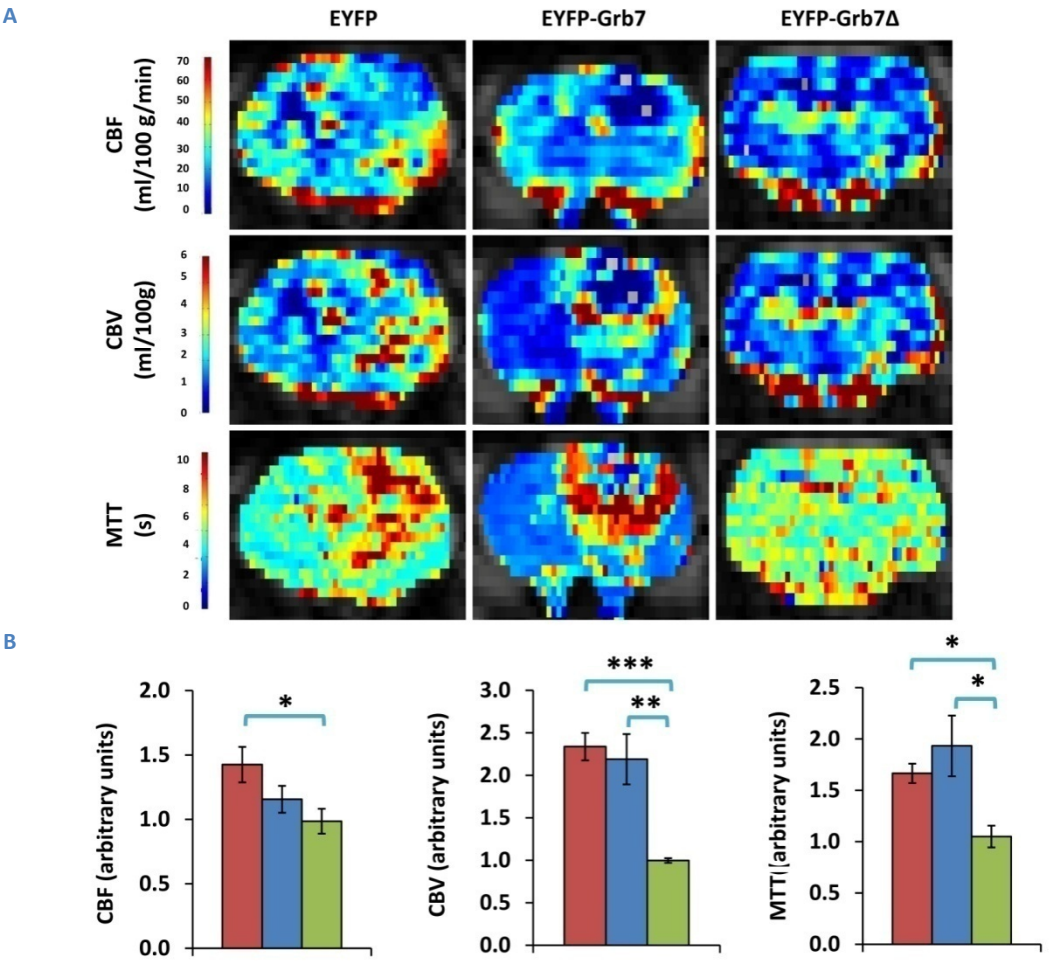

Figure 35: Expression of Grb7Δ decreases tumor-associated angiogenesis. **(A)** False-color maps of the cerebral blood flow (CBF), cerebral blood volume (CBV) and mean transit time (MMT) obtained after a bolus intra-venous injection of Magnevist® from rats bearing tumors 4 weeks post-implantation of C6 cells stably transfected with pEYFP, pEYFP-Grb7 or pEYFP-Grb7Δ. **(B)** The plots present the mean ± SEM (EYFP, n = 16; EYFP-Grb7, n = 8; EYFP-Grb7Δ, n = 3) of the relative CBF, CBV and MTT of the tumor area normalized with a similar area in the non-tumor bearing contralateral hemisphere from a set of animals similar to those in **(A)**. Significant differences were found using the Student's t test (*** $p < 0.0001$, ** $p < 0.001$ and * $p < 0.05$).

6.8.2.2 VEGF immunohistochemistry

Finally, to visualize the tumor-associated blood vessels we performed immunohistochemistry of sections of the different set of tumors using an anti-VEGF antibody **(Fig. 36A)**. In agreement with the fact that the tumor neo-vasculature could derive from the trans-differentiation of tumor stem cells (252), this marker was detected not only in the vascular endothelium, but also in the tumor cells reflecting that these cells were able to produce and to release VEGF to the extracellular media. We additionally measured the

diameter of the lumen of the blood vessels of the different tumors (Fig. 36B) demonstrating that on average, the vessels from tumors derived from EYFP-Grb7Δ-expressing C6 cells were significantly smaller than the vessels from tumors generated by EYFP- or EYFP-Grb7-expressing C6 cells.

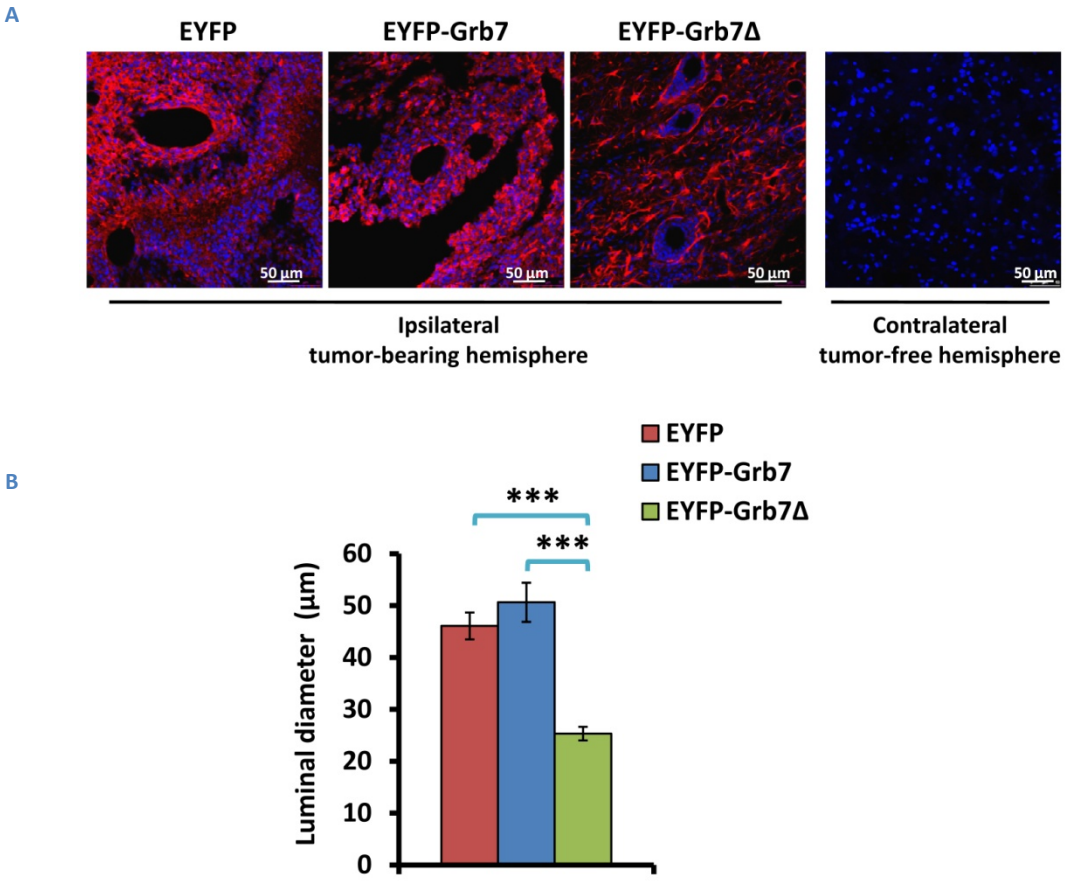

Figure 36: Tumors generated from EYFP-Grb7Δ-expressing cells are poorly vascularized. **(A)** Immunostaining using anti-VEGF and anti-rabbit IgG Alexa Fluor®-546 secondary antibodies (red) of coronal sections of brain-bearing tumors 4 weeks post-implantation of C6 cells stably transfected with pEYFP, pEYFP-Grb7 or pEYFP-Grb7Δ. Images were obtained with a confocal microscope using a 40x/1.25-0.75 oil-immersion objective exciting with the 546 nm laser. The nuclei were stained with DAPI (blue) and visualized using the UV channel. Negative immunostaining from a contralateral tumor-free hemisphere is also shown. **(B)** The plot represents the mean ± SEM (EYFP, n = 50; EYFP-Grb7, n = 12; EYFP-Grb7Δ, n = 32) diameter of the lumen of the blood vessels associated to the tumors. Significant differences were found using the Student's t test (*** $p < 0.0001$).

6.9 Identification of new Grb7 and Grb7Δ binding partners using Mass Spectrometry-based proteomics

Grb7 as an adaptor protein modulates dynamic signaling networks of many interacting signaling proteins. The known pathways in which Grb7 participates have been previously described *(see section 3.1.4)*; however, the molecular mechanisms, the proteins involved therein, and how they can crosstalk, forming different protein complexes are still poorly

known. Therefore, we considered of great relevance to study potential protein complexes and protein-protein interaction networks associated to Grb7 and if they could be somehow affected by the deletion of its CaM-BD. To perform this work, I stayed for 6 months in the laboratory of Prof. Roger J. Daly in the Garvan Institute of Medical Research in Sydney, Australia.

To identify new Grb7-associated proteins and to study if the deletion of its CaM-BD altered these associations, we used Grb7 and Grb7Δ tagged either with FLAG or EYFP and we employed ANTI-FLAG®-M2 Affinity Gel and the GFP-Trap®-A system to trap the respective proteins. To prevent unspecific associations that could occur in overexpressed proteins, we used stably transfected instead of transient transfected cells. Therefore, non-transfected HEK293 cells as negative control and HEK293 cells stably transfected with FLAG-Grb7 or FLAG-Grb7Δ on the one hand; and C6 cells stably transfected with pEFYP, pEYFP-Grb7 or pEYFP-Grb7Δ on the other were used. The cells were lysed and the tagged Grb7 and Grb7Δ were immunoprecipitated with either ANTI-FLAG®-M2 Affinity Gel system for HEK293 cells or affinity-purified with the GFP-Trap®-A system for C6 cells. The introduction of negative controls allowed us to detect potential contaminations and unspecific proteins potentially interacting with the matrixes. Samples were run in NuPAGE gels and the co-immunoprecipitated bands were detected by Sypro Ruby staining. Bands present in the Grb7 and/or Grb7Δ lanes but absent in control lanes were cut, processed for in-gel tryptic digestion and subjected to MS-based proteomics **(Fig. 10)**. Although not many specific bands were found in the Grb7 and/or Grb7Δ lanes using the ANTI-FLAG®-M2 affinity gel system to immunoprecipitate the FLAG-tagged Grb7 or Grb7Δ stably expressed in HEK293 cells, we detected one clear band at ≈ 70 KDa present only in the Grb7Δ lane, and another positive band in the Grb7 lane at ≈ 45 KDa in some of the performed experiments. The ≈ 60 KDa region, where Grb7 and Grb7Δ migrate, was also analyzed as a positive control **(Fig. 37A)**. Additionally, the GFP-Trap®-A system was used to affinity purify EYFP-Grb7 and EYFP-Grb7Δ from lysates of C6 cells stably expressing the corresponding proteins. As **Fig. 37B** shows, there was one clear ≈ 70 KDa band present in the EYFP-Grb7 and EYFP-Grb7Δ lanes but not in the control EYFP lane. Also one band present only in the EYFP-Grb7 lane at ≈100 KDa was detected. The ≈ 80 KDa region where EYFP-Grb7 and EYFP-Grb7Δ migrate was also analyzed as a positive control.

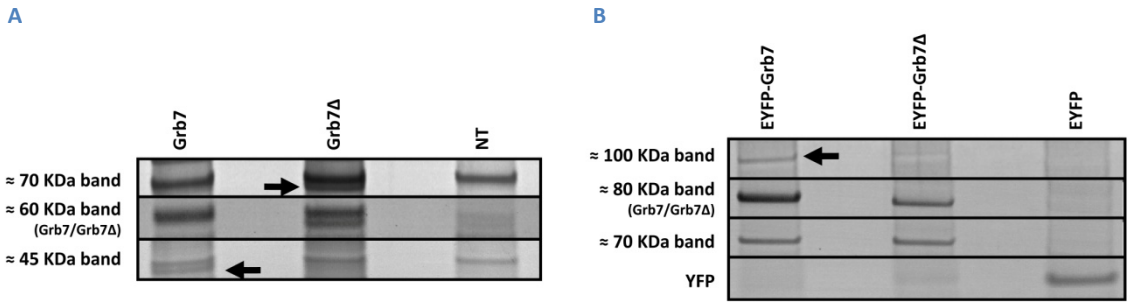

Figure 37: Proteins co-immunoprecipitated with Grb7 and/or Grb7Δ. **(A)** Sypro Ruby staining of immunoprecipitated lysates from HEK293, HEK293/FLAG-Grb7 and HEK293/FLAG-Grb7Δ cells using ANTI-FLAG®-M2 Affinity Gel system. Representative segments selected for MS analysis are shown. **(B)** Sypro Ruby staining of affinity-purified lysates from C6 cells stably expressing EYFP, EYFP-Grb7 or EYFP-Grb7Δ using the GFP-Trap®-A system. Representative segments selected for MS analysis are shown. The Grb7 and Grb7Δ bands are indicated. Arrows point to the specific bands found. Note that Grb7 and Grb7Δ presented a higher molecular mass (≈ 80 KDa) in **(B)** due to the EYFP tag.

Searches using MaxQuant in either human (for the spectra obtained from HEK293 cells), or rat (for the spectra obtained from C6 cells), databases were carried out to identify the proteins whose peptides had been detected by Mass Spectrometry. Protein hits were validated using the following criteria based on the number, rank, and score of the assigned peptides to filter and selection the proteins as potential binding partners: 1) False-positive discovery rate (FDR) < 1 %; 2) The protein must be identified in both biological replicates; 3) Cut-off of two peptides in at least one experiment. To ascertain reproducibility, two biological replicates were performed in each system, denoted as experiments A and B.

To filter the proteins that specifically interacted with Grb7 and/or Grb7Δ and not those associated with the IgG or beads in an unspecific manner, we subtracted proteins that were common among Grb7, Grb7Δ and the control lanes.

A list of candidate proteins from the two different approaches was obtained and filtered following the above detailed criteria. **Supplementary Tables 1S-5S** show potential binding partners, unique to Grb7 or Grb7Δ and those shared between Grb7 and Grb7Δ identified in two independent experiments using both the HEK293 and C6 cells stably expressing Grb7 and Grb7Δ. Importantly, Grb7 and Grb7Δ were successfully immunopurified and identified by MS.

6.9.1 Validation by Western blot

As affinity purification from lysates of C6 cells stably expressing EYFP, EYFP-Grb7 or EYFP-Grb7Δ using GFP-Trap®-A system resulted in three clear specific bands detected only in the Grb7 and/or Grb7Δ lanes, we chose from the filtered results the proteins with the highest number of peptides and intensity to be validated by Western blot. Thus, three potential binding partners were chosen: Hsc70 (≈ 70 KDa band) both present in the Grb7 and Grb7Δ

lanes; and caprin-1 (≈ 80 KDa band) and Nedd4 (≈ 100 KDa band) present only in the Grb7 lane as detected by MS.

Hsc70 is an ATP-dependent chaperone that plays critical roles in protein folding and trafficking in the cell (74, 78). As **Fig. 38A** shows, Hsc70 was affinity-purified with Grb7 and Grb7Δ in C6 cells using the GFP-Trap®-A system as determined by Western blot. To demonstrate that this was not an interaction observed only in this cellular system, immunoprecipitation was performed in HEK293 cells stably transfected with FLAG-Grb7 or FLAG-Grb7Δ using the ANTI-FLAG®-M2 Affinity Gel system, and Hsc70 was again identified by Western blot **(Fig. 38B)**. To exclude the possibility that this chaperone could be associated to Grb7 and Grb7Δ because they had been artificially transfected in both cellular systems, we immunoprecipitated Grb7 using the anti-Grb7 (N-20) antibody from human breast adenocarcinoma SK-BR-3 cells that endogenously express Grb7 and observed the positive association of Hsc70 with Grb7 **(Fig. 38C)**.

Caprin-1 is a protein involved in the regulation of the transport and translation of mRNAs of proteins involved cell proliferation and migration (264). The data obtained from MS suggested that caprin-1 was a potential binding partner of Grb7, since caprin-1 peptides were found only in the Grb7 lane. However, when Western blot analysis was performed in the Grb7 and Grb7Δ purified complexes from C6 cells, caprin-1 appeared in the Grb7 and Grb7Δ lanes but not in the control lane **(Fig. 38A)** suggesting that caprin-1 was a Grb7 binding partner independently of the deletion of its CaM-BD. The co-immunoprecipitation of caprin-1 was also validated in HEK293 cells **(Fig. 38B)**.

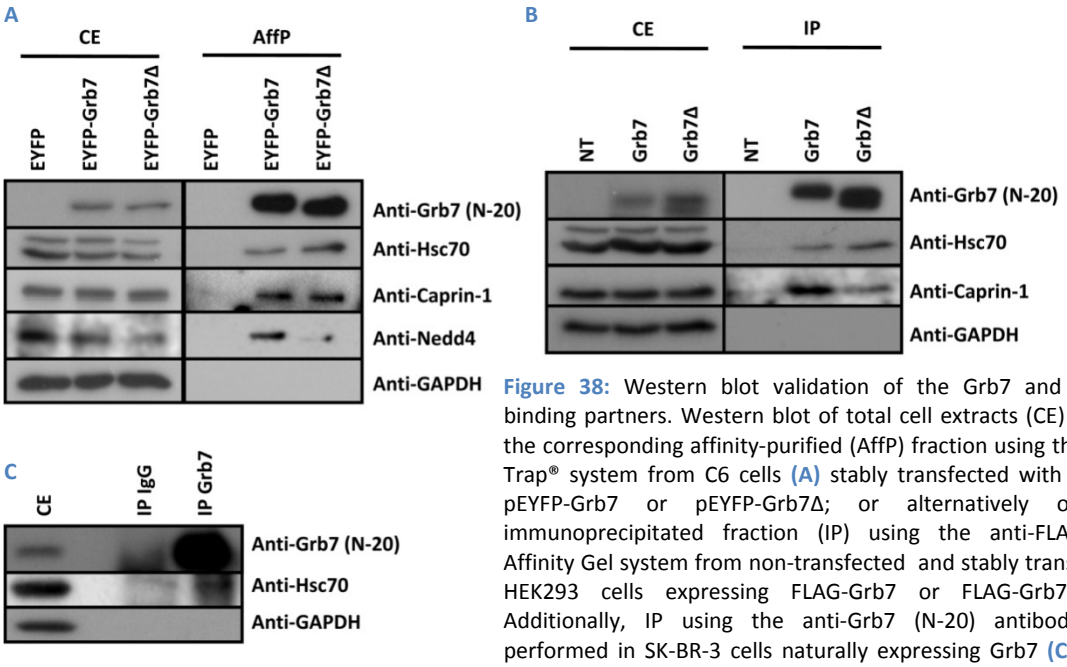

Figure 38: Western blot validation of the Grb7 and Grb7Δ binding partners. Western blot of total cell extracts (CE) and of the corresponding affinity-purified (AffP) fraction using the GFP-Trap® system from C6 cells **(A)** stably transfected with pEYFP, pEYFP-Grb7 or pEYFP-Grb7Δ; or alternatively of the immunoprecipitated fraction (IP) using the anti-FLAG®-M2 Affinity Gel system from non-transfected and stably transfected HEK293 cells expressing FLAG-Grb7 or FLAG-Grb7Δ **(B)**. Additionally, IP using the anti-Grb7 (N-20) antibody was performed in SK-BR-3 cells naturally expressing Grb7 **(C)**. Anti-GAPDH antibody was used as loading controls.

Finally, the Nedd4 protein was validated as a Grb7-associated protein. Nedd4 is an E3 ubiquitin-protein ligase which accepts ubiquitin from an E2 ubiquitin-conjugating enzyme and directly transfers the ubiquitin to target substrates (123). Western blot against Nedd4 was performed on GFP-Trap®-purified lysates of C6 cells stably expressing EYFP, EYFP-Grb7 or EYFP-Grb7Δ. As Fig. 39 shows, Nedd4 was only present in the Grb7 lane, suggesting that the CaM-BD was essential for Nedd4 binding to Grb7. Although the treatment with the CaM inhibitor W-7 did not drastically affect the binding of Nedd4 to Grb7, a slight increase of Nedd4 bound to Grb7 after the treatment with the CaM inhibitor W-7 could be observed suggesting that this interaction could be regulated by CaM (Fig. 39).

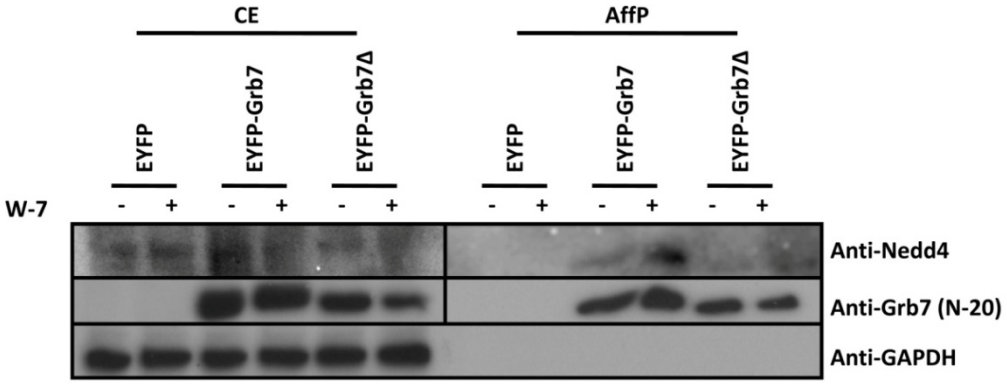

Figure 39: Effect of the calmodulin antagonist W-7 in the binding of Nedd4 to Grb7. Western blots of the total cell extract (CE) and the affinity-purified fraction (AffP) using the GFP-Trap® system from C6 cells stably expressing EYFP, EYFP-Grb7 or EYFP-Grb7Δ treated in the absence (-) or in the presence (+) of the calmodulin antagonist W-7 (30 µM) for 30 min. Anti-GAPDH antibody was used as loading control.

6.9.2 Bioinformatics analysis

To try to organize the potential functional connections between the identified proteins and conceptualized them as binding networks, the potential binding partners of Grb7, Grb7Δ and those shared between them, obtained using both the ANTI-FLAG®-M2 Affinity Gel system or the GFP-Trap®-A system, were analyzed using the STRING database resource, a database of known and predicted protein-protein interactions, which includes direct (physical) and indirect (functional) associations to extract information on potential functional protein clusters where Grb7 could be involved.

Hierarchical clustering provided a statistical approach to identify distinct protein complexes from the large number of proteins that were immuno/affinity-purified and analyzed by MS. Fig. 40 summarizes networks of predicted associations using a standard medium-confidence score of 0.4. Colored lines represent the existence of the seven types of evidence used in predicting the associations. A red line indicates fusion evidence; a green line represents neighborhood evidence; a blue line means co-occurrence evidence; a purple line shows experimental

evidence; a yellow line represents text mining evidence; a light blue line, database evidence; and finally a black line shows co-expression evidence. This representation is a useful way to represent and organize the obtained results. However, we must be extremely cautious in drawing firm conclusions because not all the evidences of interaction have the same strength. As **Fig. 40** shows, the protein network included three major distinct functional clusters: the chaperone cluster centered in Hsc70, whose ATPase activity is inhibited by HSPH1, also denoted as Hsp105 (304), and that has been found associated with HSPA90 forming an active chaperone complex (61) where both DNAJC7 and DNAJA2 act as co-chaperone of HSPA90 (251) **(Fig. 40A)**; the aminoacyl t-RNA synthetases cluster **(Fig. 40B)**; and finally the translational cluster, where translational regulatory proteins and RNA binding proteins were found **(Fig. 40C)**. It is remarkably that Grb7 has been related with translational regulation *(see section 3.1.4.2)* (282, 284), where some of the proteins implicated in translation could participate in stress granule formation *(see section 3.1.4.3)* (285) where chaperones might play a crucial role.

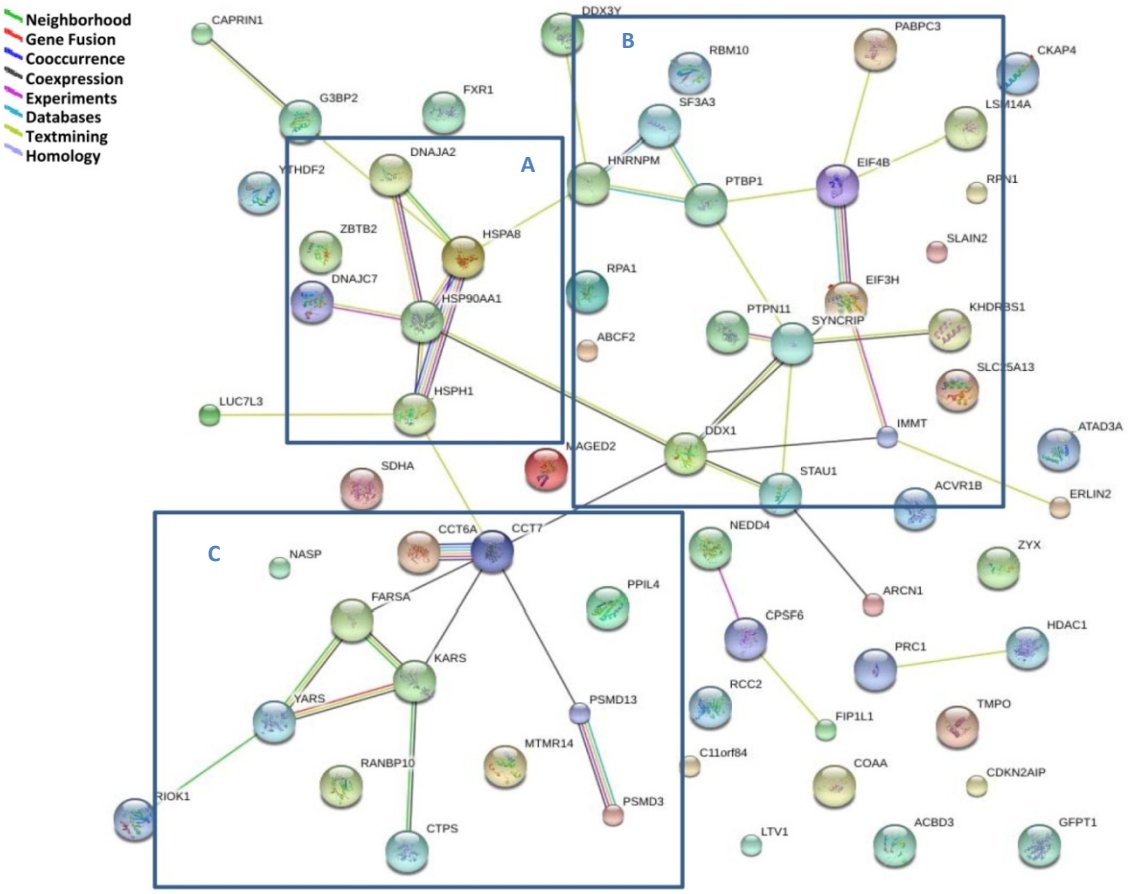

Figure 40: Pathway network from STRING showing proteins potentially associated with Grb7 and/or Grb7Δ in HEK293 and C6 cells. The network map was created with default settings, allowing for experimentally verified and predicted interactions. The three major functional clusters including chaperone-related proteins **(A)**, translational proteins **(B)** and aminoacyl t-RNA synthetases **(C)** are shown. See **Supplementary Table 6S** for a list of the abbreviations of the proteins shown above.

Grb7 and Grb7Δ binding-partners were also sorted according to their functional distribution using gene ontology. Gene ontology mining revealed enrichment for components related to mRNA binding. Other functional classes represented included: translation, transcription, cell cycle regulation and metabolism. To further analyze the data these categories were divided into sub-categories **(Fig. 41)**. It is again remarkable that Grb7 has been implicated in mRNA binding and translation *(see section 3.1.4.2)* (282, 284) and in the control of cell proliferation *(see section 6.6)*.

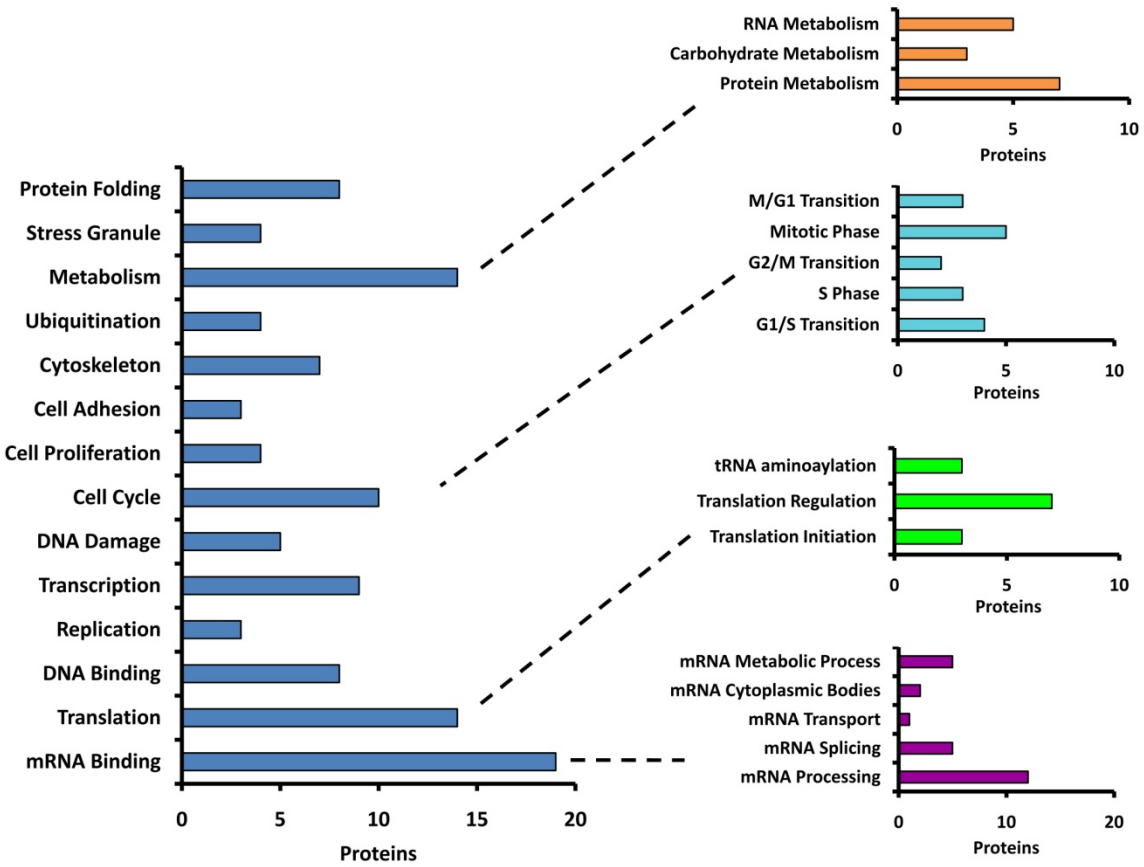

Figure 41: Classification of the potential Grb7/Grb7Δ binding partners identified by MS according to gene annotations obtained from a gene ontology search.

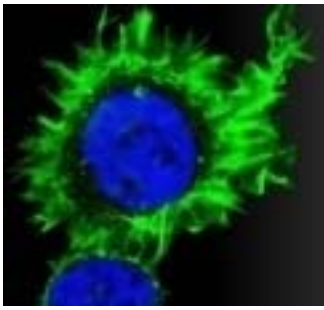

7 DISCUSSION

Grb7 is an adaptor protein that participates in crucial signaling pathways by binding to phospho-tyrosine residues of activated tyrosine kinase receptors, cytosolic tyrosine kinases and other tyrosine-phosphorylated proteins (55, 99, 167, 179, 254, 291). Among the major described roles of Grb7 are promoting cell migration, invasiveness and metastasis in several tumors (45, 98, 100-101, 255) **(Table 2)**. Our laboratory has previously described the ability of CaM to bind to hGrb7 and identified the presence of a CaM-BD located at the proximal region of its PH domain (159). The aim of this Thesis has been to describe the role that the CaM-BD of Grb7 and CaM exert on several cellular functions controlled by Grb7. To do so, we studied the differential behavior *in vitro* and *in vivo* of cells expressing Grb7Δ, a deletion mutant lacking the CaM-BD, as compared to cells expressing either its wild type counterpart or cells lacking expression of this protein.

7.1 The Grb7 protein family are calmodulin-binding proteins

The mammalian Grb7 protein family includes Grb7, Grb10 and Grb14 (38, 55, 99, 162, 167, 179, 193, 236, 254, 291). They all share a conserved structure with high sequence homology (177) **(Fig. 1)**. We have previously described Grb7 as a CaM-BP that binds CaM in a Ca^{2+}-dependent manner both *in vitro* and in living cells (159). We first aimed to test if the other members of the Grb7 family members, Grb10 and Grb14, were also able to interact with CaM. As shown in **Table 1**, *in silico* sequence prediction, showed that Grb10 and Grb14 might contain CaM-BDs homologues to the one in Grb7, comprising the sequences ^{246}KKSWKKLYVCLRRS^{259} in hGrb10β, ^{304}KKSWKKLYVCLRRS^{317} in hGrb10γ and ^{248}KKSWKKIYFFLRRS^{261} in hGrb14. CaM-affinity chromatography showed that both hGrb10γ and hGrb14 were able to bind to CaM in a Ca^{2+}-dependent manner. The fact that Grb10 and Grb14 deletion mutants in these domains did not completely lose their ability to bind CaM suggested the possibility of alternative or additional CaM-BDs present in these proteins. We have run *in silico* CaM-BD prediction and no other amphiphilic α-helix domain was found, nor any potential IQ motif. In contrast to Grb7, where direct interaction with CaM was detected *in vitro* by CaM-overlay experiments and in living cells by FRET (159), we could not discard that Grb10 and/or Grb14 could be pigy-back bound to another CaM-BP during the chromatographic process. To determine whether the proposed sequences had the capacity to bind to CaM, we requested to Prof. J. Haiech (Strasbourg University, France) to determine the affinity of peptides corresponding to the CaM-BDs of hGrb7, hGrb10γ and hGrb14 for CaM. Despite the high homology sequence shown between the three Grb7 protein family members, the affinity of these peptides for CaM was different, being the CaM-BD of Grb7 the one presenting the

highest affinity while the one corresponding to the CaM-BD of Grb10 showed the lowest, suggesting that structural differences might be found in these domains. As it has been previously described, several isoforms of hGrb10, generated by alternative splicing, have been identified, including the hGrb10α, hGrb10β and hGrb10γ (55) *(see section 3.1.3.1)*. They basically differ in their PH domain, where the CaM-BD is located. The hGrb10β and hGrb10γ isoforms show high homology sequence between their putative CaM-BD and the one of hGrb7 **(Table 1)**, whereas, the hGrb10α isoform lacks the segment harboring the sequence corresponding to the CaM-BD present in hGrb10β and hGrb10γ isoforms. Typical CaM-BDs form basic amphiphilic α-helixes (209) with basic and hydrophobic residues exposed in opposite sides of the helix (115) *(see section 3.2.2)*. **Fig. 42** shows the predicted helical projections of the CaM-BDs of hGrb7, hGrb10β/hGrb10γ and hGrb14. Although there is a noticeable segregation of basic and hydrophobic amino acids at opposite sides of all the helixes, the helix corresponding to the CaM-BD of Grb7 is the one showing a more uniform distribution, followed by the one corresponding to the CaM-BD of Grb14 and in lesser extent the one corresponding to the CaM-BD of hGrb10β/hGrb10γ. This suggests that the CaM-BD of Grb7 would be the one presenting more affinity for CaM, followed by the CaM-BDs of Grb14 and Grb10 as our results show. As the different Grb10 isoforms differ in their expression pattern in a cell compartment and tissue-specific manner (26, 202), it would be interesting to study if there is a connection between this differential expression pattern and the effect that CaM could play regulating the isoforms that contain a CaM-BD (hGrb10β, hGrb10γ) in contrast to the hGrb10α isoform lacking this domain.

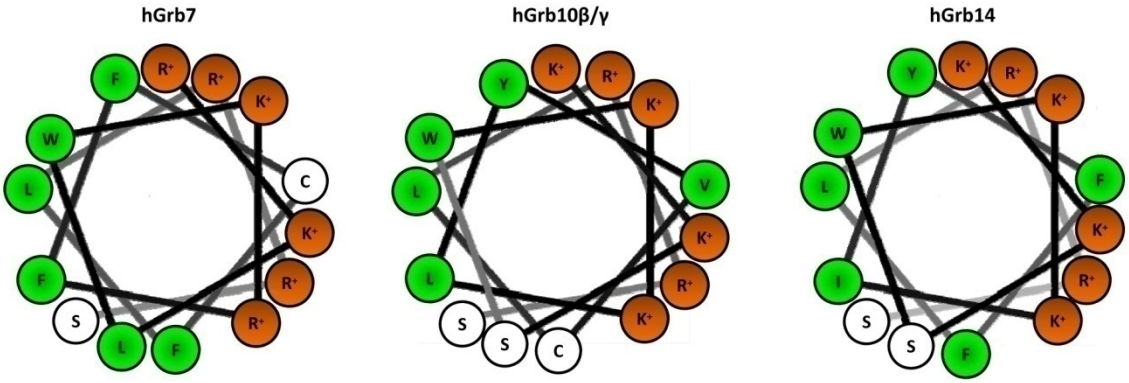

Figure 42: Helical projections of the CaM-BDs of hGrb7, hGrb10β/hGrb10γ and hGrb14. Hydrophobic residues are shown in green, while basic amino acids are shown in orange.

Crystallographic studies of the resolved PH domain of hGrb10β, where the CaM-BD is located, have shown that it is structured as a beta strand within a beta sheet (63) instead of an α-helix. This could be the reason why the affinity of the peptide corresponding to the CaM-BD

of Grb10 shows the lowest affinity for CaM, as compare to the other Grb7 family members. The lack of crystallographic structures of the whole proteins prevents us to establish whether their CaM-BDs form α-helixes or not. As we have previously described *(see section 3.2)* , the minimum number of Ca^{2+} bound to CaM required to induce an effect depends on the target protein and might vary from protein to protein, offering extra regulatory mechanisms (53, 115, 132, 289). We found specific recognition of CaM for the CaM-BD peptides of Grb7, Grb10 and Grb14, when CaM had a single Ca^{2+} bound, suggesting that although the affinity for CaM is different the recognition mechanism appears to be very similar. Nevertheless, in the case of Grb7 the affinity appeared to slightly increase upon binding of the second Ca^{2+} **(Table 4)**. Using an analogous approach, *Dagher et al.* (53), found that a peptide corresponding to the CaM-BD of EGFR, also previously described by our laboratory as a CaM-BP (7, 157-158, 160, 182, 238, 244-245), presented the highest affinity for the Ca^{2+}-CaM complex when 4 Ca^{2+} were bound to CaM (53).

7.2 Grb7Δ presents increased tendency to dimerize

Due to the deletion of the CaM-BD, the electrophoretic mobility of Grb7Δ, as detected by Western blot, was slightly higher than the observed in wild type Grb7. Furthermore, we showed how Grb7Δ exhibited a higher ability to aggregate and to form dimers, observed as a band migrating at approximately double apparent molecular mass than monomeric Grb7, even under the denaturalizing conditions of the SDS-PAGE used. In fact, the presence of aggregates found by confocal microscopy in Grb7Δ-expressing cells could be explained by this higher tendency of Grb7Δ to aggregate. Evidences supporting the existence of multimeric forms of the Grb7 protein family members (Grb7, Grb10 and Grb14) have been previously reported (62, 68, 126, 258, 269). In fact, Grb10 has not only found to dimerize, but also its tetramerization has been demonstrated both *in vitro* and in living cells (68). The specific mechanism of oligomerization is still poorly understood. *Dong et al.* (68) proposed that Grb10 is able to dimerize in a head-to-tail configuration, this is by binding of the PH, BPS and SH2 domains of one monomer with the N-terminal of the other monomer (68). However, the crystal structure of the SH2 domain of Grb10 solved by *Stein et al.* (269) showed that the SH2 domain dimerized forming a tail-to-tail complex. Although normally the SH2 domains do not tend to dimerize, the crystal structure of the SH2 domain found in the Grb7 protein family revealed that the existence of a conserved C-terminal α-helix that favors dimerization (269).

The physiological relevance of this oligomerization has not been elucidated yet; however, several studies support that it could offer an autoinhibitory mechanism. Grb14, a negative

regulator of the IGFR, has been found to increase the affinity for this receptor when it is dimerized through its SH2 domain, resulting in a stronger inhibition (62). Additionally, *Dong et al.* (68) suggested that tetramerized Grb10 failed to interact with phospho-tyrosine-containing peptides due to the steric obstruction offered by the N-terminal sequence. Two models of autoinhibitory dimerization have been proposed to describe the potential oligomerization of Grb7 **(Fig. 43)** (258). In one of them, the SH2 domain interacts with the RA domain of the protein, assisted by the BPS and PH domains and with the SH2 domain of the other Grb7 molecule in a tail-to-tail conformation **(Fig. 43A)**. Alternatively, the SH2 domain of one molecule interacts with the RA domain of another Grb7 molecule, assisted similarly by the BPS and PH domains adopting the dimer a head-to-tail conformation **(Fig. 43B)**. In any event, evidences support that despite the mechanism, the phosphorylation of Grb7 by FAK at tyrosine residues potentially located at the SH2 or PH domains triggers the separation of the Grb7 molecules into active monomers (258).

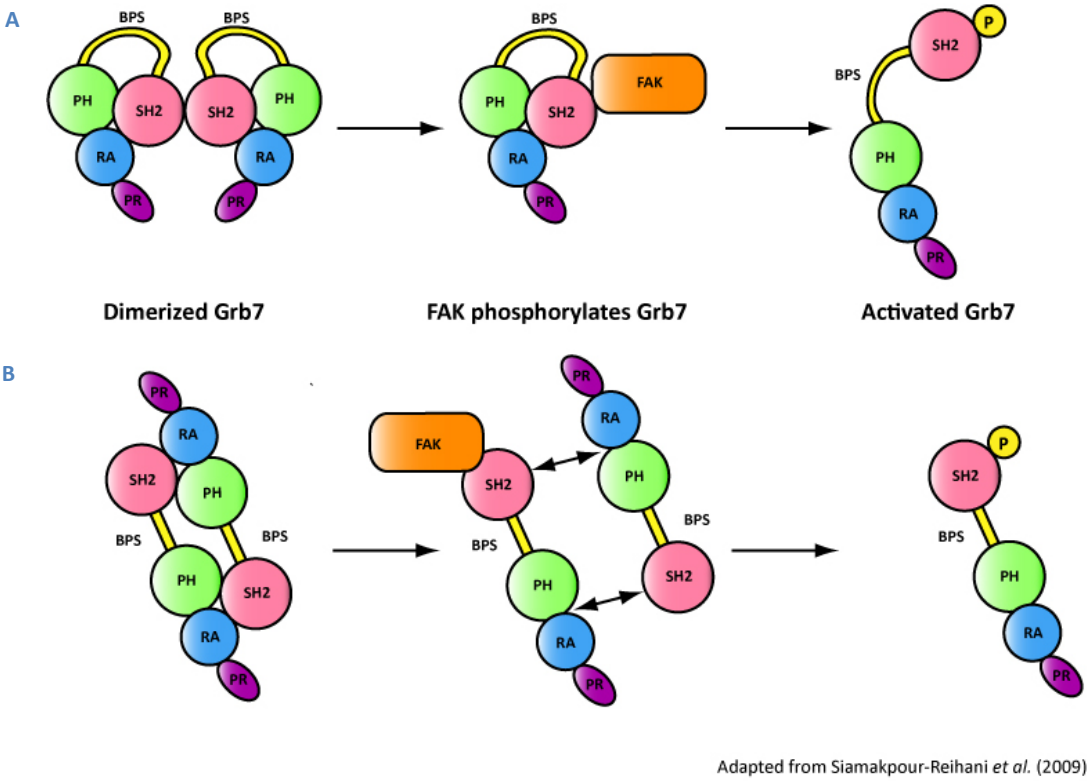

Adapted from Siamakpour-Reihani *et al.* (2009)

Figure 43: Models of the autoinhibitory dimerization of Grb7. **(A)** The SH2 domain interacts with the PH and RA domains of the same molecule and with the SH2 domain of another Grb7 molecule in a tail-to-tail conformation. **(B)** The SH2 domain interacts with the RA and PH domains of another molecule of Grb7 in a head-to-tail conformation. In both models, the phosphorylation of Grb7 by FAK triggers the disassembly of the dimer resulting in an active Grb7 monomer.

It has been shown that the PH domain plays an important role promoting this oligomerization process (68, 258, 269). We have found that deletion of the CaM-BD of Grb7, located in the proximal region of the PH domain, resulted in a higher tendency to dimerize. As

a whole, our results show that the deletion of the CaM-BD of Grb7 led to a loss of function, as compared to the wild type protein. This could, in part, be due to the higher tendency of Grb7Δ to dimerize and consequently to stronger autoinhibition. Besides, deletion of the CaM-BD could lead to an increase of some steric impediment occluding or exposing some phosphorylation sites and preventing or modifying the required access for cross-talk with other signaling proteins.

7.3 Post-translational modifications of Grb7/Grb7Δ

We observed that HEK293 cells stably transfected with Grb7Δ expressed two forms of the protein as detected by Western blot using an antibody recognizing the N-terminal of the protein, in contrast to a single band detected using an antibody recognizing its C-terminal. This phenomenon was observed in two distinct clones (clones 4 and 5). We hypothesized the possibility of a differential post-translational modification process affecting the C-terminal region of the protein occluding the C-terminal epitope. In fact, our lab previously described the existence of two apparent distinct forms of Grb7 naturally occurring in human breast adenocarcinoma SK-BR-3 cells, hinting to the existent of some post-translational modifications affecting Grb7 (159). Our results suggested that the double band could be due at least in part to phosphorylation, since treatment with phosphatases resulted in a decrease of the upper band concomitant with an increase in the lower band **(Fig. 16)**. There is one serine residue located at position 256 that is within the CaM-BD and thus absent in Grb7Δ. However, another serine residue located at position 241 and two tyrosine residues located at positions 259 and 260 are in close proximity to the CaM-BD, and could be affected by its deletion. However, it is of great relevance to highlight that both transient and stable Grb7Δ transfectants, respectively showing a single and a double band, behaved similarly in the performed experiments.

7.4 Role of the calmodulin-binding domain of Grb7 in cell migration

In agreement with the role that the *Caenorhabditis elegans* Mig10 protein, phylogenetically related with Grb7, exerts in promoting neuronal cell migration during embryonic development (177), Grb7 has been reported to play a crucial role in controlling cellular migration signaling pathways, such as the integrin-stimulated FAK activation pathway (45, 98, 100) and the EphB1-ephrin B1 pathway (101). In this work, we aimed to study the effect that the deletion of the CaM-BD could exert on the control of cell migration. Our data demonstrated that this deletion impaired migration, as cells expressing Grb7Δ presented lower migratory rate. The artificial wound healing assays performed on HEK293 cells expressing Grb7 and Grb7Δ, transiently and

stably transfected, as well as similar experiments performed on C6 cells stably transfected with the fluorescent chimeras EYFP-Grb7 or EYFP-Grb7Δ, determined that the cells expressing Grb7Δ/EYFP-Grb7Δ presented a delay in closing the wound. The observed difference between Grb7 and Grb7Δ was higher when the experiments were performed using transient transfected cells, suggesting that the initial overexpression of Grb7 and Grb7Δ occurring in the transient transfectants, led to a stronger effect. Although Grb7 is not endogenously expressed in the HEK293 and C6 cells, we postulated that as Grb7 is an adaptor, its domains might provide docking sites for proteins mediating in cellular migration processes. Thus, the deletion of the CaM-BD could alter the role of Grb7 as adaptor. In fact, the CaM-BD is located in the proximal region of the PH domain that has been described to be important for cell migration, since Grb7 needs to be in close proximity to the membrane to promote migration *(see section 3.1.4.1)* (255). *Shen et al.* (255) described that a single mutation in Arg-239 could impair Grb7-mediated cell migration by preventing Grb7 binding to phosphoinositides. Although the CaM-BD does not harbor Arg-239, our laboratory previously described that Grb7Δ lost in great extent the ability to bind to phosphoinositides (although not totally impaired since it can still bind to phosphatidyl-3-phosphate and phosphatidyl-3,5-bisphosphate) (159), a fact that could explain, at least in part, the observed decrease in cell migration rate. However, we have found that CaM is important for Grb7 to promote cell migration, since the cell permeable CaM antagonists W-13 and W-7 both retarded cell migration in Grb7-expressing cells, but not in Grb7Δ-expressing or non-expressing control cells, suggesting that CaM was essential to promote Grb7-mediated cell migration. The stronger inhibitory effect of W-7 as compared to W-13 could be explained by the apparent higher affinity of W-7 than W-13 for CaM, as determined measuring the inhibition exerted by both antagonists on different CaM-dependent systems (112, 116, 158).

Proliferation can also affect the repopulation rate of the wound, however, our *in vivo* experiments measuring the migration rate of living cells expressing EYFP-Grb7 or EYFP-Grb7Δ by time-lapse confocal fluorescence microscopy, confirmed the poor migration ability of the deletion mutant Grb7Δ. We also estimated the invasive phenotype of cells expressing Grb7 and Grb7Δ using Transwell® assays, widely used to study cell invasiveness (233). We demonstrated that the cells expressing Grb7 presented a high invasive phenotype in contrast to those expressing the CaM-BD deletion mutant Grb7Δ.

Cellular migration is critically dependent on the proper balance between cell attachment and detachment to the extracellular matrix (153). We demonstrated that HEK293 cells expressing Grb7 presented higher detachment ability than non-expressing control cells.

Besides, cells expressing the deletion mutant Grb7Δ were more easily detached from its substrate as compared to those expressing its wild type counterpart.

A successful migratory event not only requires efficient mechanisms to release focal adhesions at the rear of the cell, but also cytoskeletal reorganization to generate new attachment points at the frontal migratory edge (153). After integrin activation by fibronectin it has been described how FAK gets activated triggering phosphorylation of ERK1/2 (among other proteins) resulting in the reorganization of the cytoskeletal fibers (49, 51, 120, 146, 188, 246, 249). It has been previously demonstrated that FAK recruits Grb7 that upon fibronectin stimulation triggers a series of not well defined signaling cascades that end in the promotion of cell migration *(see section 3.1.4.1.1)* (45, 100). We aimed to study the role of the CaM-BD of Grb7 in the proper regulation of this signaling pathway. Our results showed that Grb7Δ-expressing cell presented lower and delayed phosphorylation of ERK1/2 and an altered cytoskeletal reorganization. However, we obtained no significant differences in the phosphorylation levels of FAK, between Grb7- and Grb7Δ-expressing cells. The fact that FAK is working upstream Grb7 in the signaling pathway, suggests that Grb7Δ could be correctly recruited to the signaling complex but in some way the proper transmission of the signal downstream the pathway was blocked.

Moreover, the migration rate is enhanced when the strength of cell adhesion molecules for the matrix is neither too strong nor too weak (95). We hypothesized that as Grb7-expressing cells showed high detachment ability and proper cytoskeleton reorganization they were capable of successful migration. In contrast, cells expressing Grb7Δ presented a higher ability to get detached from its substrate, meaning more labile and/or lower number of attachment points that could not offer enough support for the cell to migrate efficiently, that in conjunction with deficiency in cytoskeleton reorganization results in aborted or defective migration.

7.5 Role of Grb7 and Grb7Δ in cell proliferation

The role of Grb7 in cell proliferation has not been studied as deeply as its role in promoting cell migration. It has been shown, however, that blocking Grb7 function using several approaches, such as siRNA and shRNA silencing (45-46, 136), inhibitory peptides (220) or mutation of Grb7 phosphorylation sites, inhibited the proliferation of tumor and non-tumor cells (45). FAK has not only been related with cell migration but also plays an important role in mediating cell proliferation. Although early reports excluded the participation of Grb7 in FAK-

regulated cell cycle progression (253), more recent studies described that Grb7 is phosphorylated by FAK at Tyr-188 and Tyr-338 and that mutations of these tyrosine residues, result in lower phosphorylation levels of paxillin and ERK1/2, impairing the proliferation capacity of the cells expressing those mutants (45).

We showed that cells expressing Grb7 presented a lower proliferation capacity than non-expressing cells; however, Grb7Δ-expressing cells exhibited an even lower proliferation rate than non-expressing or Grb7-expressing cells. We also observed a decrease of the number of cells in the G_2/M phases when expressing Grb7 or Grb7Δ, underscoring a delay of cell cycle progression. A scheme depicting the control of the cell cycle by Grb7/Grb7Δ is shown in **Fig. 44**. Cell cycle control implies the crosstalk of complex mechanisms and it is mainly regulated by cyclins, proteins of cyclic expression along the cycle that form active complexes with their corresponding CDKs (190, 256). When activated, CDKs induce downstream processes by phosphorylating selected proteins that leads to the correct progression of the cell cycle (130, 191).

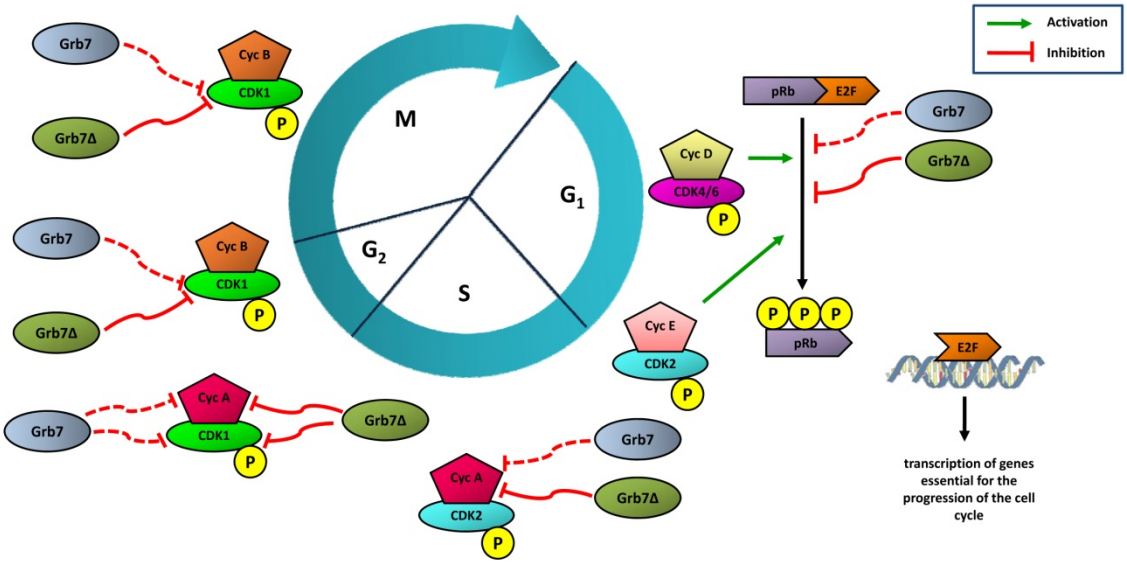

Figure 44: Schematic representation of the control of the cell cycle by Grb7 and Grb7Δ. Progression through the cell cycle is controlled by the activation and subsequent inactivation of the complexes formed by the cyclins (Cyc) and their respective associated cyclin-dependent kinases (CDK)s. To form an active complex the cyclin binds to the CDK that is then activated. The G_1/S transition is controlled by the complex cyclin D-CDK4/6 and cyclin E/CDK2 that sequentially mediates the phosphorylation of the retinoblastoma protein (pRb), releasing the E2F transcription factor that is now able to mediate the transcription of genes needed for the S phase. The S phase, in which the DNA is replicated, is controlled by the cyclin A-CDK2 complex, while the G_2/M transition is manly controlled by the cyclin A/CDK1 and cyclin B/CDK1 complexes. The cyclin B/CDK1 complex also participates in the M phase. The role of Grb7 and Grb7Δ is summarized in the figure. Green lanes mean activation and red lanes denote inhibition (continues lanes mean stronger inhibition while discontinue lanes means weaker inhibition).

A typical cell cycle is divided into several phases (190, 288). Under no growing stimuli, the cell is found quiescent in the G_0 phase. After stimulation with growth factors, the cell proceeds to the G_1 phase, where RNAs and proteins required for the division process are synthesized (190, 288). One of the key components responsible for controlling the initial steps of the cell cycle is the tumor suppressor pRb (16, 86, 300). pRb is sequentially phosphorylated by the cyclin D-CDK4/6 complex in early G_1 (41, 300) and cyclin E-CDK2 in late G_1 (71, 211) at different sites. The non-phosphorylated form of pRb is bound to the transcription factor E2F, repressing the transcription of genes essential for cell cycle progression (16, 86, 300). When the G_1 phase is initiated the cyclin D-CDK4/6 complex phosphorylates pRb causing the release of E2F (41, 300), which then activates the transcription of genes whose function is required for the S phase, including the gene that encodes cyclin E, that forms a complex with CDK2 that also phosphorylates pRb (71, 211) further mediating the transition to the S phase.

We have found that after FBS stimulation, cells expressing Grb7, and in greater extent those expressing Grb7Δ, presented lower levels of phosphorylated pRb in contrast to non-transfected cells, what could explain the observed delay in cell cycle progression and the lower proliferation rate of these cells. These differences could also explain the significant decrease of the number of cells expressing Grb7Δ in S phase as compared to those expressing the wild type Grb7 or non-transfected cells as observed by FACS. However, no significant differences were detected in the expression pattern of cyclin D1 or cyclin E. Besides, no differences in the phosphorylation levels of CDK2, that forms a complex with cyclin E essential for progression to the S phase (190-191), were found.

Once all the required proteins for the duplication of DNA have been produced, the cycle enters in the S phase in which DNA is replicated (190, 288). The transition from the S phase to the G_2 phase is controlled by the cyclin A-CDK2 complex (191). In the G_2 phase occurs the production of the microtubules required during the process of mitosis (190, 288). The G_2/M transition is controlled by cyclin A-CDK1 (191). We found that Grb7-expressing cells, and in greater extent Grb7Δ-expressing cells, presented lower levels of cyclin A concomitant with lower levels of CDK1 phosphorylation at its activating site Thr-161 (60), as compared to non-transfected cells. This resulted in impaired progression to the M phase, what could explain the lower number of Grb7- or Grb7Δ-expressing cells in G_2/M.

There are also two families of inhibitors that block the activity of cyclin-CDK complexes, the CIP/KIP family, including $p21^{Cip1/Waf1}$, $p27^{Kip1}$ and $p57^{Kip2}$ and the Ink4 family, formed by $p15^{Ink4b}$, $p16^{Ink4a}$, $p18^{Ink4c}$ and $p19^{Ink4d}$. The Cip/Kip family inhibits the activity of all cyclin-CDK complexes

formed in the G_1 phase, while the INK4 family only inhibits the activity of the complex formed by cyclin D and CDK4/6 (24, 170, 288). We studied the expression of the main members of these families including $p16^{Ink4a}$, $p19^{Ink4d}$, $p21^{Cip1/Waf1}$ and $p27^{Kip1}$ in Grb7- and Grb7Δ-expressing cells, however not reproducible results were found.

Additionally, several studies show that a proper adhesion to the substrate is essential for the cell to divide correctly (311). In fact, cell adhesion to the extracellular matrix exerts an effect in the expression levels of cyclins and CDKs inhibitors. It has been described that poorly adherent cells fail to phosphorylate pRb and that this effect can be linked to an increased association of the CDK inhibitors, $p21^{Cip1/Waf1}$ and $p27^{Kip1}$ (311). Remarkably, we found lower phospho-pRb levels, in cells expressing Grb7Δ in contrast to those expressing the wild type Grb7 or in non-transfected cells, matching the poor adhesion to the substrate of the Grb7Δ-expressing cells.

Our observations demonstrated that deletion of the CaM-BD in Grb7 decreased the proliferation rate when compared with cells expressing the wild type Grb7. However, cells expressing Grb7 also presented lower proliferation rates than non-transfected control cells suggesting that Grb7 by itself exerted and anti-proliferative effect. As previously described *(see section 3.1.5)*, the *GRB7* gene has been found co-amplified with *ERBB2* in many tumors and has been related with poor prognosis (178, 185, 262-263, 267). Although it is not well understood the mechanisms of Grb7 in tumorigenesis, co-expression of ErbB2 and Grb7 has been reported to promote Akt phosphorylation at both Thr-308 and Ser-473 facilitating tumor growth (12, 243). Thus, a key aspect to be investigated would be to elucidate how Grb7 participates in the ErbB2 signaling pathways in tumor cells and if the deletion of its CaM-BD disrupts the functionality of this receptor.

7.6 The nuclear translocation of Grb7 is regulated by calmodulin

As Grb7 and Grb7Δ appeared to affect cell cycle progression, we aimed to test the nuclear localization of the wild type and the mutant proteins, and found that Grb7, in addition to the cytosol, it was present in the nuclear fraction while its CaM-BD deletion mutant Grb7Δ failed to localize in the nucleus (82). Recent studies have described Grb7 as an mRNA-binding protein (284). In fact, it has been shown that Grb7 is able to act as a constitutive translational repressor of the KOR mRNA via netrin-1 signaling *(see section 3.1.4.2)* (284). What is more, nuclear Grb7 helps in the coordinated exit of the KOR mRNA in an EGF-dependent manner,

forming a nuclear export complex by binding to the target mRNA and other proteins such as HuR and CRM1 **(Fig. 4)** (282); however no mechanism of nuclear import has been proposed.

Nuclear proteins usually harbor a NLS in their sequence that is recognized by the nuclear translocation machinery allowing its entry into the nucleus (169). Several NLS consensus sequences have been identified to date and have been classified into classical and non-classical sequences. Classical NLSs can be subclassified into monopartite NLSs, represented by the NLS of the simian virus 40 (SV40-like) that contains short tandem clusters of basic amino acids with either a proline or glycine in between (PKKKRKV) (134-135); and bipartite NLSs, formed by two clusters of basic amino acids separated by approximately 10 unrelated amino acids, being the NLS of nucleoplasmin KR[PAATKKAGQA]KKKK the main prototype (65, 237). However, not all the experimentally described NLSs match with the above described rules. These are denoted as non-classical NLSs and include the mating type a2-like NLS, comprising short hydrophobic regions separated by one or more unrelated amino acids (KIPIK) (97), or the acidic domain of hnRNP A1 (260) among others. As the deletion mutant failed to localize in the nucleus, we proposed that the CaM-BD of Grb7 comprising the sequence ^{243}RKLWKRFFCFLRRS^{256} was a classical NLS sequence with three clusters of basic amino acids. In fact, a basic amino acidic sequence is a common feature shared by different NLSs and classical amphiphilic α-helices conforming the CaM-BD, and overlapping of both sequences frequently occurs as previously described in **Table 4.** Among these proteins we can find the EGFR that it is able to bind CaM (182) and to translocate into the nucleus (290), the small G protein Kir/Gem with one of its three NLS able to bind CaM (172), the TAP-tag protein (240), the retroviral protein BASP1 (106) and the transcription factors SRY and SOX, that present a highly conserved NLS among the different members of this family (6, 139, 173).

We also studied the role of the SH2 domain in Grb7 nuclear translocation. We described that the splicing variant Grb7V lacking the SH2 domain was able to localize in the nucleus but in lesser extent than Grb7 (82). This suggested that the SH2 domain of Grb7 also plays an important role controlling the translocation to the nucleus. SH2 domains work as docking sites for tyrosine-phosphorylated proteins, and the absence of this domain may impair the binding of phospho(Tyr)proteins that could facilitate Grb7 nuclear import. A similar process has been previously described in the TSAd protein, whose nuclear internalization is facilitated by a tyrosine-phosphorylated protein that binds to the SH2 domain of TSAd (181).

In the literature, the role of CaM controlling nuclear translocation of different proteins has been broadly described (5-6, 139, 172, 259). We have found that inhibition of CaM by the W-7

antagonist caused a massive translocation of Grb7 into the nucleus (82). CaM has also been found to inhibit the nuclear translocation of Kir/Gem (172) and of the transcription factor c-Rel (5). In contrast, the CaM antagonist calmidazolium prevents the nuclear translocation of SOX9 (6) and SRY (139, 259), while CaM antagonists prevents the nuclear localization of $p21^{Cip1/Waf1}$ (277), demonstrating that CaM positively controls the translocation process. We suggest that when CaM is bound to Grb7, it could occlude the NLS preventing its recognition by the nuclear translocation machinery. Hence, CaM acts as regulator of the amount of Grb7 that is imported into the nucleus. Therefore, inhibition of CaM exposes the NLS resulting in an increase localization of Grb7 in the nucleus. However, we cannot discard other possibilities. For instance, phosphorylation of Grb7 by CaMK-II could be blocking the translocation of the protein into the nucleus, as the inhibition of CaM by W-7 inhibits this kinase what could favor Grb7 dephosphorylation allowing its entry into the nucleus. This possibility will be studied in the future in our laboratory.

7.7 Grb7Δ inhibits tumor growth and tumor-associated angiogenesis *in vivo*

Our laboratory previously demonstrated that conditioned media from HEK293T cells transfected with the mutants Grb7Δ or Grb7VΔ presented antiangiogenic activity *in vitro* (159). In this Thesis we aimed to study the role of the CaM-BD of Grb7 in controlling tumor growth and its associated angiogenesis *in vivo* using rat C6 gliomas as a model following its development by MRI.

Our studies performed by MRI showed that tumors generated by C6 cells stably expressing EYFP-Grb7Δ were significantly smaller than those generated by cells expressing EYFP-Grb7 or by control cells expressing EYFP, although the tumors generated by Grb7-expressing cells were smaller than the control. We also measured the ADC of water by MRI. Diffusion MRI is based on the principle that water molecules cannot move in the same way through the different brain structures resulting in different ADCs that can be measured. High ADC values suggest low cellularity, while low ADC values mean high cellularity (155). The obtained results showed that the tumors derived from cells expressing EYFP-Grb7Δ presented on average higher ADC values, and therefore, less cellularity than those generated by cells expressing EYFP-Grb7 or EYFP. These results support our previous observations using MRI and were validated by histological studies.

Gliomas usually display different morphological regions, comprising an infiltration area of tumoral cells in brain tissue, a high density cell region denoted as proliferative area, and a necrotic center in which glomeruloid formations are found (241). Glomeruloid formations are vascular structures, formed by hyperplasic endothelial cells that present an altered morphological structure. Glomeruloid formations have been shown to indicate an aggressive angiogenic phenotype in human cancers (272) and have been found not only in gliomas but also in a wide variety of other malignancies (30). Histological sections showed that this typical morphology was displayed in tumors generated by EYFP-Grb7- and EYFP-expressing cells. However, the tumors derived from EYFP-Grb7Δ-expressing cells presented a smaller and more diffuse proliferative area, supporting the higher ADC values that indicated less cellularity. Besides, no glomeruloid formation was found in the central scar, suggesting that tumors derived from C6 cells expressing EYFP-Grb7Δ were less angiogenic.

To obtain further insight on the angiogenic processes associated to these tumors, we performed bolus-tracking experiments with Magnevist® to determine the CBF CBV and MTT. The results showed that these parameters were significantly lower in tumors generated by EYFP-Grb7Δ-expressing cells in contrast to the tumors generated by EYFP- and EYFP-Grb7-expressing cells, meaning a decrease in tumor-associated vascularization, a fact that was also confirmed by VEGF immunohistochemistry, where blood vessels with smaller diameters were found in the tumors derived from EYFP-Grb7Δ-expressing cells.

Angiogenesis is known to be a crucial process to sustain tumor growth since generation of new blood vessels is essential to supply nutrients to the tumor cells. As we have shown, tumor-associated angiogenesis is greatly impaired in tumors generated by cells expressing EYFP-Grb7Δ, suggesting that the CaM-BD of Grb7 might play an important role in controlling angiogenesis. Further studies on how silencing of Grb7 expression by siRNA or shRNA could affect the angiogenic phenotype of tumors naturally expressing this adaptor protein could open the possibility to use the CaM-BD of this protein as target site for new anti-angiogenic therapies.

7.8 Novel binding-partners of Grb7/Grb7Δ

Grb7, as an adaptor protein mediates signal transduction events in several pathways; however the molecular mechanisms detailing these pathways are poorly understood. The aim of this study was to identify new Grb7 binding partners, and to try to elucidate whether the

deletion of the CaM-BD affects these interactions and the transduction of signals throughout these pathways.

To identify novel Grb7/Grb7Δ binding partners we have combined Grb7/Grb7Δ immunoaffinity purification followed by MS-based protein identification. The whole MS analysis identified with high confidence 3 potential Grb7-binding partners, 42 potential Grb7Δ-binding partners and 22 potential partners shared by Grb7 and Grb7Δ **(Supplementary Table 1S-5S)**. However, we cannot conclude that all the identified proteins were indeed directly bound to Grb7 and/or Grb7Δ or if they were indirectly bound forming protein complexes. Up to date, we have validated by Western blot three candidates: Hsc70, caprin-1 and Nedd4. Further analysis will be done in the future to try to validate the rest of the candidates.

Hsc70 was the first potential candidate validated by Western blot as a Grb7 and Grb7Δ binding partner, using two different cell lines expressing Grb7 or Grb7Δ. Hsc70 is a member of the Hsp70 superfamily of molecular ATP-dependent chaperones (78) that plays critical roles in promoting appropriate folding and traffick of newly synthesized proteins and preventing aggregation of misfolded proteins in the cell (74). We also demonstrated the binding of Hsc70 to Grb7 in SK-BR-3 cells, a human breast adenocarcinoma cell line endogenously expressing Grb7, to discard the possibility that Hsc70 could be bound to Grb7 only because of its abnormal expression in HEK293 and C6 cells.

In contrast to the stress-inducible protein Hsp70, Hsc70 is constitutively expressed in the cell (78). Furthermore, Hsc70 supports the translocation of proteins into their target compartments (212, 257). Although its major described role is that of a general chaperone for unfolded proteins, other roles have been assigned to Hsc70. For instance, Hsc70 has been identified as the uncoating ATPase responsible for removing clathrin from coated vesicles and has also been found phosphorylated in response to DNA damage (102, 192, 204, 250). Although, its expression is not induced under heat shock conditions (57, 78, 164), its nuclear localization has been reported to change under heat or oxidative stresses. In eukaryotic cells, under normal growth conditions, Hsc70 has been found to move in and out of the nucleus. In contrast, when the cell is under stress Hsc70 accumulates in the nucleus (44). Upon recovery of the stress, Hsc70 can exit the nucleus by a poorly understood mechanism (149). We have already described how under stress conditions Grb7, a RNA-binding protein, exerts a major role in assembling and disassembling stress granules *(see section 3.1.4.3)* (285). Besides, under normal conditions, Hsc70 has been described to assist in the nuclear translocation of several proteins, including the SV-40 T-antigen and it has been described how the interference of

Hsc70 abolished the nuclear translocation of various NLS-bearing proteins (121, 212). This could open a new research field since we have described the presence of a NLS in Grb7 and its ability to enter into the nucleus when CaM is not blocking this site (82).

Interestingly, Hsc70 translocates into the nucleus during the early S phase in rat glioma C6 cells, suggesting a role for Hsc70 controlling cell cycle progression through the S phase (308). In addition, specific interactions of Hsc70 with cell cycle and apoptosis regulatory proteins, such as pRb and p53 have been described (83, 96, 207-208). In agreement with these reports and with our observations on the role of Grb7 and Grb7Δ in the cell cycle, it would be interesting to study if there is correlation between the amount of nuclear Grb7 and Hsc70 along the different phases of the cell cycle.

Caprin-1 was identified by MS as a unique binding partner of Grb7; however, co-immunoprecipitation showed that it was equally bound to Grb7 and Grb7Δ in both C6 and HEK293 cells, highlighting the importance of the validation by Western blot of the results obtained by MS. Caprin-1, was first described in T and B lymphocytes because its expression increased when resting lymphocytes were activated to enter into the cell cycle (93). Caprin-1 seems to be essential for a normal progression of the cell cycle through the G_1/S transition since its expression levels increased when resting cells enter in cycle, and decreased when cycling cells ceased to divide (93, 294). Caprin-1 presents several potential phosphorylation sites (93) in its sequence and also two HR domains (HR-1 and HR-2) with RGG motifs for binding to RNA (264). Caprin-1 has been described to localize within mRNPs in brain cells. mRNPs are granules that contain RNA-binding proteins like hnRNP or PABP-1 (264). This latter protein, although not yet validated was also found to be a potential Grb7 and Grb7Δ binding partner by the MS analysis **(Supplementary Table 5S).**

Also, caprin-1 has been found associated with the G3BP-1 GTPase in RNA-containing granules that are localized in the cell migration front. These granules seem to contain mRNAs from proteins required to promote the migration process (264). In addition, it has also been proposed that caprin-1 is contained in similar RNA-granules, structures composed by mRNAs encoding for cell cycle progression proteins. This supports the theory that caprin-1 could be essential for normal cell proliferation. In fact, the caprin-1/G3BP-1 complex has been found selectively bound to mRNAs encoding for c-Myc and cyclin D2 (264). Additionally, under arsenite-induced stress, caprin-1 assembles G3BP-1 leading to stress granules formation in an eIF-2α phosphorylation-dependent process (264). We have previously described the relationship between Grb7 and the assembly/disassembly of stress granules (285) *(see section*

3.1.4.3); however the specific mechanism on how this occurs is still poorly understood. The fact that caprin-1 is able to bind to Grb7, suggests that it also might cooperate with Grb7 in the formation of stress granules. Additional experiments of stress induction could elucidate the functionality of this interaction.

The last validated protein was Nedd4. We have found by MS that Nedd4 was a potential unique binding partner of Grb7. In agreement with this, our results showed that Nedd4 was efficiently co-immunoprecipitated with Grb7 but not with Grb7Δ, suggesting that the CaM-BD of Grb7 was essential for this interaction. A slight increase of Nedd4 bound to Grb7 was found in the presence of the CaM antagonist W-7 suggesting that CaM could regulate Nedd4/Grb7 binding. Nedd4 is an ubiquitin E3 ligase characterized by its modular structure containing an N-terminal C2 domain for Ca^{2+}/lipid and/or protein binding, several WW domains that allows protein-protein interaction with proline-rich PY motifs, and a HECT catalytic domain (123).

Ubiquitination is a protein modification that plays a critical role in controlling cellular homeostasis. The conjugation of ubiquitin to a target protein leads to its degradation by the 26S proteasome, as a way to control diverse processes such as degradation of misfolded and damaged proteins, endocytosis of receptors, or changes in the subcellular localization and degradation of inhibitory or activatory proteins involved in different cellular processes (47, 111). Ubiquitination, consisting in the addition of ubiquitin molecules by reaction between the carboxyl group of the C-terminal glycin residue of ubiquitin and the ε-amino group of lysine residues in the target protein, is catalyzed by a set of three enzymes with different functions denoted as E1, E2 and E3 (47, 111). Nedd4 is an E3 ligase whose role is to recognize the substrate and to promote the interaction between the E2 enzyme, containing ubiquitin, and the substrate. A protein can be monoubiquitylated, monoubiquitylated at different sites, or polyubiquitylated (presenting chains of ubiquitin molecules), and the type of ubiquitylation determines the fate of the protein (47, 111).

Interestingly, Nedd4 has been found to interact with Grb10, another Grb7 family member (194). The interaction of Nedd4 with Grb10 occurs via the C2 domain of Nedd4 and the SH2 domain of Grb10, although the BPS domain seems also to be important for this interaction (194). Due to the high sequence homology between the different members of the Grb7 family, we could hypothesize that the described binding process could be similar in Grb7 and Grb14. It would be interesting to determine whether Grb14 is also able to bind to Nedd4 and if the CaM-BD deletion mutants Grb10Δ and Grb14Δ fail to bind to Nedd4 as it happened with Grb7Δ. Although, *Huang and Szebenyi* (118) claimed that Grb7 and Grb14 were not able to

bind to the C2 domain Nedd4 protein *in vitro*, we have demonstrated, however, that Grb7 was able to bind to the full length Nedd4 suggesting that other domain(s) of the protein might be responsible for this binding.

The binding of Grb10 to Nedd4 has been shown to be essential to promote multiubiquitination, internalization and degradation of the IGF-1R (287). Additionally Grb10 has been reported to inhibit the degradation of VEGFR upon binding to Nedd4 (198). It would be interesting to study if Grb7 behaves similarly. We have previously shown that the Grb7 deletion mutant Grb7Δ presents anti-angiogenic activity. We hypothesized that the inability of Grb7Δ to bind to Nedd4 could result in the recognition of VEGFR by Nedd4 signaling its degradation and resulting in a less angiogenic phenotype. Further experiments should be performed to validate this hypothesis.

Although, the rest of the potential binding partners identified by the MS analysis are yet to be validated, bioinformatics resources are useful tools to draw preliminary conclusions. Gene ontology mining revealed enrichment for mRNA translation and RNA binding proteins among the Grb7/Grb7Δ binding partners. Additionally, we also found a great number of cell cycle-associated proteins, supporting our findings that Grb7/Grb7Δ controls the cell cycle.

The associations described by STRING are derived from different sources, including the genomic context implicating the proteins, experiments, coexpression patterns found in several types of approaches and previous knowledge found in different databases. We must be very careful, however, when making assertions derived from the results offered by this kind of analysis, but hierarchical clustering can provide a statistical approach to direct future studies.

As a summary, in this Thesis we have described the role of the CaM-BD of Grb7 in the control of major cell functions, including cell migration and invasiveness, cell attachment and cytoskeletal reorganization, cell proliferation and cell cycle progression. Furthermore, we preformed *in vivo* analysis of the phenotype of tumors expressing the CaM-BD deletion mutant Grb7Δ and described how its growth and associated angiogenesis were negatively affected by this mutant. We have also characterized new binding partners of Grb7 and/or Grb7Δ to open future work directions. However, many aspects regarding the mechanism of action of Grb7 still remain unsolved. Thus, we hope our results could open the door to get further insights into this enthralling research field.

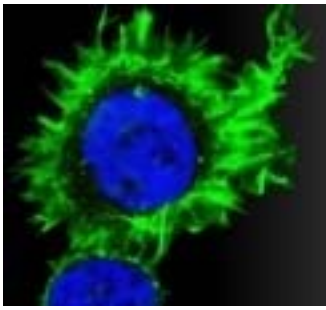

8 CONCLUSSIONS/ CONCLUSIONES

1) The three members of the Grb7 protein family, including Grb7, Grb10 and Grb14 are CaM-BPs. However, their CaM-BDs present different affinities for CaM, following the sequence: Grb7 >> Grb14 > Grb10. A single Ca^{2+} is required for the Ca^{2+}/CaM complex to efficiently bind to the CaM-BDs of these proteins.

2) Cells expressing Grb7Δ present impaired migration and invasiveness ability, underscoring the relevance of the CaM-BD in Grb7-mediated cell migration.

3) Cells expressing Grb7 are easily detached from the substrate; however those expressing Grb7Δ present a higher detachment rate suggesting that a lower number and/or more labile attachment points to the substrate are present.

4) Cells expressing Grb7Δ show a poorer reorganization of the actin cytoskeleton concomitant with lower activation of ERK1/2.

5) Grb7-expressing cells present lower proliferation rate when compared with control non-transfected cells; however this rate is even lower in cells expressing Grb7Δ, suggesting that the CaM-BD plays an important role regulating this process. This decrease in proliferation rate was caused by a slowdown of the cell cycle as a consequence of lower phosphorylation levels of pRb (Ser-780) and CDK1 (Thr-161), and lower expression of cyclin A.

6) The NLS of Grb7 overlaps with its CaM-BD. Besides, the translocation of Grb7 into the nucleus is negatively regulated by CaM.

7) Tumors generated by Grb7Δ-expressing glioma cells are on average smaller than those generated by cells expressing Grb7 or by non-expressing control cells, as shown by MRI imaging and diffusion MRI experiments *in vivo*.

8) Expression of Grb7Δ decreases tumor-associated angiogenesis as detected by perfusion MRI. Besides, the luminal diameters of the tumor-associated blood vessels were smaller on average in tumors generated by cells expressing Grb7Δ.

9) Three new Grb7 binding partners were identified by MS and subsequently validated: Hsc70 and caprin-1 associated to Grb7 and Grb7Δ; and Nedd4, associated exclusively to Grb7, suggesting that the CaM-BD is essential to promote the binding to this protein. Additional potential binding partners of Grb7 and/or Grb7Δ were identified by MS and are yet to be validated.

1) Los tres miembros de la familia de Grb7 (Grb7, Grb10 y Grb14) son proteínas de unión a CaM. Sin embargo, sus CaM-BDs presentan diferente afinidades por CaM, siendo éstas: Grb7 >> Grb14 > Grb10. La unión de un solo Ca^{2+} a la CaM es suficiente para formar un complejo Ca^{2+}/CaM para que se una eficientemente a los CaM-BDs de estas proteínas.

2) Las células que expresan Grb7Δ presentan una deficiente capacidad migratoria e invasiva, poniendo de manifiesto la importancia del CaM-BD en la migración celular mediada por Grb7.

3) Las células que expresan Grb7 se separan fácilmente del sustrato, sin embargo aquellas que expresan Grb7Δ se separan más fácilmente que éstas, sugiriendo la presencia de un menor número y/o más lábiles de puntos de anclaje al substrato.

4) La expresión de Grb7Δ resulta en una reorganización del citoesqueleto defectuosa, que viene acompañada por niveles menores de fosforilación de ERK1/2.

5) Las células que expresan Grb7 proliferan más lentamente que las células control no transfectadas. Sin embargo, la proliferación es incluso menor en células que expresan Grb7Δ, lo que sugiere una implicación del CaM-BD en la regulación de dicho proceso. La disminución de la proliferación celular se debe a un retraso en la progresión del ciclo celular como consecuencia de una menor fosforilación de pRb (Ser-780) y CDK1 (Thr-161) y una menor expresión de ciclina A.

6) LA secuencia de localización nuclear de Grb7 coincide con su CaM-BD. Además la translocación de Grb7 al núcleo está regulada negativamente por CaM.

7) Los tumores generados por células de glioma que expresan Grb7Δ son generalmente más pequeños que los generados por células que expresan Grb7 como se demuestra *in vivo* por técnicas de Imagen de Resonancia Magnética.

8) La expresión de Grb7Δ disminuye la angiogénesis asociada al tumor como se demuestra *in vivo* por técnicas de perfusión en Resonancia Magnética. Además, los diámetros medios del lumen de los vasos sanguíneos en estos tumores son menores en comparación con los tumores generados por células que expresan Grb7 o las células control.

9) Tres nuevas proteínas asociadas a Grb7 fueron identificadas mediante técnicas de Espectrometría de Masas (MS) y posterior validación: Hsc70 y caprin-1 asociadas tanto a Grb7 como a Grb7Δ; y Nedd4 asociada exclusivamente a Grb7, lo que indica que el CaM-BD está implicado en esta asociación. Adicionalmente, otros candidatos potenciales de asociarse con Grb7 y/o Grb7Δ, aún por validar, fueron identificados por MS.

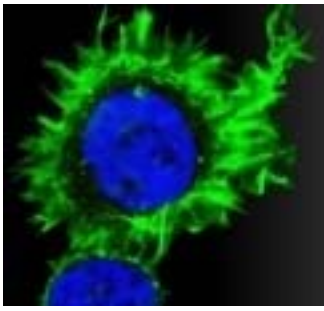

9 REFERENCES

1. **Abdel-Ghany, M., el-Gendy, K., Zhang, S., and Racker, E.** 1990. Control of src kinase activity by activators, inhibitors, and substrate chaperones. Proc Natl Acad Sci USA **87:**7061-7065.
2. **Aebersold, R., and Mann, M.** 2003. Mass spectrometry-based proteomics. Nature **422:**198-207.
3. **Altschul, S. F., Madden, T. L., Schäffer, A. A., Zhang, J., Zhang, Z., Miller, W., and Lipman, D. J.** 1997. Gapped BLAST and PSI-BLAST: a new generation of protein database search programs. Nucleic Acids Res **25:**3389-3402.
4. **Anderson, P., and Kedersha, N.** 2006. RNA granules. J Cell Biol **172:**803-808.
5. **Antonsson, Å., Hughes, K., Edin, S., and Grundström, T.** 2003. Regulation of c-Rel nuclear localization by binding of Ca^{2+}/calmodulin. Mol Cell Biol **23:**1418-1427.
6. **Argentaro, A., Sim, H., Kelly, S., Preiss, S., Clayton, A., Jans, D. A., and Harley, V. R.** 2003. A SOX9 defect of calmodulin-dependent nuclear import in campomelic dysplasia/autosomal sex reversal. J Biol Chem **278:**33839-33847.
7. **Arjona, D., Bello, M. J., Alonso, M. E., González-Gómez, P., Lomas, J., Aminoso, C., López-Marín, I., Isla, A., De Campos, J. M., Vaquero, J., Gutiérrez, M., Villalobo, A., and Rey, J. A.** 2004. Molecular analysis of the *ERBB* gene family calmodulin-binding and calmodulin-like domains in astrocytic gliomas. Int J Oncol **25:**1489-1494.
8. **Aronen, H. J., and Perkio, J.** 2002. Dynamic susceptibility contrast MRI of gliomas. Neuroimag Clin N Am **12:**501-523.
9. **Ashburner, M., Ball, C. A., Blake, J. A., Botstein, D., Butler, H., Cherry, J. M., Davis, A. P., Dolinski, K., Dwight, S. S., Eppig, J. T., Harris, M. A., Hill, D. P., Issel-Tarver, L., Kasarskis, A., Lewis, S., Matese, J. C., Richardson, J. E., Ringwald, M., Rubin, G. M., and Sherlock, G.** 2000. Gene ontology: tool for the unification of biology. The Gene Ontology Consortium. Nat Genet **25:**25-29.
10. **Babu, Y. S., Sack, J. S., Greenhough, T. J., Bugg, C. E., Means, A. R., and Cook, W. J.** 1985. Three-dimensional structure of calmodulin. Nature **315:**37-40.
11. **Bai, R. Y., Jahn, T., Schrem, S., Munzert, G., Weidner, K. M., Wang, J. Y., and Duyster, J.** 1998. The SH2-containing adapter protein GRB10 interacts with BCR-ABL. Oncogene **17:**941-948.
12. **Bai, T., and Luoh, S.-W.** 2008. GRB-7 facilitates HER-2/Neu-mediated signal transduction and tumor formation. Carcinogenesis **29:**473-479.
13. **Baker, E., Sutherland, G. R., Sutherland, R. L., and Daly, R. J.** 1996. Assignment of the human *GRB14* gene to chromosome 2q22-q24 by fluorescence *in situ* hybridization. Genomics **36:**218-220.

14. **Barbier, E. L., Lamalle, L., and Décorps, M.** 2001. Methodology of brain perfusion imaging. J Magn Reson Imaging **13:**496-520.

15. **Bardeesy, N., and DePinho, R. A.** 2002. Pancreatic cancer biology and genetics. Nat Rev Cancer **2:**897-909.

16. **Bartek, J., Bartkova, J., and Lukas, J.** 1996. The retinoblastoma protein pathway and the restriction point. Curr Opin Cell Biol **8:**805-814.

17. **Basso, A. D., Kirschmeier, P., and Bishop, W. R.** 2006. Thematic review series: lipid posttranslational modifications. Farnesyl transferase inhibitors. J Lipid Res **47:**15-31.

18. **Benaim, G., and Villalobo, A.** 2002. Phosphorylation of calmodulin. Functional implications. Eur J Biochem **269:**3619-3631.

19. **Benguría, A., Hernández-Perera, O., Martínez-Pastor, M. T., Sacks, D. B., and Villalobo, A.** 1994. Phosphorylation of calmodulin by the epidermal-growth-factor-receptor tyrosine kinase. Eur J Biochem **224:**909-916.

20. **Benguría, A., Martín-Nieto, J., Benaim, G., and Villalobo, A.** 1995. Regulatory interaction between calmodulin and the epidermal growth factor receptor. Ann N Y Acad Sci **766:**472-476.

21. **Benguría, A., Soriano, M., Joyal, J. L., Sacks, D. B., and Villalobo, A.** 1995. Phosphorylation of calmodulin by plasma-membrane-associated protein kinase(s). Eur J Biochem **234:**50-58.

22. **Bereziat, V., Kasus-Jacobi, A., Perdereau, D., Cariou, B., Girard, J., and Burnol, A. F.** 2002. Inhibition of insulin receptor catalytic activity by the molecular adapter Grb14. J Biol Chem **277:**4845-4852.

23. **Bernstein, J. J., Goldberg, W. J., Laws, E. R., Jr., Conger, D., Morreale, V., and Wood, L. R.** 1990. C6 glioma cell invasion and migration of rat brain after neural homografting: ultrastructure. Neurosurgery **26:**622-628.

24. **Besson, A., Dowdy, S. F., and Roberts, J. M.** 2008. CDK Inhibitors: cell cycle regulators and beyond. Dev Cell **14:**159-169.

25. **Biemann, K.** 1988. Contributions of mass spectrometry to peptide and protein structure. Biomed Environ Mass Spectrom **16:**99-111.

26. **Blagitko, N., Mergenthaler, S., Schulz, U., Wollmann, H. A., Craigen, W., Eggermann, T., Ropers, H.-H., and Kalscheuer, V. M.** 2000. Human *GRB10* is imprinted and expressed from the paternal and maternal allele in a highly tissue- and isoform-specific fashion. Hum Mol Genet **9:**1587-1595.

27. **Bosl, G. J., and Motzer, R. J.** 1997. Testicular germ-cell cancer. N Engl J Med **337:**242-253.

28. **Bradford, M. M.** 1976. A rapid and sensitive method for the quantitation of microgram quantities of protein utilizing the principle of protein-dye binding. Anal Biochem **72:**248-254.

29. **Brantley-Sieders, D. M., and Chen, J.** 2004. Eph receptor tyrosine kinases in angiogenesis: from development to disease. Angiogenesis **7:**17-28.

30. **Brat, D. J., and Van Meir, E. G.** 2001. Glomeruloid microvascular proliferation orchestrated by VPF/VEGF: a new world of angiogenesis research. Am J Pathol **158:**789-796.

31. **Brunberg, J. A., Chenevert, T. L., McKeever, P. E., Ross, D. A., Junck, L. R., Muraszko, K. M., Dauser, R., Pipe, J. G., and Betley, A. T.** 1995. *In vivo* MR determination of water diffusion coefficients and diffusion anisotropy: correlation with structural alteration in gliomas of the cerebral hemispheres. Am J Neuroradiol **16:**361-371.

32. **Buchan, J. R., and Parker, R.** 2009. Eukaryotic stress granules: the ins and outs of translation. Mol Cell **36:**932-941.

33. **Cailliau, K., Le Marcis, V., Béréziat, V., Perdereau, D., Cariou, B., Vilain, J. P., Burnol, A.-F., and Browaeys-Poly, E.** 2003. Inhibition of FGF receptor signalling in *Xenopus* oocytes: differential effect of Grb7, Grb10 and Grb14. FEBS Lett **548:**43-48.

34. **Cammoun, D., Hendee, W. R., and Davis, K. A.** 1985. Clinical applications of magnetic resonance imaging-current status. West J Med **143:**793-803.

35. **Carafoli, E.** 1987. Intracellular calcium homeostasis. Annu Rev Biochem **56:**395-433.

36. **Carafoli, E., Santella, L., Branca, D., and Brini, M.** 2001. Generation, control, and processing of cellular calcium signals. Crit Rev Biochem Mol Biol **36:**107-260.

37. **Caravan, P., Ellison, J. J., McMurry, T. J., and Lauffer, R. B.** 1999. Gadolinium (III) chelates as MRI contrast agents: structure, dynamics, and applications. Chem Rev **99:**2293-2352.

38. **Cariou, B., Bereziat, V., Moncoq, K., Kasus-Jacobi, A., Perdereau, D., Le Marcis, V., and Burnol, A. F.** 2004. Regulation and functional roles of Grb14. Front Biosci **9:**1626-1636.

39. **Chattopadhyaya, R., Meador, W. E., Means, A. R., and Quiocho, F. A.** 1992. Calmodulin structure refined at 1.7 Å resolution. J Mol Biol **228:**1177-1192.

40. **Chen, H. C., and Guan, J. L.** 1994. Stimulation of phosphatidylinositol 3'-kinase association with focal adhesion kinase by platelet-derived growth factor. J Biol Chem **269:**31229-31233.

41. **Chen, P. L., Scully, P., Shew, J. Y., Wang, J. Y., and Lee, W. H.** 1989. Phosphorylation of the retinoblastoma gene product is modulated during the cell cycle and cellular differentiation. Cell **58:**1193-1198.

42. **Chenevert, T. L., and Ross, B. D.** 2009. Diffusion imaging for therapy response assessment of brain tumor. Neuroimag Clin N Am **19:**559-571.

43. **Cho, H. J., Xie, Q. W., Calaycay, J., Mumford, R. A., Swiderek, K. M., Lee, T. D., and Nathan, C.** 1992. Calmodulin is a subunit of nitric oxide synthase from macrophages. J Exp Med **176:**599-604.

44. **Chu, A., Matusiewicz, N., and Stochaj, U.** 2001. Heat-induced nuclear accumulation of hsc70s is regulated by phosphorylation and inhibited in confluent cells. FASEB J **15:**1478-1480.

45. **Chu, P. Y., Huang, L. Y., Hsu, C. H., Liang, C. C., Guan, J. L., Hung, T. H., and Shen, T. L.** 2009. Tyrosine phosphorylation of growth factor receptor-bound protein-7 by focal adhesion kinase in the regulation of cell migration, proliferation, and tumorigenesis. J Biol Chem **284:**20215-20226.

46. **Chu, P. Y., Li, T. K., Ding, S. T., Lai, I. R., and Shen, T. L.** 2010. EGF-induced Grb7 recruits and promotes Ras activity essential for the tumorigenicity of SK-BR-3 breast cancer cells. J Biol Chem **285:**29279-29285.

47. **Ciechanover, A.** 2005. Proteolysis: from the lysosome to ubiquitin and the proteasome. Nat Rev Mol Cell Biol **6:**79-87.

48. **Clapham, D. E.** 2007. Calcium signaling. Cell **131:**1047-1058.

49. **Clark, E., and Brugge, J.** 1995. Integrins and signal transduction pathways: the road taken. Science **268:**233-239.

50. **Cooney, G. J., Lyons, R. J., Crew, A. J., Jensen, T. E., Molero, J. C., Mitchell, C. J., Biden, T. J., Ormandy, C. J., James, D. E., and Daly, R. J.** 2004. Improved glucose homeostasis and enhanced insulin signalling in Grb14-deficient mice. EMBO J **23:**582-593.

51. **Cox, B. D., Natarajan, M., Stettner, M. R., and Gladson, C. L.** 2006. New concepts regarding focal adhesion kinase promotion of cell migration and proliferation. J Cell Biochem **99:**35-52.

52. **Crivici, A., and Ikura, M.** 1995. Molecular and structural basis of target recognition by calmodulin. Annu Rev Biophys Biomol Struct **24:**85-116.

53. **Dagher, R., Peng, S., Gioria, S., Fève, M., Zeniou, M., Zimmermann, M., Pigault, C., Haiech, J., and Kilhoffer, M.-C.** 2011. A general strategy to characterize calmodulin-calcium complexes involved in CaM-target recognition: DAPK and EGFR calmodulin

binding domains interact with different calmodulin-calcium complexes. Biochim Biophys Acta-Mol Cell Res **1813:**1059-1067.

54. **Dahlberg, P. S., Jacobson, B. A., Dahal, G., Fink, J. M., Kratzke, R. A., Maddaus, M. A., and Ferrin, L. J.** 2004. *ERBB2* amplifications in esophageal adenocarcinoma. Ann Thorac Surg **78:**1790-1800.
55. **Daly, R. J.** 1998. The Grb7 family of signalling proteins. Cell Signal **10:**613-618.
56. **Daly, R. J., Sanderson, G. M., Janes, P. W., and Sutherland, R. L.** 1996. Cloning and characterization of *GRB14*, a novel member of the *GRB7* gene family. J Biol Chem **271:**12502-12510.
57. **Daugaard, M., Rohde, M., and Jäättelä, M.** 2007. The heat shock protein 70 family: highly homologous proteins with overlapping and distinct functions. FEBS Lett **581:**3702-3710.
58. **Davis, H. W., Crimmins, D. L., Thoma, R. S., and Garcia, J. G.** 1996. Phosphorylation of calmodulin in the first calcium-binding pocket by myosin light chain kinase. Arch Biochem Biophys **332:**101-109.
59. **Davy, A., and Soriano, P.** 2005. Ephrin signaling *in vivo*: look both ways. Dev Dynam **232:**1-10.
60. **De Smedt, V., Poulhe, R., Cayla, X., Dessauge, F., Karaiskou, A., Jessus, C., and Ozon, R.** 2002. Thr-161 phosphorylation of monomeric cdc2. J Biol Chem **277:**28592-28600.
61. **Demand, J., Luders, J., and Hohfeld, J.** 1998. The carboxy-terminal domain of Hsc70 provides binding sites for a distinct set of chaperone cofactors. Mol Cell Biol **18:**2023-2028.
62. **Depetris, R. S., Hu, J., Gimpelevich, I., Holt, L. J., Daly, R. J., and Hubbard, S. R.** 2005. Structural basis for inhibition of the insulin receptor by the adaptor protein Grb14. Mol Cell **20:**325-333.
63. **Depetris, R. S., Wu, J., and Hubbard, S. R.** 2009. Structural and functional studies of the Ras-associating and pleckstrin-homology domains of Grb10 and Grb14. Nat Struct Mol Biol **16:**833-839.
64. **Dey, B. R., Frick, K., Lopaczynski, W., Nissley, S. P., and Furlanetto, R. W.** 1996. Evidence for the direct interaction of the insulin-like growth factor I receptor with IRS-1, Shc, and Grb10. Mol Endocrinol **10:**631-641.
65. **Dingwall, C., and Laskey, R. A.** 1991. Nuclear targeting sequences - a consensus? Trends Biochem Sci **16:**478-481.
66. **Domon, B., and Aebersold, R.** 2006. Mass spectrometry and protein analysis. Science **312:**212-217.

67. **Dong, L. Q., Du, H., Porter, S. G., Kolakowski, L. F., Jr., Lee, A. V., Mandarino, L. J., Fan, J., Yee, D., and Liu, F.** 1997. Cloning, chromosome localization, expression, and characterization of an Src homology 2 and pleckstrin homology domain-containing insulin receptor binding protein hGrb10γ. J Biol Chem **272:**29104-29112.

68. **Dong, L. Q., Porter, S., Hu, D., and Liu, F.** 1998. Inhibition of hGrb10 binding to the insulin receptor by functional domain-mediated oligomerization. J Biol Chem **273:**17720-17725.

69. **Drum, C. L., Yan, S. Z., Bard, J., Shen, Y. Q., Lu, D., Soelaiman, S., Grabarek, Z., Bohm, A., and Tang, W. J.** 2002. Structural basis for the activation of anthrax adenylyl cyclase exotoxin by calmodulin. Nature **415:**396-402.

70. **Duval, A., Rolland, S., Compoint, A., Tubacher, E., Iacopetta, B., Thomas, G., and Hamelin, R.** 2001. Evolution of instability at coding and non-coding repeat sequences in human MSI-H colorectal cancers. Hum Mol Genet **10:**513-518.

71. **Dynlacht, B. D., Flores, O., Lees, J. A., and Harlow, E.** 1994. Differential regulation of E2F transactivation by cyclin/cdk2 complexes. Genes Dev **8:**1772-1786.

72. **Egea, J., and Klein, R.** 2007. Bidirectional Eph-ephrin signaling during axon guidance. Trends Cell Biol **17:**230-238.

73. **Eggermann, T., Meyer, E., and Wollmann, H. A.** 2004. Quantification of *GRB10* in 7p12-p14 by fluorogenic 5' nuclease chemistry and application for genetic diagnosis in Silver-Russell syndrome. Ann Genet **47:**99-102.

74. **Ellis, R. J., van der Vies, S. M., and Hemmingsen, S. M.** 1989. The molecular chaperone concept. Biochem Soc Symp **55:**145-153.

75. **Fenn, J. B., Mann, M., Meng, C. K., Wong, S. F., and Whitehouse, C. M.** 1989. Electrospray ionization for mass spectrometry of large biomolecules. Science **246:**64-71.

76. **Fiddes, R. J., Campbell, D. H., Janes, P. W., Sivertsen, S. P., Sasaki, H., Wallasch, C., and Daly, R. J.** 1998. Analysis of Grb7 recruitment by heregulin-activated ErbB receptors reveals a novel target selectivity for ErbB3. J Biol Chem **273:**7717-7724.

77. **Flynn, D. C.** 2001. Adaptor proteins. Oncogene **20:**6270-6272.

78. **Forreiter, C., and Nover, L.** 1998. Heat induced stress proteins and the concept of molecular chaperones. J Biosci **23:**287-302.

79. **Frantz, J. D., Giorgetti-Peraldi, S., Ottinger, E. A., and Shoelson, S. E.** 1997. Human GRB-IRβ/GRB10. Splice variants of an insulin and growth factor receptor-binding protein with PH and SH2 domains. J Biol Chem **272:**2659-2667.

80. **Fukami, Y., and Lipmann, F.** 1985. Purification of the Rous sarcoma virus src kinase by casein-agarose and tyrosine-agarose affinity chromatography. Proc Natl Acad Sci USA **82:**321-324.

81. **Gale, N. W., Holland, S. J., Valenzuela, D. M., Flenniken, A., Pan, L., Ryan, T. E., Henkemeyer, M., Strebhardt, K., Hirai, H., Wilkinson, D. G., Pawson, T., Davis, S., and Yancopoulos, G. D.** 1996. Eph receptors and ligands comprise two major specificity subclasses and are reciprocally compartmentalized during embryogenesis. Neuron **17:**9-19.

82. **García-Palmero, I., and Villalobo, A.** 2012. Calmodulin regulates the translocation of Grb7 into the nucleus. FEBS Lett **586:**1533-1539.

83. **Garimella, R., Liu, X., Qiao, W., Liang, X., Zuiderweg, E. R. P., Riley, M. I., and Van Doren, S. R.** 2006. Hsc70 contacts helix III of the J domain from Polyomavirus T antigens: addressing a dilemma in the chaperone hypothesis of how they release E2F from pRb. Biochemistry **45:**6917-6929.

84. **Geiger, B., and Bershadsky, A.** 2001. Assembly and mechanosensory function of focal contacts. Curr Opin Cell Biol **13:**584-592.

85. **Ghosh, S., Nunziato, D. A., and Pitt, G. S.** 2006. KCNQ1 assembly and function is blocked by long-QT syndrome mutations that disrupt interaction with calmodulin. Circul Res **98:**1048-1054.

86. **Giacinti, C., and Giordano, A.** 2006. RB and cell cycle progression. Oncogene **25:**5220-5227.

87. **Gilks, N., Kedersha, N., Ayodele, M., Shen, L., Stoecklin, G., Dember, L. M., and Anderson, P.** 2004. Stress granule assembly is mediated by prion-like aggregation of TIA-1. Mol Biol Cell **15:**5383-5398.

88. **Gingras, A. C., Gstaiger, M., Raught, B., and Aebersold, R.** 2007. Analysis of protein complexes using mass spectrometry. Nat Rev Mol Cell Biol **8:**645-654.

89. **Giorgetti-Peraldi, S., Murdaca, J., Mas, J. C., and Van Obberghen, E.** 2001. The adapter protein, Grb10, is a positive regulator of vascular endothelial growth factor signaling. Oncogene **20:**3959-3968.

90. **Glynn, R. W., Miller, N., and Kerin, M. J.** 2010. 17q12-21 – The pursuit of targeted therapy in breast cancer. Cancer Treat Rev **36:**224-229.

91. **González-Fernández, O., Jiménez, A., and Villalobo, A.** 2008. Differential p38 mitogen-activated protein kinase-controlled hypophosphorylation of the retinoblastoma protein induced by nitric oxide in neuroblastoma cells. Free Radic Biol Med **44:**353-366.

92. **Gossmann, A., Helbich, T. H., Kuriyama, N., Ostrowitzki, S., Roberts, T. P. L., Shames, D. M., van Bruggen, N., Wendland, M. F., Israel, M. A., and Brasch, R. C.** 2002. Dynamic contrast-enhanced magnetic resonance imaging as a surrogate marker of tumor response to anti-angiogenic therapy in a xenograft model of glioblastoma multiforme. J Magn Reson Imaging **15:**233-240.

93. **Grill, B., Wilson, G. M., Zhang, K.-X., Wang, B., Doyonnas, R., Quadroni, M., and Schrader, J. W.** 2004. Activation/division of lymphocytes results in increased levels of cytoplasmic activation/proliferation-associated protein-1: prototype of a new family of proteins. J Immunol **172:**2389-2400.

94. **Grobben, B., De Deyn, P., and Slegers, H.** 2002. Rat C6 glioma as experimental model system for the study of glioblastoma growth and invasion. Cell Tissue Res **310:**257-270.

95. **Gupton, S. L., and Waterman-Storer, C. M.** 2006. Spatiotemporal feedback between actomyosin and focal-adhesion systems optimizes rapid cell migration. Cell **125:**1361-1374.

96. **Hainaut, P., and Milner, J.** 1992. Interaction of heat-shock protein 70 with p53 translated *in vitro*: evidence for interaction with dimeric p53 and for a role in the regulation of p53 conformation. EMBO J **11:**3513-3520.

97. **Hall, M. N., Hereford, L., and Herskowitz, I.** 1984. Targeting of *E. coli* β-galactosidase to the nucleus in yeast. Cell **36:**1057-1065.

98. **Han, D. C., and Guan, J. L.** 1999. Association of focal adhesion kinase with Grb7 and its role in cell migration. J Biol Chem **274:**24425-24430.

99. **Han, D. C., Shen, T. L., and Guan, J. L.** 2001. The Grb7 family proteins: structure, interactions with other signaling molecules and potential cellular functions. Oncogene **20:**6315-6321.

100. **Han, D. C., Shen, T. L., and Guan, J. L.** 2000. Role of Grb7 targeting to focal contacts and Its phosphorylation by focal adhesion kinase in regulation of cell migration. J Biol Chem **275:**28911-28917.

101. **Han, D. C., Shen, T. L., Miao, H., Wang, B., and Guan, J. L.** 2002. EphB1 associates with Grb7 and regulates cell migration. J Biol Chem **277:**45655-45661.

102. **Hannan, L. A., Newmyer, S. L., and Schmid, S. L.** 1998. ATP- and cytosol-dependent release of adaptor proteins from clathrin-coated vesicles: a dual role for Hsc70. Mol Biol Cell **9:**2217-2229.

103. **Hansen, H., Svensson, U., Zhu, J., Laviola, L., Giorgino, F., Wolf, G., Smith, R. J., and Riedel, H.** 1996. Interaction between the Grb10 SH2 domain and the insulin receptor carboxyl terminus. J Biol Chem **271:**8882-8886.

104. **Haran, M., Chebatco, S., Flaishon, L., Lantner, F., Harpaz, N., Valinsky, L., Berrebi, A., and Shachar, I.** 2004. Grb7 expression and cellular migration in chronic lymphocytic leukemia: a comparative study of early and advanced stage disease. Leukemia **18:**1948-1950.

105. **Haring, H. U., White, M. F., Kahn, C. R., Ahmad, Z., DePaoli-Roach, A. A., and Roach, P. J.** 1985. Interaction of the insulin receptor kinase with serine/threonine kinases *in vitro*. J Cell Biochem **28:**171-182.

106. **Hartl, M., Nist, A., Khan, M. I., Valovka, T., and Bister, K.** 2009. Inhibition of Myc-induced cell transformation by brain acid-soluble protein 1 (BASP1). Proc Natl Acad Sci USA **106:**5604-5609.

107. **He, W., Rose, D. W., Olefsky, J. M., and Gustafson, T. A.** 1998. Grb10 interacts differentially with the insulin receptor, insulin-like growth factor I receptor, and epidermal growth factor receptor via the Grb10 Src homology 2 (SH2) domain and a second novel domain located between the pleckstrin homology and SH2 domains. J Biol Chem **273:**6860-6867.

108. **Hendee, W. R., and Morgan, C. J.** 1984. Magnetic resonance imaging. Part I-physical principles. West J Med **141:**491-500.

109. **Hendee, W. R., and Morgan, C. J.** 1984. Magnetic resonance imaging. Part II-clinical applications. West J Med **141:**638-648.

110. **Hendrick, R. E., Nelson, T. R., and Hendee, W. R.** 1984. Optimizing tissue contrast in magnetic resonance imaging. Magn Reson Imaging **2:**193-204.

111. **Hershko, A., and Ciechanover, A.** 1998. The ubiquitin system. Annu Rev Biochem **67:**425-479.

112. **Hidaka, H., and Tanaka, T.** 1983. Naphthalenesulfonamides as calmodulin antagonists. Methods Enzymol **102:**185-194.

113. **Himanen, J. P., Saha, N., and Nikolov, D. B.** 2007. Cell-cell signaling via Eph receptors and ephrins. Curr Opin Cell Biol **19:**534-542.

114. **Hitchins, M. P., Monk, D., Bell, G. M., Ali, Z., Preece, M. A., Stanier, P., and Moore, G. E.** 2001. Maternal repression of the human *GRB10* gene in the developing central nervous system; evaluation of the role for *GRB10* in Silver-Russell syndrome. Eur J Hum Genet **9:**82-90.

115. **Hoeflich, K. P., and Ikura, M.** 2002. Calmodulin in action: diversity in target recognition and activation mechanisms. Cell **108:**739-742.

116. **Hope, W. C., Chen, T., and Morgan, D. W.** 1993. Secretory phospholipase A2 inhibitors and calmodulin antagonists as inhibitors of cytosolic phospholipase A2. Agents Actions **39 Spec No:**C39-C42.

117. **Hoskins, W. J.** 1995. Prospective on ovarian cancer: why prevent? J Cell Biochem **Suppl 23:**189-199.

118. **Huang, Q., and Szebenyi, D. M. E.** 2010. Structural basis for the interaction between the growth factor-binding protein Grb10 and the E3 ubiquitin ligase Nedd4. J Biol Chem **285:**42130-42139.

119. **Hubbard, T., Barker, D., Birney, E., Cameron, G., Chen, Y., Clark, L., Cox, T., Cuff, J., Curwen, V., Down, T., Durbin, R., Eyras, E., Gilbert, J., Hammond, M., Huminiecki, L., Kasprzyk, A., Lehvaslaiho, H., Lijnzaad, P., Melsopp, C., Mongin, E., Pettett, R., Pocock, M., Potter, S., Rust, A., Schmidt, E., Searle, S., Slater, G., Smith, J., Spooner, W., Stabenau, A., Stalker, J., Stupka, E., Ureta-Vidal, A., Vastrik, I., and Clamp, M.** 2002. The Ensembl genome database project. Nucleic Acids Res **30:**38-41.

120. **Hynes, R. O.** 2002. Integrins: bidirectional, allosteric signaling machines. Cell **110:**673-687.

121. **Imamoto, N., Matsuoka, Y., Kurihara, T., Kohno, K., Miyagi, M., Sakiyama, F., Okada, Y., Tsunasawa, S., and Yoneda, Y.** 1992. Antibodies against 70-kD heat shock cognate protein inhibit mediated nuclear import of karyophilic proteins. J Cell Biol **119:**1047-1061.

122. **Imamura, H., Takaishi, K., Nakano, K., Kodama, A., Oishi, H., Shiozaki, H., Monden, M., Sasaki, T., and Takai, Y.** 1998. Rho and Rab small G proteins coordinately reorganize stress fibers and focal adhesions in MDCK cells. Mol Biol Cell **9:**2561-2575.

123. **Ingham, R. J., Gish, G., and Pawson, T.** 2004. The Nedd4 family of E3 ubiquitin ligases: functional diversity within a common modular architecture. Oncogene **23:**1972-1984.

124. **Itoh, S., Taketomi, A., Tanaka, S., Harimoto, N., Yamashita, Y.-i., Aishima, S.-i., Maeda, T., Shirabe, K., Shimada, M., and Maehara, Y.** 2007. Role of growth factor receptor bound protein 7 in hepatocellular carcinoma. Mol Cancer Res **5:**667-673.

125. **Ivancic, M., Daly, R. J., and Lyons, B. A.** 2003. Solution structure of the human Grb7-SH2 domain/ErbB2 peptide complex and structural basis for Grb7 binding to ErbB2. J Biomol NMR **27:**205-219.

126. **Ivancic, M., Spuches, A. M., Guth, E. C., Daugherty, M. A., Wilcox, D. E., and Lyons, B. A.** 2005. Backbone nuclear relaxation characteristics and calorimetric investigation of the human Grb7-SH2/ErbB2 peptide complex. Protein Sci **14:**1556-1569.

127. **James, P., Vorherr, T., and Carafoli, E.** 1995. Calmodulin-binding domains: just two faced or multi-faceted? Trends Biochem Sci **20:**38-42.

128. **Janes, P. W., Lackmann, M., Church, W. B., Sanderson, G. M., Sutherland, R. L., and Daly, R. J.** 1997. Structural determinants of the interaction between the ErbB2 receptor and the Src homology 2 domain of Grb7. J Biol Chem **272:**8490-8497.

129. **Jarrett, H. W., and Madhavan, R.** 1991. Calmodulin-binding proteins also have a calmodulin-like binding site within their structure. The flip-flop model. J Biol Chem **266:**362-371.

130. **Jonathon, P.** 1995. Cyclins, CDKs and cancer. Sem Cancer Biol **6:**63-72.

131. **Jones, N., Master, Z., Jones, J., Bouchard, D., Gunji, Y., Sasaki, H., Daly, R. J., Alitalo, K., and Dumont, D. J.** 1999. Identification of Tek/Tie2 binding partners. Binding to a multifunctional docking site mediates cell survival and migration. J Biol Chem **274:**30896-30905.

132. **Jurado, L. A., Chockalingam, P. S., and Jarrett, H. W.** 1999. Apocalmodulin. Physiol Rev **79:**661-682.

133. **Kairouz, R., Parmar, J., Lyons, R. J., Swarbrick, A., Musgrove, E. A., and Daly, R. J.** 2005. Hormonal regulation of the Grb14 signal modulator and its role in cell cycle progression of MCF-7 human breast cancer cells. J Cell Physiol **203:**85-93.

134. **Kalderon, D., Richardson, W. D., Markham, A. F., and Smith, A. E.** 1984. Sequence requirements for nuclear location of simian virus 40 large-T antigen. Nature **311:**33-38.

135. **Kalderon, D., and Smith, A. E.** 1984. *In vitro* mutagenesis of a putative DNA binding domain of SV40 large-T. Virology **139:**109-137.

136. **Kao, J., and Pollack, J. R.** 2006. RNA interference-based functional dissection of the 17q12 amplicon in breast cancer reveals contribution of coamplified genes. Genes Chromosom Cancer **45:**761-769.

137. **Kasus-Jacobi, A., Bereziat, V., Perdereau, D., Girard, J., and Burnol, A. F.** 2000. Evidence for an interaction between the insulin receptor and Grb7. A role for two of its binding domains, PIR and SH2. Oncogene **19:**2052-2059.

138. **Kasus-Jacobi, A., Perdereau, D., Auzan, C., Clauser, E., Van Obberghen, E., Mauvais-Jarvis, F., Girard, J., and Burnol, A. F.** 1998. Identification of the rat adapter Grb14 as an inhibitor of insulin actions. J Biol Chem **273:**26026-26035.

139. **Kaur, G., Delluc-Clavieres, A., Poon, I. K., Forwood, J. K., Glover, D. J., and Jans, D. A.** 2010. Calmodulin-dependent nuclear import of HMG-box family nuclear factors: importance of the role of SRY in sex reversal. Biochem J **430:**39-48.

140. **Kauraniemi, P., Barlund, M., Monni, O., and Kallioniemi, A.** 2001. New amplified and highly expressed genes discovered in the *ERBB2* amplicon in breast cancer by cDNA microarrays. Cancer Res **61:**8235-8240.

141. **Kauraniemi, P., and Kallioniemi, A.** 2006. Activation of multiple cancer-associated genes at the *ERBB2* amplicon in breast cancer. Endocr Relat Cancer **13:**39-49.

142. **Kauraniemi, P., Kuukasjarvi, T., Sauter, G., and Kallioniemi, A.** 2003. Amplification of a 280-kilobase core region at the *ERBB2* locus leads to activation of two hypothetical proteins in breast cancer. Am J Pathol **163:**1979-1984.

143. **Keegan, K., and Cooper, J. A.** 1996. Use of the two hybrid system to detect the association of the protein-tyrosine-phosphatase, SHPTP2, with another SH2-containing protein, Grb7. Oncogene **12:**1537-1544.

144. **Kimball, S. R., Horetsky, R. L., Ron, D., Jefferson, L. S., and Harding, H. P.** 2003. Mammalian stress granules represent sites of accumulation of stalled translation initiation complexes. Am J Physiol Cell Physiol **284:**C273-C284.

145. **Klee, C. B., and Vanaman, T. C.** 1982. Calmodulin. Adv Protein Chem **35:**213-321.

146. **Klemke, R. L., Cai, S., Giannini, A. L., Gallagher, P. J., de Lanerolle, P., and Cheresh, D. A.** 1997. Regulation of cell motility by mitogen-activated protein kinase. J Cell Biol **137:**481-492.

147. **Knuutila, S., Bjorkqvist, A. M., Autio, K., Tarkkanen, M., Wolf, M., Monni, O., Szymanska, J., Larramendy, M. L., Tapper, J., Pere, H., El-Rifai, W., Hemmer, S., Wasenius, V. M., Vidgren, V., and Zhu, Y.** 1998. DNA copy number amplifications in human neoplasms: review of comparative genomic hybridization studies. Am J Pathol **152:**1107-1123.

148. **Kobayashi, S., Kohda, T., Miyoshi, N., Kuroiwa, Y., Aisaka, K., Tsutsumi, O., Kaneko-Ishino, T., and Ishino, F.** 1997. Human PEG1/MEST, an imprinted gene on chromosome 7. Hum Mol Genet **6:**781-786.

149. **Kodiha, M., Chu, A., Lazrak, O., and Stochaj, U.** 2005. Stress inhibits nucleocytoplasmic shuttling of heat shock protein hsc70. Am J Physiol Cell Physiol **289:**C1034-C1041.

150. **Kuijper, S., Turner, C. J., and Adams, R. H.** 2007. Regulation of angiogenesis by Eph-ephrin interactions. Trends Cardiovas Med **17:**145-151.

151. **Kullander, K., and Klein, R.** 2002. Mechanisms and functions of Eph and ephrin signalling. Nat Rev Mol Cell Biol **3:**475-486.

152. **Laemmli, U. K.** 1970. Cleavage of structural proteins during the assembly of the head of bacteriophage T4. Nature **227:**680-685.

153. **Lauffenburger, D. A., and Horwitz, A. F.** 1996. Cell migration: a physically integrated molecular process. Cell **84:**359-369.

154. **Laviola, L., Giorgino, F., Chow, J. C., Baquero, J. A., Hansen, H., Ooi, J., Zhu, J., Riedel, H., and Smith, R. J.** 1997. The adapter protein Grb10 associates preferentially with the insulin receptor as compared with the IGF-I receptor in mouse fibroblasts. J Clin Invest **99:**830-837.

155. **Le Bihan, D.** 2003. Looking into the functional architecture of the brain with diffusion MRI. Nat Rev Neurosci **4:**469-480.

156. **Lee, H., Volonte, D., Galbiati, F., Iyengar, P., Lublin, D. M., Bregman, D. B., Wilson, M. T., Campos-González, R., Bouzahzah, B., Pestell, R. G., Scherer, P. E., and Lisanti, M. P.** 2000. Constitutive and growth factor-regulated phosphorylation of caveolin-1 occurs at the same site (Tyr-14) *in vivo*: identification of a c-Src/Cav-1/Grb7 signaling cassette. Mol Endocrinol **14:**1750-1775.

157. **Li, H., Panina, S., Kaur, A., Ruano, M. J., Sánchez-González, P., la Cour, J. M., Stephan, A., Olesen, U. H., Berchtold, M. W., and Villalobo, A.** 2012. Regulation of the ligand-dependent activation of the epidermal growth factor receptor by calmodulin. J Biol Chem **287:**3273-3281.

158. **Li, H., Sánchez-Torres, J., Del Carpio, A., Salas, V., and Villalobo, A.** 2004. The ErbB2/Neu/HER2 receptor is a new calmodulin-binding protein. Biochem J **381:**257-266.

159. **Li, H., Sánchez-Torres, J., del Carpio, A. F., Nogales-González, A., Molina-Ortiz, P., Moreno, M. J., Török, K., and Villalobo, A.** 2005. The adaptor Grb7 is a novel calmodulin-binding protein: functional implications of the interaction of calmodulin with Grb7. Oncogene **24:**4206-4219.

160. **Li, H., and Villalobo, A.** 2002. Evidence for the direct interaction between calmodulin and the human epidermal growth factor receptor. Biochem J **362:**499-505.

161. **Li, W., Lee, J., Vikis, H. G., Lee, S. H., Liu, G., Aurandt, J., Shen, T. L., Fearon, E. R., Guan, J. L., Han, M., Rao, Y., Hong, K., and Guan, K. L.** 2004. Activation of FAK and Src are receptor-proximal events required for netrin signaling. Nat Neurosci **7:**1213-1221.

162. **Lim, M. A., Riedel, H., and Liu, F.** 2004. Grb10: more than a simple adaptor protein. Front Biosci **9:**387-403.

163. **Lin, S. Y., Makino, K., Xia, W., Matin, A., Wen, Y., Kwong, K. Y., Bourguignon, L., and Hung, M. C.** 2001. Nuclear localization of EGF receptor and its potential new role as a transcription factor. Nat Cell Biol **3:**802-808.

164. **Lindquist, S., and Craig, E. A.** 1988. The heat-shock proteins. Annu Rev Genet **22:**631-677.

165. **Liu, F., and Roth, R. A.** 1995. Grb-IR: a SH2-domain-containing protein that binds to the insulin receptor and inhibits its function. Proc Natl Acad Sci USA **92:**10287-10291.

166. **Liu, G., Beggs, H., Jurgensen, C., Park, H. T., Tang, H., Gorski, J., Jones, K. R., Reichardt, L. F., Wu, J., and Rao, Y.** 2004. Netrin requires focal adhesion kinase and Src family kinases for axon outgrowth and attraction. Nat Neurosci **7:**1222-1232.

167. **Lucas-Fernández, E., García-Palmero, I., and Villalobo, A.** 2008. Genomic organization and control of the Grb7 gene family. Curr Genomics **9:**60-68.

168. **Lynch, T. J., and Cheung, W. Y.** 1979. Human erythrocyte Ca^{2+}-Mg^{2+}-ATPase: mechanism of stimulation by Ca^{2+}. Arch Biochem Biophys **194:**165-170.

169. **Macara, I. G.** 2001. Transport into and out of the nucleus. Microbiol Mol Biol Res **65:**570-594.

170. **MacLachlan, T. K., Sang, N., and Giordano, A.** 1995. Cyclins, cyclin-dependent kinases and cdk inhibitors: implications in cell cycle control and cancer. Crit Rev Eukaryot Gene **5:**127-156.

171. **Maffucci, T., and Falasca, M.** 2001. Specificity in pleckstrin homology (PH) domain membrane targeting: a role for a phosphoinositide-protein co-operative mechanism. FEBS Lett **506:**173-179.

172. **Mahalakshmi, R. N., Nagashima, K., Ng, M. Y., Inagaki, N., Hunziker, W., and Beguin, P.** 2007. Nuclear transport of Kir/Gem requires specific signals and importin α5 and is regulated by calmodulin and predicted serine phosphorylations. Traffic **8:**1150-1163.

173. **Malki, S., Boizet-Bonhoure, B., and Poulat, F.** 2010. Shuttling of SOX proteins. Int J Biochem Cell Biol **42:**411-416.

174. **Manalan, A. S., and Klee, C. B.** 1987. Affinity selection of chemically modified proteins: role of lysyl residues in the binding of calmodulin to calcineurin. Biochemistry **26:**1382-1390.

175. **Mano, H., Ohya, K., Miyazato, A., Yamashita, Y., Ogawa, W., Inazawa, J., Ikeda, U., Shimada, K., Hatake, K., Kasuga, M., Ozawa, K., and Kajigaya, S.** 1998. Grb10/GrbIR as an *in vivo* substrate of Tec tyrosine kinase. Genes Cells **3:**431-441.

176. **Manser, J., Roonprapunt, C., and Margolis, B.** 1997. *C. elegans* cell migration gene mig-10 shares similarities with a family of SH2 domain proteins and acts cell nonautonomously in excretory canal development. Dev Biol **184:**150-164.

177. **Manser, J., and Wood, W. B.** 1990. Mutations affecting embryonic cell migrations in *Caenorhabditis elegans*. Dev Genet **11:**49-64.

178. **Maqani, N., Belkhiri, A., Moskaluk, C., Knuutila, S., Dar, A. A., and El-Rifai, W.** 2006. Molecular dissection of 17q12 amplicon in upper gastrointestinal adenocarcinomas. Mol Cancer Res **4:**449-455.

179. **Margolis, B.** 1994. The GRB family of SH2 domain proteins. Prog Biophys Mol Biol **62:**223-244.

180. **Margolis, B., Silvennoinen, O., Comoglio, F., Roonprapunt, C., Skolnik, E., Ullrich, A., and Schlessinger, J.** 1992. High-efficiency expression/cloning of epidermal growth factor-receptor-binding proteins with Src homology 2 domains. Proc Natl Acad Sci USA **89:**8894-8898.

181. **Marti, F., and King, P. D.** 2005. The p95-100 kDa ligand of the T cell-specific adaptor (TSAd) protein Src-homology-2 (SH2) domain implicated in TSAd nuclear import is p97 valosin-containing protein (VCP). Immunol Lett **97:**235-243.

182. **Martín-Nieto, J., and Villalobo, A.** 1998. The human epidermal growth factor receptor contains a juxtamembrane calmodulin-binding site. Biochemistry **37:**227-236.

183. **Maurer-Stroh, S., and Eisenhaber, F.** 2005. Refinement and prediction of protein prenylation motifs. Genome Biol **6:**R55.

184. **McHugh, L., and Arthur, J. W.** 2008. Computational methods for protein identification from mass spectrometry data. PLoS Comput Biol **4:**e12.

185. **McIntyre, A., Summersgill, B., Jafer, O., Rodriguez, S., Zafarana, G., Oosterhuis, J. W., Gillis, A. J., Looijenga, L., Cooper, C., Huddart, R., Clark, J., and Shipley, J.** 2004. Defining minimum genomic regions of imbalance involved in testicular germ cell tumors of adolescents and adults through genome wide microarray analysis of cDNA clones. Oncogene **23:**9142-9147.

186. **McIntyre, A., Summersgill, B., Spendlove, H. E., Huddart, R., Houlston, R., and Shipley, J.** 2005. Activating mutations and/or expression levels of tyrosine kinase receptors *GRB7*, *RAS*, and *BRAF* in testicular germ cell tumors. Neoplasia **7:**1047-1052.

187. **Meggio, F., Brunati, A. M., and Pinna, L. A.** 1987. Polycation-dependent, Ca^{2+}-antagonized phosphorylation of calmodulin by casein kinase-2 and a spleen tyrosine protein kinase. FEBS Lett **215:**241-246.

188. **Mitra, S. K., Hanson, D. A., and Schlaepfer, D. D.** 2005. Focal adhesion kinase: in command and control of cell motility. Nat Rev Mol Cell Biol **6:**56-68.

189. **Moncoq, K., Broutin, I., Larue, V., Perdereau, D., Cailliau, K., Browaeys-Poly, E., Burnol, A. F., and Ducruix, A.** 2003. The PIR domain of Grb14 is an intrinsically unstructured protein: implication in insulin signaling. FEBS Lett **554:**240-246.

190. **Morgan, D. O.** 2007. The cell cycle, principles of control. Integr Comp Biol **47:**794-795.

191. **Morgan, D. O.** 1995. Principles of CDK regulation. Nature **374:**131-134.

192. **Morgan, J. R., Prasad, K., Jin, S., Augustine, G. J., and Lafer, E. M.** 2001. Uncoating of clathrin-coated vesicles in presynaptic terminals: roles for Hsc70 and auxilin. Neuron **32:**289-300.

193. **Morrione, A.** 2003. Grb10 adapter protein as regulator of insulin-like growth factor receptor signaling. J Cell Physiol **197:**307-311.

194. **Morrione, A., Plant, P., Valentinis, B., Staub, O., Kumar, S., Rotin, D., and Baserga, R.** 1999. mGrb10 interacts with Nedd4. J Biol Chem **274:**24094-24099.

195. **Morrione, A., Valentinis, B., Li, S., Ooi, J. Y., Margolis, B., and Baserga, R.** 1996. Grb10: A new substrate of the insulin-like growth factor I receptor. Cancer Res **56:**3165-3167.

196. **Mounier, C., Lavoie, L., Dumas, V., Mohammad-Ali, K., Wu, J., Nantel, A., Bergeron, J. J. M., Thomas, D. Y., and I. Posner, B.** 2001. Specific inhibition by hGRB10ζ of insulin-induced glycogen synthase activation: evidence for a novel signaling pathway. Mol Cell Endocrinol **173:**15-27.

197. **Moutoussamy, S., Renaudie, F., Lago, F., Kelly, P. A., and Finidori, J.** 1998. Grb10 identified as a potential regulator of growth hormone (GH) signaling by cloning of GH receptor target proteins. J Biol Chem **273:**15906-15912.

198. **Murdaca, J., Treins, C., Monthouël-Kartmann, M.-N., Pontier-Bres, R., Kumar, S., Van Obberghen, E., and Giorgetti-Peraldi, S.** 2004. Grb10 prevents Nedd4-mediated vascular endothelial growth factor receptor-2 degradation. J Biol Chem **279:**26754-26761.

199. **Murtaugh, T. J., Wright, L. S., and Siegel, F. L.** 1986. Posttranslational modification of calmodulin in rat brain and pituitary. J Neurochem **47:**164-172.

200. **Myllykangas, S., Junnila, S., Kokkola, A., Autio, R., Scheinin, I., Kiviluoto, T., Karjalainen-Lindsberg, M. L., Hollmen, J., Knuutila, S., Puolakkainen, P., and Monni, O.** 2008. Integrated gene copy number and expression microarray analysis of gastric cancer highlights potential target genes. Int J Cancer **123:**817-825.

201. **Nakajo, S., Hayashi, K., Daimatsu, T., Tanaka, M., Nakaya, K., and Nakamura, Y.** 1986. Phosphorylation of rat brain calmodulin *in vivo* and *in vitro*. Biochem Int **13:**687-693.

202. **Nantel, A., Huber, M., and Thomas, D. Y.** 1999. Localization of endogenous Grb10 to the mitochondria and its interaction with the mitochondrial-associated Raf-1 pool. J Biol Chem **274:**35719-35724.

203. **Nantel, A., Mohammad-Ali, K., Sherk, J., Posner, B. I., and Thomas, D. Y.** 1998. Interaction of the Grb10 adapter protein with the Raf1 and MEK1 kinases. J Biol Chem **273:**10475-10484.

204. **Newmyer, S. L., and Schmid, S. L.** 2001. Dominant-interfering Hsc70 mutants disrupt multiple stages of the clathrin-coated vesicle cycle *in vivo*. J Cell Biol **152:**607-620.

205. **Niggli, V., Penniston, J. T., and Carafoli, E.** 1979. Purification of the (Ca^{2+}-Mg^{2+})-ATPase from human erythrocyte membranes using a calmodulin affinity column. J Biol Chem **254:**9955-9958.

206. **Niggli, V., Ronner, P., Carafoli, E., and Penniston, J. T.** 1979. Effects of calmodulin on the (Ca^{2+} and Mg^{2+})ATPase partially purified from erythrocyte membranes. Arch Biochem Biophys **198:**124-130.

207. **Nihei, T., Sato, N., Takahashi, S., Ishikawa, M., Sagae, S., Kudo, R., Kikuchi, K., and Inoue, A.** 1993. Demonstration of selective protein complexes of p53 with 73 kDa heat shock cognate protein, but not with 72 kDa heat shock protein in human tumor cells. Cancer Lett **73:**181-189.

208. **Nihei, T., Takahashi, S., Sagae, S., Sato, N., and Kikuchi, K.** 1993. Protein interaction of retinoblastoma gene product pRb110 with M(r) 73,000 heat shock cognate protein. Cancer Res **53:**1702-1705.

209. **O'Neil, K. T., and DeGrado, W. F.** 1990. How calmodulin binds its targets: sequence independent recognition of amphiphilic α-helices. Trends Biochem Sci **15:**59-64.

210. **O'Neill, T. J., Rose, D. W., Pillay, T. S., Hotta, K., Olefsky, J. M., and Gustafson, T. A.** 1996. Interaction of a GRB-IR splice variant (a human GRB10 homolog) with the insulin and insulin-like growth factor I receptors. Evidence for a role in mitogenic signaling. J Biol Chem **271:**22506-22513.

211. **Ohtani, K., DeGregori, J., and Nevins, J. R.** 1995. Regulation of the cyclin E gene by transcription factor E2F1. Proc Natl Acad Sci USA **92:**12146-12150.

212. **Okuno, Y., Imamoto, N., and Yoneda, Y.** 1993. 70-kDa heat-shock cognate protein colocalizes with karyophilic proteins into the nucleus during their transport *in vitro*. Exp Cell Res **206:**134-142.

213. **Ooi, J., Yajnik, V., Immanuel, D., Gordon, M., Moskow, J. J., Buchberg, A. M., and Margolis, B.** 1995. The cloning of Grb10 reveals a new family of SH2 domain proteins. Oncogene **10:**1621-1630.

214. **Østergaard, L.** 2004. Cerebral perfusion imaging by bolus tracking. Top Magn Reson Imaging **15:**3-9.

215. **Østergaard, L.** 2005. Principles of cerebral perfusion imaging by bolus tracking. J Magn Reson Imaging **22:**710-717.

216. **Østergaard, L., Weisskoff, R. M., Chesler, D. A., Gyldensted, C., and Rosen, B. R.** 1996. High resolution measurement of cerebral blood flow using intravascular tracer bolus passages. Part I: Mathematical approach and statistical analysis. Magn Reson Med **36:**715-725.

217. **Pagani, E., Bizzi, A., Di Salle, F., De Stefano, N., and Filippi, M.** 2008. Basic concepts of advanced MRI techniques. Neuro Sci **29:**290-295.

218. **Pandey, A., Liu, X., Dixon, J. E., Di Fiore, P. P., and Dixit, V. M.** 1996. Direct association between the Ret receptor tyrosine kinase and the Src homology 2-containing adapter protein Grb7. J Biol Chem **271:**10607-10610.

219. **Panina, S., Stephan, A., la Cour, J. M., Jacobsen, K., Kallerup, L. K., Bumbuleviciute, R., Knudsen, K. V., Sánchez-González, P., Villalobo, A., Olesen, U. H., and Berchtold, M. W.** 2012. Significance of calcium binding, tyrosine phosphorylation, and lysine trimethylation for the essential function of calmodulin in vertebrate cells analyzed in a novel gene replacement system. J Biol Chem **287:**18173-18181.

220. **Pero, S. C., Shukla, G. S., Cookson, M. M., Flemer, S., Jr., and Krag, D. N.** 2007. Combination treatment with Grb7 peptide and doxorubicin or trastuzumab (herceptin) results in cooperative cell growth inhibition in breast cancer cells. Br J Cancer **96:**1520-1525.

221. **Phizicky, E. M., and Fields, S.** 1995. Protein-protein interactions: methods for detection and analysis. Microbiol Rev **59:**94-123.

222. **Plancke, Y. D., and Lazarides, E.** 1983. Evidence for a phosphorylated form of calmodulin in chicken brain and muscle. Mol Cell Biol **3:**1412-1420.

223. **Poliakov, A., Cotrina, M., and Wilkinson, D. G.** 2004. Diverse roles of Eph receptors and ephrins in the regulation of cell migration and tissue assembly. Dev Cell **7:**465-480.

224. **Porter, C. J., Matthews, J. M., Mackay, J. P., Pursglove, S. E., Schmidberger, J. W., Leedman, P. J., Pero, S. C., Krag, D. N., Wilce, M. C., and Wilce, J. A.** 2007. Grb7 SH2 domain structure and interactions with a cyclic peptide inhibitor of cancer cell migration and proliferation. BMC Struct Biol **7:**58-73.

225. **Porter, C. J., and Wilce, J. A.** 2007. NMR analysis of G7-18NATE, a nonphosphorylated cyclic peptide inhibitor of the Grb7 adapter protein. Biopolymers **88:**174-181.

226. **Radivojac, P., Vacic, V., Haynes, C., Cocklin, R. R., Mohan, A., Heyen, J. W., Goebl, M. G., and Iakoucheva, L. M.** 2010. Identification, analysis, and prediction of protein ubiquitination sites. Proteins **78:**365-380.

227. **Ramos, F. J., Langlais, P. R., Hu, D., Dong, L. Q., and Liu, F.** 2006. Grb10 mediates insulin-stimulated degradation of the insulin receptor: a mechanism of negative regulation. Am J Physiol Endocrinol Metab **290:**E1262-E1266.

228. **Ramsey, B., Bai, T., Hanlon Newell, A., Troxell, M., Park, B., Olson, S., Keenan, E., and Luoh, S.-W.** 2011. GRB7 protein over-expression and clinical outcome in breast cancer. Breast Cancer Res Treat **127:**659-669.

229. **Rao, S. T., Wu, S., Satyshur, K. A., Ling, K. Y., Kung, C., and Sundaralingam, M.** 1993. Structure of *Paramecium tetraurelia* calmodulin at 1.8 Å resolution. Protein Sci **2:**436-447.

230. **Rasband, W. S.** 1997-2011. http://imagej.nih.gov/ij/.

231. **Reiske, H. R., Kao, S. C., Cary, L. A., Guan, J. L., Lai, J. F., and Chen, H. C.** 1999. Requirement of phosphatidylinositol 3-kinase in focal adhesion kinase-promoted cell migration. J Biol Chem **274:**12361-12366.

232. **Ren, X. R., Ming, G. L., Xie, Y., Hong, Y., Sun, D. M., Zhao, Z. Q., Feng, Z., Wang, Q., Shim, S., Chen, Z. F., Song, H. J., Mei, L., and Xiong, W. C.** 2004. Focal adhesion kinase in netrin-1 signaling. Nat Neurosci **7:**1204-1212.

233. **Repesh, L. A.** 1989. A new *in vitro* assay for quantitating tumor cell invasion. Inv Metast **9:**192-208.

234. **Rhoads, A. R., and Friedberg, F.** 1997. Sequence motifs for calmodulin recognition. FASEB J **11:**331-340.

235. **Rice, N. A., Nadeau, O. W., Yang, Q., and Carlson, G. M.** 2002. The calmodulin-binding domain of the catalytic γ subunit of phosphorylase kinase interacts with its inhibitory α subunit: evidence for a Ca^{2+} sensitive network of quaternary interactions. J Biol Chem **277:**14681-14687.

236. **Riedel, H.** 2004. Grb10 exceeding the boundaries of a common signaling adapter. Front Biosci **9:**603-618.

237. **Robbins, J., Dilworth, S. M., Laskey, R. A., and Dingwall, C.** 1991. Two interdependent basic domains in nucleoplasmin nuclear targeting sequence: identification of a class of bipartite nuclear targeting sequence. Cell **64:**615-623.

238. **Rodríguez-Viciana, P., Sabatier, C., and McCormick, F.** 2004. Signaling specificity by Ras family GTPases is determined by the full spectrum of effectors they regulate. Mol Cell Biol **24:**4943-4954.

239. **Rodríguez, S., Jafer, O., Goker, H., Summersgill, B. M., Zafarana, G., Gillis, A. J., van Gurp, R. J., Oosterhuis, J. W., Lu, Y. J., Huddart, R., Cooper, C. S., Clark, J., Looijenga, L. H., and Shipley, J. M.** 2003. Expression profile of genes from 12p in testicular germ

cell tumors of adolescents and adults associated with i(12p) and amplification at 12p11.2-p12.1. Oncogene **22:**1880-1891.

240. **Rohila, J. S., Chen, M., Cerny, R., and Fromm, M. E.** 2004. Improved tandem affinity purification tag and methods for isolation of protein heterocomplexes from plants. Plant J **38:**172-181.

241. **Rojiani, A. M., and Dorovini-Zis, K.** 1996. Glomeruloid vascular structures in glioblastoma multiforme: an immunohistochemical and ultrastructural study. J Neurosurgery **85:**1078-1084.

242. **Ross, B. D., Zhao, Y. J., Neal, E. R., Stegman, L. D., Ercolani, M., Ben-Yoseph, O., and Chenevert, T. L.** 1998. Contributions of cell kill and posttreatment tumor growth rates to the repopulation of intracerebral 9L tumors after chemotherapy: an MRI study. Proc Natl Acad Sci USA **95:**7012-7017.

243. **Saito, M., Kato, Y., Ito, E., Fujimoto, J., Ishikawa, K., Doi, A., Kumazawa, K., Matsui, A., Takebe, S., Ishida, T., Azuma, S., Mochizuki, H., Kawamura, Y., Yanagisawa, Y., Honma, R., Imai, J.-i., Ohbayashi, H., Goshima, N., Semba, K., and Watanabe, S.** 2012. Expression screening of 17q12–21 amplicon reveals *GRB7* as an *ERBB2*-dependent oncogene. FEBS Lett**:**doi: 10.1016/j.febslet.2012.1005.1003.

244. **Salas, V., Sánchez-Torres, J., Cusidó-Hita, D. M., García-Marchán, Y., Sojo, F., Benaim, G., and Villalobo, A.** 2005. Characterisation of tyrosine-phosphorylation-defective calmodulin mutants. Protein Expr Purif **41:**384-392.

245. **Sánchez-González, P., Jellali, K., and Villalobo, A.** 2010. Calmodulin-mediated regulation of the epidermal growth factor receptor. FEBS J **277:**327-342.

246. **Schaller, M. D., Borgman, C. A., Cobb, B. S., Vines, R. R., Reynolds, A. B., and Parsons, J. T.** 1992. pp125FAK, a structurally distinctive protein-tyrosine kinase associated with focal adhesions. Cell Biol **89:**5192-5197.

247. **Scharf, P. J., Witney, J., Daly, R., and Lyons, B. A.** 2004. Solution structure of the human Grb14-SH2 domain and comparison with the structures of the human Grb7-SH2/erbB2 peptide complex and human Grb10-SH2 domain. Protein Sci **13:**2541-2546.

248. **Scherzinger, A. L., and Hendee, W. R.** 1985. Basic principles of magnetic resonance imaging - an update. West J Med **143:**782-792.

249. **Schlaepfer, D. D., Mitra, S. K., and Ilic, D.** 2004. Control of motile and invasive cell phenotypes by focal adhesion kinase. Biochim Biophys Acta **1692:**77-102.

250. **Schmid, S. L.** 1997. Clathrin-coated vesicle formation and protein sorting: an integrated process. Annu Rev Biochem **66:**511-548.

251. **Schnaider, T., Sőti, C., Cheetham, M. E., Miyata, Y., Yahara, I., and Csermely, P.** 2000. Interaction of the human DnaJ homologue, HSJ1b with the 90 kDa heat shock protein, Hsp90. Life Sci **67:**1455-1465.

252. **Shen, R., Ye, Y., Chen, L., Yan, Q., Barsky, S. H., and Gao, J. X.** 2008. Precancerous stem cells can serve as tumor vasculogenic progenitors. PLoS One **3:**e1652.

253. **Shen, T. L., and Guan, J. L.** 2001. Differential regulation of cell migration and cell cycle progression by FAK complexes with Src, PI3K, Grb7 and Grb2 in focal contacts. FEBS Lett **499:**176-181.

254. **Shen, T. L., and Guan, J. L.** 2004. Grb7 in intracellular signaling and its role in cell regulation. Front Biosci **9:**192-200.

255. **Shen, T. L., Han, D. C., and Guan, J. L.** 2002. Association of Grb7 with phosphoinositides and its role in the regulation of cell migration. J Biol Chem **277:**29069-29077.

256. **Sherr, C. J.** 1994. G1 phase progression: cycling on cue. Cell **79:**551-555.

257. **Shi, Y., and Thomas, J. O.** 1992. The transport of proteins into the nucleus requires the 70-kilodalton heat shock protein or its cytosolic cognate. Mol Cell Biol **12:**2186-2192.

258. **Siamakpour-Reihani, S., Argiros, H. J., Wilmeth, L. J., Haas, L. L., Peterson, T. A., Johnson, D. L., Shuster, C. B., and Lyons, B. A.** 2009. The cell migration protein Grb7 associates with transcriptional regulator FHL2 in a Grb7 phosphorylation-dependent manner. J Mol Recognit **22:**9-17.

259. **Sim, H., Rimmer, K., Kelly, S., Ludbrook, L. M., Clayton, A. H., and Harley, V. R.** 2005. Defective calmodulin-mediated nuclear transport of the sex-determining region of the Y chromosome (SRY) in XY sex reversal. Mol Endocrinol **19:**1884-1892.

260. **Siomi, H., and Dreyfuss, G.** 1995. A nuclear localization domain in the hnRNP A1 protein. J Cell Biol **129:**551-560.

261. **Sircoulomb, F., Bekhouche, I., Finetti, P., Adelaide, J., Ben Hamida, A., Bonansea, J., Raynaud, S., Innocenti, C., Charafe-Jauffret, E., Tarpin, C., Ben Ayed, F., Viens, P., Jacquemier, J., Bertucci, F., Birnbaum, D., and Chaffanet, M.** 2010. Genome profiling of *ERBB2*-amplified breast cancers. BMC Cancer **10:**539-557.

262. **Skotheim, R. I., Abeler, V. M., Nesland, J. M., Fossa, S. D., Holm, R., Wagner, U., Florenes, V. A., Aass, N., Kallioniemi, O. P., and Lothe, R. A.** 2003. Candidate genes for testicular cancer evaluated by *in situ* protein expression analyses on tissue microarrays. Neoplasia **5:**397-404.

263. **Skotheim, R. I., Monni, O., Mousses, S., Fossa, S. D., Kallioniemi, O. P., Lothe, R. A., and Kallioniemi, A.** 2002. New insights into testicular germ cell tumorigenesis from gene expression profiling. Cancer Res **62:**2359-2364.

264. **Solomon, S., Xu, Y., Wang, B., David, M. D., Schubert, P., Kennedy, D., and Schrader, J. W.** 2007. Distinct structural features of caprin-1 mediate its interaction with G3BP-1 and its induction of phosphorylation of eukaryotic translation initiation factor 2α, entry to cytoplasmic stress granules, and selective interaction with a subset of mRNAs. Mol Cell Biol **27:**2324-2342.

265. **Sotak, C. H.** 2004. Nuclear magnetic resonance (NMR) measurement of the apparent diffusion coefficient (ADC) of tissue water and its relationship to cell volume changes in pathological states. Neurochem Int **45:**569-582.

266. **Spratlin, J. L., Chu, Q., Koski, S., King, K., and Mulder, K.** 2011. Targeting metastatic upper gastrointestinal adenocarcinomas. World J Clin Oncol **2:**135-149.

267. **Stein, D., Wu, J., Fuqua, S. A., Roonprapunt, C., Yajnik, V., D'Eustachio, P., Moskow, J. J., Buchberg, A. M., Osborne, C. K., and Margolis, B.** 1994. The SH2 domain protein *GRB-7* is co-amplified, overexpressed and in a tight complex with *HER2* in breast cancer. EMBO J **13:**1331-1340.

268. **Stein, E., Cerretti, D. P., and Daniel, T. O.** 1996. Ligand activation of ELK receptor tyrosine kinase promotes its association with Grb10 and Grb2 in vascular endothelial cells. J Biol Chem **271:**23588-23593.

269. **Stein, E. G., Ghirlando, R., and Hubbard, S. R.** 2003. Structural basis for dimerization of the Grb10 Src homology 2 domain. Implications for ligand specificity. J Biol Chem **278:**13257-13264.

270. **Stein, E. G., Gustafson, T. A., and Hubbard, S. R.** 2001. The BPS domain of Grb10 inhibits the catalytic activity of the insulin and IGF1 receptors. FEBS Lett **493:**106-111.

271. **Stoclet, J. C., Gérard, D., Kilhoffer, M.-C., Lugnier, C., Miller, R., and Schaeffer, P.** 1987. Calmodulin and its role in intracellular calcium regulation. Prog Neurobiol **29:**321-364.

272. **Straume, O., Chappuis, P. O., Salvesen, H. B., Halvorsen, O. J., Haukaas, S. A., Goffin, J. R., Bégin, L. R., Foulkes, W. D., and Akslen, L. A.** 2002. Prognostic importance of glomeruloid microvascular proliferation indicates an aggressive angiogenic phenotype in human cancers. Cancer Res **62:**6808-6811.

273. **Takada, Y., Ye, X., and Simon, S.** 2007. The integrins. Genome Biol **8:**215-224.

274. **Tanaka, S., Mori, M., Akiyoshi, T., Tanaka, Y., Mafune, K., Wands, J. R., and Sugimachi, K.** 1997. Coexpression of Grb7 with epidermal growth factor receptor or Her2/ErbB2 in human advanced esophageal carcinoma. Cancer Res **57:**28-31.

275. **Tanaka, S., Mori, M., Akiyoshi, T., Tanaka, Y., Mafune, K., Wands, J. R., and Sugimachi, K.** 1998. A novel variant of human Grb7 is associated with invasive esophageal carcinoma. J Clin Invest **102:**821-827.

276. **Tanaka, S., Pero, S. C., Taguchi, K., Shimada, M., Mori, M., Krag, D. N., and Arii, S.** 2006. Specific peptide ligand for Grb7 signal transduction protein and pancreatic cancer metastasis. J Natl Cancer Inst **98:**491-498.

277. **Taulés, M., Rodríguez-Vilarrupla, A., Rius, E., Estanyol, J. M., Casanovas, O., Sacks, D. B., Pérez-Payá, E., Bachs, O., and Agell, N.** 1999. Calmodulin binds to $p21^{Cip1}$ and is involved in the regulation of its nuclear localization. J Biol Chem **274:**24445-24448.

278. **Terada, M., Sakamoto, H., Ohmura, Y., Tsuruta, H., Akiyama, N., Sasaki, H., Katoh, M., Hattori, Y., and Yoshida, T.** 1991. Biological significance of gene amplification in carcinogenesis. Princess Takamatsu Symp **22:**371-380.

279. **Thiry, P., Vandermeers, A., Vandermeers-Piret, M. C., Rathe, J., and Christophe, J.** 1980. The activation of brain adenylate cyclase and brain cyclic-nucleotide phosphodiesterase by seven calmodulin derivatives. Eur J Biochem **103:**409-414.

280. **Thommes, K., Lennartsson, J., Carlberg, M., and Ronnstrand, L.** 1999. Identification of Tyr-703 and Tyr-936 as the primary association sites for Grb2 and Grb7 in the c-Kit/stem cell factor receptor. Biochem J **341:**211-216.

281. **Traxler, K. W., Norcum, M. T., Hainfeld, J. F., and Carlson, G. M.** 2001. Direct visualization of the calmodulin subunit of phosphorylase kinase via electron microscopy following subunit exchange. J Struct Biol **135:**231-238.

282. **Tsai, N. P., Lin, Y. L., Tsui, Y. C., and Wei, L.-N.** 2010. Dual action of epidermal growth factor: extracellular signal-stimulated nuclear-cytoplasmic export and coordinated translation of selected messenger RNA. J Cell Biol **188:**325-333.

283. **Tsai, N. P., Bi, J., Loh, H. H., and Wei, L. N.** 2006. Netrin-1 signaling regulates *de novo* protein synthesis of κ opioid receptor by facilitating polysomal partition of its mRNA. J Neurosci **26:**9743-9749.

284. **Tsai, N. P., Bi, J., and Wei, L. N.** 2007. The adaptor Grb7 links netrin-1 signaling to regulation of mRNA translation. EMBO J **26:**1522-1531.

285. **Tsai, N. P., Ho, P. C., and Wei, L. N.** 2008. Regulation of stress granule dynamics by Grb7 and FAK signalling pathway. EMBO J **27:**715-726.

286. **Vayssiere, B., Zalcman, G., Mahe, Y., Mirey, G., Ligensa, T., Weidner, K. M., Chardin, P., and Camonis, J.** 2000. Interaction of the Grb7 adapter protein with Rnd1, a new member of the Rho family. FEBS Lett **467:**91-96.

287. **Vecchione, A., Marchese, A., Henry, P., Rotin, D., and Morrione, A.** 2003. The Grb10/Nedd4 complex regulates ligand-induced ubiquitination and stability of the insulin-like growth factor I receptor. Mol Cell Biol **23:**3363-3372.

288. **Vermeulen, K., Van Bockstaele, D. R., and Berneman, Z. N.** 2003. The cell cycle: a review of regulation, deregulation and therapeutic targets in cancer. Cell Prolif **36:**131-149.

289. **Vetter, S. W., and Leclerc, E.** 2003. Novel aspects of calmodulin target recognition and activation. Eur J Biochem **270:**404-414.

290. **Villalobo, A., García-Andrés, C., and Molina-Ortiz, P.** 2003. Translocation of ErbB receptors into the nucleus. Clin Transl Oncol **5:**381-389.

291. **Villalobo, A., Li, H., and Sánchez-Torres, J.** 2003. The Grb7 protein family. Curr Top Biochem Res **5:**105-114.

292. **Waksman, G., Kominos, D., Robertson, S. C., Pant, N., Baltimore, D., Birge, R. B., Cowburn, D., Hanafusa, H., Mayer, B. J., Overduin, M., Resh, M. D., Rios, C. B., Silverman, L., and Kuriyan, J.** 1992. Crystal structure of the phosphotyrosine recognition domain SH2 of v-src complexed with tyrosine-phosphorylated peptides. Nature **358:**646-653.

293. **Walch, A., Specht, K., Braselmann, H., Stein, H., Siewert, J. R., Hopt, U., Hofler, H., and Werner, M.** 2004. Coamplification and coexpression of GRB7 and ERBB2 is found in high grade intraepithelial neoplasia and in invasive Barrett's carcinoma. Int J Cancer **112:**747-753.

294. **Wang, B., David, M. D., and Schrader, J. W.** 2005. Absence of caprin-1 results in defects in cellular proliferation. J Immunol **175:**4274-4282.

295. **Wang, K. K., Villalobo, A., and Roufogalis, B. D.** 1992. The plasma membrane calcium pump: a multiregulated transporter. Trends Cell Biol **2:**46-52.

296. **Wang, X. W., Hussain, S. P., Huo, T.-I., Wu, C.-G., Forgues, M., Hofseth, L. J., Brechot, C., and Harris, C. C.** 2002. Molecular pathogenesis of human hepatocellular carcinoma. Toxicology **181–182:**43-47.

297. **Wang, Y., Chan, D. W., Liu, V. W., Chiu, P., and Ngan, H. Y.** 2010. Differential functions of growth factor receptor-bound protein 7 (GRB7) and its variant GRB7V in ovarian carcinogenesis. Clin Cancer Res **16:**2529-2539.

298. **Watterson, D. M., Iverson, D. B., and Van Eldik, L. J.** 1980. Spinach calmodulin: isolation, characterization, and comparison with vertebrate calmodulins. Biochemistry **19:**5762-5768.

299. **Watterson, D. M., Sharief, F., and Vanaman, T. C.** 1980. The complete amino acid sequence of the Ca^{2+}-dependent modulator protein (calmodulin) of bovine brain. J Biol Chem **255:**962-975.

300. **Weinberg, R. A.** 1995. The retinoblastoma protein and cell cycle control. Cell **81:**323-330.

301. **Wennerberg, K., Rossman, K. L., and Der, C. J.** 2005. The Ras superfamily at a glance. J Cell Sci **118:**843-846.

302. **Williamson, M. P.** 1994. The structure and function of proline-rich regions in proteins. Biochem J **297:**249-260.

303. **Wulf, E., Deboben, A., Bautz, F. A., Faulstich, H., and Wieland, T.** 1979. Fluorescent phallotoxin, a tool for the visualization of cellular actin. Proc Natl Acad Sci USA **76:**4498-4502.

304. **Yamagishi, N., Ishihara, K., and Hatayama, T.** 2004. Hsp105α suppresses Hsc70 chaperone activity by inhibiting Hsc70 ATPase activity. J Biol Chem **279:**41727-41733.

305. **Yap, K. L., Kim, J., Truong, K., Sherman, M., Yuan, T., and Ikura, M.** 2000. Calmodulin target database. J Struct Funct Genomics **1:**8-14.

306. **Yazawa, M., Kawamura, E., Minowa, O., Yagi, K., Ikura, M., and Hikichi, K.** 1984. N-terminal region (domain 1) of calmodulin is the low affinity site for Ca^{2+}. A ^{13}C NMR study of S-cyanocalmodulin. J Biochem **95:**443-446.

307. **Yokote, K., Margolis, B., Heldin, C. H., and Claesson-Welsh, L.** 1996. Grb7 is a downstream signaling component of platelet-derived growth factor α- and β-receptors. J Biol Chem **271:**30942-30949.

308. **Zeise, E., Kuhl, N., Kunz, J., and Rensing, L.** 1998. Nuclear translocation of stress protein Hsc70 during S phase in rat C6 glioma cells. Cell Stress Chap **3:**94-99.

309. **Zetterberg, A., Engstrom, W., and Larsson, O.** 1982. Growth activation of resting cells: induction of balanced and imbalanced growth. Ann N Y Acad Sci **397:**130-147.

310. **Zhou, R., Mazurchuk, R., and Straubinger, R. M.** 2002. Antivasculature effects of doxorubicin-containing liposomes in an intracranial rat brain tumor model. Cancer Res **62:**2561-2566.

311. **Zhu, X., Ohtsubo, M., Bohmer, R. M., Roberts, J. M., and Assoian, R. K.** 1996. Adhesion-dependent cell cycle progression linked to the expression of cyclin D1,

activation of cyclin E-cdk2, and phosphorylation of the retinoblastoma protein. J Cell Biol **133:**391-403.

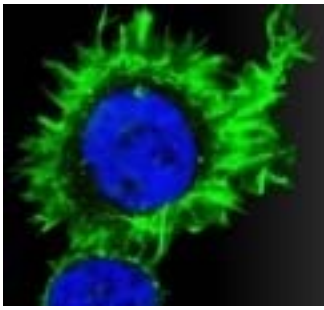

10 APPENDIX

10.1 Supplementary material

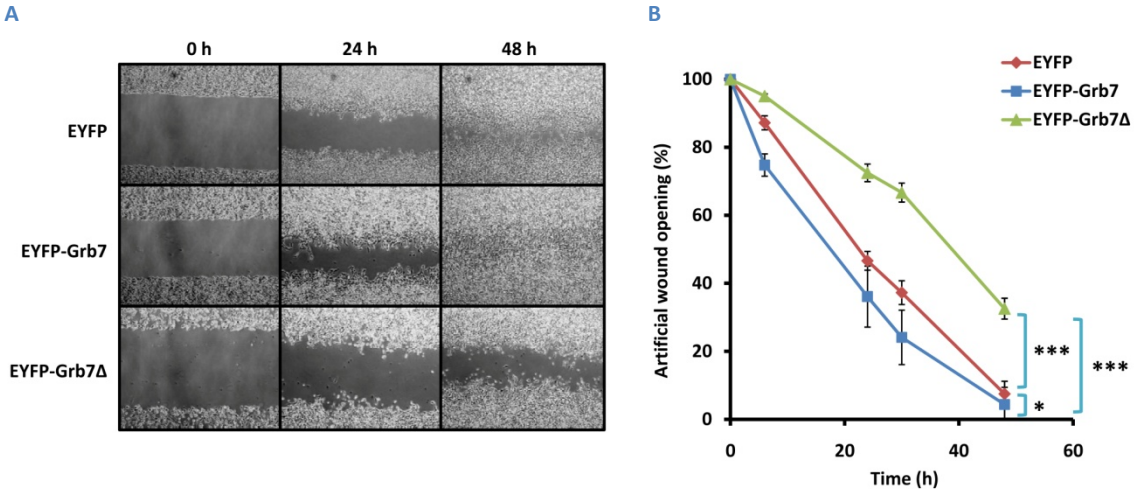

Supplementary Fig. 1S: Grb7Δ-expressing C6 cells present a lower repopulation rate of artificial wounds. Artificial wounds were performed in monolayers of confluent C6 cells stably expressing EYFP, EYFP-Grb7 or EYFP-Grb7Δ **(A)**. Photographs taken at different times to follow the repopulation of the artificial wounds using a Nikon Eclipse TS100 microscope with 4x objective are shown. **(B)** The plot represents the mean ± SEM (n = 4) opening of the wound in a set of experiments similar to the one shown in **(A)**. Significant differences were found when comparing the curves using the two-way ANOVA test (*** $p < 0.0001$ and * $p < 0.05$).

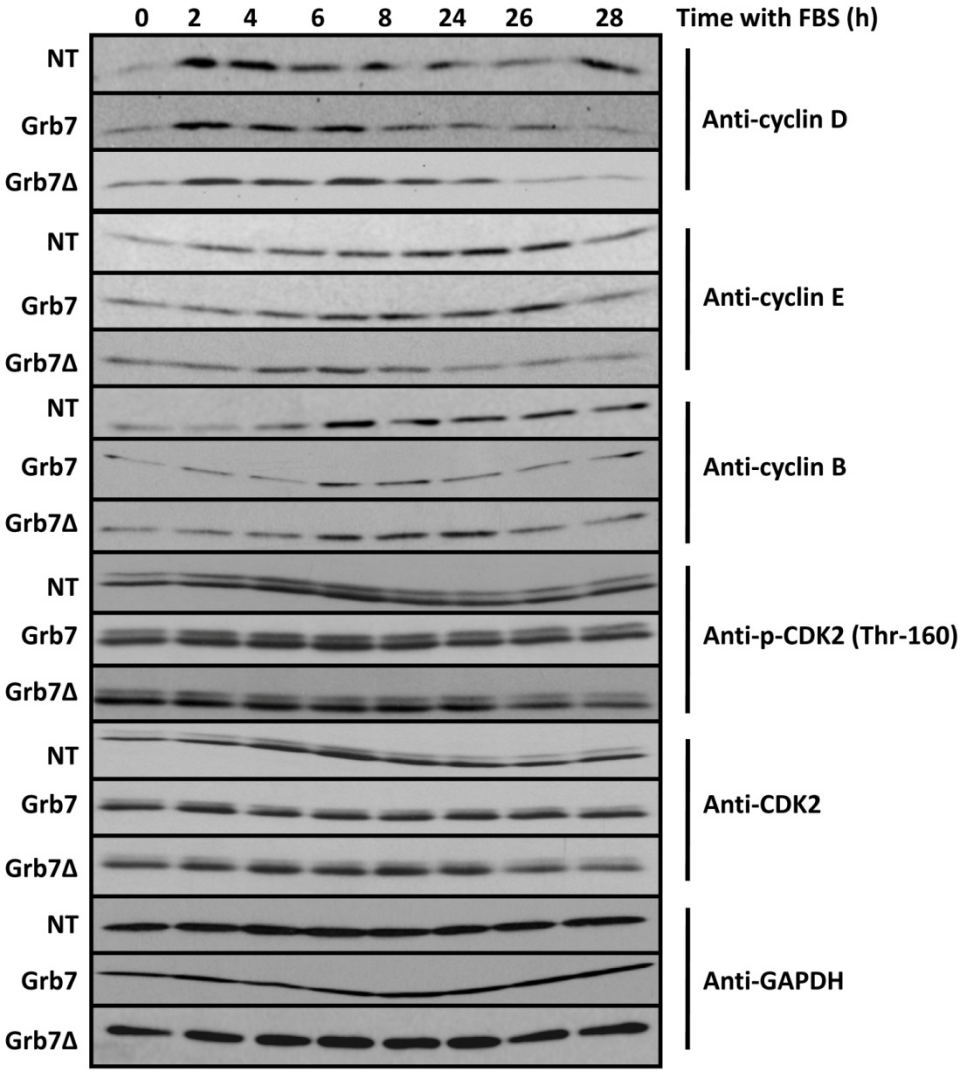

Supplementary Fig. 2S: Effect of Grb7 and Grb7Δ expression in different cell cycle regulators. The cell cycle of non-transfected (NT) and stably transfected HEK293 cells expressing Grb7 or Grb7Δ was synchronized by serum deprivation and proliferation started by the addition of 10 % (v/v) FBS. Total cell extracts were prepared to test by Western blot the expression and/or phosphorylation of the indicated proteins implicated in cell cycle regulation. Anti-GAPDH or the corresponding antibody against the total protein when comparing phosphorylation patterns, were used as loading controls.

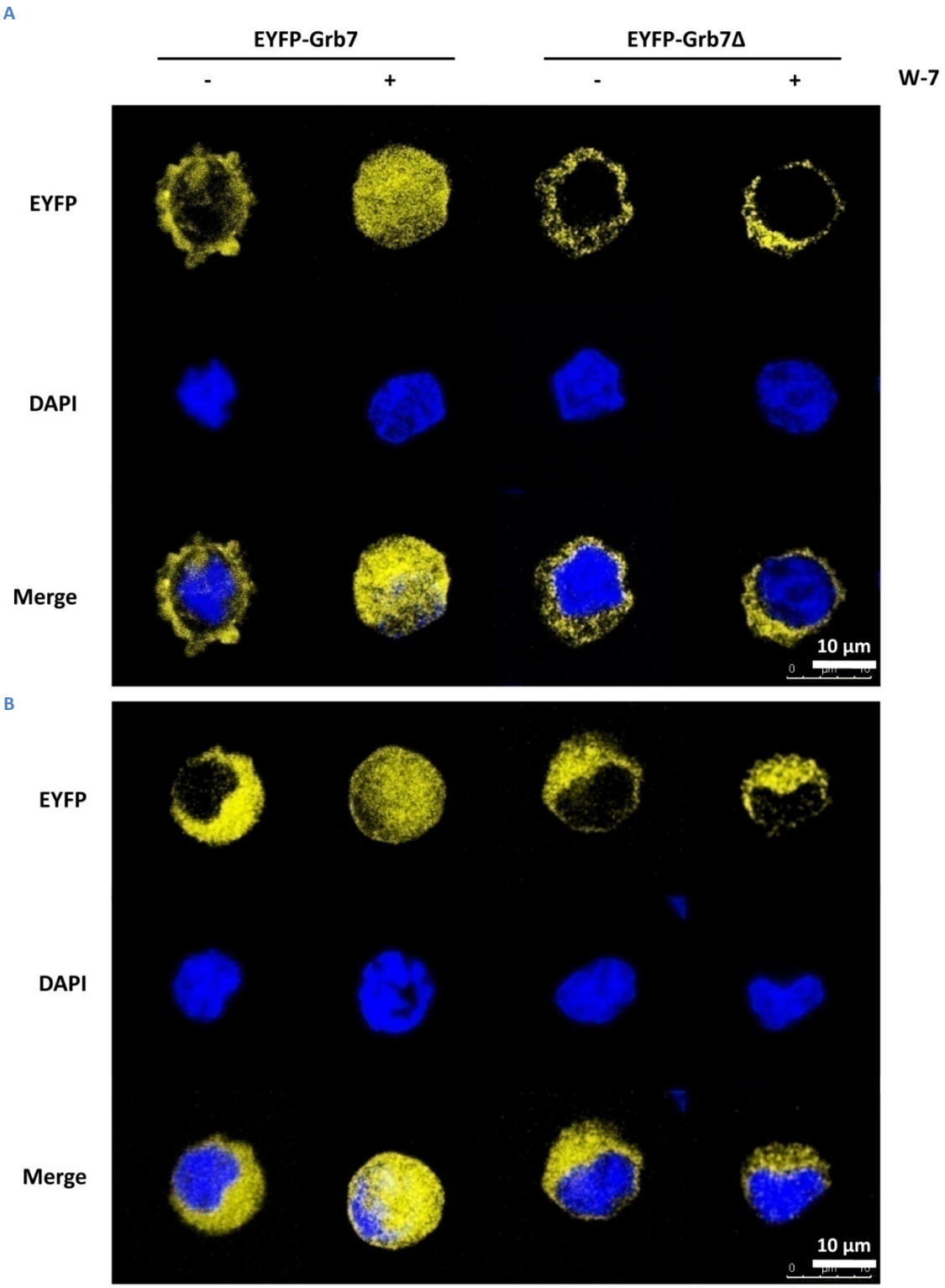

Supplementary Fig. 3S: The calmodulin (CaM) antagonist W-7 enhances the translocation of Grb7 into the nucleus in C6 cells. Transiently **(A)** or stably **(B)** transfected C6 cells with pEYFP-Grb7 or pEYFP-Grb7Δ were incubated in the absence and presence of W-7 (15 µM) for 30 min as described in Materials and Methods and seeded in fibronectin-coated plates. The cells were then fixed and the nuclei were stained with DAPI to be observed in a confocal microscope using a 63x (HCS PL APO lambda blue) oil-immersion objective exciting with a 488 nm laser to detect the EYFP and the UV channel to observe the nuclei. The localization of the chimeras EYFP-Grb7 and EYFP-Grb7Δ (EYFP) (yellow) and their corresponding nuclei visualized by DAPI staining (blue) are shown. Merge represents the overlay of the EYFP and the DAPI signals.

Acession	Name	Band	Peptides A	Peptides B	Intensity A	Intensity B	PEP
O94905	Erlin-2	~45 KDa	3	4	135190	86915	3.47×10^{-27}
Q9BUA3	Uncharacterized protein C11orf84	~45 KDa	2	1	27475	12183	1.02×10^{-2}
Q9UNM6	26S proteasome non-ATPase regulatory subunit 13	~45 KDa	2	1	77411	10218	5.88×10^{-2}
O15372	Eukaryotic translation initiation factor 3 subunit H	~45 KDa	2	1	118890	59233	1.42×10^{-3}
O60884	DNAJ homolog subfamily A member 2	~45 KDa	3	1	132610	19768	2.70×10^{-4}
P54577	Tyrosyl-tRNA synthetase. cytoplasmic	~60 KDa	4	2	104660	22579	1.20×10^{-3}
P40227	T-complex protein 1 subunit zeta	~60 KDa	2	1	168630	42882	3.80×10^{-3}
P48444	Coatomer subunit delta	~60 KDa	3	1	60328	21778	2.01×10^{-2}
P49321	Nuclear autoantigenic sperm protein isoform 2	~60 KDa	2	1	103670	29550	1.74×10^{-3}
Q07666	KH domain-containing. RNA-binding. signal transduction-associated protein 1	~60 KDa	2	3	233470	95770	1.18×10^{-4}
Q12874	Splicing factor 3A subunit 3	~60 KDa	3	1	71276	33517	2.41×10^{-4}
Q15482	Activin receptor type-1B	~60 KDa	2	1	87719	38589	3.40×10^{-3}
Q8ND56	Protein LSM14 homolog A	~60 KDa	2	1	173440	64839	1.36×10^{-3}
Q99615	DnaJ homolog subfamily C member 7	~60 KDa	6	7	229580	320470	4.51×10^{-44}
Q9P258	Regulator of chromosome condensation 2 RCC2	~60 KDa	5	3	193440	53049	1.21×10^{-9}

Supplementary Table 1S: Potential Grb7Δ binding partners in HE293 cells as detected by Mass Spectrometry. List of the identified proteins by Mass Spectrometry as unique potential binding partners to Grb7Δ after immunoprecipitation of FLAG-Grb7Δ from lysates of HEK293 cells stably expressing FLAG-Grb7Δ using the anti-FLAG®-M2 affinity gel as described in Materials and Methods. Two biological replicates denoted as experiments A and B were performed. PEP score indicating the probability of error in the identification of the protein is shown.

Acession	Name	Band	Peptides A	Peptides B	Intensity A	Intensity B	PEP
Q9UJS0	Calcium-binding mitochondrial carrier protein Aralar2	~70 KDa	6	4	236990	76244	2.75×10^{-11}
Q9H3P7	Golgi resident protein GCP60	~70 KDa	4	3	85372	50150	5.49×10^{-41}
Q9UG63	ATP-binding cassette sub-family F member 2	~70 KDa	4	2	127380	36155	2.93×10^{-9}
P17812	CTP synthase 1	~70 KDa	3	2	60064	41525	7.37×10^{-15}
Q6UN15	Pre-mRNA 3'-end-processing factor FIP1	~70 KDa	2	1	45696	26780	7.37×10^{-20}
Q6VN20	Ran-binding protein 10	~70 KDa	6	2	138160	20336	4.47×10^{-16}
O43663	Protein regulator of cytokinesis 1	~70 KDa	2	1	44315	14656	1.10×10^{-3}
O60506	Heterogeneous nuclear ribonucleoprotein Q	~70 KDa	3	2	163810	42874	1.67×10^{-13}
P27694	Replication protein A 70 kDa DNA-binding subunit	~70 KDa	2	2	51762	23382	2.74×10^{-3}
P51114	Fragile X mental retardation syndrome-related protein 1	~70 KDa	5	2	206200	92382	2.78×10^{-19}
Q06124	Tyrosine-protein phosphatase non-receptor type 11	~70 KDa	3	2	62797	32658	7.53×10^{-28}
Q06210	Glucosamine-fructose-6-phosphate aminotransferase	~70 KDa	4	2	164830	26273	2.57×10^{-62}
Q07065	Cytoskeleton-associated protein 4	~70 KDa	5	2	137320	44448	8.35×10^{-29}
Q15046	Lysyl-tRNA synthetase	~70 KDa	3	2	79155	48107	4.31×10^{-24}
Q15942	Zyxin	~70 KDa	7	3	670420	56485	2.22×10^{-34}
Q16630	Cleavage and polyadenylation specificity factor subunit6	~70 KDa	3	2	184920	82010	3.31×10^{-40}
Q8N680	Zinc finger and BTB domain-containing protein 2	~70 KDa	4	2	115840	38730	1.13×10^{-5}
Q8NCE2	Myotubularin-related protein 14	~70 KDa	2	1	38343	21715	2.25×10^{-8}
Q9BRS2	Serine/threonine-protein kinase RIO1	~70 KDa	10	1	975520	22534	6.33×10^{-26}
Q9NVI7	ATPase family AAA domain-containing protein 3A	~70 KDa	6	5	412820	270720	6.65×10^{-39}
Q9NXV6	CDKN2A-interacting protein	~70 KDa	2	2	23931	21281	8.29×10^{-2}
Q9P270	SLAIN motif-containing protein 2	~70 KDa	6	2	199840	28650	1.32×10^{-22}
Q9UNF1	Melanoma-associated antigen D2	~70 KDa	4	2	101730	56831	6.02×10^{-16}
Q9Y5A9	YTH domain family protein 2	~70 KDa	3	1	82702	35619	1.84×10^{-11}

Supplementary Table 1S: Potential Grb7Δ binding partners in HE293 cells as detected by Mass Spectrometry. (continuation).

			Grb7				Grb7Δ				
Acession	Name	Band	Peptides B	Peptides A	Intensity A	Intensity B	Peptides A	Peptides B	Intensity A	Intensity B	PEP
Q92769	Histone deacetylase 2	~60 KDa	3	1	97482	14958	3	2	168970	87491	1.03×10^{-6}
P98175	RNA-binding protein 10	~60 KDa	2	1	27657	10630	2	1	83333	12559	2.32×10^{-4}
Q96GA3	Protein LTV1 homolog	~60 KDa	2	1	31933	10531	3	1	44063	16599	2.40×10^{-4}
Q8WUA2	Peptidyl-prolyl cis-trans isomerase-like 4	~60 KDa	3	1	85188	22669	5	2	261600	23982	1.98×10^{-19}
O43242	26S proteasome non-ATPase regulatory subunit 3	~60 KDa	2	2	45018	32285	9	5	265620	172310	1.31×10^{-21}
O95232	Luc7-like protein 3	~60 KDa	2	1	59424	38226	8	3	400530	98817	8.58×10^{-69}
O95793	Double-stranded RNA-binding protein Staufen homolog 1	~60 KDa	3	1	67435	13724	3	1	62467	14962	1.04×10^{-11}
P26599	Polypyrimidine tract-binding protein 1	~60 KDa	4	1	259660	65798	3	3	312340	170940	6.03×10^{-5}
Q99832	T-complex protein 1 subunit eta	~60 KDa	3	1	60227	15984	8	6	675630	301230	2.92×10^{-28}
Q9UHX	Poly(U)-binding-splicing factor PUF60	~60 KDa	3	2	62017	32854	2	1	89069	16356	6.83×10^{-20}
Q9UN86	GTPase activating protein binding protein 2 G3PB2	~60 KDa	2	1	94859	53483	2	1	111610	37195	4.95×10^{-5}
Q9Y285	Phenylalanyl-tRNA synthetase alpha chain	~60 KDa	5	4	65799	294110	6	4	59237	250270	8.99×10^{-13}
Q14451	Growth factor receptor bound 7	~60 KDa	15	12	30151000	27543000	17	11	33753000	24142000	1.08×10^{-112}
P04843	Dolichyl-diphospho-oligosaccharide-protein glycosyltransferase subunit 1	~70 KDa	3	1	44567	16426	5	3	239360	75404	5.11×10^{-31}
P23588	EIF4B: Eukaryotic translation initiation factor 4B	~70 KDa	3	5	50633	110830	8	8	444000	168760	2.96×10^{-115}
P31040	Succinate dehydrogenase [ubiquinone] flavoprotein subunit, mitochondrial	~70 KDa	4	1	81087	12037	4	1	216320	15756	5.10×10^{-19}
P52272	Heterogeneous nuclear ribonucleoprotein M	~70 KDa	1	5	92356	158790	8	3	527720	89675	8.19×10^{-10}
Q96PK6	RNA-binding protein 14	~70 KDa	1	2	20593	36987	5	3	252120	79488	4.80×10^{-24}

Supplementary Table 2S: Potential binding partners shared by Grb7 and Grb7Δ in HE293 cells as detected by Mass Spectrometry. List of the identified proteins by Mass Spectrometry as potential binding partners shared between Grb7 and Grb7Δ after immunoprecipitation of FLAG-Grb7 or FLAG-Grb7Δ from lysates of HEK293 cells stably expressing FLAG-Grb7 or FLAG-Grb7Δ using the anti-FLAG®-M2 affinity gel as described in Materials and Methods. Two biological replicates denoted as experiments A and B were performed. PEP score indicating the probability of error in the identification of the protein is shown.

Acession #	Name	Band	Peptides A	Peptides B	Intensity A	Intensity B	PEP
D4ACJ0	Histone deacetylase 10	~70 KDa	1	2	17399	19725	3.94 x 10-3
Q5M9G3	Caprin-1	~80 KDa	3	6	14871	42619	5.28×10^{-9}
F1LQ82	Nedd-4	~100 KDa	15	13	942790	613340	1.9×10^{-77}

Supplementary Table 3S: Potential Grb7 binding partners in C6 cells as detected by Mass Spectrometry. List of the identified proteins by Mass Spectrometry as unique potential binding partners to Grb7 after purification of EYFP-Grb7 from lysates of C6 cells stably expressing EYFP-Grb7 using the GFP-Trap®-A system as described in Materials and Methods. Two biological replicates denoted as experiments A and B were performed. PEP score indicating the probability of error in the identification of the protein is shown.

Acession	Name	Band	Peptides A	Peptides B	Intensity A	Intensity B	PEP
D3ZSD1	Mitochondrial inner membrane protein	~70 KDa	2	3	19777	23771	2.83×10^{-34}
D3ZNL2	Thymopoietin, isoform CRA_a	~70 KDa	2	2	34007	14672	2.22×10^{-4}
Q641Y8	ATP-dependent RNA helicase DDX1	~70 KDa	1	2	6840	13943	1.35×10^{-3}

Supplementary Table 4S: Potential Grb7Δ binding partners in C6 cells as detected by Mass Spectrometry. List of the identified proteins by Mass Spectrometry as unique potential binding partners to Grb7Δ after purification of EYFP-Grb7Δ from lysates of C6 cells stably expressing EYFP-Grb7Δ using the GFP-Trap®-A system as described in Materials and Methods. Two biological replicates denoted as experiments A and B were performed. PEP score indicating the probability of error in the identification of the protein is shown.

			Grb7				Grb7Δ				
Acession	Name	Band	Peptides B	Peptides A	Intensity A	Intensity B	Peptides A	Peptides B	Intensity A	Intensity B	PEP
D4ADE8	Ddx3x Helicase	~70 KDa	1	5	14074	101570	3	3	41914	27771	2.49×10^{-14}
Q9EPH8	Polyadenylate-binding protein 1	~70 KDa	2	6	47422	143720	4	1	37511	9669	6.88×10^{-25}
P63018	Heat shock cognate 70	~70 KDa	22	24	4077900	7188300	22	22	5800100	4122400	0
P82995	Heat shock protein HSP 90-alpha	~80 KDa	1	2	4065	11479	3	2	30480	24583	1.02×10^{-100}
Q9QZC5	Growth factor receptor bound 7	~80 KDa	9	8	5977000	6592900	5	4	307900	1988700	1.73×10^{-65}
Q66HA8	Heat shock protein 105	~100 KDa	1	2	8229	16901	1	2	7481	13812	1.20×10^{-2}

Supplementary Table 5S: Potential binding partners shared by Grb7 and Grb7Δ in C6 cells as detected by Mass Spectrometry. List of the identified proteins by Mass Spectrometry as potential binding partners shared between Grb7 and Grb7Δ after purification of EYFP-Grb7 or EYFP-Grb7Δ from lysates of C6 cells stably expressing EYFP-Grb7 or EYFP-Grb7Δ using the GFP-Trap®-A system as described in Materials and Methods. Two biological replicates denoted as experiments A and B were performed. PEP score indicating the probability of error in the identification of the protein is shown.

Access	Abbreviature	Protein name
O00571	DDX3Y	DEAD (Asp-Glu-Ala-Asp) box polypeptide 3, Y-linked
O15372	EIF3H	eukaryotic translation initiation factor 3, subunit H
O43242	PSMD3	proteasome 26S subunit, non-ATPase, 3
O43663	PRC1	protein regulator of cytokinesis 1
O60506	SYNCRIP	synaptotagmin binding
O60884	DNAJA2	DnaJ (Hsp40) homolog, subfamily A, member 2
O94905	ERLIN2	ER lipid raft associated 2
O95232	LUC7L3	LUC7-like 3
O95793	STAU1	Double-stranded RNA-binding protein Staufen homolog 1
P04843	RPN1	Dolichyl-diphosphooligosaccharide--protein glycosyltransferase subunit 1
P82995	HSP90AA1	Heat shock protein HSP 90-alpha
P11142	HSPA8	heat shock 70kDa protein 8
P11940	PABPC3	poly(A) binding protein, cytoplasmic 3
P23588	EIF4B	eukaryotic translation initiation factor 4B
P26599	PTBP1	Polypyrimidine tract-binding protein 1
P27694	RPA1	Replication protein A 70 kDa DNA-binding subunit
P31040	SDHA	Succinate dehydrogenase complex, subunit A
P40227	CCT6A	Chaperonin containing TCP1, subunit 6A
P42166	TMPO	Thymopoietin
P46934	NEDD4	Neural precursor cell expressed, developmentally down-regulated 4
P48444	ARCN1	archain 1
P49321	NASP	nuclear autoantigenic sperm protein
P51114	FXR1	fragile X mental retardation, autosomal homolog 1
P52272	HNRNPM	heterogeneous nuclear ribonucleoprotein M
P54577	YARS	Tyrosyl-tRNA synthetase
P98175	RBM10	RNA-binding motif protein 10
Q06124	PTPN11	Tyrosine phosphatase, non-receptor type 11
Q06210	GFPT1	Glucosamine-fructose-6-phosphate aminotransaminase
Q07065	CKAP4	Cytoskeleton-associated protein 4
Q07666	KHDRBS1	KH domain-containing, RNA-binding, signal transduction associated 1
Q12874	SF3A3	Splicing factor 3A, subunit 3
Q14444	CAPRIN1	Cell cycle associated protein 1
Q15046	KARS	Lysyl-tRNA synthetase
Q15482	ACVR1B	Activin A receptor type-1B
Q15942	ZYX	Zyxin
Q16630	CPSF6	Cleavage and polyadenylation specificity factor subunit 6
D3ZSD1	IMMT	Mitochondrial inner membrane protein
Q6UN15	FIP1L1	Pre-mRNA 3'-end-processing factor FIP1
Q6VN20	RANBP10	Ran-binding protein 10
Q8N680	ZBTB2	Zinc finger and BTB domain-containing 2
Q8NCE2	MTMR1	Myotubularin-related protein 14
Q8ND56	LSM14A	Protein LSM14 homolog A
Q8WUA2	PPIL4	Peptidyl-prolyl cis-trans isomerase-like 4
Q92499	DDX1	ATP-dependent RNA helicase DDX1
Q641Y8	HSPH1	Heat shock 105kDa/110kDa protein 1
Q92769	HDAC1	Histone deacetylase
Q96GA3	LTV1	Protein LTV1 homolog
Q96PK6	COAA	RNA-binding protein 14
Q99615	DNAJC7	DnaJ homolog subfamily C member 7
Q99832	CCT7	T-complex protein 1 subunit eta
Q9BRS2	RIOK1	Serine/threonine-protein kinase RIO1
Q9BUA3	C11orf84	Uncharacterized protein C11orf84
Q9H3P7	ACBD3	Golgi resident protein GCP60
Q9NVI7	ATAD3A	ATPase family AAA domain-containing 3A
Q9NXV6	CDKN2AIP	CDKN2A-interacting protein
Q9P258	RCC2	regulator of chromosome condensation 2
Q9P270	SLAIN2	SLAIN motif-containing protein 2
Q9UG63	ABCF2	ATP-binding cassette sub-family F member 2
Q9UJS0	SLC25A13	Calcium-binding mitochondrial carrier protein Aralar2
Q9UN86	G3BP2	GTPase activating protein binding protein 2
Q9UNF1	MAGED2	Melanoma-antigen family D2
Q9UNM6	PSMD13	26S proteasome non-ATPase regulatory subunit 13
Q9Y285	FARSA	Phenylalanyl-tRNA synthetase, alpha subunit
Q9Y5A9	YTHDF2	YTH domain family protein 2

Supplementary Table 6S: Abbreviation list of proteins shown in the STRING analysis shown in **Fig. 40**.

10.2 Publication list

Lucas-Fernández, E., García-Palmero I., and Villalobo A. 2008. Genomic organization and control of the Grb7 gene family. Curr Genomics **9:**60-68.

García-Palmero, I., and Villalobo A. 2012. Calmodulin regulates the translocation of Grb7 into the nucleus. FEBS Lett **586:**1533-1539.

García-Palmero, I., López-Larrubia P., Cerdán S., and Villalobo A. 2012. Nuclear magnetic resonance imaging of tumor growth and neovasculature performance *in vivo* reveals Grb7 as a novel antiangiogenic target. *(Submitted).*

Genomic Organization and Control of the Grb7 Gene Family

E. Lucas-Fernández, I. García-Palmero and A. Villalobo*

Instituto de Investigaciones Biomédicas, Consejo Superior de Investigaciones Científicas & Universidad Autónoma de Madrid. Arturo Duperier 4, E-28029 Madrid, Spain

Abstract: Grb7 and their related family members Grb10 and Grb14 are adaptor proteins, which participate in the functionality of multiple signal transduction pathways under the control of a variety of activated tyrosine kinase receptors and other tyrosine-phosphorylated proteins. They are involved in the modulation of important cellular and organismal functions such as cell migration, cell proliferation, apoptosis, gene expression, protein degradation, protein phosphorylation, angiogenesis, embryonic development and metabolic control. In this short review we shall describe the organization of the genes encoding the Grb7 protein family, their transcriptional products and the regulatory mechanisms implicated in the control of their expression. Finally, the alterations found in these genes and the mechanisms affecting their expression under pathological conditions such as cancer, diabetes and some congenital disorders will be highlighted.

Received on: January 9, 2008 - Revised on: February 20, 2008 - Accepted on: February 21, 2008

Key Words: Adaptor proteins, cancer, congenital disorders, diabetes, genetic imprinting, Grb7, Grb10, Grb14, uniparental disomy, splice variants.

INTRODUCTION

The so-called adaptors form an ample group of proteins that generally lack enzymatic activity, but play an important role in multiple signal transduction processes in the cell. They function by bringing together in a proper conformational manner, different components of given signaling pathways to achieve their correct functionality in transmitting signals along defined routes. Among the adaptors found in mammalian cells, the growth factor receptor bound protein 7 (Grb7) family that is formed by three members: Grb7, Grb10 and Grb14, has acquired certain relevance. These proteins mediate the interaction between many activated (phosphorylated) tyrosine kinase receptors located at the cell surface, from this its acronym Grb pertaining to Growth factor receptor bound, and their downstream signaling effector proteins came into existence. In addition, these adaptor proteins are able to interact with other non-receptor tyrosine-phosphorylated proteins involved in signaling events (see [1-4] for reviews and references therein).

The mammalian Grb7 family members show significant homology to the *Caenorhabditis elegans* protein denoted Mig10, which is implicated in embryonic neuronal cell migration [5]. These proteins exhibit a conserved multidomain structure. Hence, in their central section they present a region termed GM, for Grb and Mig, that includes a Ras-associating (RA) domain, which allows for their interaction with members of the Ras superfamily of small G proteins; and a pleckstrin homology (PH) domain whose function is to allow their binding to cell membrane phosphoinositides, and where our group has additionally identified (in Grb7) a functional calmodulin-binding domain overlapping its proximal region [6]. In their N-terminus, these proteins present a proline-rich (PR) domain for interaction with proteins containing a Src homology 3 (SH3) domain. Distal to the GM region is located the BPS domain (for between PH and SH2), which is responsible for interaction with the insulin and insulin-like growth factor-I (IGF-I) receptors and finally, the C-terminus contains the all-important Src homology 2 (SH2) domain, whereby the Grb7 family proteins interact with phosphotyrosine residues present in activated receptors and signaling proteins. The *C. elegans* Mig10 protein lacks, however, an SH2 domain and contains instead an additional PR domain in its C-terminus (see [1-4] for reviews and references therein).

Grb7 interacts with many tyrosine kinase receptors, including the epidermal growth factor receptor (EGFR/ErbB1) and others, erytoblastic leukemia viral oncogene homolog receptors (ErbB2, ErbB3, ErbB4) just to give some examples of a set of receptors involved in tumor biology and it has been implicated in cellular migration because of its interaction with focal adhesion kinase (FAK) and the erythropoietin-producing hepatocellular carcinoma cells receptor B1 (EphB1), an ephrin receptor. This adaptor protein also plays a prominent role in the metastatic spread of tumor cells, where it is frequently overexpressed (see [1-4, 7] for reviews and references therein). In addition, Grb7 appears to be involved in cellular processes controlling angiogenesis [6], and its role in the negative control of protein translation has recently been shown [8].

Grb10 translocates to the plasma membrane upon insulin stimulation and binds with high affinity to the insulin receptor, and also with the IGF-I receptor, thereby inhibiting their tyrosine kinase activity. Grb10 also acts as a positive regulator of phosphatidylinositol 3-kinase (PI3K)/Akt (for v-*akt* murine thymoma viral oncogene homolog)-mediated cellular

*Address correspondence to this author at the Instituto de Investigaciones Biomédicas, Consejo Superior de Investigaciones Científicas and Universidad Autónoma de Madrid. Arturo Duperier 4, E-28029 Madrid, Spain; Tel: 34-91-585-4424; Fax: 34-91-585-4401;
E-mail: antonio.villalobo@iib.uam.es

1389-2029/08 $55.00+.00

functions and it has been shown to associate to the mitochondrial outer membrane in response to IGF-I or serum treatment, from where it could exert an anti-apoptotic action. Grb10 possibly regulates the ubiquitination of target proteins, such as tyrosine kinase receptors, because of its interaction with Nedd4, a ubiquitin protein ligase. Furthermore, Grb10 seems to play a leading role in development by negatively affecting cell proliferation because of its actions on the signaling pathways, which are the insulin and IGF-I receptors, but by the growth hormone receptor as well (see [1-4, 9-11] for reviews and references therein). Nevertheless, the negative control of Grb10 on mitogenesis is not a universal event, since a stimulatory role of this protein on cell proliferation mediated by platelet-derived growth factor-BB (PDGF-BB), insulin and IGF-I has also been reported [12].

Grb14 exerts its functional roles upon its association with the insulin and the fibroblast growth factor receptors, thereby inhibiting both cell proliferation and insulin-mediated glycogen synthesis (see [1-4, 13] for reviews and references therein).

As we have seen, the Grb7 protein family members control numerous cellular functions because of the variegated spectrum of receptors they interact with and the multiplicity of receptor-controlled signaling pathways in which these adaptor proteins intervene. In order to illustrate the global physiological impact of these proteins on the control of cellular functions, Fig. (**1**) summarizes the main biological processes in which the Grb7/Grb10/Grb14 proteins appear to play a relevant role.

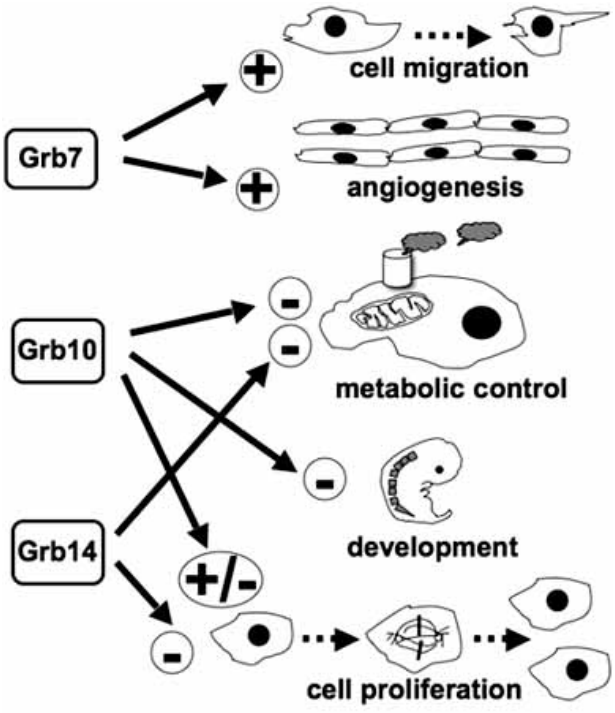

Fig. 1. Control exerted by the Grb7/Grb10/Grb14 proteins on cellular and physiological processes. The cartoon represents a selected series of cellular and physiologically relevant processes in which the Grb7 family member proteins exert a positive or negative control by participating in defined signaling pathways. These processes are: cell migration (Grb7), angiogenesis (Grb7), metabolic control (Grb10 and Grb14), development (Grb10), and cell proliferation (Grb10 and Grb14). Encircled plus and minus symbols represent, respectively, activation and inhibition of the indicated processes. See text for additional details.

THE *GRB7* GENE

Human *GRB7* maps to the large arm of chromosome 17 at the 17q12-q21.1 locus (see Fig. (**2**) left panel), near to the *ERBB2* gene within the 17q12 amplicon, which is also called the *ERBB2* amplicon [14, 15]. Transgenic mouse models expressing activated ErbB2 under the control of its endogenous promoter(s), but not under the control of a mouse mammary tumor virus-based promoter, express high levels of Grb7 and other genes within the same *ERBB2* amplicon, such as *CAB1* [16]. The major human *GRB7* mRNA transcript is 2.4 kb long and is accompanied by a less abundant transcript of 4.1 kb [15, 17]. The *GRB7* gene comprises 15 exons, of which only 14 have total or partial coding capacity, yielding three transcripts of 2,107, 2,197 and 2,228 pb that differ only in their 5'-untraslated region (5'-UTR) and all encoding the same 532 amino acids (59.7 kDa) Grb7 protein. The C-terminal truncated variant Grb7V lacking the SH2 domain has 447 amino acids (49.4 kDa) and is encoded by a 1,667 pb transcript expressed by an altered gene with only 13 exons of which only 12 have total or partial coding capacity [18, 19].

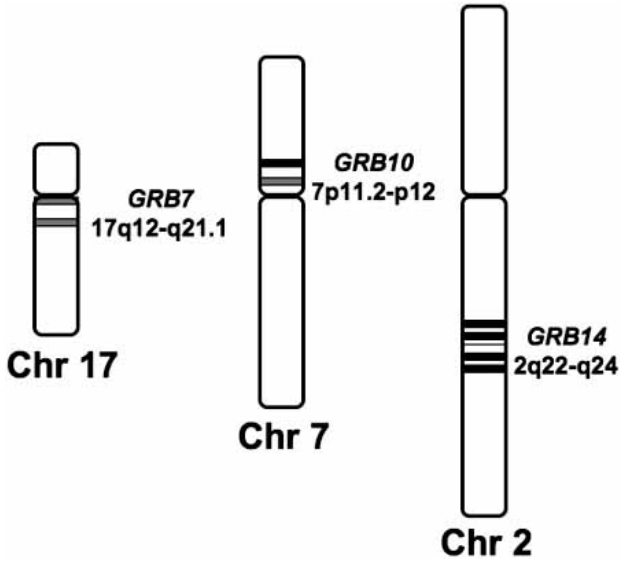

Fig. 2. Chromosomal localization of the human *GRB7, GRB10* and *GRB14* genes. The cartoon represents partial ideograms of human chromosomes (Chr) 17, 7 and 2 where the *GRB7, GRB10,* and *GRB14* genes are respectively located. The approximate distribution of chromosome bands corresponding to the loci: 17q12-q21.1 (for *GRB7*), close to the centromere in the long arm of chromosome 17; 7p11.2-p12 (for *GRB10*), close to the centromere of the small arm of chromosome 7; and 2q22-q24 (for *GRB14*), in the middle part of the long arm of chromosome 2, are shown. See text for additional details.

Mouse *Grb7* is located in chromosome 11 [14, 20] but in rats this gene maps in chromosome 10 [21, 19]. In pig, *GRB7* maps in chromosome 12 [22] and in chimpanzee is located in chromosome 17 like in human [19, 21]. The human and mouse chromosomal loci where *GRB7* reside, are evolutionarily conserved regarding the order and orientation of the genes they contain [20]. Murine *Grb7* mRNA is highly expressed in liver and kidney and to a lesser extent, in testis

and ovary with trace levels in lung, yielding a transcript of approximately 2.3 kb [23].

Among the new uncovered functional roles of the Grb7 protein, it has been recently described that it can act as a translational repressor upon binding to the 5'-UTR of a targeted mRNA, thereby blocking the recruitment of the translation eukaryotic initiation factor 4E (eIF4E) and silencing protein expression [8].

IMPLICATION OF *GRB7* IN CANCER

The *GRB7* and *ERBB2* genes are co-amplified and/or overexpressed in human gastric and esophageal carcinoma cell lines, and in primary gastric and esophageal cancers, particularly within the lower segment of the esophagus [14, 15, 24-26]. In some human esophageal carcinoma patients, amplification of the *GRB7* gene was not detected but its mRNA was overexpressed and co-expressed with the *ERBB2* and/or *EGFR* genes [27, 28]. In contrast, a positive correlation between an increased number of copies of the *GRB7* gene and elevated mRNA expression levels was found in gastric cancers [29]. The aforementioned Grb7 truncated isoform Grb7V, in which the SH2 domain was substituted by a short hydrophobic tail, was detected in highly invasive human esophageal carcinomas, presenting a particularly enhanced expression in metastasized lymph nodes, underscoring the role of the Grb7 protein in tumor invasion [18]. Genomic hybridization analysis using cDNA microarrays detected the co-amplification of the *ERBB2* and *GRB7* genes in a series of human gastric cancer xenographs, primary tumors and tumor cell lines, although overexpression was apparent for *ERBB2* but not for *GRB7* [25].

Co-amplification of *ERBB2* and *GRB7* was also found in human breast cancer cell lines [17], and has been additionally detected in non-invasive ductal carcinomas *in situ* [16]. Increased expression of *GRB7* correlates with a lower survival rate in breast cancer patients with tumors with either high or low expression of *ERBB2* [30, 31]. A subset of the estrogen receptor (ER)-negative breast cancer subtype presents overexpression of the genes within the *ERBB2* amplicon including *GRB7* [32]. *GRB7* expression not only positively correlates with *ERBB2* expression in human breast carcinoma but with *ERBB3* expression as well [33], although the latter maps at chromosome 12q13 [34]. Nevertheless, no association was found between common single-nucleotide polymorphisms (SNPs) in genes within the *ERBB2* amplicon and the risk of developing breast cancer in a study conducted in over two thousand patients when compared to a similar number of control subjects [35].

The *GRB7* gene also co-amplifies with additional genes located within the *ERBB2* amplicon such as *CAB1, A39, C51* and *MLN64* in gastric and breast cancers [17, 24]. However, the minimum region of recurrent amplification within the 17q12 amplicon includes just the *STARD3, ERBB2* and *GRB7* genes in human breast cancer [36].

An increased *GRB7* gene copy number was also detected in human testicular germ cell tumors, exhibiting a particularly high expression in immature teratoma, embryonal carcinoma, choriocarcinoma and some (but not all) seminoma, in contrast to its rare incidence in normal testicular tissues [37, 38]. In fact, *GRB7* is approximately 5-fold downregulated in most seminomas as compared to embryonal carcinomas [39]. However, no elevated *ERBB2* expression was found in these testicular tumors [37]. Instead, there is a positive correlation between the co-expression of *GRB7* and *KIT* (a gene encoding the v-*kit* Hardy-Zuckerman 4 feline sarcoma viral oncogene homolog receptor, another tyrosine kinase receptor that interacts with Grb7 and which maps at the locus 4q11-q12) in seminomas, but not in non-seminoma testicular tumors. In the latter, however, there was a positive correlation between the co-expression of *GRB7* and *KRAS2*, a gene encoding a small G protein of the Ras family, which maps to the 12p12.1-p11.2 locus [40].

The expression of the *GRB7* gene was also increased in cells from chronic lymphocytic leukemia patients, in which the highest expression levels were found in the advanced stages of the disease (stage IV) as compared to less advanced stages (stage I) [41].

THE *GRB10* GENE

In human, as in chimpanzee, the *GRB10* gene is located in chromosome 7 (see Fig. (**2**) center panel). The DOPA-decarboxylase (*DDC*) and Cordon-bleu (*COBL*) genes flank it and maps at the 7p11.2-p12 locus (or as described by others at the 7p11.1-p12 or 7p11.2-p12.2 locus), close to any event of the *EGFR* gene, which is located at ≈ 3.7 Mb toward the centromere [19, 21, 42-45]. This gene is alternatively spliced yielding transcripts that may encode a protein with a partial deletion of the PH domain and/or an N-terminal sequence addition. High expression of a prominent 4.7 kb transcript for the human *GRB10* splice variant denoted GRB10/IR-SV1 (insulin receptor bind spliced variant 1) (hGrb10α), a 548 amino acid (61.9 kDa) protein, with a deletion of 80 amino acids in the PH domain and a distinct N-terminus addition as compared to the mouse Grb10, are found in skeletal muscle and pancreas, and in lesser quantities in heart, brain, placenta, lung, liver and kidney [46]. A second *GRB10* 5.6 kb transcript encoding a 536 amino acid (60.7 kDa) protein with an intact PH domain named GRB-IRβ/GRB10 (hGrb10β) was later described and its expression also detected to be elevated in pancreas and skeletal muscle although it is also present in most tissues [47]. A third isoform of 594 amino acids (67.1 kDa) denoted hGrb10γ, containing the same N-terminal extension as hGrb10α but with an intact PH domain, was also described [43]. Its expression was also high in skeletal muscle and in some tumor cells, as HeLa cells and diverse breast cancer cell lines [43]. The detailed cloning and sequence analysis of the human *GRB10* gene shows the presence of 17 exons (or 22 if subdivided exons are considered) among translated and untranslated ones (see [19]), of which 14 participate in the translation of all isoforms described up to day, including not only the mentioned hGrb10α, hGrb10β and, hGrb10γ but also the additional described hGrb10ζ, hGrb10ε and hGrb10σ isoforms, while 3 additional exons are translated in at least one of the isoforms [48].

The mouse *Grb10* gene maps to chromosome 11, and is also flanked by the *Ddc* and *Cobl* genes. Like its human ortholog, *Grb10* is in the proximity of the *Egfr* gene, located at a distance of ≈ 4.9 Mb toward the centromere [44, 49]. It

was initially proposed that mouse *Grb10* encodes several isoforms of the protein (mGrb10) because of the existence of alternative translational start sites [49]. The most abundant transcripts are 5.5 kb and 1.5 kb long and the transcription of the mGrb10α and mGrb10δ isoforms is initiated at exon 1, although the mGrb10δ isoform originates from a spliced variant transcript lacking exon 5 as compared to the full-length transcript encoding the mGrb10α isoform [50]. The start of the translation occurs in exon 3 and ends at exon 18. The correlation between *Grb10* exons and the protein functional domains is as follows: exon 4 encodes the PR domain, exons 10-13 the PH domain, exons 13-16 encode the BPS domain and part of the SH2 domain and exons 16-18 the rest of the SH2 domain [50].

The expression of two prominent *GRB10* transcripts was also detected in the adipose tissue of the rhesus monkey [46]. Overexpression of *Grb10* mRNA occurs in fetal rat liver as compared to adult liver, where it nearly disappears, suggesting a role of this gene in tissue growth [51]. This was further supported by the enhanced expression of the *Grb10* gene found in fast growing cultured pre-implantation mouse embryos (blastocytes) [52].

IMPRINTING OF THE *GRB10* GENE

Genetic imprinting consists in the selective expression of a single allele of a given gene either that residing in the mother or in the father homologous chromosome, what results in a non-Mendelian inheritance pattern. The mechanism of imprinting may underlie the methylation of CpG dinucleotides lying in selected sectors of the gene such as the promoter region, catalyzed by specific DNA methyl-transferases; and/or chromatin modification, involving the posttranslational acetylation and/or methylation of histones bound to the targeted gene catalyzed by histone acetyl-transferases and methyl-transferases, respectively. These processes usually occur at the gametes and the imprinted mark is thereafter transmitted during embryonic development and through the subsequent developmental stages up to adulthood. In general, these differential DNA and histone modifications result in the epigenetic silencing of the targeted genes.

The human *GRB10* gene may be imprinted either paternally or maternally, or expressed from both alleles depending on the tissue and the protein isoform under consideration. Thus, in human fetal brain, the paternal allele is the one transcribed for most of the Grb10 isoforms, while in skeletal muscle, the transcribed allele for the Grb10γ1 isoform is from maternal origin [48], whereas biallelic expression was detected in other fetal peripheral tissues [53]. These and other authors noticed that the paternal-specific expression of human *GRB10* in the fetal central nervous system (brain and spinal cord) appositely differs from the maternal allele-only transcription in the mouse brain [48, 53]. Despite the imprinted nature of *GRB10*, no allele-specific methylation of most of the 5' CpG island of this gene in human fetal brain was found by these authors [48] and the silenced mouse *Grb10* allele remained inactive despite the exposure of cells to inhibitors of DNA methylation and of histone deacetylases [54]. Additional work revealed the maternal expression of *Grb10* in mouse embryos, adult kidney and liver; while in adult brain the paternal allele was mainly expressed [55]. Also, *Grb10* is paternally imprinted in bovine embryos, being expressed in both *in vitro*-fertilized and parthenogenetically activated blastocysts [56].

Uniparental disomy (UPD) consists in the inheritance of two homologous copies of a given chromosome (or part of a chromosome) from a single parent, either the mother or the father. This is most likely due to the rescue-driven loss of a third copy of the chromosome in an otherwise non-viable trisomic zygote, among other mechanisms. As earlier reviewed, paternal uniparental disomy (patUPD) affecting the mouse *Grb10* gene results in embryonic and postnatal overgrowth while maternal uniparental disomy (matUPD) results in undergrowth [57].

Within the promoter region of mouse *GRB10* are located two major 1.4 kb long CpG islands, the first encompassing exon 1a and the second encompassing exon 1b [50, 55]. These CpG islands are also present at analogous positions in human *GRB10*, presenting notorious sequence homologies in both species, except for a 600 bp mouse-specific tandem repeat in the promoter region of the parentally expressed gene [55, 58]. Both in mouse and human, DNA methylation at the *GRB10* promoter was not different in the paternal and maternal expressed alleles in the first CpG island, which was hipomethylated, but increased methylation was found in the second CpG island in the maternal allele as compared to the paternal one [55, 58]. Most recently, however, a third CpG island was identified around the subdivided exon 1c in mouse *Grb10* that exhibits extensive methylation in both maternal and parental alleles in neurons and glial cells [59]. Two distinct promoters, a major one active in most tissues and a brain-specific promoter located downstream of the first one were thus proposed to exist in the mouse and human *GRB10* genes [55]. In mouse, methylation of the CpG islands was not only detected during oocyte growth but they kept extensively methylated into adulthood [60]. Most interestingly, differential acetylation and methylation of histones in the nucleosomes containing the CpG islands 1 and 2 in the promoter of the parental alleles of the mouse *Grb10* gene have been detected in neurons, glia and fibroblasts, what may contribute to the epigenetic control of the expression of this gene [59].

As a consequence of imprinting, a deviation of a Mendelian 1:1 female/male transmission ratio of the grandparental alleles in the paternal chromosome containing the imprinted gene *GRB10* was found in females as compared to males where the fraction of the transmitted grandmaternal alleles was 0.38 and 0.5 respectively due to uneven loss of human embryos in the former [61].

IMPLICATION OF *GRB10* IN PATHOLOGICAL PROCESSES

Several connections between Grb10 and cancer have been reported. Thus, *Grb10* was shown to be overexpressed more than three-fold in mouse cells infected with tumorigenic adenovirus 12 as compared with cells infected with non-tumorigenic adenovirus 5 [62]. Also, increased expression of *GRB10* mRNA was detected in primary cervical squamous carcinomas in human as compared to normal uterine squamous cell tissues [63]. Furthermore, dysregulation of

GRB10 has been detected in human metastatic malignant melanomas [64].

Several transgenic mouse lines with ectopic overexpression of *Grb10* have been shown to present growth retardation after weaning and hyperinsulinemia due to insulin resistance [65]. Conversely, knockout mice with a disrupted *Grb10* gene exhibited body overgrowth, particularly due to muscle mass increase accompanied by decreased adiposity, as well as increased glucose tolerance, insulin sensitivity and insulin-mediated cellular signaling [66, 67]. These observations appear to link Grb10 to the pathogenesis of type 2 diabetes. In this context, it has been shown that some SNPs in the *GRB10* gene correlates indeed with type 2 diabetes in human [68].

Albeit the important role of Grb10 in organismal development, and in contrast to the RET tyrosine kinase, which is one of its upstream signaling receptors, mutations in *GRB10* were not linked to Hirschsprung disease, a congenital condition characterized by the absence of intrinsic enteric ganglion cells in some sectors of the gastrointestinal track, including the colon, which results in a distended atonic megacolon [69].

The Silver-Russell syndrome (SRS) is an inherited condition characterized by intrauterine and postnatal growth retardation resulting in typical dysmorphic features, such as a small triangular face with down-turned corners of the mouth, prominent forehead, skeletal asymmetry of the trunk and limbs, and clinodactyly of the fifth finger, which consists in its inner bending due to an undeveloped middle phalange [70]. Multiple genetic alterations have been associated with SRS. Among them and of particular importance to us are: the maternal uniparental disomy of chromosome 7 (matUPD7) occurring in 7-10 % of SRS patients, in which disruption of genomic imprinting takes place; and a few patients where maternal duplication of the 7p11.2-p13 region was detected [70-72]. Although *GRB7* maps close to a translocation breakpoint in chromosome 17 detected in three SRS patients, the implication of the *GRB7* gene in this syndrome was soon discarded [73].

The first indication, however, of the possible implication of *GRB10* as a candidate gene for the SRS was obtained in the mouse, where the imprinted gene *Meg1/Grb10* was associated with the maternal or paternal duplication of proximal chromosome 11, where this gene is located, which was correlated with prenatal growth retardation or growth promotion, respectively [74]. Soon thereafter, sub-microscopic duplication of the 7p12.1-p13 region of human chromosome 7, which includes the *GRB10* gene among others, was detected in mothers and daughters with SRS phenotypes [75, 76], although this duplication was found in only 2.4 % of 32 additional SRS patients screened [77]. Interestingly, a partial matUPD7 was described in an SRS patient in which only a small segment of matUPD7 occurred while the rest of chromosome 7 was of biparental inheritance, including *GRB10* [78]. This particular segmental matUPD7 led to suggest that *GRB10* may not be central to SRS etiology [71], although SRS patients with three *GRB10* copies were later detected [79]. Also, against the implication of *GRB10* in the etiology of SRS it has been argued that the imprinting of this gene in brain and skeletal muscle is incomplete and isoform-specific, and that there is absence of *GRB10* imprinting in the growth cartilage plates, a tissue involved in very active growth in young subjects [80].

Also, mutations in *GRB10* accounting for a proline to serine substitution at residue 95 of Grb10 were detected in two out of 58 screened SRS patients [81], although an additional study did not reveal *GRB10* mutations in a subset of 18 SRS patients with non-matUPD7 [53]. In contrast, although frequent SNPs were found in exons 3 and 12, and intron 3, as well as a heterozygous microsatellite repeat in intron 14 of the *GRB10* gene of SRS patients, no other alterations have been detected, further suggesting to those authors that this gene does not play a major role in the etiology of SRS [48]. Furthermore, no epimutations in the differentially-methylated region of the *GRB10* gene were found in a large set of 46 screened SRS patients performed in two independent studies [58, 82].

THE *GRB14* GENE

Using fluorescence *in situ* hybridization, the *GRB14* gene was located in the long arm of human chromosome 2, most precisely in the 2q22-q24 locus (see Fig. (**2**) right panel), relatively close to the *ERBB4* gene located at the 2q33.3-q34 locus [83]. These authors also detected minor hybridization signals at 12q13 and 6q27, which they suggested were derived from other *GRB7* related genes [83]. The *GRB14* gene comprises 14 exons, which yield the 2,382 bp *GRB14* transcript that encodes for the 540 amino acid residues (60.9 kDa) protein (see [19, 21]). The human *GRB14* mRNA is highly expressed in liver, kidney, pancreas, ovary, testis, heart and skeletal muscles and it is also very abundantly present in kidney embryonic cells, some prostate cancer cell lines and breast cancer cells [84], particularly in ER-positive cell lines [84, 85]. Originally, three most prominent mRNA transcripts of 2.3, 2.4 and 2.5 kb were detected, which were frequently accompanied by a less abundant 9.5 kb transcript [84].

The chimpanzee and mouse *GRB14* orthologs are located in chromosome 2, whereas the rat gene maps in chromosome 3 (see [19]). In both mouse and rat, Grb14 is a 538 amino acid protein highly expressed in insulin-responsive tissues such as liver, heart, skeletal muscle, pancreas and white adipose tissues, as well as in the brain, and is encoded by a major 2.5 kb transcript and a lesser 1.9 kb transcript [86]. Mouse Grb14 bears 93 % sequence identity to rat Grb14 and 85 % sequence identity to human Grb14 [87].

IMPLICATION OF *GRB14* IN PATHOLOGICAL PROCESSES

The *GRB14* gene is highly transcribed in human breast and prostate tumor cells [84, 85], which might underscore its potential implication in cancer biology. Moreover, a high mutation frequency of this gene has been found in human colorectal cancers showing microsatellite instability (30 % of primary tumors and 50 % of tumor cell lines), as they are prone to failure in repairing errors occurring during DNA replication [88]. *GRB14* expression is under hormonal control since it is downregulated by estradiol and upregulated by

insulin [85], and overexpression of *GRB14* has been detected in animal models and human patients exhibiting insulin resistance due to type 2 diabetes [89].

FUTURE PERSPECTIVES

The study of the organization and control of the genes encoding the three Grb7 family members is still in its infancy. Among the relevant issues that still require great experimental attention we should mention the full characterization of the promoter regions of *GRB7, GRB10,* and *GRB14*, the complete identification of the panel of transcription factors and accessory proteins involved in their expression and the potential role of iRNAs controlling the translation of their respective transcriptional products. Among the specific issues related to the alterations observed in the organization of these genes, it should be of interest to unravel the underlying mechanisms of amplicon duplication involving the *GRB7* and *ERBB2* genes, as observed in some human cancers (see [1-3, 7] for reviews and references therein); as well as the mechanisms responsible for the observed segmental UPD of chromosome 7 in a number of Silver-Russell syndrome patients that, although appears not to affect the *GRB10* gene [78], might clarify the basis of this congenital defect. Given the negative control exerted by the Grb10 and Grb14 proteins on cell proliferation (see [1-4, 9-11, 13] for reviews and references therein), it should be of interest to perform a systematic screening of tumors in search of disabling mutations affecting the *GRB10* and *GRB14* genes, in order to determine whether they might work as tumor suppressor genes. Alternatively, and given that Grb10 also appears to exert a promitogenic function in some context [12], it should be of interest to explore whether mutations in the *GRB10* gene, in addition to those already known, could be of relevance to explain the high proliferation rate of some tumors. Poly(ADP-ribose) polymerases catalyze the poly-ADP-ribosylation of proteins, including those involved in the control of the maintenance of genomic functionality and integrity, because of their participation in single- and double-strand DNA repair, recombination and replication, gene transcription and control of telomeric functions [90]. Tankyrase-2, which belongs to this group of poly(ADP-ribose) polymerases, has been shown to bind to the Grb14 protein [91]. As this enzyme has a relevance in telomere maintenance [90], further work should be performed to determine whether or not the *GRB14* gene might control processes related to cellular senescence. Finally, given the variety of signaling pathways in which the three family members Grb7/Grb10/Grb14 appear to be involved, it may not be out of the ordinary that mutations and/or rearrangements affecting their encoding genes, and hence the stability of their transcripts and/or the functionality of their protein products, are found in additional congenital pathological processes in human and/or animal models, and hence clarifying their etiologies. A prediction that only a sustained experimental effort in this direction may only confirm this or contrarily falsify.

ACKNOWLEDGEMENTS

Work in the authors' laboratory was financed by grants (to A.V.) from the Dirección General de Investigación, Ministerio de Educación y Ciencia (SAF2005-00631), the Consejería de Educación de la Comunidad de Madrid (S-BIO-0170-2006), the Agencia Española de Cooperación Internacional (A/5444/06) and the European Commission (MRTN-CT-2005-19561). We are thankful to Dr. José Martín-Nieto from the Universidad de Alicante for critical reading of the manuscript and useful suggestions.

ABBREVIATIONS

Akt	=	v-*akt* murine thymoma viral oncogene homolog
BPS	=	Between PH and SH2
COBL	=	Cordon-bleu gene
DDC	=	DOPA-decarboxylase gene
EGFR	=	Epidermal growth factor receptor
eIF4E	=	Eukaryotic initiation factor 4E
Eph	=	Erythropoietin-producing hepatocellular carcinoma cells
ER	=	Estrogen receptor
ERBB	=	Erythroblastic leukemia viral oncogene homolog
FAK	=	Focal adhesion kinase
Grb	=	Growth factor receptor bound
IGF-I	=	Insulin-like growth factor-I
IR	=	Insulin receptor
KIT	=	v-*kit* Hardy-Zuckerman 4 feline sarcoma viral oncogene homolog
matUPD	=	Maternal UPD
matUPD7	=	matUPD of chromosome 7
PDGF-BB	=	Platelet-derived growth factor-BB
patUPD	=	Paternal UPD
PH	=	Pleckstrin homology
PI3K	=	Phosphatidylinositol 3-kinase
PR	=	Proline-rich
RA	=	Ras-associating
SH2	=	Src homology 2
SH3	=	Src homology 3
SNP	=	Single-nucleotide polymorphism
UPD	=	Uniparental disomy
5'-UTR	=	5'-untraslated region

REFERENCES

[1] Daly, R. J. The Grb7 family of signalling proteins. *Cell. Signal.* **1998**, *10:* 613-618.

[2] Han, D. C., Shen, T.-L., Guan, J.-L. The Grb7 family proteins: structure, interactions with other signaling molecules and potential cellular functions. *Oncogene* **2001**, *20:* 6315-6321.

[3] Villalobo, A., Li, H., Sánchez-Torres, J. The Grb7 protein family. *Curr. Topics Biochem. Res.* **2003**, *5:* 105-114.

[4] Holt, L., Siddle, K. Grb10 and Grb14: enigmatic regulators of insulin action - and more? *Biochem. J.* **2005**, *388:* 393-406.

[5] Manser, J., Roonprapunt, C., Margolis, B. *C. elegans* cell migration gene mig-10 shares similarities with a family of SH2 domain pro-

teins and acts cell nonautonomously in excretory canal development. *Dev. Biol.* **1997**, *184:* 150-164.

[6] Li, H., Sánchez-Torres, J., del Carpio, A. F., Nogales-González, A., Molina-Ortiz, P., Moreno, M. J., Török, K., Villalobo, A. The adaptor Grb7 is a new calmodulin-binding protein: functional implications of the interaction of calmodulin with Grb7. *Oncogene* **2005**, *24:* 4206-4219.

[7] Shen, T.-L., Guan, J.-L. GRB7 in intracellular signaling and its role in cell regulation. *Front. Biosci.* **2004**, *9:* 192-200.

[8]** Tsai, N.-P., Bi, J., Wei, L.-N. The adaptor Grb7 links netrin-1 signaling to regulation of mRNA translation. *EMBO J.* **2007**, *26*, 1522-1531.
(This work identify a new mechanism by which Grb7 binds to mRNA, silencing protein translation by preventing the recruitment of the eukaryotic initiation factor 4E. The mechanism operate by transmitting netrin-1 signals to the translation machinery via the focal adhesion kinase)

[9] Morrione, A. Grb10 adapter protein as regulator of insulin-like growth factor receptor signaling. *J. Cell. Physiol.* **2003**, *197:* 307-311.

[10] Riedel, H. GRB10 exceeding the boundaries of a common signaling adapter. *Front. Biosci.* **2004**, *9:* 603-618.

[11] Lim, M. A., Riedel, H., Liu, F. GRB10: more than a simple adaptor protein. *Front. Biosci.* **2004**, *9:* 387-403.

[12] Wang, J., Day, H., Yousaf, N., Moussaif, M., Deng, Y., Boufelliga, A., Swamy, O. R., Leone, M. E., Riedel, H. Grb10, a positive signaling adapter in platelet-derived growth factor BB-, insulin-like growth factor I-, and insulin-mediated mitogenesis. *Mol. Cell. Biol.* **1999**, *19:* 6217-6228.

[13] Cariou, B., Bereziat, V., Moncoq, K., Kasus-Jacobi, A., Perdereau, D., Le Marcis, V., Burnol, A.-F. Regulation and functional roles of GRB14. *Front. Biosci.* **2004**, *9:* 1626-1636.

[14] Stein, D., Wu, J., Fuqua, S.A.W., Roonprapunt, C., Yajnik, V., D'Eustachio, P., Moskow, J.J., Buchberg, A.M., Osborne, C.K., Margolis, B. The SH2 domain protein GRB-7 is co-amplified, overexpressed and in a tight complex with HER2 in breast cancer. *EMBO J.* **1994**, *13:* 1331-1340.

[15] Akiyama, N., Sasaki, H., Ishizuka, T., Kishi, T., Sakamoto, H., Onda, M., Hirai, H., Yazaki, Y., Sugimura, T., Terada, M. Isolation of a candidate gene, *CAB1*, for cholesterol transport to mitochondria from the c-*ERBB*-2 amplicon by a modified cDNA selection method. *Cancer Res.* **1997**, *57:* 3548-3553.

[16] Andrechek, E.R., Laing, M.A., Girgis-Gabardo, A.A., Siegel, P.M., Cardiff, R.D., Muller W.J. Gene expression profiling of neu-induced mammary tumors from transgenic mice reveals genetic and morphological similarities to ErbB2-expressing human breast cancer. *Cancer Res.* **2003**, *63:* 4920-4926.

[17] Kauraniemi, P., Bärlund, M., Monni, O., Kallioniemi, A. (2001) New amplified and highly expressed genes discovered in the *ERBB2* amplicon in breast cancer by cDNA microarrays. *Cancer Res.* **2001**, *61:* 8235-8240.

[18] Tanaka, S., Mori, M., Akiyoshi, T., Tanaka, Y., Mafune, K., Wands, J.R., Sugimachi, K. A novel variant of human Grb7 is associated with invasive esophageal carcinoma. *J. Clin. Invest.* **1998**, *102:* 821-827.

[19] Ensembl Genome Database. http://www.ensembl.org/index.html

[20] Katoh, M., Katoh, M. Identification and characterization of mouse Erbb2 gene in silico. *Int. J. Oncol.* **2003**, *23:* 831-835.

[21] GenBank NCBI Database. http://www.ncbi.nlm.nih.gov/sites/entrez?db=gene

[22] Yang, J., Li, K., Liu, B., Yerle, M., Fan, B., Xiong, T., Yu, M. Assignments of *GRB7*, *GCN5L2*, *COL1A1* and *TBCD* to pig chromosome 12 by radiation hybrid mapping. *Cytogenet. Genome Res.* **2003**, *103:* 204L.

[23] Margolis, B., Silvennoinen, O., Comoglio, F., Roonprapunt, C., Skolnik, E., Ullrich, A., Schlessinger, J. High-efficiency expression/cloning of epidermal growth factor-receptor-binding proteins with Src homology 2 domains. *Proc. Natl. Acad. Sci. USA* **1992**, *89:* 8894-8898.

[24] Kishi, T., Sasaki, H., Akiyama, N., Ishizuka, T., Sakamoto, H., Aizawa, S., Sugimura, T., Terada, M. Molecular cloning of human *GRB-7* co-amplified with *CAB1* and c-*ERBB-2* in primary gastric cancer. *Biochem. Biophys Res. Commun.* **1997**, *232:* 5-9.

[25] Varis, A., Wolf, M., Monni, O., Vakkari, M.-L., Kokkola, A., Moskaluk, C., Frierson, H.Jr., Powell, S.M., Knuutila, S., Kallioniemi, A., El-Rifai W. Targets of gene amplification and overexpression at 17q in gastric cancer. *Cancer Res.* **2002**, *62:* 2625-2629.

[26] Maqani, N., Belkhiri, A., Moskaluk, C., Knuutila, S., Dar, A.A., El-Rifai, W. Molecular dissection of 17q12 amplicon in upper gastrointestinal adenocarcinomas. *Mol. Cancer Res.* **2006**, *4:* 449-455.

[27] Tanaka, S., Mori, M., Akiyoshi, T., Tanaka, Y., Mafune, K., Wands, J.R., Sugimachi, K. Coexpression of Grb7 with epidermal growth factor receptor or Her2/erbB2 in human advanced esophageal carcionoma. *Cancer Res.* **1997**, *57:* 28-31.

[28] Dahlberg, P.S., Jacobson, B.A., Dahal, G., Fink, J.M., Kratzke, R.A., Maddaus, M.A., Ferrin, L.J. ERBB2 amplifications in esophageal adenocarcinoma. *Ann. Thoracic Surg.* **2004**, *78:* 1790-1800.

[29] Yang, S., Jeung, H.-C., Jeong, H.J., Choi, Y.H., Kim, J.E., Jung, J.-J., Rha, S.Y., Yang, W.I., Chung, H.C. Identification of genes with correlated patterns of variations in DNA copy number and gene level in gastric cancer. *Genomics* **2007**, *89:* 451-459.

[30] Vinatzer, U., Dampier, B., Streubel, B., Pacher, M., Seewald, M.J., Stratowa, C., Kaserer, K., Schreiber, M. Expression of *HER2* and the coamplified genes *GRB7* and *MLN64* in human breast cancer: quantitative real-time reverse transcription-PCR as a diagnostic alternative to immunochemistry and fluorescence *in situ* hybridization. *Clin. Cancer Res.* **2005**, *11:* 8348-8357.

[31] Cobleigh, M.A., Tabesh, B., Bitterman, P., Baker, J., Cronin, M., Liu, M.-L., Borchik, R., Mosquera, J.-M., Walker, M.G., Shak S. Tumor gene expression and prognosis in breast cancer patients with 10 or more positive lymph nodes. *Clin. Cancer Res.* **2005**, *11:* 8623-8631.

[32] Carrivick, L., Rogers, S., Clark, J., Campbell, C., Girolami, M., Cooper, C. Identification of prognostic signatures in breast cancer microarray data using Bayesian techniques. *J. R. Soc. Interface* **2006**, 3: 367-381.

[33] Bièche, I., Onody, P., Tozlu, S., Driouch, K., Vidaud, M., Lidereau, R. Prognostic value of *ERBB* family mRNA expression in breast carcinomas. *Int. J. Cancer* **2003**, *106:* 758-765.

[34] Kraus, M.H., Issing, W., Miki, T., Popescu, N.C., Aaronson, S.A. Isolation and characterization of *ERBB3*, a third member of the *ERBB*/epidermal growth factor receptor family: evidence for overexpression in a subset of human mammary tumors. *Proc. Natl. Acad. Sci. USA* **1989**, *86:* 9193-9197.

[35] Benusiglio, P.R., Pharoah, P.D., Smith, P.L., Lesueur, F., Conroy, D., Luben, R.N., Dew, G., Jordan, C., Dunning, A., Easton, D.F., Ponder, B.A.J. HapMap-based study of the 17q21 *ERBB2* amplicon in susceptibility to breast cancer. *Br. J. Cancer* **2006**, *95:* 1689-1695

[36] Kao, J., Pollack, J.R. RNA interference-based functional dissection of the 17q12 amplicon in breast cancer reveals contribution of coamplified genes. *Genes Chromos. Cancer* **2006**, *45:* 761-769.

[37] Skotheim, R.I., Monni, O., Mousses, S., Fosså, S.D., Kallioniemi. O.-P., Lothe, R.A., Kallioniemi, A. New insights into testicular germ cell tumorigenesis from gene expression profiling. *Cancer Res.* **2002**, *62:* 2359-2364.

[38] Skotheim, R.I., Abeler, V.M., Nesland J.M., Fosså, S.D., Holm, R., Wagner, U., Flørenes, V.A., Aass, N., Kallioniemi, O.P., Lothe R.A. Candidate genes for testicular cancer evaluate by *in situ* protein expression analyses on tissue microarrays. *Neoplasia* **2003**, 5: 397-404.

[39] Hofer, M.D., Browne, T.J., He, L., Skotheim, R.I., Lothe, R.A., Rubin, M.A. Identification of two molecular groups of seminomas by using expression and tissue microarrays. *Clin. Cancer Res.* **2005**, *11:* 5722- 5729.

[40] McIntyre, A., Summersgill, B., Spendlove, H., Huddart, R., Houlston, R., Shipley, J. Activating mutations and/or expression levels of tyrosine kinase receptors *GRB7*, *RAS*, and *BRAF* in testicular germ cell tumors. *Neoplasia* **2005**, *7:* 1047-1052.

[41] Haran, M., Chebatco, S., Flaishon, L., Lantner, F., Harpaz-Berrebi, N., Shachar, I. Grb7 expression and cellular migration in chronic lymphocytic leukemia: a comparative study of early and advanced stage disease. *Leukemia* **2004**, *18:* 1948-1950.

[42] Jerome, C.A., Scherer, S.W., Tsui, L.-C., Gietz, R.D., Triggs-Raine B. Assignment of growth factor receptor-bound protein 10 (*GRB10*) to human chromosome 7p11.2-p12. *Genomics* **1997**, *40:* 215-216.

[43] Dong, L. Q., Du, H., Porter, S. G., Kolakowski, L. F. Jr., Lee, A. V., Mandarino, J., Fan, J., Yee, D., Liu, F. Cloning, chromosome location, expression, and characterization of an Src homology 2

and pleckstrin homology domain-containing insulin receptor binding protein hGrb10γ. *J. Biol. Chem.* **1997**, *272:* 29104-29112.

[44] Hitchins, M.P., Bentley, L., Monk, D., Beechey, C., Peters, J., Kelsey, G., Ishino, F., Preece, M.A., Stainer, P., Moore G.E. *DDC* and *COBL*, flanking the imprinted *GRB10* gene on 7p12, are biallelically expressed. *Mammalian Genet.* **2002a**, *13:* 686-691.

[45] Katoh, M., Katoh M. Identification and characterization of human ZPBP-like gene *in silico*. *Int. J. Mol. Med.* **2003b**, *12:* 399-404.

[46] O´Neill, T.J., Rose, D.W., Pillay, T.S., Hotta, K., Olefsky, J.M., Gustafson T.A. Interaction of a GRB-IR splice variant (a human Grb10 homolog) with the insulin and the insulin-like growth factor I receptors. *J. Biol. Chem.* **1996**, *271:* 22506-22513.

[47] Frantz, J.D., Giorgetti-Peraldi, S., Ottinger E.A., Schoelson, S.E. Human GRB-IRβ/GRB10: splice variants of an insulin and growth factor receptor-binding protein with PH and SH2 domains. *J. Biol. Chem.* **1997**, *272:* 2659-2667.

[48] Blagitko, N., Mergenthaler, S., Schulz, U., Wollmann, H.A., Craigen, W., Eggermann, T., Ropers, H.-H., Kalscheuer, V.M. Human *GRB10* is imprinted and expressed from the paternal and maternal allele in a highly tissue- and isoform-specific fashion. *Hum. Mol. Genet.* **2000**, *9:* 1587-1696

[49] Ooi, J., Yajnik, V., Immanuel, D., Gordon, M., Moskow, J.J., Buchwerg, A.M., Margolis, B. The cloning of Grb10 reveals a new family of SH2 domain proteins. *Oncogene* **1995**, *10:* 1621-1630

[50] Charalambous, M., Smith, F.M., Bennett, W.R., Crew, T.E., Mackenzie, F., Ward, A. Disruption of the imprinted *Grb10* gene leads to disproportionate overgrowth by an *Igf2*-independent mechanism. *Proc. Natl. Acad. Sci. USA* **2003**, *100:* 8292-8297.

[51] Gruppuso, P.A., Boylan, J.M., Vaslet C.A. Identification of candidate growth-regulating genes that are overexpressed in late gestation fetal liver in the rat. *Biochim. Biophys. Acta* **2000**, *1494:* 242-247.

[52] Khosla, S., Dean, W., Brown, D., Reik, W., Feil R. Culture of preimplantation mouse embryos affects fetal development and the expression of imprinted genes. *Biol. Reprod.* **2001**, *64:* 918-926

[53] Hitchins, M.P., Monk, D., Bell, G.M., Ali, Z., Preece, M.A., Stainer, P., Moore, G.E. Maternal repression of the human *GRB10* gene in the developing central nervous system; evaluation of the role for *GRB10* in Silver-Russell syndrome. *Eur. J. Hum. Genet.* **2001** *9:* 82-90.

[54] El Kharroubi, A., Piras, G., Stewart, C.L. DNA demethylation reactives a subset of imprinted genes in uniparental mouse embryonic fibroblasts. *J. Biol. Chem.* **2001**, *276:* 8674-8680.

[55] Hikichi, T., Kohda, T., Kaneko-Ishino, T., Ishino, F. Imprinting regulation of the murine *Meg1/Grb10* and human *GRB10* genes; roles of brain specific promoters and mouse specific CTCF-binding sites. *Nucleic Acids Res.* **2003**, *31:* 1398-1406

[56] Ruddock, N.T., Wilson, K.J., Cooney, M.A., Korfiatis, N.A., Tercirlioglu, R.T., French, A.J. Analysis of imprinted messenger RNA expression during bovine preimplantation development. *Biol. Reprod.* **2004**, *70:* 1131-1135.

[57] Smith, F.M., Garfield, A.S., Ward A. Regulation of growth and metabolism by imprinted genes. *Cytogenet. Genome Res.* **2006**, *113:* 279-291.

[58] Arnaud, P., Monk, D., Hitchins, M., Gordon, E., Dean, W., Beechey, C.V., Peters, J., Craigen, W., Preece, M., Stanier, P., Moore, G.E., Kelsey, G. Conserved methylation imprints in the human and mouse GRB10 genes with divergent allelic expression suggests differential reading of the same mark. *Hum. Mol. Genet.* **2003**, *12:* 1005-1019.

[59]** Yamasaki-Ishizaki, Y., Kayashima, T., Mapendano, C.K., Soejima, H., Ohta, T., Masuzaki, H., Kinoshita, A., Urano. T., Yoshiura, K., Matsumoto, N., Ishimaru, T., Mukai, T., Niikawa, N., Kishino, T. Role of DNA methylation and histone H3 lysine 27 methylation in tissue-specific imprinting of mouse *Grb10*. *Mol. Cell. Biol.* **2007**, *27:* 732-742.
(This work describes in great detail the regulation of the tissue-specific imprinting mechanism of Grb10 by DNA methylation and chromatin remodeling by Polycomb group proteins)

[60] Hiura, H., Obata, Y., Komiyama, J., Shirai, M., Kono, T. Oocyte growth-dependent progression of maternal imprinting in mice. *Genes Cells* **2006**, *11:* 353-361.

[61] Naumova, A.K., Greenwood, C.M.T., Morgan, K. Imprinting and deviation from Mendelian transmission ratios. *Genome* **2001**, *44:* 311-320.

[62] Guan, H., Smirnov, D.A., Ricciardi, R.P. Identification of genes associated with adenovirus 12 tumorigenesis by microarray. *Virology* **2003**, *309:* 114-124.

[63] Okino, K., Konishi, H., Doi, D., Yoneyama, K., Ota, Y., Jin, E., Kawanami, O., Takeshita, T. Up-regulation of growth factor receptor-bound protein 10 in cervical squamous cell carcinoma. *Oncol. Rep.* **2005**, *13:* 1069-1074.

[64] Mirmohammadsadegh, A., Baer, A., Nambiar, S., Bardenheuer, W., Hengge, U.R. Rapid identification of dysregulated genes in cutaneous malignant melanoma metastases using cDNA technology. *Cells Tissues Organs* **2004**, *177:* 119-123.

[65] Shiura, H., Miyoshi, N., Konishi, A., Wakisaka-Saito, N., Suzuki, R., Muguruma, K., Kohda, T., Wakana, S., Yokoyama, M., Ishino, F., Kaneko-Ishino, T. *Meg1/Grb10* overexpression causes postnatal growth retardation and insulin resistance via negative modulation of the IGF1R and IR cascades. *Biochem. Biophys. Res. Commun.* **2005**, *329:* 909-916.

[66]** Smith, F.M., Holt, L.J., Garfield, A.S., Charalambous, M., Koumanov, F., Perry, M., Bazzani, R., Sheardown, S.A., Hegarty, B.D., Lyons, R.J., Cooney, G.J., Daly, R.J., Ward, A. Mice with a disruption of the imprinted *Grb10* gene exhibit altered body composition, glucose homeostasis, and insulin signaling during postnatal life. *Mol. Cell. Biol.* **2007**, *27:* 5871-5886.
(The work described in this paper shows that disruption of the *Grb10* gene in a mouse model enhances insulin signaling thus increasing glucose tolerance and insulin sensitivity. This demonstrates the negative regulatory role of the adaptor protein on the insulin receptor *in vivo*, which together with the related paper in Ref. 67 hints to the implication of the Grb10 protein in the pathogenesis of diabetes mellitus type II)

[67]** Wang, L., Balas, B., Christ-Roberts, C.Y., Kim, R. Y., Ramos, F.J., Kikani, C.K., Li, C., Deng, C., Reyna, S., Musi, N., Dong, L.Q., DeFronzo, R.A., Liu, F. Peripheral disruption of the Grb10 gene enhances insulin signaling and sensitivity *in vivo*. *Mol. Cell. Biol.* **2007**, *27:* 6497-6505.
(This work describes in a peripheral-tissue-specific *Grb10* knockout mouse model the resulting increase in glucose tolerance and insulin sensitivity in peripheral tissues. Further supporting, as the related paper in Ref. 66, the possible implication of Grb10 in the pathogenesis of diabetes mellitus type II)

[68] Di Paola, R., Ciociola, E., Boonyasrisawat, W., Nolan, D., Duffy, J., Miscio, G., Cisternino, C., Fini, G., Tassi, V., Doria, A., Trischitta, V. Association of hGrb10 genetic variations with type 2 diabetes in caucasian subjects. *Diabetes Care* **2006**, *29:* 1181-1182.

[69] Angrist, M., Bolk, S., Bentley, K., Nallasamy, S., Halushka, M.K., Chakravarti, A. Genomic structure of the gene for the SH2 and pleckstrin homology domain-containing protein *GRB10* and evaluation of its role in Hirschsprung disease. *Oncogene* **1998**, *17:* 3065-3070.

[70] Hitchins M.P., Stanier P, Preece MA, Moore GE. Silver-Russell syndrome: a dissection of the genetic aetiology and candidate chromosomal regions. *J. Med. Genet.* **2001**, *38:* 810-819.

[71] Aldred, M. Homing in on Russell-Silver. *Trends Mol. Med.* **2001**, *7:* 100.

[72] Kim, Y., Kim, S.-S., Kim, G., Park, S., Park, I.S., Yoo, H.-W. Detection of maternal uniparental disomy at the two imprinted genes on chromosome 7, *GRB10* and *PEG1/MEST*, in a Silver-Russell syndrome patient using methylation-specific PCR assays. *Clin. Genet.* **2004**, *67:* 267-269.

[73] Hitchins, M.P., Abu-Amero, S., Apostolidou, S., Monk ,D., Stanier, P., Preece, M.A., Moore, G.E. Investigation of the *GRB2*, *GRB7*, and *CSH1* genes as candidates for the Silver-Russell syndrome (SRS) on chromosome 17q. *J. Med. Genet.* **2002**, *39:* E13.

[74] Miyoshi, N., Kuroiwa, Y., Kohda, T., Shitara, H., Yonekawa, H., Kawabe, T., Hasegawa, H., Barton, S.C., Surani, M.A., Kaneko-Ishino, T., Ishino, F. Identification of the *Meg1/Grb10* imprinted gene on mouse proximal chromosome 11, a candidate for the Silver-Russell syndrome gene. *Proc. Natl. Acad. Sci. USA* **1998**, *95:* 1102-1107.

[75] Joyce, C.A., Sharp, A., Walker, J.M., Bullman, H., Temple, I.K. Duplication of 7p12.1-p13, including *GRB10* and *IGFBP1*, in a mother and daughter with features of Silver-Russell syndrome. *Hum. Genet.* **1999**, *105:* 273-280.

[76] Monk, D., Wakeling, E.L., Proud, V., Hitchins, M., Abu-Amero, S.N., Stainer, P., Preece, M.A., Moore, G.E. Duplication of 7p11.2-

p13, including *GRB10*, in Silver-Russell syndrome. *Am. J. Hum. Genet.* **2000**, *66:* 36-46.

[77] Mergenthaler, S., Sharp, A., Ranke, M.B., Kalscheuer, V.M., Wollmann, H.A., Eggermann, T. (2001) Gene dosage analysis in Silver-Russell syndrome: use of quantitative competitive PCR and dual-color FISH to estimate the frequency of duplications in 7p11.2-p13. *Genet. Testing* **2001**, *5:* 261-266.

[78] Hannula K., Lipsanen-Nyman M., Kontiokari T. and Kere J. A narrow segment of maternal uniparental disomy of chromosome 7q31-qter in Silver-Russell syndrome delimits a candidate gene region. *Am. J. Hum. Genet.* **2001**, *68:* 247-253.

[79] Eggermann, T., Meyer, E., Wollmann, H.A. Quantification of GRB10 in 7p12-p14 by fluorogenic 5´ nuclease chemistry and application for genetic diagnosis in Silver-Russell syndrome. *Ann. Gen.* **2004**, *47:* 99-102.

[80] McCann, J.A., Zheng, H., Islam, A., Goodyer, C.G., Polychronakos, C. Evidence against *GRB10* as the gene responsible for Silver-Russell syndrome. *Biochem. Biophys. Res. Commun.* **2001**, *286:* 943-948.

[81] Yoshihashi, H., Maeyama, K., Kosaki, R., Ogata, T., Tsukahara, M., Goto, Y., Hata, J., Matsuo, N., Smith, R.J., Kosaki, K. Imprinting of human *GRB10* and its mutations in two patients with Russell-Silver syndrome. *Am. J. Hum. Genet.* **2000**, *67:* 476-482.

[82] Monk, D., Smith, R., Arnaud, P., Preece, M.A., Stanier, P., Beechey, C.V, Peters, J., Kelsey, G., Moore, G.E. Imprinted methylation profiles for proximal mouse chromosomes 11 and 7 as revealed by methylation-sensitive representational difference analysis. *Mammalian Gen.* **2003**, *14:* 805-816.

[83] Baker, E., Sutherland, G.R., Sutherland, R.L., Daly J. Assignment of the human *GRB14* gene to chromosome 2q22-q24 by fluorescence *in situ* hybridization. *Genomics* **1996**, *36:* 218-220.

[84] Daly, R.J., Sanderson, G.M., Janes, P.W., Sutherland R. L. Cloning and characterization of *GRB14*, a novel member of the *GRB7* gene family. *J. Biol. Chem.* **1996**, *271:* 12502-12510.

[85] Kairouz, R., Parmar, J., Lyons, R. J., Swarbrick, A., Musgrove, E.A., Daly, R. J. Hormonal regulation of the Grb14 signal modulator and its role in cell cycle progression of MCF-7 human breast cancer cells. *J. Cell.* Physiol. **2005**, *203:* 85-93.

[86] Kasus-Jacobi, A., Perdereau, D., Auzan, C., Clauser, E., Van Obberghen, E., Mauvais-Jarvis, F., Girard, J., Burnol, A.-F. Identification of the rat adapter Grb14 as an inhibitor of insulin actions. *J. Biol. Chem.* **1998**, *273:* 26026-26035.

[87] Reilly, J.F., Mickey, G., Maher, P.A. Association of fibroblast growth factor receptor 1 with the adaptor protein Grb14: characterization of a new receptor binding partner. *J. Biol. Chem.* **2000**, *275:* 7771-7778.

[88] Duval, A., Rolland, S., Compoint, A., Tubacher, E., Iacopetta, B., Thomas, G., Hamelin R. Evolution of instability at coding and non-coding repeat sequences in human MSI-H colorectal cancers. *Hum. Mol. Genet.* **2001**, *10:* 513-518.

[89] Cariou, B., Capitaine, N., Le Marcis, V., Vega, N., Béréziat, V., Kergoat, M., Laville, M., Girard, J., Vidal, H., Burnol, A.-F. Increased adipose tissue expression of Grb14 in several models of insulin resistance. *FASEB J.* **2004**, *18:* 965-967.

[90] Petermann, E., Keil, C., Oei, S. L. Importance of poly(ADP-ribose) polymerases in the regulation of DNA-dependent processes. *Cell. Mol. Life Sci.* **2005**, *62:* 731-738.

[91] Lyons, R. J., Deane, R., Lynch, D. K., Ye, Z. S., Sanderson, G. M., Eyre, H. J., Sutherland, G. R., Daly, R. J. Identification of a novel human tankyrase through its interaction with the adaptor protein Grb14. *J. Biol. Chem.* **2001**, *276:* 17172-17180.

FEBS Letters 586 (2012) 1533–1539

journal homepage: www.FEBSLetters.org

Calmodulin regulates the translocation of Grb7 into the nucleus

Irene García-Palmero, Antonio Villalobo *

Instituto de Investigaciones Biomédicas, Consejo Superior de Investigaciones Científicas and Universidad Autónoma de Madrid, Department of Cancer Biology, c/ Arturo Duperier 4, E-28029 Madrid, Spain

ARTICLE INFO

Article history:
Received 17 February 2012
Revised 30 March 2012
Accepted 12 April 2012
Available online 25 April 2012

Edited by Gianni Cesareni

Keywords:
Calmodulin
Grb7
Nuclear localization sequence/signal (NLS)
Nuclear translocation
W-7

ABSTRACT

We describe in this report the presence of a nuclear localization signal (NLS) overlapping the calmodulin-binding domain (CaM-BD) of the growth factor receptor bound protein 7 (Grb7). We show that deletion of the CaM-BD of Grb7 prevents its nuclear localization, and that its Src homology 2 (SH2) domain might participate as well in the translocation process. Also, treating cells with the CaM antagonist *N*-(6-aminohexyl)-5-chloro-1-naphthalenesulfonamide (W-7) enhances the presence of Grb7 in the nucleus. We propose that CaM inhibits the translocation of Grb7 to the nucleus after binding to its CaM-BD and therefore occluding its overlapping NLS.

1. Introduction

The growth factor receptor bound protein 7 (Grb7) is an adaptor that regulates multiple cellular functions by interacting with different tyrosine kinase receptors and other phospho-tyrosine proteins. It gives name to a family of proteins, which also includes Grb10 and Grb14 [1–6]. The Grb7 family members share a similar structural organization, composed by an amino-terminal PR region, a central GM region (for *G*rb and *M*ig10) [6] that includes a RA domain, a PH domain and a BPS domain (for *b*etween *P*H and *S*H2). The SH2 domain, important because of its binding to phospho-tyrosine residues in target proteins, is located at its carboxyl-terminal [1,2,4,6].

We have previously described the presence of a CaM-BD located at the proximal region of the PH domain forming a predicted amphiphilic α-helix, and that a Grb7 mutant lacking the CaM-BD loses the ability to bind CaM and membrane phosphoinositides [7]; however the functional relevance of this CaM-BD is still unknown.

A basic amino acidic sequence is a common feature shared by different NLSs and classical amphiphilic α-helices that conform the CaM-BDs of many proteins. Overlapping of both sequences frequently occurs (see Table 1 and references therein). In other instances, both regions do not overlap but are in close proximity, as in the nuclear matrix protein denoted matrin 3 [8]. This close association also suggests a regulatory role of CaM on the translocation process.

Nuclear Grb7 has been shown to aid in the coordinated exit of a KOR specific mRNA–protein export complex from the nucleus after the EGF-mediated dephosphorylation of Grb7 by SHP-2, and the subsequent rephosphorylation of the adaptor protein by FAK inducing the release of the mRNA to start translation [12].

In this report we investigate the role of CaM regulating Grb7 translocation into the nucleus, as Grb7Δ (a deletion mutant lacking the CaM-BD), is unable of nuclear localization. Moreover, cell treatment with the CaM antagonist W-7 results in a massive translocation of Grb7 into the nucleus, suggesting that CaM is regulating this process.

Abbreviations: 5′-UTR, 5′-untranslated region; CaM, calmodulin; CaM-BD, CaM-binding domain; CRM1, chromosomal region maintenance 1; DAPI, 4′,6-diamidino-2-phenylindole; DMEM, Dulbecco's modified Eagle's medium; EGFR, epidermal growth factor receptor; EYFP, enhanced yellow fluorescent protein; FAK, focal adhesion kinase; FBS, fetal bovine serum; Grb7, growth factor receptor bound protein 7; GRK5, G protein-coupled receptor kinase 5; HEK, human embryonic kidney; HRP, horseradish peroxidase; HuR, Hu antigen R; KOR, κ-opioid receptor; NLS, nuclear localization sequence/signal; NF, nuclear fraction; NNF, non-nuclear fraction; PARP, poly-ADP ribose polymerase; PBS, phosphate buffered saline; PH, pleckstrin homology; PR, proline-rich; RA, Ras-associating; SH2, Src homology 2; SHP-2, SH2 domain-containing phosphatase-2; SOX, Sry-related high-mobility-box; SRY, sex-determining region on the Y chromosome; TSAd, T cell-specific adapter; W-7, *N*-(6-aminohexyl)-5-chloro-1-naphthalenesulfonamide

* Corresponding author. Fax: +34 91 585 4401.
E-mail address: antonio.villalobo@iib.uam.es (A. Villalobo).

0014-5793/$36.00
http://dx.doi.org/10.1016/j.febslet.2012.04.017

Table 1
Overlapping of the CaM-BD and NLS.

Protein	CaM-BD/NLS	Reference
hGrb7	**RK**LW**KR**FFCFL**RR**S	[7]
BASP1	GG**K**LS**KKKK**	[32]
EGFR	**RRR**HIV**RKR**TL**RR**LLQ	[16,17]
hSOX1	**KR**PMNAFMVWS**R**GQ**RRK**	[18,20]
hSOX9	**RR**PMNAFMVWAQAA**RRK**	[18,20]
hSRY	**KR**PMNAFIVWS**R**DQ**RR**K	[19]
Kir/Gem	**KRK**ESMP**RK**A**RR**	[22]
TAP-Tag	**KRR**W**KK**NFIAVSAAN**RF**K**K**	[33]

The sequences corresponding to the CaM-BD and the overlapping NLS of different proteins are indicated. Clusters of basic amino acid residues are highlighted in bold.

2. Materials and methods

2.1. Reagents

ProLong Gold antifade reagent, FBS, DMEM, and DAPI were obtained from Invitrogen, and W-7 from Calbiochem. The X-ray films (Curix RP2 Plus) were from Agfa Healthcare. The ExSite mutagenesis kit was from Stratagene. The rabbit polyclonal anti-Grb7 (N-20 and C-20) and the goat polyclonal anti-lamin B (C-20) antibodies were from Santa Cruz Biotechnology. Rabbit monoclonal anti-GAPDH and anti-PARP antibodies were from Cell Signaling Technology. HRP-conjugated goat anti-rabbit IgG (H+L) antibody was from Zymed Laboratories. Fibronectin (from bovine plasma), FLAG®-M2 affinity gel and anti-FLAG®-M2 monoclonal mouse antibody were purchased from Sigma. The HRP-conjugated donkey anti-goat IgG antibody was from Promega Co. The anti-GFP antibody, also recognizing the variant EYFP, was from Roche Diagnostics.

2.2. Vectors preparation

The FLAG-tagged Grb7 and Grb7V open reading frames were amplified by PCR using the vector pCR3/FLAG-Grb7 and pCR3/FLAG-Grb7V as templates and the following oligonucleotides: for Grb7 forward primer 5′-GAT GAC GAT CAT ATG GAG CCG GAT CTG TCT CCA CCT CAT C-3′ containing a *NdeI* restriction site (underlined), reverse primer 5′-GCC AGT CCA CGC TCG AGT CAG AGG GCC ACC CGC GTG CAG C-3′ containing a *XhoI* restriction site (underlined); for Grb7V the same forward primer was used and the reverse primer was 5′-GCA GGA TGA GAT CTC GAG TCA CTT TCT GCA GGT GGC ACA AAG-3′ containing a *XhoI* restriction site (underlined) [7]. The CaM-BD deletion (residues 243–256) mutants Grb7Δ and Grb7VΔ were generated with the ExSite mutagenesis kit (Stratagene) using pCR3/FLAG-Grb7 and pCR3/FLAG-Grb7V as templates and the following oligonucleotides: forward primer 5′-TCC TGA ACC CCG CAG CTG CAG AAA GCC CTG-3′ and reverse primer 5′ GGC GTC TAT TAC TCC ACC AAG GGC ACC TCT AAG-3′ [7]. The PCR products were subcloned into pcDNA3 using the *EcoRI* and *XhoI* restriction enzymes yielding the pcDNA3/FLAG-Grb7, pcDNA3/FLAG-Grb7Δ, pcDNA3/FLAG-Grb7V and pcDNA3/FLAG-Grb7VΔ vectors. The pEYFP-Grb7 and pEYFP-Grb7Δ vectors were prepared by subcloning the inserts from pCR3-FLAG-Grb7 and pCR3-FLAG-Grb7Δ into pEYFP-C1 using the restriction enzymes *XhoI* and *KpnI* after elimination of the FLAG tag as previously described [7].

2.3. Cell culture and transfection

Authenticated human embryonic kidney HEK293 (ATCC number CRL-1573), and rat glioma C6 (ATCC number CCL-107) cells were obtained from the American Type Culture Collection (Manassas, VA). The cell lines were grown in DMEM supplemented with 10% (v/v) FBS, 2 mM L-glutamine, 40 μg/ml gentamicin (plus 1 mg/ml G418 in the case of the stable transfectants) at 37 °C in a humified atmosphere containing 5% CO_2. The HEK293 and C6 cells were, respectively, transfected with the calcium phosphate method [7] or the jetPEI™ transfection kit as described by the manufacturer using the following plasmids: pcDNA3.1, pcDNA3/FLAG-Grb7, pcDNA3/FLAG-Grb7Δ, pEYFP, pEYFP-Grb7 or pEYFP-Grb7Δ.

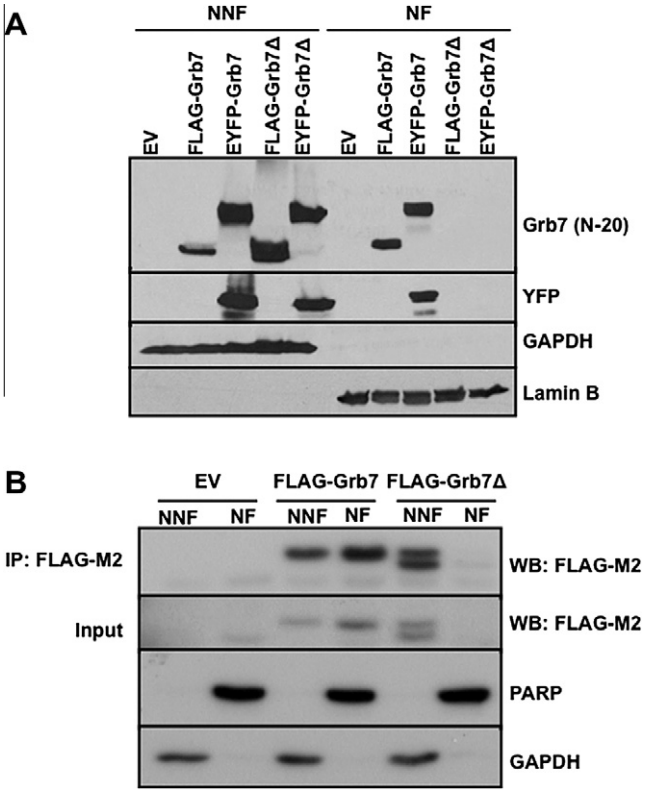

Fig. 1. Deletion of the CaM-BD in FLAG-Grb7 and EYFP-Grb7 prevents its presence in the nucleus. (A) The non-nuclear fraction (NNF) and the nuclear fraction (NF) from HEK293 cells transiently transfected with either pcDNA3.1, pcDNA3/FLAG-Grb7, pcDNA3/FLAG-Grb7Δ, pEYFP, pEYFP-Grb7 or pEYFP-Grb7Δ were processed for Western blots as described in Section 2 using the anti-Grb7 (N-20) and anti-YFP antibodies. (B) Immunoprecipitation (IP) of FLAG-Grb7 and FLAG-Grb7Δ from NNF and NF using anti-FLAG®M2 affinity gel. Anti-GAPDH and anti-lamin B or anti-PARP antibodies were used as loading controls and to ascertain the absence of cross-contamination between the NNF and NF.

2.4. Nuclear fractionation

The nuclear fractions were prepared as described [9]. Briefly: HEK293 cells transiently transfected with pcDNA3.1, pcDNA3/FLAG-Grb7, pcDNA3/FLAG-Grb7Δ, pEYFP, pEYFP-Grb7 or pEYFP-Grb7Δ vectors were collected in a hypotonic lysis buffer containing 20 mM Hepes-NaOH (pH 7.0), 10 mM KCl, 2 mM $MgCl_2$, 0.5% (v/v) Nonidet P-40, 1 mM Na_3VO_4 and a protease inhibitors cocktail, and homogenized on ice by 30 strokes using a Dounce homogenizer. After centrifugation at $1500g_{max}$ for 5 min, the supernatant (non-nuclear fraction) was collected, and the pellet containing the nuclei was washed four times with the same buffer. The nuclei were resuspended in the same buffer supplemented with 0.5 M NaCl to extract the nuclear proteins. The samples were centrifuged at $15000g_{max}$ for 10 min and the supernatant (nuclear fraction) was collected. The protein concentration was determined using the BCA™ protein assay kit.

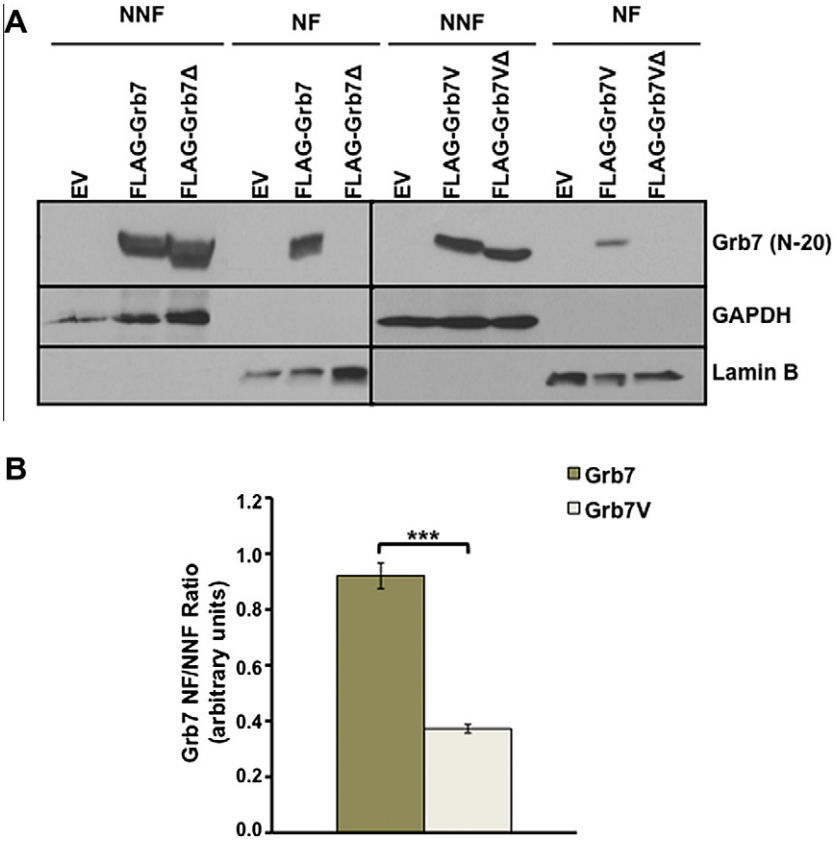

Fig. 2. The truncated variant Grb7V is present in the nucleus in lesser amount than wild type Grb7. (A) Western blot analysis of the NNF and the NF from HEK293 cells transiently transfected with pcDNA3.1, pcDNA3/FLAG-Grb7, pcDNA3/FLAG-Grb7Δ, pcDNA3/FLAG-Grb7V or pcDNA3/FLAG-Grb7VΔ. Anti-GAPDH and anti-lamin B antibodies were used as loading controls and to ascertain the absence of cross-contamination between the NNF and NF. (B) The plot presents the NF/NNF ratio of the mean ± S.E.M. ($n = 3$) densitometric signal of Grb7. $^{***}p < 0.001$.

2.5. Immunoprecipitation

Proteins from both nuclear and non-nuclear fractions were immunoprecipitated at 4 °C overnight with anti-FLAG®-M2 Affinity Gel. The next day, beads were washed four times and the immunocomplexes eluted with loading buffer (60 mM Tris–HCl pH 6.8, 5% (v/v) glycerol, 1.5% (w/v) SDS, 100 mM dithiothreitol and 0.05% (w/v) bromophenol-blue).

2.6. W-7 treatment and fibronectin seeding

Forty-eight hours post-transfection, trypsin-detached serum-starved HEK293 cells were resuspended in DMEM, treated with 15 μM W-7 for 30 min and reseeded on 10 μg/ml fibronectin-coated plastic plates or glass cover slips. The cells were collected 30–60 min later for nuclear fractionation or for confocal microscopy. Long-term treatment was performed by adding daily 30 μM W-7 to the cells.

2.7. Confocal microscopy

Cells transfected with pEYFP-Grb7 or pEYFP-Grb7Δ were washed twice with PBS and fixed with 4% (v/v) paraformaldehyde for 20 min and then permeabilized with 0.5% (v/v) Triton X-100 for 10 min. The cells were washed again with PBS and stained with DAPI (1:500 dilution) for 10 min. The ProLong Gold Antifade Reagent was used as mounting solution. Cells were visualized using a Leica TCS SP5 confocal fluorescence microscope with a 63× (HCS PL APO lambda blue) oil-immersion objective using the UV and 488 nm lasers.

2.8. Statistical analysis

The Student's *t* test was performed using the GraphPad Prism software program (GraphPad Software Inc.). Differences were considered significant at $p \leqslant 0.05$.

3. Results

3.1. The CaM-BD deletion mutant Grb7Δ fails to localize in the nucleus

We first studied the localization on Grb7 inside the nucleus. Subcellular fractionation showed that both FLAG-Grb7 and EYFP-Grb7 were detectable in the NF as well as in the NNF of transiently transfected cells. However, the CaM-BD deletion mutant Grb7Δ failed to localize in the NF (Fig. 1A) suggesting that the CaM-BD is essential for nuclear localization. These observations were supported by immunoprecipitation using anti-FLAG-M2 affinity gel from both the NNF and NF from HEK293 cells stably expressing FLAG-Grb7 or FLAG-Grb7Δ (Fig. 1B). The upper band of Grb7Δ in the stable transfectants most likely represents some phosphorylation of the protein at its C-terminal, as only the lower band was detected using an anti-Grb7 (C-20) antibody recognizing its C-terminal end, and alkaline phosphatase treatment significantly affect the migration of the upper band (not shown).

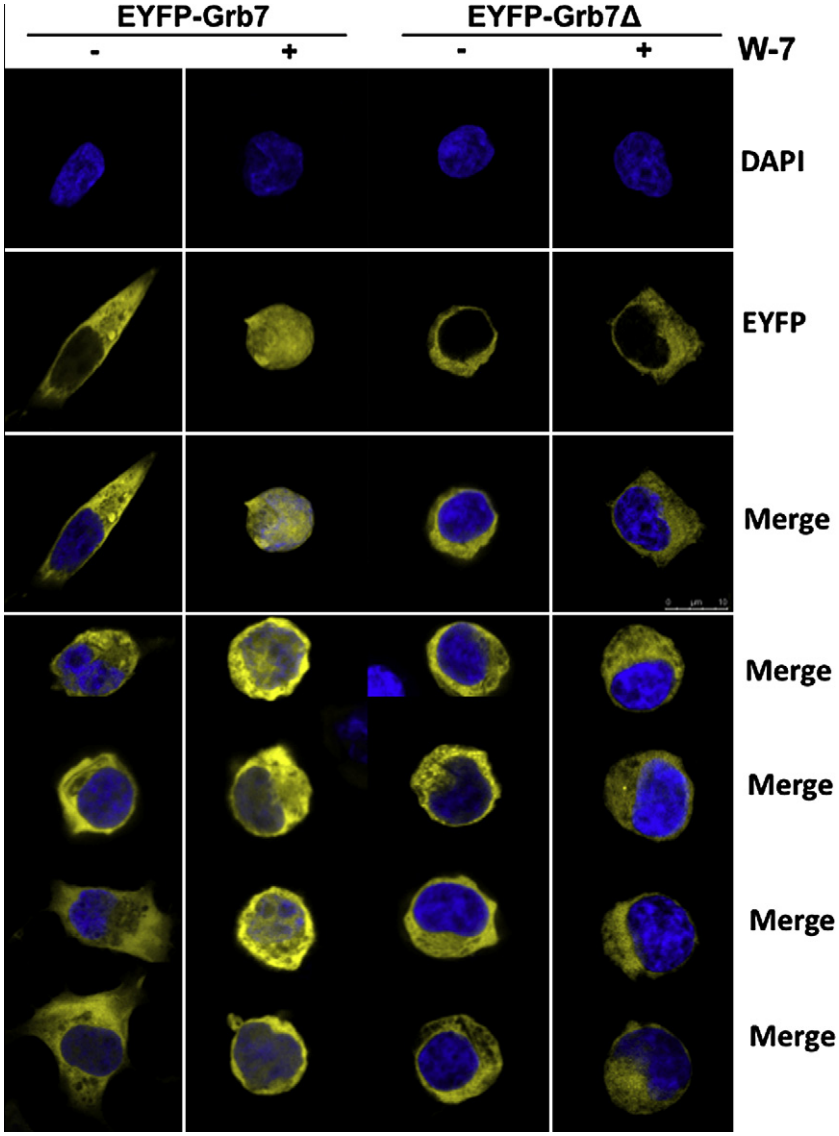

Fig. 3. The CaM antagonist W-7 enhances the translocation of EYFP-Grb7 into the nucleus. HEK293 cells transiently transfected with pEYFP-Grb7 and pEYFP-Grb7Δ were incubated for 60 min (*top panel*) or 30 min (*bottom panel*) in the absence (−) and presence (+) of 15 μM W-7. Thereafter, the cells were seeded on fibronectin-coated plates, and 30 min later the cells were fixed, stained with DAPI and observed in a confocal fluorescence microscope as described in Section 2. Representative images of cells expressing EYFP-Grb7 and EYFP-Grb7Δ are shown.

3.2. The SH2 domain of Grb7 is necessary for efficient nuclear localization

To determine whether the SH2 domain of Grb7 was required for its nuclear translocation we compared the location of Grb7 and Grb7V, a truncated variant that lacks the SH2 domain [10], at the nuclear fraction. Fig. 2 shows that Grb7V was detectable in the nuclear fraction but in lesser extent (≈40%) than Grb7. The deletion of the CaM-BD in both Grb7 and Grb7Δ prevented this localization. This suggests that the SH2 domain plays a relevant role in the nuclear translocation process.

3.3. W-7 enhances Grb7 translocation into the nucleus

To study the role of CaM in the control of the nuclear translocation of Grb7, we used W-7 to inhibit CaM. Confocal fluorescence studies of HEK293 cells transiently transfected with pEYFP-Grb7 and pEYFP-Grb7Δ showed that inhibition of CaM by W-7 led to a massive translocation of EYFP-Grb7 into the nucleus, while this inhibitor had no effect on EYFP-Grb7Δ localization (Fig. 3). Similar results were obtained in rat glioma C6 cells expressing both transiently and stably transfected EYFP-Grb7 and EYFP-Grb7Δ (not shown). These results were confirmed by Western blot of the NNF and NF of HEK239 cells transiently transfected with FLAG-Grb7 (Fig. 4). To test for long-term effects of the CaM antagonist, we treated HEK293 cells with W-7 for several days. Fig. 5 shows the progressive increase of Grb7 in the NF at longer times of exposure to W-7.

4. Discussion

Grb7 is an adaptor protein that plays important roles in transmitting signals from the cell surface to the cell interior. This adaptor has recently been identified as an RNA-binding protein, interacting through the PR domain with KOR mRNA [11]. Grb7 works as a constitutive translational repressor, when it binds directly to the 5′-UTR of the target mRNA, blocking the recognition of the mRNA by the translational initiator complex. Grb7 when

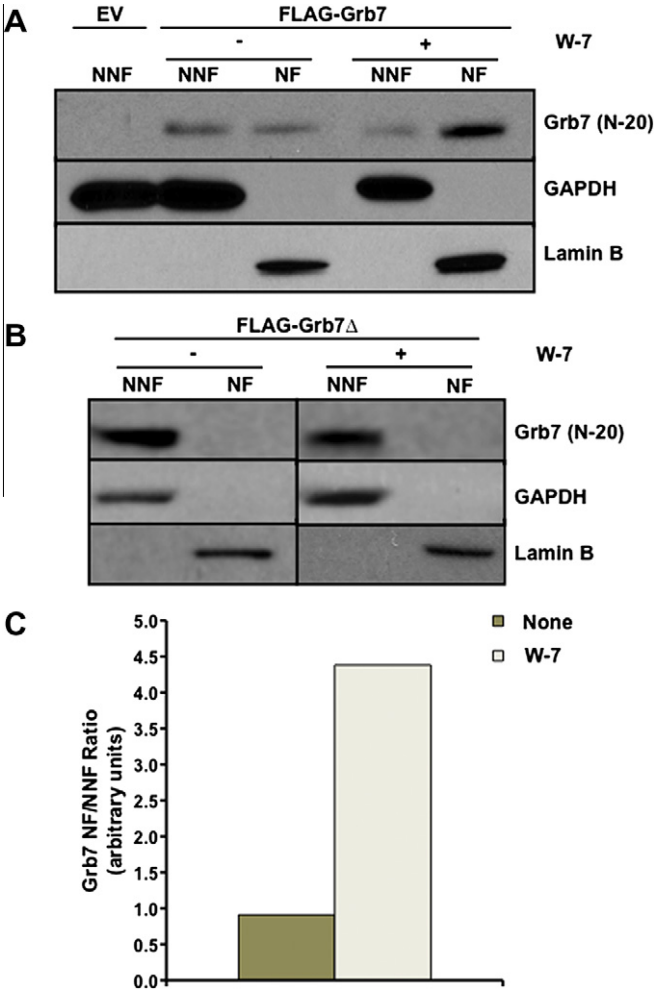

Fig. 4. The CaM antagonist W-7 enhances the presence of Grb7 in the nucleus. HEK293 cells transiently transfected with pcDNA3/FLAG-Grb7 (A) or pcDNA3/FLAG-Grb7Δ (B) were treated with 15 μM W-7 for 30 min prior to subcellular fractionation. A control of cells transfected with the empty vector (EV) pcDNA3.1 is also shown. (A, B) Western blot analyses of the NNF and the NF using an anti-Grb7 (N-20) antibody. Anti-GAPDH and anti-lamin B antibodies were used as loading controls and to ascertain the absence of cross-contamination between the NNF and NF. (C) The plot presents the densitometric NF/NNF ratio of Grb7 in the absence and presence of W-7 corresponding to the experiment shown in panel A.

bound to KOR mRNA is able to transport the target mRNA from the nucleus to the cytoplasm in a EGF-dependent manner, forming a nuclear export complex with other proteins such as HuR and CRM1 [12]. However, no mechanism of nuclear import of Grb7 has been proposed yet. Large proteins harboring a NLS enter in the nucleus by an energy-dependent process [13]. Several NLS consensus sequences have been described. The classical NLS consensus sequence consists of clusters of basic amino acids separated by some unrelated amino acids [14,15]. We propose that the CaM-BD of Grb7 comprising the sequence ^{243}RKLWKRFFCFLRRS^{256} is a classical basic NLS sequence.

As Table 1 shows many CaM-BDs in different proteins overlap with their known NLSs. This occurs in the EGFR that binds CaM and is also translocated into the nucleus [16,17]. Moreover, the translocation of the transcription factors SRY and SOX into the nucleus is mediated by two NLSs: one working through importin α1 (α-NLS), and the other by binding calmodulin (CaM-NLS) [18–20]. The CaM-NLS sequence of these proteins is highly conserved [18,20]. Nuclear translocation of SRY occurs by a mutual exclusive mechanism involving only one of the two NLSs, where switching between both of them depends on the concentration of intracellular calcium available at a given time [21]. Three NLSs have been identified in the small G protein Kir/Gem one of which has CaM binding capacity as well [22]. p21^{Cip1} translocation into the nucleus is also controlled by CaM [23]. A peptide encoding amino acids 145–164 of p21^{Cip1}, binds CaM and also comprises part of its previously described NLS [23]. The export of proteins out of the nucleus can also be regulated by CaM, as for example GRK5 where the Ca^{2+}/CaM complex binds to the N-terminal CaM-BD to aid in the export process [24].

The region responsible for the localization of the SV40 large-T antigen in the nucleus was identified by deletion of a basic sequence defining its NLS [25,26]. Using a similar approach we have demonstrated that deletion of a basic sequence of Grb7 corresponding to its CaM-BD also prevents its nuclear localization.

We have described that the truncated variant Grb7V lacking the SH2 domain is able to localize in the nucleus but in lesser extent than Grb7. This suggests that the SH2 domain of Grb7 plays an important role controlling its entry into the nucleus. SH2 domains work as docking sites allowing the binding to phospho-tyrosine residues of target proteins. We hypothesized that the absence of this domain may impair the binding of a phospho-protein(s) that could facilitate Grb7 nuclear import. In this context, the nuclear entry of TSAd facilitated by a tyrosine-phosphorylated protein ligand interacting with the SH2 domain has been described [27].

The SH2 structure of Grb7 in solution shows two external α-helices and two central β-sheets exposing an overall net high negative electrostatic surface potential [28]. We speculated that the SH2 and PH domains of Grb7 could suffer an intermolecular electrostatic interaction helping to expose the overlapping CaM-BD/NLS to the nuclear translocating machinery. The absence of a crystallographic structure of the whole Grb7 molecule prevents us to elaborate further on this hypothetical interaction. If confirmed it could explain why Grb7V is less efficiently translocated than Grb7.

The CaM antagonist calmidazolium prevents the nuclear translocation of SOX9 [18] and SRY [19,29] demonstrating that CaM positively controls the translocation process. A similar effect is observed in p21^{Cip1} translocation [23]. In contrast, CaM inhibits the translocation of Kir/Gem [22] and the transcription factor c-Rel [30] into the nucleus, similarly to what occurs with Grb7.

The crystallographic structure of the full-length Grb7 has not been established yet. Therefore, it is not known the structure of the identified CaM-BD in the proximal region of the PH domain, although a helical conformation was proposed [7]. However, the structure of the RA and PH domains of Grb10 shows that this segment is not helical but a β-strand within a β-sheet [31], suggesting that this might be the same in Grb7 because of the high homology sequence of this segment. We have found that the three Grb7/10/14 proteins are indeed CaM-binding proteins (García-Palmero and Villalobo, unpublished results). However, deletion of this homologous segment has a differential effect on CaM binding, being Grb7Δ the one with far lower capacity to bind CaM, as compared to Grb10Δ and Grb14Δ (García-Palmero and Villalobo, unpublished results).

In conclusion, we propose that binding of CaM to Grb7 occludes its NLS, preventing the translocation of this adaptor protein into the nucleus. Conversely, inhibition of CaM leads to a higher exposition of the NLS resulting in increased nuclear localization. Hence, CaM plays an important role controlling the nuclear localization of Grb7.

Acknowledgements

This work was financed by grants (to A.V.) from the *Secretaría de Estado de Investigación, Desarrollo e Innovación* (SAF2011-23494), the European Commission (contract PITN-GA-2011-289033), and

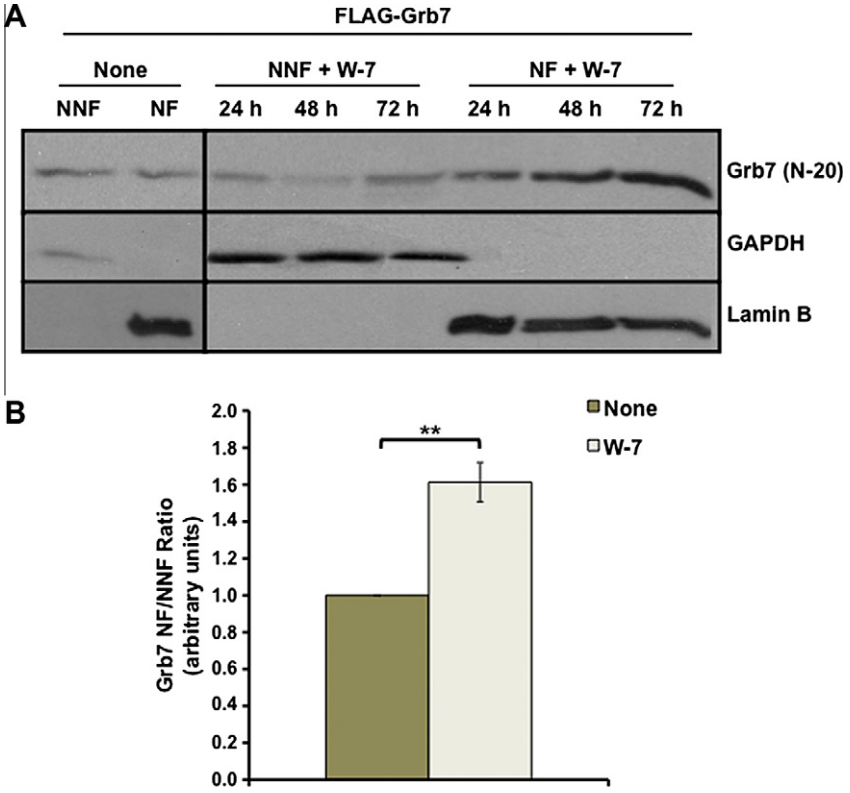

Fig. 5. Long-term treatment with W-7 enhances the presence of Grb7 in the nucleus. HEK293 cells stably transfected with pcDNA3/FLAG-Grb7 were treated with 30 μM W-7 for 24, 48 and 72 h as described in Section 2. (A) The panel shows Western blots of the NNF and the NF during the treatment using an anti-Grb7 (N-20) antibody. Anti-GAPDH and anti-lamin B antibodies were used as loading controls and to ascertain the absence of cross-contamination between the NNF and NF. (B) The plot presents the mean ± S.E.M. ($n = 3$) densitometric signal of the NF/NNF ratio of Grb7 at 72 h in independent experiments similar to the one shown in panel A. $^{**}p < 0.01$.

the *Consejería de Educación de la Comunidad de Madrid* (S2011/BMD-2349). IG-P was supported by a predoctoral fellowship from the *Ministerio de Ciencia e Innovación*.

References

[1] Daly, R.J. (1998) The Grb7 family of signalling proteins. Cell Signal. 10, 613–618.
[2] Han, D.C., Shen, T.L. and Guan, J.L. (2001) The Grb7 family proteins: structure, interactions with other signaling molecules and potential cellular functions. Oncogene 20, 6315–6321.
[3] Shen, T.L. and Guan, J.L. (2004) Grb7 in intracellular signaling and its role in cell regulation. Front. Biosci. 9, 192–200.
[4] Villalobo, A., Li, H. and Sánchez-Torres, J. (2003) The Grb7 protein family. Curr. Top. Biochem. Res. 5, 105–114.
[5] Lucas-Fernandez, E., Garcia-Palmero, I. and Villalobo, A. (2008) Genomic organization and control of the Grb7 gene family. Curr. Genomics 9, 60–68.
[6] Margolis, B. (1994) The GRB family of SH2 domain proteins. Prog. Biophys. Mol. Biol. 62, 223–244.
[7] Li, H., Sanchez-Torres, J., del Carpio, A.F., Nogales-Gonzalez, A., Molina-Ortiz, P., Moreno, M.J., Török, K. and Villalobo, A. (2005) The adaptor Grb7 is a novel calmodulin-binding protein: functional implications of the interaction of calmodulin with Grb7. Oncogene 24, 4206–4219.
[8] Valencia, C.A., Ju, W. and Liu, R. (2007) Matrin 3 is a Ca^{2+}/calmodulin-binding protein cleaved by caspases. Biochem. Biophys. Res. Commun. 361, 281–286.
[9] Lin, S.Y., Makino, K., Xia, W., Matin, A., Wen, Y., Kwong, K.Y., Bourguignon, L. and Hung, M.C. (2001) Nuclear localization of EGF receptor and its potential new role as a transcription factor. Nat. Cell. Biol. 3, 802–808.
[10] Tanaka, S., Mori, M., Akiyoshi, T., Tanaka, Y., Mafune, K., Wands, J.R. and Sugimachi, K. (1998) A novel variant of human Grb7 is associated with invasive esophageal carcinoma. J. Clin. Invest. 102, 821–827.
[11] Tsai, N.P., Bi, J. and Wei, L.N. (2007) The adaptor Grb7 links netrin-1 signaling to regulation of mRNA translation. EMBO J. 26, 1522–1531.
[12] Tsai, N.-P., Lin, Y.-L., Tsui, Y.-C. and Wei, L.-N. (2010) Dual action of epidermal growth factor: extracellular signal-stimulated nuclear-cytoplasmic export and coordinated translation of selected messenger RNA. J. Cell Biol. 188, 325–333.
[13] Macara, I.G. (2001) Transport into and out of the nucleus. Microbiol. Mol. Biol. Rev. 65, 570–594.
[14] Dingwall, C. and Laskey, R.A. (1991) Nuclear targeting sequences – a consensus? Trends Biochem. Sci. 16, 478–481.
[15] Robbins, J., Dilworth, S.M., Laskey, R.A. and Dingwall, C. (1991) Two interdependent basic domains in nucleoplasmin nuclear targeting sequence. Identification of a class of bipartite nuclear targeting sequence. Cell 64, 615–623.
[16] Martín-Nieto, J. and Villalobo, A. (1998) The human epidermal growth factor receptor contains a juxtamembrane calmodulin-binding site. Biochemistry 37, 227–236.
[17] Villalobo, A., García-Andrés, C. and Molina-Ortiz, P. (2003) Translocation of ErbB receptors into the nucleus. Clin. Transl. Oncol. 5, 381–389.
[18] Argentaro, A., Sim, H., Kelly, S., Preiss, S., Clayton, A., Jans, D.A. and Harley, V.R. (2003) A SOX9 defect of calmodulin-dependent nuclear import in campomelic dysplasia/autosomal sex reversal. J. Biol. Chem. 278, 33839–33847.
[19] Kaur, G., Delluc-Clavieres, A., Poon, I.K., Forwood, J.K., Glover, D.J. and Jans, D.A. (2010) Calmodulin-dependent nuclear import of HMG-box family nuclear factors: importance of the role of SRY in sex reversal. Biochem. J. 430, 39–48.
[20] Malki, S., Boizet-Bonhoure, B. and Poulat, F. (2010) Shuttling of SOX proteins. Int. J. Biochem. Cell Biol. 42, 411–416.
[21] Kaur, G. and Jans, D.A. (2011) Dual nuclear import mechanisms of sex determining factor SRY: intracellular Ca^{2+} as a switch. FASEB J. 25, 665–675.
[22] Mahalakshmi, R.N., Nagashima, K., Ng, M.Y., Inagaki, N., Hunziker, W. and Beguin, P. (2007) Nuclear transport of Kir/Gem requires specific signals and importin α5 and is regulated by calmodulin and predicted serine phosphorylations. Traffic 8, 1150–1163.
[23] Taulés, M., Rodríguez-Vilarupla, A., Rius, E., Estanyol, J.M., Casanovas, O., Sacks, D.B., Pérez-Payá, E., Bachs, O. and Agell, N. (1999) Calmodulin binds to p21Cip1 and is involved in the regulation of its nuclear localization. J. Biol. Chem. 274, 24445–24448.
[24] Johnson, L.R., Scott, M.G. and Pitcher, J.A. (2004) G protein-coupled receptor kinase 5 contains a DNA-binding nuclear localization sequence. Mol. Cell. Biol. 24, 10169–10179.
[25] Kalderon, D. and Smith, A.E. (1984) In vitro mutagenesis of a putative DNA binding domain of SV40 large-T. Virology 139, 109–137.
[26] Kalderon, D., Richardson, W.D., Markham, A.F. and Smith, A.E. (1984) Sequence requirements for nuclear location of simian virus 40 large-T antigen. Nature 311, 33–38.
[27] Marti, F. and King, P.D. (2005) The p95–100 kDa ligand of the T cell-specific adaptor (TSAd) protein Src-homology-2 (SH2) domain implicated in TSAd nuclear import is p97 valosin-containing protein (VCP). Immunol. Lett. 97, 235–243.

[28] Ivancic, M., Daly, R.J. and Lyons, B.A. (2003) Solution structure of the human Grb7-SH2 domain/erbB2 peptide complex and structural basis for Grb7 binding to ErbB2. J. Biomol. NMR 27, 205–219.
[29] Sim, H., Rimmer, K., Kelly, S., Ludbrook, L.M., Clayton, A.H. and Harley, V.R. (2005) Defective calmodulin-mediated nuclear transport of the sex-determining region of the Y chromosome (SRY) in XY sex reversal. Mol. Endocrinol. 19, 1884–1892.
[30] Antonsson, Å., Hughes, K., Edin, S. and Grundström, T. (2003) Regulation of c-Rel nuclear localization by binding of Ca^{2+}/calmodulin. Mol. Cell. Biol. 23, 1418–1427.
[31] Depetris, R.S., Wu, J. and Hubbard, S.R. (2009) Structural and functional studies of the Ras-associating and pleckstrin-homology domains of Grb10 and Grb14. Nat. Struct. Mol. Biol. 16, 833–839.
[32] Hartl, M., Nist, A., Khan, M.I., Valovka, T. and Bister, K. (2009) Inhibition of Myc-induced cell transformation by brain acid-soluble protein 1 (BASP1). Proc. Nat. Acad. Sci. 106, 5604–5609.
[33] Rohila, J.S., Chen, M., Cerny, R. and Fromm, M.E. (2004) Improved tandem affinity purification tag and methods for isolation of protein heterocomplexes from plants. Plant J. 38, 172–181.